Open Research Online

The Open University's repository of research publications
and other research outputs

Evaluation of the complexity of cell cycle effects induced by anticancer drugs

Thesis

How to cite:

Lupi, Monica (2006). Evaluation of the complexity of cell cycle effects induced by anticancer drugs. PhD thesis The Open University.

For guidance on citations see FAQs.

© 2006 Monica Lupi

Version: Version of Record

Copyright and Moral Rights for the articles on this site are retained by the individual authors and/or other copyright owners. For more information on Open Research Online's data policy on reuse of materials please consult the policies page.

oro.open.ac.uk

UNRESTRICTED

EVALUATION OF THE COMPLEXITY OF CELL CYCLE EFFECTS INDUCED BY ANTICANCER DRUGS

Thesis submitted for the degree of Doctor of Philosophy

at the Open University

Discipline of Life Sciences

By

Monica Lupi, Degree in Physics

Mario Negri Institute for Pharmacological Research

Milan, Italy

The Open University, UK

Advanced School of Pharmacology
Dean, Enrico Garattini M D

Mario Negri Institute for Pharmacological Research

September 2005

7/6/2006

DATE OF SUBMISSION 19 SEPTEMBER 2005
DATE OF AWARD 25 JANUARY 2006

ProQuest Number: 13917267

All rights reserved

INFORMATION TO ALL USERS
The quality of this reproduction is dependent upon the quality of the copy submitted.

In the unlikely event that the author did not send a complete manuscript
and there are missing pages, these will be noted. Also, if material had to be removed,
a note will indicate the deletion.

ProQuest 13917267

Published by ProQuest LLC (2019). Copyright of the Dissertation is held by the Author.

All rights reserved.
This work is protected against unauthorized copying under Title 17, United States Code
Microform Edition © ProQuest LLC.

ProQuest LLC.
789 East Eisenhower Parkway
P.O. Box 1346
Ann Arbor, MI 48106 – 1346

ACKNOWLEDGEMENTS

At the end of this work I cannot forget all the people that supported me during these years. First of all I would like to thank Paolo Ubezio, Paul Smith and Maurizio D'Incalci for their advice and suggestions about this project and its development.

A special thought is for my parents, that always encouraged me during my travel in the scientific world, but a big thank is also for all of my friends and colleagues that made more pleasant these years of work. It would take too long to cite all their names, but I'm very grateful to each one of them, in particular to those that helped me in the realization of this project: Giada, Davide, Claudia and Valentina.

CONTENTS

LIST OF FIGURES

LIST OF TABLES

ABSTRACT

The time- and dose-dependence of the blocking activity, cell loss and recycling from block that follow a treatment with anticancer agents is not always easy to interpret, especially because of the superimposition of cytostatic and cytotoxic effects. Their separate quantification, in terms of the cellular control mechanisms that regulate the response to a drug treatment, is important to deeply understand the mode of action of an anticancer compound.

We investigated cell cycle effects induced by different drugs on a cell line growing *in vitro* with an approach including experimental data coming from cell counting and different flow cytometric techniques and a mathematical model reproducing the perturbed cell growth after drug treatment. In this way we could quantify the effects induced by treatments performed with topotecan, doxorubicin and melphalan on IGROV1 cells, evaluating separately cytostatic and cytotoxic effects. For each one of the considered drugs we obtained and compared a set of parameters describing the time- and dose-dependence of cell cycle effects. These results were compared with those previously published by our group (Sena et al., 1999; Montalenti et al., 1998).

Besides the classical flow cytometric techniques, we used the method of carboxyfluorescein diacetate succinimidyl ester staining to quantify and appreciate the heterogeneity of the effects induced by a treatment on the cells of the same population. The results obtained could be simulated with our mathematical model.

In the last part of the project, the previously listed tools were used to obtain two sets of parameters describing the effects induced by a short treatment of cisplatin on HCT-116 and HCT-116 p53-/-. This allowed the quantification of the role of p53 in the cell response to cisplatin treatment, finding that this protein has a more important role in the activation of the apoptosis than in the cytostatic effects induced by this drug.

CHAPTER 1: Introduction

1.1 CELL CYCLE IN NORMAL AND TUMOUR CELLS

The cell cycle is the mechanism by which cells divide. It is controlled by numerous mechanisms ensuring correct cell division. Cell division consists of two consecutive processes: DNA replication and segregation of replicated chromosomes into two separate cells. Originally, cell division was divided into two stages: mitosis (M) and interphase. Interphase cells simply grow in size, but different techniques revealed that the interphase includes G_1, S and G_2 phase (Howard and Pelc, 1953). Replication of DNA occurs in a specific part of the interphase called S phase. S phase is preceded by a gap called G_1 during which the cell is preparing for DNA synthesis and is followed by a gap called G_2 during which the cell prepares for mitosis (reviewed by Norbury and Nurse, 1992; Vermeulen et al., 2003).

Different cellular proteins regulate the transition from one cell cycle phase to another. Key regulatory proteins are the cyclin-dependent kinases (CDK), a family of serine/threonine protein kinases that are activated at specific points of the cell cycle. When activated, CDKs induce downstream processes by phosphorylating selected proteins. CDK protein levels remain stable during the cell cycle, in contrast to the cyclins. Cyclin protein levels rise and fall during the cell cycle and in this way they periodically activate CDK (Evans et al., 1983; Pines, 1991).

The three D-type cyclins (cyclin D1, cyclin D2, cyclin D3) bind to CDK4 and to CDK6 and they are essential for entry in G_1 (Sherr, 1994). Unlike the other cyclins, cyclin D is not expressed periodically, but it is synthesised as long as growth factor stimulation persists (Assoian and Zhu, 1997). Another G_1 cyclin is cyclin E which associates with CDK2 to regulate the progression from G_1 into S phase (Ohtsubo et al., 1995). Cyclin A binds CDK2 and this complex is required during S phase (Girard et al., 1991). In late G_2 and early M, cyclin A complexes with CDK1 (CDC2)

to promote entry into mitosis. Mitosis is further regulated by cyclin B in complex with CDK1 (King et al., 1994; Arellano and Moreno, 1997).

CDK activity is modulated by cell cycle inhibitory proteins called CDK inhibitors (CKI), which bind to CDK alone or to the CDK-cyclin complex. Two distinct families of CKI have been discovered (Sherr and Roberts, 1995), the INK4 family which specifically inactivates G_1 CDK and the Cip/Kip family, that includes p21, p27 and p57. The first family forms stable complexes with the CDK enzyme before cyclin binding, the second one inactivates CDK-cyclin complexes. Moreover, p21 inhibits DNA synthesis by binding and inhibiting the proliferating cell nuclear antigen (PCNA) (Pan et al., 1995; Waga et al., 1997). CKI are regulated both by internal and external signals: the expression of *p21* is under transcriptional control of the *p53* tumour suppressor gene. The *p21* gene promoter contains a p53-binding site that allows p53 to transcriptionally activate the *p21* gene (El Deiry et al., 1993).

CDKs present different substrates and when they are active, target proteins become phosphorylated on CDK consensus sites, resulting in changes that are physiologically relevant for cell cycle progression. For instance, during early G_1, Rb becomes phosphorylated and this leads to disruption of the complex with the histone deacetylase protein (HDAC) and release of the transcription factors E2F-1, which positively regulates the transcription of genes whose products are required for S phase progression (Buchkovic et al., 1989; Kato et al., 1993). pRb remains hyperphosphorylated for the remainder of the cell cycle and CDK2-cyclin E complex participates in maintaining this hyperphosphorylated state. During G_1/S the CDK2-cyclin E complex also phosphorylates its inhibitor p27, inducing its proteasome-dependent degradation (Hinds et al., 1992; Montagnoli et al., 1999).

1.1.1 Checkpoints

In response to DNA damage, checkpoints arrest the cell cycle in order to provide time for DNA repair. DNA damage checkpoints are positioned before S phase or after DNA replication, even though control systems are located also during S and M phase (Iliakis et al., 2003).

At the G_1/S checkpoint, cell cycle arrest induced by DNA damage is characterised by two kinetically distinct components. The initial, acute phase operates by inactivating CDK2-cyclin E through inhibition of the activating phosphatase Cdc25A and is followed by a more delayed and sustained G_1 arrest, also mediated by CDK2-cyclin E inactivation through stabilisation of the p53 tumour suppressor protein (Bao et al., 2001; Lukas et al., 2001).

Both components of the checkpoint response utilise the ATM/ATR and Chk1/Chk2 kinases (Costanzo et al., 2000; Falck et al., 2001). Downstream, inactivation of Cdc25A deprives the cell from an activator of the CDK2-cyclin E kinase, operating by removing inhibitory phosphatase from CDK2. This keeps the kinase in an inactive state and inhibits further downstream events required for the progression of cells into S phase.

The central element of the second branch of the G_1 component of the DNA damage checkpoint is the stabilisation of the p53 protein and the activation of its transcriptional activity. These effects lead to the transcription of a large number of genes, including *p21*, *Mdm2* and *Bax* (Agarwal et al., 1998). The induction of p21 results in CDK inhibition and cell cycle arrest, preventing the replication of damaged DNA (Ko and Prives, 1996). Mdm2 plays an important role in the regulation of p53: it binds to and inhibits p53 transcriptional activity and contributes to the proteolytic degradation of p53 by facilitating its ubiquitination (Oren, 1999). In the case of severely damaged cells, p53 induces cell death by activating genes, such as *Bax*, that are involved in apoptotic signalling.

When DNA is damaged during early part of the DNA synthesis phase, the S-phase checkpoint is activated (Larner et al., 1997). The length of the S-phase delay may be determined by the repair requirements imposed in this phase of the cell cycle. In contrast to the G_1/S checkpoint a role for p53 or p21 could not be established for the S-phase checkpoint (Lee et al., 1997; Guo et al., 1999). In presence of DNA damage ATM is activated and phosphorylates several substrates that are candidate components of the S-phase checkpoint including Chk2 (Matsuoka et al., 2000). Inhibition of CDK2 activity through Cdc25A degradation leads to delay in S-phase progression that correlates timely with the S-phase checkpoint response.

The G_2/M checkpoint is operational in late G_2 phase and it was initially considered a passive consequence of the presence of damaged DNA, but extensive investigations led to speculations for an active response with a role in DNA repair (Hartwell and Weinert, 1989). A key effector of the G_2 checkpoint is the CDK1 kinase. Chk1 and Chk2, which are activated during DNA damage in an ATM-dependent manner, phosphorylate Cdc25C, a specific phosphatase required for the removal of the inhibiting phosphorylation of tyrosine 15 of CDK1 (Matsuoka et al., 1998; Yu et al., 1998). Nuclear CDK1 remains phosphorylated in the absence of active Cdc25C and the cells remain arrested in the G_2 phase.

1.1.2 Cell Cycle and Cancer

In cancer cells the genetic control of cell division presents fundamental alterations that determine an unscheduled cell proliferation. Inactivation of tumour suppressor genes like *pRb* and *p53* results in dysfunction of proteins that normally inhibit cell cycle progression. In cancer, mutations have been observed in genes encoding CDK, cyclins, CDK-activating enzymes, CKI, CDK substrates and checkpoint proteins (Sherr, 1996; McDonald and El Deiry, 2000).

Alterations of CDK molecules in cancer have been reported, although with low frequency (Wolfel et al., 1995; Easton et al., 1998). On the other side aberrant cyclin D1 expression has been observed in many tumours. *Cyclin D1* gene amplification occurs in breast, oesophageal, bladder, lung and squamous cell carcinomas (Hall and Peters, 1996) and cyclin E has been found to be amplified or overexpressed in some cases of breast and colon cancer and in acute lymphoblastic and acute myeloid leukaemias (Leach et al., 1993; Keyomarsi et al., 1995; Iida et al., 1997).

Genetic analysis of human cancers has revealed that checkpoint proteins are inactivated in a large fraction of cases, and that alterations of the DNA damage checkpoint are likely to contribute to resistance of tumour cell to chemotherapeutic agents or irradiation. In particular, the *p53* gene is known to be the most frequently mutated gene in human cancer (Miller and Koeffler, 1993; Greenblatt et al., 1994). Point and mis-sense mutations lead to conformational changes and inactivation of the protein. p53 function can be altered or blocked also by other mechanisms, such as gene deletion or inactivation due to the binding of viral oncoproteins (for further details see 9.1.1).

On the other side overexpression by gene amplification of *Mdm2* has been reported in leukaemia and lymphoma, breast carcinoma, sarcoma and glioma and this can represent an alternative to p53 mutation to escape p53-mediated growth control (Moller et al., 1999).

Cell cycle checkpoints play a crucial role in the cell response to drug treatment with conventional chemotherapeutic and radiotherapeutic agents and with new compounds that target specific proteins, many of which belong to the cell cycle engine.

1.2 CANCER CHEMOTHERAPY

Before 1950, surgery was essentially the only available cancer therapy. With the invention of the linear accelerator, radiation therapy became a valuable tool to control local and regional disease after 1960 (reviewed by Chabner and Roberts, 2005). Both radiation therapy and surgery could eradicate localized tumours. Thus it was required to develop systemic therapies potentially active against metastasis. The employment of nitrogen mustard in 1942 as an effective treatment for some systemic human neoplasms such as lymphoma marked the beginnings of the modern era of chemotherapy (Gilman, 1963). The mechanism of action of nitrogen mustards was elucidated four years later by Gilman and Phillips (1946) who hypothesized that its therapeutic effects were due to alkylation of macromolecules. After the Second World War the employment of folic acid analogues in patients with leukaemia were investigated (Farber et al., 1948). The folate analogues, like methotrexate, were found to be active in haematological malignancies inducing remission in children with acute lymphoblastic leukaemia (ALL). In addition to antifolates other compounds, structurally related to pyrimidines and purines present in nucleic acids and active as antimetabolites, were successfully employed for the therapy of different neoplasms (Galmarini et al., 2002).

A further step toward the therapeutic cure of ALL was represented by the use of Vincristine, a natural product acting as inhibitor of microtubule polymerization. More recently many other natural or semisynthetic compounds that act by targeting the cell proliferative process have been discovered, such as novel inhibitors of mitosis, like taxanes (Manfredi and Horwitz, 1986) or topoisomerase I- and topoisoperase II-poisons, like camptothecin or epipodophillotoxins and anthracyclines (Minocha and Long, 1984; Hsiang et al., 1985).

In the late 1980s, molecular and genetic approaches to understanding cell biology uncovered new signalling networks that regulate cellular activities such as

proliferation and survival. Many of these networks were found to be altered in cancer cells, thus the aim of cancer therapy became the repair of these molecular defects or their use as specific targets. One of the most paradigmatic compounds of this category is imatinib mesylate. This product is a selective inhibitor of the BCR-ABL kinase (Druker et al., 1996), the fusion protein product of a chromosomal translocation that is involved in the pathogenesis of chronic myeloid leukaemia (CML).

The series of events that prompts a human cell out of quiescence and into cell division involves a complicated progression of signals. It is a highly regulated process, frequently altered in cancer cells leading to abnormal proliferation. A variety of novel agents that interfere with discrete elements of the signal transduction cascade are now in clinical development. Some of these compounds may inhibit the activation of membrane receptors involved in the transmission of proliferative signals, such as the epidermal growth factor receptor (EGFR) inhibitors. Multiple lines of evidence indicate that dysregulation of the EGFR signal transduction pathway plays a critical role in the process of tumour pathogenesis, growth and metastasis. At the cellular level, three major signalling pathways mediate the downstream effects of EGFR activation. The first pathway involves the Ras-Raf-MAP kinase pathways, the second involves phosphatidylinositol 3-kinase and Akt and the third involves the stress-activated protein kinase pathway. Thus different strategies for targeting the EGFR are under evaluation. These include monoclonal antibodies against EGFR and small molecules acting as inhibitors of the receptor tyrosine kinase domain. Monoclonal antibodies (e.g. cetuximab) generally act binding the extracellular domain of the EGFR and inhibiting ligand binding to the receptor, whereas tyrosine kinase inhibitors (e.g. gefitinib) compete with ATP for the intracellular catalytic site of EGFR (El-Rayes and Lo Russo, 2004).

Over the last decade also cell cycle and apoptotic pathways have emerged as interesting targets in the treatment of cancer. In particular, the inhibition or the modulation of CDK activity may promote different responses to the treatment including cell cycle arrest, induction of differentiation, apoptosis and inhibition of transcription. The induced effect depends not only on which specific CDK is modulated but also on the growth state of the cell, the presence of specific cell cycle components, and many other environmental factors. At least four molecules of this family are under clinical investigation, such as Flavopiridol, UCN-01, CYC202 and BMS-387032 (reviewed by Senderowicz, 2004).

On the other side, the fact that most tumours are aneuploid, reflecting abnormal sister chromatid separation, has motivated increasing interest in the mitotic checkpoints. Depletion of one of several mitotic components by small molecules, intracellular antibodies, dominant negative alleles or siRNA promotes cell death in *in vitro* cancer models. There are at least two serine-threonine kinases relevant to mitotic checkpoints that are being targeted by small molecules: aurora and polo-like kinases.

Even though a significant progress in the design of potentially cancer-selective compounds has been recently made there are still unresolved questions including finding ways of targeting these agents specifically to tumours, the development of effective combinations of new molecular target-directed agents with standard therapies and overcoming resistance mechanisms.

1.2.1 Anticancer Drugs

Conventional chemical or physical anticancer agents are generally cytotoxic and cytostatic, that means that they exert their antitumour activity inducing cell death or inhibiting cell proliferation. In general, they act interfering, directly or indirectly, with the mechanisms of cell division or with the basic machinery of DNA synthesis and

function. The most part of anticancer agents has DNA as principal target and this is probably responsible for both therapeutic effects and adverse side effects, but the clinical use of these compounds is based on the rationale that rapidly proliferating tumour cells are more sensitive than normal cells to their action (De Vita et al., 2001).

From the point of view of the antiproliferative effect, drugs have been traditionally divided into three different classes. In the first group are classified the non cycle-specific drugs. This kind of drugs exerts its killing activity against both proliferating and non-proliferating cells, which in solid tumour are the most part. However, only a few compounds, like melphalan and nitrosureas, were classified in this category.

In general, many anticancer drugs exert their prevalent action against proliferating cells (cycle-specific compounds) and among them it is possible to distinguish between phase-specific and non phase-specific agents. Phase-specific agents, like antimetabolites, preferentially kill the cells that are in a particular phase of the cell cycle at the time of treatment, by causing cells to transiently accumulate in a limited part of the cell cycle.

On the other side non phase-specific agents had cytotoxic and cytostatic effects on proliferating cells independently of the phase that they occupied at the time of treatment (Gianni et al., 1999). However this classification has not to be interpreted as a rigid subdivision, in fact some cycle-specific drugs, like anthracyclines, are able to kill resting cells too and phase-specific agents can exert certain cytostatic or cytotoxic effects in more than one cell cycle phase (see chapter 4).

A further subdivision of these compounds can be made taking into account their chemical origin or their mode of action. Cytotoxic drugs conventionally used in clinical practice can be divided in alkylating agents (e.g. nitrogen mustards, nitrosureas and tetrazines), platinum based compounds, antimetabolites (e.g. folic

acid analogues, pyrimidine or purine analogues), DNA-topoisomerase I or II inhibitors (e.g. camptothecins, epipodophillotoxins and anthracyclines) and antimitotic agents (e.g. *Vinca* alkaloids and taxanes).

1.2.2 Extracellular Determinants of Drug Effects

The therapy-induced effects depend both on the pharmacologic and pharmacokinetic properties of the therapeutic agent and on the sensitivity of cancer cells that is related to biochemical and cytokinetic response following treatment. The importance of the cell cycle traverse properties of normal and tumour cell populations in the development of anticancer strategies has been studied and debated for a long time (Steel, 1977). It has become clear that substantial cytokinetic differences exist in humans among tumours and normal cell populations, this contributes to the variability of the individual outcome of treatments. In addition, a substantial number of drugs have been identified to exhibit cell cycle specific effects. At the most elementary level, it was recognized that cell cycle specific agents would more heavily affect populations in which the majority of cells were actively proliferating than populations in which relatively few cells were actively proliferating. This concept has led to preferential application of phase-specific drugs to fast growing tumours. The knowledge of the cytokinetics and of the mechanisms regulating cells death is expected to be crucial also for the development of new therapeutic strategies and for the comprehension of the drug resistance.

The effects of the treatment schedule have been investigated empirically in animal tumour model systems, but the application of cytokinetic concepts in the clinic has been limited for different reasons. The experimental techniques used in cytokinetic studies often yield inaccurate or insufficient information and the rapidly proliferating rodent tumours used in anticancer studies are usually poor cytokinetic

models of slowly proliferating human tumours. In spite of these deficiencies, the potential for the improvement of cancer therapy using cytokinetic principles remains, especially because newly developed techniques allow a more accurate cytokinetic information *in vivo*. These techniques include measurement of the rate of growth of tumour volume and cell number, of rates of cell production and cell loss, of cell survival and regrowth after treatment. Thus, the use of a mathematical model would allow the connection between the kinetic properties of the population and the experimentally obtained data, such as the fraction of cells in a particular cell cycle phase or cell cycle phase duration, variability and growth fraction.

1.2.3 Cellular Determinants of Drug Effects

Even at the cellular level the effectiveness of the drug is variable, resulting in a real "resistance" in many cases. The concept of cancer resistance is in part derived from the work of Luria and Delbruck (1943), who found that bacteria spontaneously developed mutations that make them resistant to bacteriophages. When applying this concept to cancer, Goldie and Coldman (1979; 1985) proposed that the probability that a given tumour will contain resistant clones at the time of diagnosis would be a function of the mutation rate of the cancer and the size of the tumour at diagnosis (Shah and Schwartz, 2001).

While treatment of certain malignancies with chemotherapy is successful, in most cases the effectiveness is limited by the occurrence of tumour drug resistance and by side effects on normal tissues. Drug resistance is one of the biggest obstacles to the success of cancer chemotherapy, especially because of its complexity and because of its multifactorial origin. In fact, many tumours are intrinsically resistant to many of the more potent cytotoxic agents used in cancer therapy. Other tumours, initially sensitive, recur and are resistant not only to the initial therapeutic agents, but also to other drugs not used in the treatment. Studies focused on the

causes leading the cells to drug resistance at the same time give information about the ways to improve the drug efficacy at the cellular level.

However, in spite of the efforts that have been made to advance the understanding of the mechanisms involved in drug effectiveness/resistance, the knowledge of this phenomenon is still not complete, even though we can recognize different molecular processes that determine it. The principal mechanisms of cell sensitivity/resistance to anticancer drugs can be divided into the following categories: intracellular transport of the drug, extracellular transport of the drug, activation of the drug, inactivation of the drug, alteration of the target and DNA repair.

1.2.3.a Intracellular transport

Anticancer drugs can be divided into two types, on the base of their mechanism of entry into the cell. There are compounds, like nitrogen mustard and melphalan, that can be actively transported and others, like nitrosureas, that are passively diffusing. In both the cases the uptake can be heterogeneous and, in the case of malphalan, for instance, it depends on the cellular content of L-leucine and L-glutamine, that share a common transport mechanisms with melphalan (Vistica et al., 1978). Moreover alkylation of membrane components may effect both active and passive transport with a consequent reduction of the cellular uptake of the drug (Fisher et al., 1983).

1.2.3.b Extracellular transport

Resistance to a broad spectrum of chemotherapeutic agents in cancer cell lines and human tumours has been defined multidrug resistance (MDR). This phenotype is associated with increased drug efflux from the cells that is mediated

by an energy-dependent mechanism that involves transporter proteins like MDR-associated Protein (MRP) and P-glycoprotein (P-gp).

1.2.3.c Activation or detoxification

This mechanism involves the drugs that need to be converted in an active form in order to elicit their action. For instance, cytosine arabinoside (Ara-C) needs to be converted to its metabolite ara-CTP to become active. The first step in the conversion process is phosphorylation of Ara-C to Ara-CMP by cytoplasmic deoxycytidine kinase (Durham and Ives, 1969), for this reason cells with altered activity or low levels of deoxycytidine kinases seem to be resistant to this drug (Rogers et al., 1980).

On the other side, drug resistance can be also ascribed to detoxification processes. One of the molecules responsible for this phenomenon is GSH. Increased levels of GSH or glutathione S-transferases (GST) seem to be correlated with the resistance to DDP and alkylating agents (Morrow and Cowan, 1990; Black and Wolf, 1991; Tew, 1994; Kartalou and Essigmann, 2001). In particular, DDP can be covalently linked to GSH after nucleophilic attack of the glutathione thiolate anion, and this complex can be transported out of the cell by an ATP-dependent pump (Ishikawa and Ali-Osman, 1993). In addition, conjugation with GSH inhibits the conversion of DNA cross-linkable monoadducts to cross-links, thereby reducing the cytotoxic potential of the adducts (Eastman, 1987).

Intracellular levels of GSH have also been shown to affect the sensitivity of cells to cell death-inducing stimuli, as well as the mode of cell death, but the results are often contradictory (Vahrmeijer et al., 1999), and direct evidence that GSTs are responsible for altering drug sensitivities is limited.

1.2.3.d Alteration of drug target

Tumour cells can become resistant to anticancer drugs by altering the specific target of the considered compound. In the case of treatment with topoisomerase I inhibitors, whose toxicity is due to the formation of a complex with DNA, drug and enzyme, cancer cells become resistant by reducing the level of topoisomerase, or expressing a mutant form of it with reduced drug affinity (Pommier et al., 1999).

1.2.3.e DNA repair and apoptotic pathways

The most part of classical anticancer agents targets DNA. DNA damage responses, and particularly DNA repair, influence the outcome of therapy, in fact DNA repair normally excises lethal DNA lesions and for this reason the mechanisms that are able to increase the repair of DNA damage can be a key event in the induction of drug resistance. There is evidence that reduced levels of DNA nucleotide excision repair are associated with a good therapeutic outcome, especially for treatments performed with platinum compounds (Koberle et al., 1999) or alkylating agents (Grant et al., 1998). A more contradictory relationship has been reported between DNA mismatch repair (MMR) and drug sensitivity, where the difference between repair-proficient and -defective variants is highly dependent on the drug (Bignami et al., 2003).

In addition to increased DNA repair, adduct tolerance could also be attained by inhibition of apoptosis. Apoptotic process may be either p53-dependent or independent, but frequently the cellular response to DNA damage is regulated by this protein (Bellamy, 1997). Depending on the particular cell type and damage, p53 may then initiate one of two possible pathways: apoptosis or a process of cell-cycle arrest and repair. In cells where the apoptotic pathway dominates, changes that cause dysfunction or deletion of p53 are likely to result in reduced apoptosis in response to DNA damage, leading to relative resistance and cell survival with

damage. In cells where the p53-dependent cell-cycle arrest and repair response dominates deletion or mutation of p53 might be expected to result in decreased cell-cycle arrest and repair leading to accumulated DNA damage and hence an increased sensitivity to the chemotherapeutic agent.

Besides p53 there are other families of genes regulating apoptotic process. The Bcl-2 and Bax family proteins comprise several important regulators of apoptosis. Bcl-2 proteins (Bcl-2, Bcl-XL, Bcl-w, A1, and Mcl-1) are antiapoptotic, whereas Bax family is constituted by proapoptotic proteins (Bax, Bak, Bad, Bik, and Bid). Their expression can influence the relative sensitivity of cells to toxic stress. Indeed it has been proposed that increased levels of antiapoptotic proteins may result in reduced sensitivity to DNA-damaging anticancer drugs (Walton et al., 1993). Thus, the expression of mutant and wild type p53, Bcl-2 family members, and other proteins associated with the control of apoptosis may contribute significantly to the sensitivity of tumour cells (Dole et al., 1994; Eliopoulos et al., 1995; Miyake et al., 1999).

1.2.4 Therapeutic Concepts

For more than 30 years anticancer drugs were used as single agents following a daily or weekly schedule of treatment with an alternation of the different compounds in order to counteract drug resistance. The concept of combining chemotherapeutic agents to increase cytotoxic efficacy has evolved greatly over the past several years. The rationale for combination chemotherapy has centred on attacking different biochemical targets, overcoming drug resistance in heterogeneous tumours. Moreover the employment of agents with different side effects can increase the tolerance of the patient towards the toxic action of the drugs, trying to improve clinical efficacy with acceptable toxicity.

Combination chemotherapy has been crucial in the development of regimens more effective than single agent therapies in haematological malignancies and in the majority of solid tumours including breast, lung, gastrointestinal, ovarian and testicular cancer (Frei, 1972; Frei, 1985).

However combination treatment can induce a cell cycle-mediated antagonism, a phenomenon that can be observed when one chemotherapeutic agent impacts the cell cycle such that the other chemotherapeutic agent given in combination becomes less effective. This is particularly relevant with the use of cell cycle-specific inhibitors but also has relevance for the action of standard less specific chemotherapeutic agents currently in clinical practice. A greater understanding of chemotherapeutic cell cycle effects can be essential to counteract cell cycle mediated resistance, providing the rationale for investigating appropriate sequencing and scheduling of agents in combination chemotherapy.

In principle the clinical investigation should be performed following the indications derived from preclinical studies aimed to evaluate the cytostatic and cytotoxic effects induced by anticancer agents and to explore the synergism or antagonism of a combination therapy.

1.3 EVALUATION OF DRUG EFFECTS

Several methods have been developed since the 1950s to determine the *in vitro* sensitivity of human tumour cells to various anticancer agents. Studies performed by using reliable *in vitro* drug-response assays raised the possibility of selecting effective anticancer agents to be used either alone or in combination. *In vitro* identification of agents with an extremely low probability of response or ineffective in a particular regimen makes possible to stop further *in vivo* evaluation and clinical trials of such agents (Chu and De Vita, 1997).

Clonogenic assay, cell viability assay, growth inhibition assay and chemotherapeutic treatment of athymic nude mice with human tumour xenografts are only some of the different methods that can be used to investigate the sensitivity of tumours and tumour cell lines. The major distinction among these methods is the end point used to measure cell viability. Cell toxicity is usually assessed from the fraction of cells killed by exposure to the therapeutic agent. These studies depend critically upon the criterion by which cell kill is assessed. Some scientist score as dead, those cells lacking membrane integrity and thus unable to exclude dyes such as trypan blue or ethidium bromide. Others consider as dead, every cell not capable of self-reproduction (clonogenicity). Thus, assay end points include colony formation from a single cell, incorporation of tritiated thymidine, microscopic examination of cells with vital dyes, mitochondrial enzyme activity and many other parameters. For each assay type the difficulties arise not only in the evaluation of the precision of the results obtained, but also in their interpretation, once that the level of precision is defined. During this phase it is necessary to take into account all the limitations and the drawbacks that are included in the considered method (Bellamy, 1992). Without such exercise the use of different methods might easily lead to contradictory conclusions.

One of the factors that can influence the utility of the *in vitro* assays as predictors of the sensitivity of a patient's tumour response is the high heterogeneity of the tumour *in vivo* and its environment. In fact, cells in culture lack the architectural and cellular complexity of "real" tumours, which include inflammatory cells, vasculature and stromal components. Nevertheless, cell lines can be considered useful models for the evaluation of drug effects on the proliferative core of the tumour.

Xenograft models too present differences from human tumours. Human tumours develop over a number of years, whereas mouse xenografts are chosen because

they are rapidly growing and their growth can be monitored in the timeframe of days or weeks (Kamb, 2005).

Besides the limitations in the models used for preclinical studies, there are also problems coming from the experimental techniques that often yield inaccurate or insufficient information.

Despite the acknowledged importance of cell cycle events to determine the outcome of a treatment with anticancer drugs, classical methods of measuring drug efficacy seem to overlook the complex relationship between cell cycle perturbations and the measured quantity, even at the *in vitro* level. For instance, an evaluation of growth inhibition, by a colorimetric assay, measures the percentage of absorbance of treated respect to untreated samples at a given -arbitrary- time. The same value can be obtained by blocking cycle progression of all cells without killing them, or by killing a fraction and leaving the other unaffected. More, infinite combinations of a partial cytostatic effect with a partial cytotoxic effect will produce the same measured outcome. Obviously, different results should be expected by measures performed at a different sampling time, and one should be very cautious to make numerical comparisons between cell lines with different rate of unperturbed growth (which strongly affects the measure). There are methods oriented to measure cell survival (like a properly performed colony assay) or to evaluate blocking activity (like DNA flow cytometry), but also in these cases a closer analysis reveals that the connection between the number given as "datum" and the underlying phenomenon is not straightforward. For instance, cells blocked for a few days and then recovering will not be considered "surviving" if their colony had not time to reach an arbitrarily set threshold size. More badly, the culture (and treatment) conditions required in clonogenic assay are often far from being optimal for tumour cells, resulting in low plating efficiency. In that respect, an *in vitro* treatment of an exponentially growing

cell population, minimises manipulations and potential artefacts and maintains the possibility of cell interaction. For these reasons, a similar condition is preferred in most studies of cell cycle perturbations performed by DNA flow cytometry. But even the interpretation of flow cytometric data is not exempt from ambiguities when more than one cell cycle effect occurs at the same time, as it often happens. In the two following sections advantages and disadvantages of the methods more frequently used in studies aimed to investigate the cell response to a treatment with anticancer agents will be presented.

1.3.1 Classical Methods for the Evaluation of Drug Effects: Advantages and Disadvantages

The methods that are classically used to evaluate the impact of a drug treatment on a cell population, such as growth inhibition or clonogenic assays, generally lack of connection with phase related events. In many classical studies authors overcame this limitation by synchronizing the cell population in a certain cell cycle phase and then performed a clonogenic assay. This was the most used experimental approach to evaluate the phase specificity of a particular anticancer agent.

1.3.1.a Cell synchronization and clonogenic assay

Cell synchronization can be achieved with different methods, but, independently of the method used to synchronize the cells, this technique presents some negative aspects. For instance, using centrifugal elutriation it is possible to obtain cells enriched in the various phases of the cell cycle with minimal loss of cell viability. In a typical experiment, cells are treated with the drug, harvested, dissociated into single cells, elutriated and assayed for cell survival. However the stress induced by harvesting, centrifugation, collection and re-seeding is not negligible and its

contribution to the drug effect eventually observed is unknown (Mikulits et al., 1997). Moreover pure populations of G_1, S, and G_2M cells were not obtained with elutriation, thus true phase specific plating efficiencies cannot be determined experimentally and a correction taking into account of the $\%G_1$, %S and $\%G_2M$ (independently measured by flow cytometry) has been proposed (Linfoot et al., 1986). In addition, the plating efficiency of reference untreated cells may vary fraction by fraction, and this is seldom reported and compared with the plating efficiency of exponentially growing cells not subjected to the elutriation procedure.

Synchronisation can also be achieved by techniques that metabolically block cells in specific phases, using for instance hydroxyurea, 5-fluorouridine, aphidicolin, methotrexate or isoleucine deprivation etc. but all of them have the limitation that only partial synchrony is achieved. The population is spread at various points through a phase and even in other stages of the cycle (Knehr et al., 1995). Moreover the cells do not exit the block at the same time and the synchrony decays due to random rates of transit through cell cycle stages (Drewinko and Barlogie, 1976).

As demonstrated by Urbani et al. (1995) and Ji et al. (1997) cell synchronization introduces alteration in cell cycle kinetics and in protein expression. In particular Ji and coworkers investigated the level of p53 and p21 in cell synchronized with mimosine and aphidicolin, demonstrating the presence of high levels of both proteins for 48h following release from block. That means that, in any case, caution should be exercised in the interpretation of the results obtained by this kind of experiments.

The clonogenic assay that generally follows cell synchronization and treatment is considered the optimal test system for *in vitro* radiation studies. A treated cell is considered clonogenic if at about ten days after treatment it has been able to generate a colony with at least 50 cells. For this reason this test is not only

laborious but it also requires long times before obtaining the results. Furthermore, it is limited by the need of cells to form colonies and is less reliable for cells with low colony forming capacity (Pauwels et al., 2003), possibly due to the lack of cell interactions and/or optimal growth conditions.

1.3.1.b Growth inhibition assays

The two most important members of this family of techniques employed for *in vitro* studies about drug interactions are Sulphorhodamine Blue assay (SRB) and tetrazolium-based assay (MTT).

MTT assay depends on cellular capacity to metabolise the MTT dye to a highly coloured formazan product. The tetrazolium salt is metabolised to a formazan product through the action of a mitochondrial succinic dehydrogenase. The UV absorbance of the solubilised formazan crystals is measured spectrophotometrically and directly correlates with the number of cells, which are metabolically active. This assay depends on cellular reductive capacity and makes the assumption that the reductive capacity remains constant through out the time duration of experiment.

Factors which may lead to problems with proper interpretation of the MTT assay include: (a) alterations in pH of the media; (b) chemical interference with the cellular reduction of the dye, and chemical reduction of the dye due to factors within the media, including the test agents; and (c) the quality of reagents used to solubilise the formazan crystals (Carmichael et al., 1987; Twentyman and Luscombe, 1987), moreover MTT assay can only assesses metabolically active cells.

In SRB assay cell growth and viability are based on whole culture protein determination. The protein stain SRB binds electrostatically to basic amino acids of cellular macromolecules. The assay is reported to provide a sensitive index of

cellular protein content that is linear over a cell density range of two orders of magnitude (Rubinstein et al., 1990).

The advantages for this assay include that it is simple to perform, faster, more sensitive and less affected by environmental factors than the MTT assay. The assay also has a stable endpoint, which does not require immediate reading. On the other hand SRB assay could not discriminate live cells from debris of freshly lysed cells. However, by 24h after cell lysis, the SRB assay was reported to be comparable to the MTT assay, indicating that at this point the SRB assay was not staining cellular debris (Keepers et al., 1991). Therefore it seems likely that the SRB does not overestimate the survival fraction of cells in chemosensitivity assays under normal growth conditions.

However, in general, all growth inhibition assays do not discriminate between cytostatic and cytotoxic effects and the frequent choice of a short-time endpoint might result in an overestimation of the cell survival due to delayed cell killing induced by anticancer agents.

1.3.2 Flow Cytometric Approach: Advantages and Disadvantages

Since its origin, flow cytometry has been used to evaluate the kinetic of cell proliferation *in vitro* and *in vivo* in basal conditions and after treatment with chemical or physical anticancer agents (Mauro et al., 1986).

Monoparametric staining of DNA and biparametric staining of DNA and the use of BrdUrd made possible to monitor the cell distribution and flow through the different phases of the cycle. In presence of cells that are growing without any perturbation, flow cytometric data can be related to some parameters, such as phase duration, doubling time, potential doubling time and so on, that describe the kinetics of proliferation of the population (Steel, 1977; Bertuzzi et al., 1997).

After treatment with an anticancer agent, damaged cells interact with molecular cell cycle control mechanisms and the percentage of cells in G_1, S and G_2M that can be obtained by analysing flow cytometric data is the result of this interaction. These percentages are the result of the superimposition of cytostatic and cytotoxic effects and of their time dependence. The situation becomes much more complex, if we take into account the heterogeneity of the cell population and its response to the anticancer agent. For instance, we can suppose that not all treated cells are damaged and that at the time of their passage through G_1 phase only some of them are intercepted by the checkpoint and remain blocked in G_1 phase. A similar behaviour can be observed for cells passing through G_2M phase, whereas damaged cells traversing S phase cannot be intercepted in a particular region within this phase. In this case treated cells can slow down their progression through the phase, trying to repair the damage or shifting towards cell death if they are not able to complete successfully repair processes. In the next paragraph evidence will be provided that combinations of different microscopic effects can generate similar DNA distributions, requiring a proper experimental plan and a tool as the model presented in 3.6 to interpret univocally all the experimental data.

The starting point of the following examples is an asynchronously growing cell population with mean phase duration of 9.1, 8.7 and 3.1h for G_1, S and G_2M respectively. Different scenarios of cell cycle perturbations were hypothesized and the corresponding flow cytometric data were simulated (see paragraph 3.6 for further details about the simulation program).

1.3.3 Interpretation of Flow Cytometric Results

1.3.3.a Perturbations in G_1 phase

In this first case the hypothesis is that drug treatment activates a cell response in G_1 phase, by intercepting at the checkpoint a high percentage of cells which can

subsequently repair the damage. DNA histograms generated by this situation are represented in figure 1.1. The block in G_1 causes a depletion of cells in S and in G_2M phase. 18h after treatment cells leave G_1 and a wave of semisynchronized cells is detected at 21 and 24h while traversing S phase and in G_2M at 30h. At 48h the histograms of treated samples are essentially equivalent to those of the control.

This example demonstrates that a sequence of DNA histograms at different times after treatment is necessary for the comprehension and interpretation of the phenomena, that could not be caught by a single histogram of those shown in figure 1.1.

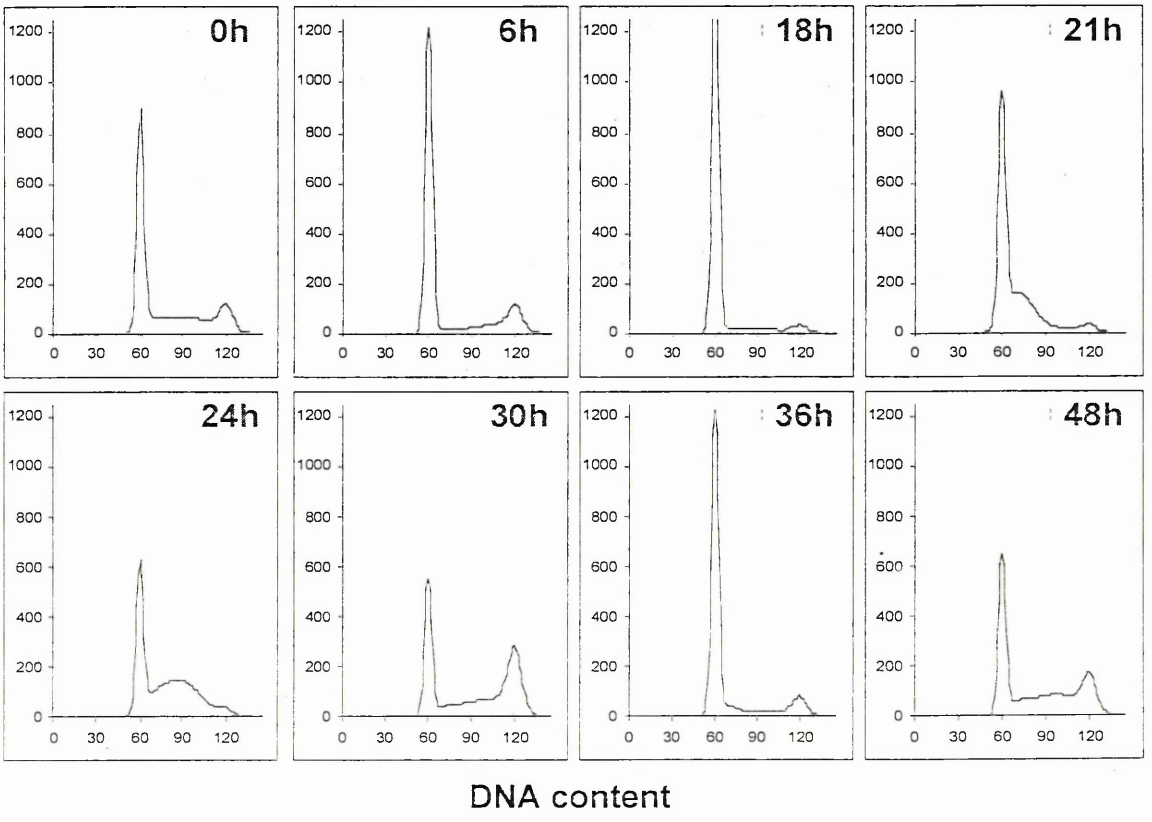

Figure 1.1: Time-course of DNA distributions obtained by the simulation. We hypothesized the presence of a blocking activity in G_1 phase for 18h, in particular 80% of cells passing through G_1 phase remained blocked. After 18h, blocked cells start cycling again and the rate of entering S phase is of 20% of cells every hour.

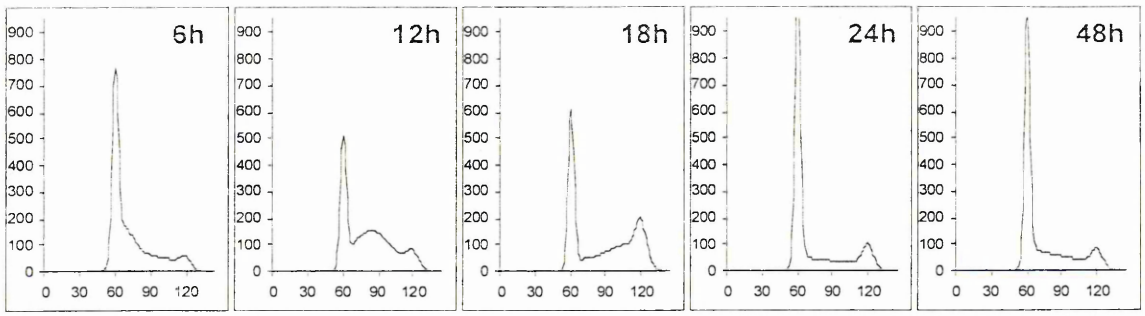

Figure 1.2: Time-course of DNA distributions obtained by the simulation. We hypothesized the presence of a delay in the cell progression through S phase. We supposed that just after treatment DNA synthesis is totally inhibited, but the parameters describing this effect halves its value every 8h.

DNA histogram of control cells is that reported in figure 1.1 (histogram at 0h).

1.3.3.b Perturbations in S phase

In figure 1.2 are reported DNA histograms of a cell population with a delayed progression through S phase, this phenomenon can be a consequence of a drug treatment with an agent inhibiting DNA synthesis. When the drug is removed the delay of cell progression through S phase decreases.

If we compare figure 1.1 (histogram at 24h) with figure 1.2 (histogram at 12h), we can observe that the DNA distributions look very similar. However, in the first case the hump in the S region is a consequence of a release from G_1 block, whereas in the second case it is a consequence of a delayed progression through S phase. This demonstrates that the interpretation of flow cytometric data, obtained by a simple analysis of DNA distribution, is not always univocal.

A BrdUrd pulse-and-chase experiment (see 3.4.2) performed at short times after treatment would allow the discrimination between these two situations.

1.3.3.c Perturbations in G_2M phase

In figure 1.3 two different effects in G_2M phase were represented. The histograms in the first row (figure 1.3a) have been obtained by supposing the existence of a checkpoint able to intercept the 80% of cells passing through G_2M phase and after 18h the previously blocked cells repair their damage and start cycling again. Very similar DNA distributions can be obtained by considering the same blocking activity, but supposing that blocked cells die and are lost 18h after treatment (figure 1.3b). In these two cases the information coming from the cell count become a crucial datum to discriminate between the hypotheses that can be made just analysing DNA histograms.

In real cases the situation is not always so clear: the competition between cell loss and proliferation could cause an increase in the number of cells. In any case the association of DNA distribution with cell number greatly improves our ability in interpreting the experimental data.

1.3.3.d Perturbations in all cell cycle phases

The scenario shown in figure 1.4 takes into account the possibility that drug treatment affects every cell cycle phase, as often occurs in the real situation. All the perturbations hypothesized in the previous examples are now considered together.

At short times after treatment blocking activity and delay are quite strong, and the DNA distribution at 6h looks very similar to that of control cells at 0h, as expected in the presence of a generalized freezing effect. As delay in S phase decreases, 18h after treatment the cells that were in S phase at the time of treatment are able to reach G_1 and G_2M checkpoints. In fact at this time a subpopulation of blocked cells is present in these two phases. After 18h both G_1 and G_2M blocking activity end and this determines a decrease in the percentage of cells in G_2M and the

presence of a wave of synchrony in S phase formed by those cells that left G_1 at 18h. Passing from 24 to 30h the wave becomes always less detectable and the DNA histograms become more similar to asynchronous distribution of the controls.

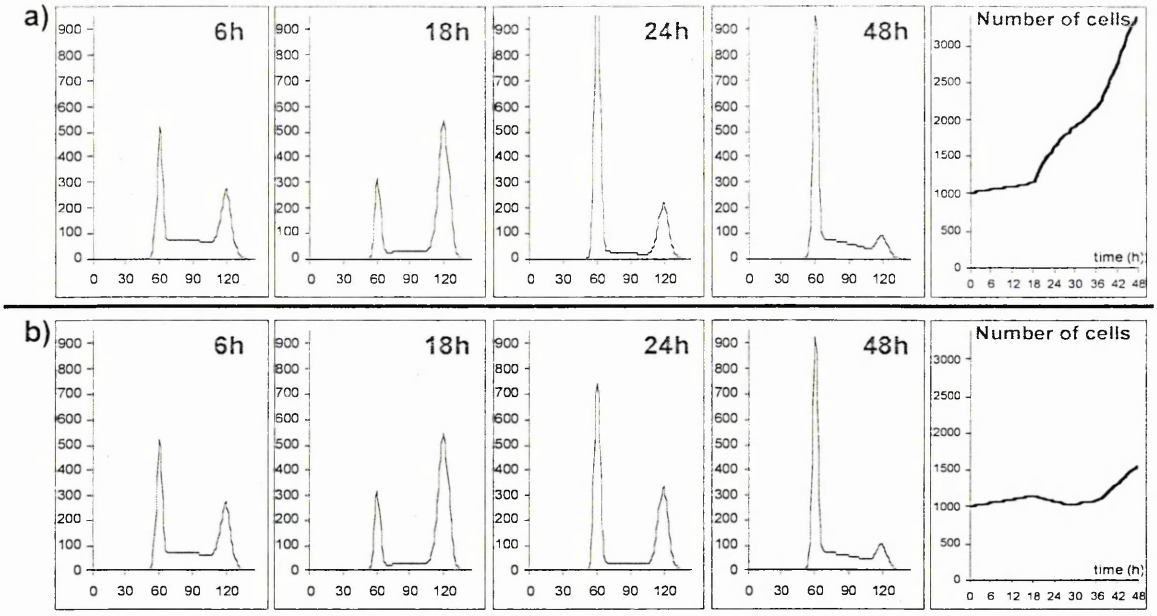

Figure 1.3: Time-course of DNA distributions obtained by the simulation. We hypothesized the presence of a blocking activity in G_2M for 18h. 80% of cells passing through G_2M phase remained blocked. 18h after treatment 5% of blocked cells per hour start cycling again (panel a) or die (panel b).

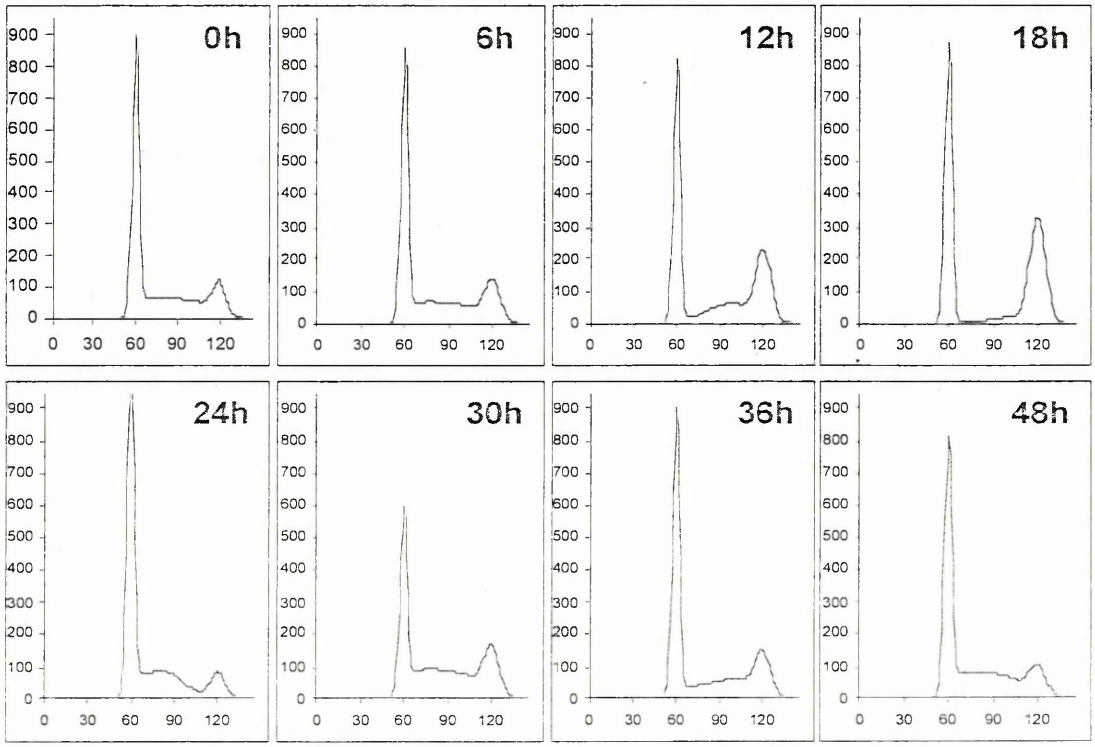

Figure 1.4: Time-course of DNA distributions obtained by the simulation, hypothesizing the presence of effects in every cell cycle phase.

The parameters used to describe these effects are the same that were considered in the previous examples.

Considering together the previously described examples, we have the demonstration that flow cytometric experiments can give us a lot of information about cell cycle effects induced by treatment with anticancer agents. However, only combining DNA histograms with cell count and other flow cytometric methods, like BrdUrd labelling, we can attempt to distinguish between cytostatic and cytotoxic effects and determine their time- and dose-dependence. Moreover the use of BrdUrd allows the recognition of any possible differential effect between cells that were in S phase at the time of treatment and those that were in G_1 and in G_2M phase, without any synchronization procedure.

On the other side, as we have shown in the considered examples, flow cytometric data could be easily misinterpreted or there is the risk of focusing the attention only on particularly evident effects, such as accumulation of cells in a cell cycle phase. The situation becomes much more complex when more than one cell cycle effect occurs at the same time, as it often happens. For instance, no difference may be detected in the DNA profile between well growing untreated cells and another sample treated with drug concentration causing a complete freezing of the cycle (figure 1.4). Moreover the presence of a block in G_2M phase, for instance, reduce the percentage of cycling cells and as a consequence the presence of a possible block in G_1 phase could be hidden by the small number of cells passing through this phase.

In well-designed experiments, replicated flasks are sampled at different times during/after treatment, in the attempt to catch the dynamics of cell cycle perturbations. But then the analysis of such sequence of data is not simple, because the cell cycle distribution observed at a given time depends on that observed at the previous time (soon diverging and unrelated to control distribution a few hours post treatment) plus the normal cycle flux of cells growing normally,

plus the recycling or death of previously blocked cells, plus the result of new blocking or killing activity carried on by checkpoint and apoptotic machinery. In order to face this complex situation a computer simulation tool was developed in our laboratory (Montalenti et al. 1998) with the aim to objectively support the interpretation of the available data and reach a comprehensive view of all cell cycle perturbations.

1.4 MATHEMATICAL MODELS

Mathematical modelling is currently a common tool in the study of physiological and biochemical systems. In recent years, it has become increasingly clear that sophisticated computational methods will be needed to manage, interpret and understand the complexity of biological information. The representation of complex biological systems in terms of mathematical equations allows us to increase the comprehension of the system itself by providing a concise and objective description of dynamic processes and by defining the relationships between quantitative measurements. This approach can also be used to improve experimental designs, by testing different hypotheses about physiological or biochemical phenomena (Tyson et al., 2001).

The model is a mathematical description of a real process that can help the comprehension of the phenomenon considered. The modelling process is an iterative process: it is possible to distinguish in it a number of steps, which usually must be repeated.

i. The first step is represented by empirical observations of the considered system, performing experiments and data collection.
ii. State variables that are taken to be sufficient to summarize the properties of interest in the study system have to be listed and the properties that have been observed during the experiments have to be formalized using known

relationships (stoichiometric relations, biochemical reactions, pressure-force relationships in mechanics and fluids etc.).

iii. The mathematization by algebraic and/or differential equations with constraints and initial and/or boundary conditions of the relationships recognized at the previous step contribute to the final design of the mathematical model.

iv. The analysis of the model can be approached in two different ways: (a) mathematically, so that it is possible to find an analytical solution of the problem or (b) translating the equations into computer code to obtain numerical solutions for state variable trajectories.

v. The results have to be compared with the real system, in order to verify the hypotheses that have been made at the beginning of the process. On the other side the results can help a more precise design of new experiments.

From this point of view the construction of successful models is constrained by what we can measure, either to estimate parameters that are part of the model formulation or to validate model predictions. Moreover, in the field of mathematical modelling it is possible to distinguish between at least two basic types of scientific models: descriptive and phenomenological models. Descriptive models are those designed to fit observed data with arbitrary functions, whereas phenomenological models reproduce the behaviour of a biological system on the basis of some *a priori* knowledge of the underlying "mechanisms".

Cancer biology is one of the fields were both descriptive and phenomenological modelling has been applied (reviewed by Komarova, 2005).

1.4.1 Models in Cancer Biology

The mathematical investigation of cancer began in the 1950s, when Nordling (1953), Armitage and Doll (1954, 1957), and Fisher (1958) set out to explain the age-dependent incidence curves of human cancers. In the early 1970s, Knudson

(1971) used a statistical analysis of the incidence of retinoblastoma in children to explain the role of tumour-suppressor genes in sporadic and inherited cancers. Later on, other studies were devoted to the development of specific theories for drug resistance (Goldie and Coldman, 1979; Goldie and Coldman, 1983), angiogenesis (Anderson and Chaplain, 1998) and immune responses against tumours (Owen and Sherratt, 1999) and genetic instability (Chang et al., 2001).

In this context we recognize the two different cited approaches. The application of mathematical modelling in the context of epidemiology, where simple arbitrary functions are used to fit the existing data, or statistical tests performed to recognize the existence of relationships or differences between measured data can be considered as descriptive models. In the same category we found the models trying to reproduce and interpret the trend of a dose-response curve after drug treatment and all the statistical tools that are applied to analyse microarrays and other data coming from high throughput discovery technologies.

The category of phenomenological modelling in cancer research includes a large amount of examples that are listed in table 1.1. In general, mathematical modelling in cancer and cancer therapy has been attempted at different levels, starting from the most microscopic one that describes molecular interactions or protein networks of specific cellular functions (Kohn, 1998; Qu, 2003), to cell cycle and *in vitro* cell proliferation, up to the most macroscopic level describing tumour growth *in vivo*.

Experimental Level	System	Variables	Parameters
Molecular	Molecular networks	Concentration of molecules	Association and disassociation rates
In vitro	Cell population	Number of cells at different stages of maturity (age and cell cycle phases)	Transition rate from one state to another and killing rate in the different cell cycle phases to simulate drug effects
In vivo	Tumour	Mass of the tumour (volume, number of cells, number of quiescent and resistant cells)	Proliferation rate and loss rate to simulate tumour growth in normal conditions. Killing rate, diffusion and resistance rate to simulate drug effects
	Pharmacokinetic systems	Drug concentration	Transition rate from one body compartment to another, representing the absorption, distribution and transformation of drugs within the body
	Tumours and normal tissues	Mass of tumour and normal tissues	Interaction among populations and killing rate

Table 1.1: Overview of the different examples of phenomenological models in cancer biology.

1.4.1.a Models of molecular interactions

At the most microscopic level molecular interactions are studied, using biophysical models to elaborate the atomic structure of the molecules, their binding sites and chemical bonds. Research focuses on a single or a group of molecules isolated from the cellular environment, investigating their possible bonds with chemical agents (Albert, 2005). At a more macroscopic level, the issue is the comprehension of cellular mechanisms that control the production of the proteins necessary for the cell life and proliferation or necessary to perform other specific tasks (Tyson et al., 2001). In this case, mathematicians work by modelling molecular networks, trying to explain the global behaviour of such complex systems of intertwined molecular relationships that molecular biology studies focusing on a single cells or on a cell èxtract.

1.4.1.b Models of cell proliferation

The demonstration by autoradiographic methods of the existence of different cell cycle phases (Howard and Pelc, 1953) provided a base for most of the mathematical modelling in cell kinetics. The cell cycle is an ordered sequence of biochemical events leading up to cell division. The cycle can be divided into four phases, G_1, S, G_2 and M and after mitosis a daughter cell can again traverse the cycle or can shift to a quiescent state during which cells do not divide for long periods. The time for a cell to traverse the cycle is defined "cycle time", and this parameter is not equal for all the cells even in a homogenous population (Sisken and Morasca, 1965). Thus the models of cell kinetics aim to quantify the biological aspects and to define the relationships that regulate the cell cycle.

In the literature the time evolution of a cell is often defined by either its chronological age or its position in the cell cycle. The main body of modelling is the

reproduction of the cell cycle dynamics. From this point of view cell cycle models can be divided into two categories. In the first group there are models in which the cell position in the cycle is represented by its belonging to one of a finite number of stages. In the models of the second group the cell position in the cycle is represented by a continuous variable, that was called "maturity". In any case, in discrete stage models each successive stage corresponds to an increased maturity value, so a cell maturity distribution for the population can be considered both in the continuous and in the discrete models (Bertuzzi et al., 1981).

1.4.1.c Spatial models of tumour growth

A different approach to the problem is that adopted by the researchers that aim to study spatial aspects of tumour growth. In this case, tumour was described as a fluid with a production term proportional to concentration of nutrients (Franks et al., 2003), or as a mixture of solid (tumour) and liquid (extracellular fluid with nutrients) phases (Byrne and Preziosi, 2003). The phenomena of migration of tumour cells (Mansury and Deisboeck, 2003) and the vascular stage involving the mechanisms responsible for angiogenesis can be also investigated with this kind of approach (Breward et al., 2003; Chaplain and Anderson, 2004).

The tools of applied mathematics, such as nonlinear partial differential equations and discrete cellular automaton approach are used to describe these phenomena (Qi et al., 1993), but modelling can also be used to address practical questions of drug dosage and therapy timing. For instance, Swanson et al. (2003) studied cancerous growth for gliomas in the context of drug therapy. Their model included both cell proliferation and motility and took account of inhomogeneities of the brain tissue.

1.4.1.d Models of tumour growth and drug efficacy *in vivo*

From measurements made in preclinical studies or in clinical investigations it is possible to know the volume of the tumour growing in animals or in humans and it is possible to monitor its variation after drug treatment. Because of the simplicity of these outlines, simplified models of tumour growth were used. For instance Skipper et al. (1964) adopted a model of exponential growth, defined by the number of tumour cells at a given time, typically the beginning of the observation period, and by the doubling time. This model was able to reproduce leukaemia amplification in mice and drug effect was described by the fraction of cells killed at each administration. Norton and Simon (1977) improved the Skipper's model using a Gompertz function that takes into account the decline of the growth rate as the tumour mass increases. This shape is able to fit many experimental time courses of solid tumours, particularly in animals, where the whole story of the tumour may be followed. Reduction of drug efficacy in massive tumours was described by a simple link between the fraction of surviving cells at each treatment and the growth rate. Goldie and Coldman (1979) tackled the issue of drug resistance and they described its rising by considering the probability of spontaneous mutation(s) towards a resistant phenotype.

1.4.1.e Pharmacokinetic and parmacodynamic models

The starting point of pharmacokinetic-pharmacodynamic model is the formulation of a model describing the progression of the disease, then a link has to be made between the administration regimen of a particular compound and tumour growth dynamics. In the model of perturbed growth the effects of an anticancer compound are related to plasma drug concentrations. Plasma drug concentrations in input to the pharmacodynamic model are derived from the pharmacokinetic parameters using the appropriate dosing regimen (Simeoni et al., 2004). These models have

been developed with the aim of making a quantitative characterisation of the relationship between drug dose, plasma concentration and haematological toxicity. The knowledge of this relationship is of importance in drug development, dose finding, schedule optimisation and drug combination studies.

One of the principal differences in all these models is represented by the consideration and the use of the data available at a given level. Some models are more theoretical and catch qualitative information from the experimental scientific literature, while some others try to fit specific data sets. For instance, the models connected with cell proliferation can start from experimental data coming from the most common tests used to evaluate *in vitro* toxicity of different anticancer agents. In this case the measured quantities are probabilistic data, like the percentage of surviving cells. At this level the mathematical models have to take into account the cell cycle, including intercell variability due to differences in protein levels or drug uptake, simulating the time course of cytostatic and cytotoxic effects of drugs. Flow cytometric techniques can also provide information about cell response to a drug treatment and in the literature there are attempts of reproducing experimental flow cytometric results with mathematical models of cell cycle (Kozusko et al., 2001; Basse et al., 2004). In these studies the starting point is the description of the unperturbed growth of the considered cell population. Parameters describing cell loss and cell transition from one phase into the next one are changed in order to fit the DNA distributions obtained after treatment. However, in this kind of approach, the experimental data are used as tools to validate the hypotheses made in the model.

On the other side pharmacodynamic studies are focused on the investigation of killing effects that occur after drug treatment, whereas cytostatic effects are not deepened.

In this rich context of modelling in cancer therapy our contribution was aimed to face the study of the time- and dose-dependence of cytostatic and cytotoxic effects in the different cell cycle phases, taking into account the current knowledge about cell cycle checkpoints. Our point of view is to consider the model as an instrument to interpret "macroscopic" data, coming from flow cytometric experiments and cell count, in function of more "microscopic" quantities describing blocking activity, recycling from block and cell loss, trying in this way to make a connection between the molecular level and the measured parameters (Montalenti et al., 1998; Sena et al., 1999; Lupi et al., 2004).

CHAPTER 2: Aims

2.1 GENERAL AIM

After treatments with all anticancer agents, either classical compounds or new drugs with specific targets, cell cycle perturbations occur. The perturbations are usually classified as cytostatic (cell cycle arrest) or cytotoxic (cell killing). Molecular research is now focusing on the molecular pathways exploited by a cell when challenged by chemical and physical agents, triggering cell cycle arrest, particularly at checkpoints within phases G_1 and G_2, or apoptotic death. The knowledge of the kinetics of such events is particularly relevant in cancer research, both applied and basic. However, no substantial progress has been made on how to describe these effects in quantitative terms, with a clear separation between cytostatic and cytotoxic effects: this work aims to provide a contribution in that direction.

Drug effects are still described by growth inhibition and clonogenic assays, often overlooking the limitations of these measures, such as unresolved overlapping of cytostatic and cytotoxic effects, and the lack of connection with phase-related events (Cook and Mitchell, 1989; Lamb and Friend, 1997; Waldman et al., 1997), and not considering the time-course of the response to treatment. On the other hand, DNA flow cytometry allows the study of cell cycle perturbations, by detecting accumulation or depletion of cells in G_1, S and G_2M. However, a single flow cytometric measure of DNA content takes a picture of the cell distribution in the different cell cycle phases at a given time, which is the result of the superimposition of the effects of cell block and death and their time evolution. In addition, the cell response to treatment is heterogeneous: only a fraction of cells is blocked, some of them repair DNA damage and start cycling again, some others die. Moreover, the values of these fractions depend on the treatment dose. In such a situation, even a time-course of cytometric data cannot univocally discriminate among different kinds of effect. Indeed, as shown in the section

1.3.2, different combinations of the underlying cytostatic and cytotoxic effects may give similar values of $\%G_1$, %S, and $\%G_2M$.

The first solution to this problem was the enrichment of the experimental plan, adding other kinds of independent measures to the basic time-course of DNA histograms at different drug concentrations. Thus, biparametric flow cytometric DNA-BrdUrd measures and absolute cell count made by Coulter Counter were included in the experimental plan. This allowed the reconstruction of cell flow into the different phases of the cell cycle after treatment with a sub-lethal drug concentration (Ubezio et al., 1991).

In our laboratory the use of a mathematical model was attempted to face the complexity of data analysis in presence of cytotoxic effects. The model adopted for data analysis and interpretation is the result of a merging of two models, one for the cell cycle and the other for the drug effects. The inputs are parameters that describe the cell cycle during unperturbed growth and the effects induced in each phase by the treatment. The simulation gives the temporal evolution of cell flow into the different cell cycle phases and a set of values that are equivalent to the measured data and can be directly compared with them. The parameters that describe in a quantitative way the effects induced by the treatment are directly linked to the phenomena of cell cycle arrest, DNA repair and cell death in each phase (for further details see section 3.6).

This particularly rich experimental plan and the analysis using mathematical simulation were already applied to study the effects of two classical anticancer drugs: DDP and paclitaxel (Montalenti et al., 1998; Sena et al., 1999). During this project, the presented approach was not only used to investigate the effects induced by treatments with other anticancer drugs but it was also improved by considering new experimental data and performing deeper mathematical analysis.

In particular, the methodology was further implemented by:

1- Including new flow cytometric information (obtained from CFSE staining) in the experimental data.

2- Doing a sensitivity analysis of the parameters considered in the simulation model.

3- Collecting a relevant number of data reproducing the time-course of the cell response to drug treatment, considering, besides cisplatin and paclitaxel, three other different anticancer drugs (TPT, DXR and L-PAM). This allowed the creation of a database for a panel of five different drugs (belonging to the principal classes of classical anticancer drugs) using the same experimental plan and the same cell line.

4- Obtaining, with the use of the simulation program, the time- and dose-dependence of each specific cytostatic and cytotoxic effect. This allowed us to perform the first comparative analysis of the response of the same cell line to treatment with five different drugs.

5- Performing experiments and simulation analysis with a p53-defective cell line and its wild type counterpart to explore the capability of the methodology to catch the contribution of a specific protein in the cell cycle response to drug treatment.

2.2 SPECIFIC AIMS

2.2.1 Application of a New Method to the Study of Classical Drugs with Different Mode of Action

Extensive experiments were set up in order to study the time- and dose-dependence of cytostatic and cytotoxic effects of classical drugs, L-PAM, DXR and TPT, on IGROV1 cells, an ovarian carcinoma cell line growing *in vitro*. Cells were treated for 1h with different drug concentrations, in order to cover all

sensitivity ranges from low to high drug efficacy, qualitatively assessed by preliminary experiments.

In the basic experimental plan, three replicated flasks were harvested at different times after treatment with each concentration, counted and fixed for flow cytometric analyses. This part of the project was specifically aimed to collect a suitable amount of data to cover a wide range of time and drug concentrations, and to construct a database of such data. Preliminary qualitative evaluation of the results was made at this level. Then the database was used in the simulation to evaluate separately the time- and dose-dependence of blocks in G_1, in G_2M, recycling from blocks, S-phase delay and killing in G_1, S and G_2M phase.

2.2.2 Study of the Sensitivity of the Mathematical Model and Comparison between Cell Cycle Effects Induced by Different Drugs

A work similar to that described in 2.2.1 was already done in our research group to study the effects induced on IGROV1 cells by treatments with DDP and paclitaxel. As in this part of the project we aimed to compare the response of the same cell line to different anticancer compounds with various mechanisms of action, we needed to evaluate the sensitivity of the mathematical model that we use to interpret the data.

In particular, several sets of parameters describing the drug effects were tested by computer simulation. The aim of the analysis was to find a set (or the sets) of descriptors coherent with the data, i.e. producing simulated measures in the range of the real measures with their experimental error.

In case of coexistence of more than one scenarios compatible with the data, the discrimination between them was performed experimentally (not mathematically), by additional experiments suggested by the simulation itself. At

the end of the procedure, only a single set of parameter values gave the scenario coherent with the experimental measures. Then, we studied the sensitivity of the parameters considered in the best-fit simulation, in order to evaluate the range of parameters' values in keeping with the data.

We studied the sensitivity of parameters not only for L-PAM, TPT and DXR, but also for the previously evaluated drugs DDP and paclitaxel. On the basis of this analysis, we approached the final aim, i.e. the comparison of the dynamics of cytostatic and cytotoxic effects of the five drugs in each cell cycle phase, trying to reach a better appreciation of the complexity of the cell cycle response, but also possible common features among the drugs.

2.2.3 Integration of Cytometric Data with Information Coming from CFSE Staining

CFSE is a fluorescent dye that allows the detection of cell division, because it is equally divided between subsequent cell generations. For its characteristics CFSE has normally been used to stain lymphocytes and to determine the number of cell divisions (see 8.1).

From this technique we could obtain additional information about the impact that a drug treatment has on the proliferating ability of a cell population. However the common cytochemical protocol was set up for lymphocytes and it was not suitable for exponentially growing tumour cells. For this reason, the first aim of this part of the project was the optimisation of CFSE staining and the interpretation of the data, in order to adapt the protocol to the study of cell cycle and cell kinetic effects of anticancer drugs. Subsequent aim, upon success of the first part, was to introduce the information provided by CFSE (i.e. the percentage of cells at the different cell cycle divisions) in our process of reconstruction of drug effects by mathematical model.

2.2.4 Study of the Impact of p53 on Cell Cycle Response to Drug Treatment

In parallel with the comparison of the effects of different drugs on the same biological model, we attempted the comparison of the response of different biological models to the same drug. The specific aim of this part of the project was the evaluation of the contribution of p53 to the cell cycle response after drug treatment.

For this purpose we used a colon carcinoma cell line HCT-116 and its isogenic cell line lacking for the gene coding for p53 (HCT-116 p53-/-) and we applied the experimental and mathematical approach listed above to quantify the parameters describing the effects induced by DDP in the two cell lines. The comparison of the results in the two cell lines could allow the estimation of the role of p53 in each cell cycle effect.

CHAPTER 3: Materials and Methods

3.1 CELL CULTURE

In order to test cell cycle effects induced by a treatment with an anticancer agent three different cell lines where used:

IGROV1, an ovarian cancer cell line with wild type p53 (ATCC) (Benard J et al., 1985). This line is maintained as monolayers in T-25 cm^2 tissue culture flasks (Iwaki, Bobby Sterilin, Staffordshire, UK) and routinely subcultured twice a week. The culture medium consisted of RPMI-1640 (Cambrex, Verviers, Belgium) with 10% foetal bovine serum (Sigma, St. Louis, MO, USA) and 1% L-glutamine (Cambrex). Culture was maintained in an incubator with 5% CO_2 in air at 37°C and 96% relative humidity.

To allow cells to reach exponential growth, they were seeded at about 20,000 cells/ml 72h before drug treatment.

HCT-116 and HCT-116 p53-/-, two isogenic colon carcinoma cell lines which respectively express p53 wild type (Brattain et al., 1981) or with p53 disrupted by homologous recombination (Bunz et al., 1998) (kindly provided by Dr. B. Vogelstein from John Hopkins University Baltimora, MA, USA). The cell line is maintained as monolayers in T-25 cm^2 tissue culture flasks and routinely subcultured twice a week. The culture medium consisted of Iscove's Modified Dulbecco's Medium (IMDM) (Cambrex) with 10% foetal bovine serum and 1% L-glutamine. Culture was maintained in an incubator with 5% CO_2 in air at 37°C and 96% relative humidity.

To allow cells to reach exponential growth, they were seeded at about 10,000 cells/ml 72h before drug treatment.

3.2 DRUG TREATMENT

Exponentially growing cells were treated for 1h with different drugs at different concentrations.

TPT (generously provided by Glaxo Smithkline, Middlesex, UK) was dissolved in dimethylsulfoxide (DMSO) (ICN Biomedicals, Irvine, CA) and the stock solution of 5 mM was stored at -20°C until required, further dilutions were performed in culture medium. IGROV1 cells were treated with 0.05, 0.2, 1, 10 and 100 μM TPT. Multiple treatments were done using the lowest drug concentrations (0.05 and 0.2 μM). We consider as 0h the time of the first treatment, so the cells were treated at 0, 24 and 48h. Each treatment lasted 1h, and the cells were counted and fixed every 24h for 96h.

L-PAM (Sigma) was dissolved in $4*10^{-3}$ N HCl in sterile water. The stock solution of 3 mM was prepared just before using it. IGROV1 cells were treated with 3, 10, 30, 50, 100 and 300 μM L-PAM.

DXR (generously provided by Pharmacia, Nerviano, Italy) was dissolved in sterile water and the stock solution of 3 mM was stored at -20°C until required, further dilutions were performed in culture medium. IGROV1 cells were treated with 0.5, 1, 3, 6, 10 and 30 μM DXR.

DDP (Sigma) was dissolved in culture medium at a concentration of 1 mM. The stock solution was prepared just before using it. HCT-116 and HCT-116 p53-/- cells were treated with 10, 30 and 100 μM DDP.

After treatment the cells were washed twice with warm PBS (Cambrex) and left in drug-free medium for 0, 6, 24, 48, 72 or sometimes also 96h. At each time the cells were detached, using 1ml 0.05% trypsin - 0.02% EDTA (Cambrex) in PBS, counted with a Coulter Counter ZM (Coulter Electronics, Harpenden, UK), then fixed in cold 70% ethanol and stored at 4°C.

3.3 FLOW CYTOMETRY

The basic principles of flow cytometry arise from some very old ideas generated early in the 20th century and follow the principles of laminar flow defined by Reynolds in the late 19th century.

3.3.1 Fluidic System

Reynolds formulated the relationship for fluid flow as $Re = vd\rho/\eta$ where Re is the Reynolds number (a dimensionless number), v the average velocity, d the tube diameter, ρ the fluid density, and η the viscosity. Below a Reynolds number of 2300, flow will be laminar, a necessary factor for quality optical measurements in flow cytometry. Maintenance of nonturbulent flow requires careful design of fluidic systems in flow cytometers, particularly the flow cell components.

Cells are hydrodynamically focused in a core stream encased within a sheath. This sheath-flow system is constituted by a needle that deposits cells within a flowing stream of sheath fluid (usually water or saline), creating a coaxial flow that moves from a larger to a smaller orifice. In this way it is possible to obtain a parabolic distribution of the velocity profile (figure 3.1). Because of the hydrodynamic focusing effect, cells that are injected through the injection tube remain in the centre of the core fluid, thus allowing very accurate excitation with subsequent excellent sensitivity and precision of measurement within the flowing stream.

There is a small differential pressure between the sheath and the sample (core), forcing alignment of cells in single file throughout the core.

3.3.2 Optical System

The key to the efficiency and sensitivity of flow cytometers is the laser-based coherent light source. The light source needs to be focused to a spot and a desired shape. This is accomplished by using a beam-shaping optic to obtain the desired crossed-cylindrical beam shape. The most desirable beam shape is an elliptical beam of approximately 15 by 60 microns, which at typical flow rates can be traversed by the cell in a few microseconds. Moreover its large and relatively flat cross-section reduces the variation in intensity of the excitation spot.

The most used excitation sources employed argon ion laser tuned to 488 nm. This wavelength is optimal because is close to the absorption maximum of the common fluorochrome fluorescein isothiocyanate (FITC) and other commonly used fluorochromes. On more sophisticated cytometers two or more lasers can be used to analyse the stream of cells in sequence enabling complex combinations of fluorochromes to be examined.

When a cell passes through the laser beam several physical processes take place, such as absorption, diffraction, refraction and reflection of the incident light and also fluorescence emmission. In flow cytometers, after blocking the direct laser beam, any low angle scattered light is focused by a lens onto a photoelectric diode. This signal represents an important parameter commonly referred to as forward angle light scatter. At higher angles refraction and reflection become increasingly important, these processes result from structural features of the cell such as granularity and surface convolutions. This measurement is made orthogonal to the stream and is referred to as side scatter (SS, SSC). Fluorescence measurements are also made in the orthogonal direction after separating various components by optical filtration. A typical arrangement for measuring four components is shown in figure 3.2.

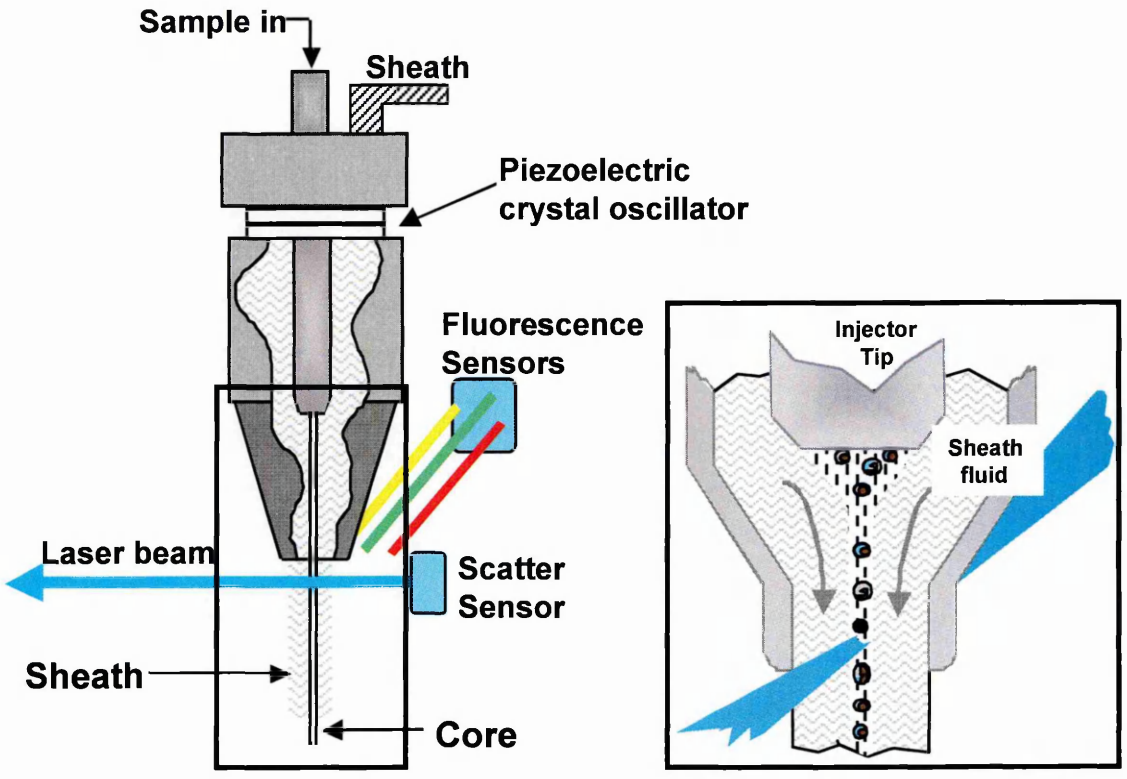

Figure 3.1: Schematic representation of the fluidic system. Sheath fluid flows through a large area and under pressure is forced into a much smaller orifice. In the centre of the cell is an injection tube that injects cells or particles into the centre of the flowing stream, forcing the cells to undergo hydrodynamic focusing, which will result in laminar flow if Reynolds number does not exceed 2300. In particular, in the square is shown the coaxial cross section of the sheath and core.

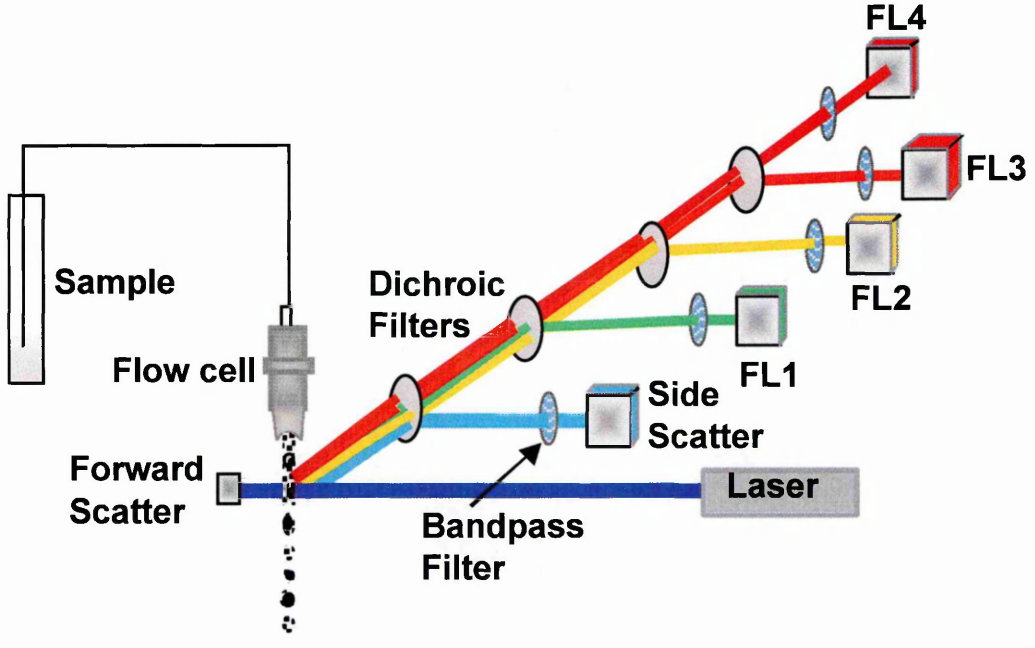

Figure 3.2: Schematic representation of the optical system.

3.3.3 Spectral Compensation

When a particle or cell contains fluorophores of multiple spectral bands, the identification and analysis become more complex. For example, a detector with a band pass filter designed to collect fluorescence from FITC (525 nm) and another detector designed to collect signals at 550 nm (PE) will register photons in both detectors. It is impossible to determine which detector is detecting the real photons from FITC. To achieve this, it is necessary to perform spectral compensation whereby a percentage of signal from one detector is subtracted from the other. At this point it is necessary to consider a cell labelled with only FITC, in this case, a large fraction of the emission (F) will be detected through the FITC bandpass filter and a small fraction f = (kF) through the PE bandpass filter. The true PE signal is known to be zero and can be obtained by electronically reducing the apparent PE signal by an amount kF. The same process is applied using a sample labelled with only PE to obtain a correction factor to subtract from the apparent FITC signal. These correction factors can then applied to all simultaneous measurements of FITC and PE.

3.3.4 Electronic System

Flow cytometers collect a lot of data very quickly. Every particle that passes through the laser beam is individually collected on every detector.

The relationship between incident electrons and output voltage from PMT's is sigmoid i.e. the output voltage reaches a saturation level. The sensitivity is also a function of high voltage, if this is increased too far the dynamic range of a tube will be severely limited by the saturating level.

The amplified signal can be used directly or subject to a logarithmic transformation, which effectively increases resolution for low input level.

Linear amplifiers produce signals that are proportional to their inputs but most immunofluorescence applications have huge dynamic ranges that are beyond amplification in the linear domain. For this reason, logarithmic amplifiers with scales covering three to five decades are required. This is particularly useful for samples in which some cells exhibit very small amounts of signal, while others have signals four orders of magnitude larger.

The final stage before storing signals is converting from analogue to digital. Many systems operate on an eight-bit conversion giving 256 channels. This allows one measurement per byte (8 bits) with a sufficient resolution for most flow cytometric measurements. Ten-bit conversion allows 1024 channels and is commonly used for measurements where fine detail is essential.

3.4 FLOW CYTOMETRIC ANALYSIS

3.4.1 Monoparametric Staining of DNA Content

About $1*10^6$ fixed cells were washed with cold PBS and resuspended in 1 ml of 25 µg/ml propidium iodide (PI) (Calbiochem, Darmstad, Germany) in PBS plus 25 µl of 1 mg/ml RNAse (Sigma) in water. The samples were measured with a FACS Calibur (Becton Dickinson, San Jose, CA, USA) flow cytometer after at least 2h incubation at room temperature in the dark.

3.4.2 5-Bromo-2'-Deoxyuridine (BrdUrd) Incorporation

Short-term perturbations were investigated by BrdUrd pulse-and-chase analysis. 30 µM BrdUrd (Sigma) was added to the cell culture during the last 20 min of treatment. After drug and BrdUrd washout the cells were left in drug- and BrdUrd-free medium for 6h. During the labelling BrdUrd, which is an analogue of thymidine, was incorporated by the cells that were synthesizing DNA (in S phase).

BrdUrd pulse-and-chase 6h after treatment detected the cell movement through the S phase and the outflow of unlabelled G_1 and G_2M cells.

At the same way cells can be labelled with BrdUrd at the time of treatment, washed and let in BrdUrd-free medium until 72h. In this case BrdUrd pulse-and-chase analysis allows the appreciation of a selective cell killing of the considered anticancer agent against BrdUrd-positive or BrdUrd-negative cells. If the percentage of BrdUrd-positive or BrdUrd-negative cells is not different from that of the control we conclude that the drug does not specifically affect one of the two subpopulations.

For BrdUrd pulse labelling experiment the cells were labelled with 30 µM BrdUrd 20 min before detaching them. This was generally done at 24, 48 or, in some cases, 96h after treatment and it allows us to obtain qualitative information about the reduction of DNA synthesis.

For BrdUrd continuous labelling cells were incubated with 30 µM BrdUrd and deoxycytidine for at least 48h (this depends on the doubling time of the considered cell line) so that all cycling cells can incorporate BrdUrd. At the end of incubation the cells were fixed in 70% ethanol.

3.4.3 Two-parameter Flow Cytometry Analysis: DNA Content and BrdUrd Incorporation

About $2*10^6$ fixed cells were washed with PBS and resuspended in 3 N HCl for 30 min. After washing with 0.1 M $Na_2B_4O_7$, pH 8.5, to stop acid depurination, the cells were resuspended with 180 µl 0.5% Tween 20 (Sigma) with 1% NGS (Dako, Glostrup, Denmark) in PBS. After this, 20 µl anti-BrdUrd monoclonal antibody (Becton Dickinson) was added and the mixture was incubated for 1h at room temperature. After washing with PBS, cells were incubated for 1h with fluorescein (FITC)-conjugated affinity pure F(ab')2 fragment goat antimouse IgG (Jackson,

West Grove, PA, USA) diluted 1:50 in PBS with 0.5% Tween 20 and 1% NGS. After incubation with antibody, cells were centrifuged, resuspended in 2.5 µg/ml PI in PBS plus 25 µl of 1 mg/ml RNAse in water, incubated overnight and analysed.

In the case of direct BrdUrd immunostaining, we added 20 µl of anti-BrdUrd FITC (Becton Dickinson) at the cells resuspended in 180 µl 0.5% Tween 20. After 1h incubation the cells were washed with PBS and resuspended in 2.5 µg/ml PI in PBS plus 25 µl of 1 mg/ml RNAse in water, incubated overnight and analysed.

3.4.4 Two-parameter Flow Cytometry Analysis: DNA Content and FITC-Conjugated dUTP

DNA fragmentation was detected by the TdT-mediated dUTP nick end labelling technique (TUNEL), which uses terminal deoxynucleotidyl transferase (TdT) to catalyze the binding of FITC-conjugated dUTP to DNA strand breaks. This technique detects DNA fragmentation induced during apoptosis. $2*10^6$ fixed cells were washed in PBS and permeabilized for 2 min on ice in 0.1% Triton X-100, 0.1% sodium citrate. The cells were washed, resuspended in 50 µl of TUNEL reaction mixture (Roche, Mannheim, Germany) containing dUTP-FITC and TdT, and incubated for 90 min at 37°C in the dark. After that, the samples were washed and resuspended in 1 µg/ml PI plus 25 µl of 1 mg/ml RNAse in water and incubated overnight at 4°C.

3.4.5 CFSE Loading and Drug Treatment

Cells were detached and loaded with 1 µM CFSE (Molecular Probes, Eugene, Oregon) in PBS for 15 min in a tube kept at 37°C under gentle shaking. After labelling the cells were washed with warm PBS and then seeded in T-25 cm^2 tissue culture flasks. Experiment started at least 24h after seeding.

In particular CFSE-loaded IGROV1 cells were treated for 1h with TPT, whereas CFSE-loaded HCT-116 and HCT-116 p53-/- cells were treated for 1h with DDP, washed twice using warm PBS and left in drug-free culture medium. At the appropriate times, cells were detached, counted and immediately analysed in the flow cytometer or fixed in cold 70% ethanol and stored at 4°C.

3.4.6 DNA Staining of CFSE-loaded Cells

For biparametric flow cytometric analysis cells fixed in 70% ethanol were washed with cold PBS and stained with a standard procedure for detection of DNA content with 2.5 µg/ml PI plus 25 µl of 1 mg/ml RNAse.

3.4.7 Triparametric Staining CFSE/BrdUrd/DNA

CFSE-loaded cells were treated for 1h with different drug concentrations, 20 min before the end of the treatment the cells were labelled with 30 µM BrdUrd, then washed and left in drug- and BrdUrd-free medium. The cells were counted and fixed in 70% ethanol at 24, 48 and 72h after treatment. In this way we were able to follow the fate of BrdUrd-positive and BrdUrd-negative cells at different times after treatment, monitoring in particular their ability of generating descendant.

About $1*10^6$ fixed cells were washed with cold PBS and resuspended in 2 N HCl for 30 min. After washing with 0.1 M $Na_2B_4O_7$, pH 8.5, to stop acid depurination, the cells were resuspended with 160 µl 0.5% Tween 20 with 1% NGS in PBS. After this, 40 µl of PE-conjugated Anti-BrdUrd Monoclonal Antibody (PharMingen, BD Biosciences, San Jose, CA, USA) was added and the mixture was incubated for 1h at room temperature. After incubation the cells were washed with PBS and resuspended in 1 ml of 0.25 µM TO-PRO3 (Molecular Probes) in PBS plus 25 µl 1% RNAse in water, incubated for 2h at room temperature in the dark and analysed.

For each samples we acquired at least 10,000 events on a 256-channel scale. FITC fluorescence of BrdUrd-indirect immunostaining and CFSE fluorescence were detected in FL1 (530 ± 30 nm) with a logarithmic amplifier, while dUTP-FITC fluorescence was detected in FL1 with a liner amplifier. BrdUrd-direct immunostained cells were detected in FL1 when stained with anti-BrdUrd FITC or in FL2 (585 ± 4 nm) when stained with anti-BrdUrd PE, but always with a liner amplifier.

DNA content was detected in FL3 (>620 nm) when stained with PI and in FL4 (>658 nm) when stained with TO-PRO3, always with a linear amplifier.

FITC, CFSE, PE and PI were excited with an argon laser (488 nm), whereas a diode laser emitting at 635 nm excited TO-PRO3.

3.5 COLONY ASSAY

Chemosensitivity of single and repeated treatments with TPT (0.2, 0.2 triple treatments, 1, 10 and 100 μM) was assessed by a clonogenic assay. IGROV1 cells were seeded at low density (about 250 cells/ml) in a six-well plate (Iwaki) and treated 48h later with different drug concentrations. The wells corresponding to triple treatment were treated with 0.2 μM TPT for 1h every 24h. One week after treatment the plates were washed with PBS and colonies were stained for 3 min with Gram's crystal violet solution (Fluka Chemie GmbH, Buchs, Switzerland). The colonies (>50 cells) were counted using an image analyser (Immagini & Computer, Milano, Italy). Surviving fractions were obtained by normalizing the plating efficiencies to the respective control values (plating efficiency of untreated cells: 40%). Each value is the mean of four replicates.

3.6 MATHEMATICAL MODEL

3.6.1 Unperturbed Growth

The study of cell kinetics of a cell proliferating population is the determination of the law which gives N(t) and the values of percentage of occupation of different intermitotic phases.

In steady state conditions a cell population grows following an exponential trend. That means that proliferating cells arrive in a condition of dynamic equilibrium after a short time and this condition is described by the following equation:

$N(t) = N_0 \exp(bt)$, where N(t) is the number of cells at the time t, N_0 is the initial cell number and b is a parameter related to the doubling time (T_C) in the following way: $b = \log 2 / T_C$.

In cell kinetic studies theory and simulation are based on the age distribution $n(\alpha,t)$, where $n(\alpha,t)d\alpha$ gives the cell fraction which has an age between α and $\alpha+d\alpha$ at the time t. If the age distribution is known it is possible to calculate the percentage of occupation for each intermitotic phase:

$$\%G_1(t) = 100 * \int_0^{T_{G1}} n(\alpha,t)d\alpha$$

$$\%S(t) = 100 * \int_{T_{G1}}^{T_S} n(\alpha,t)d\alpha \qquad (a)$$

$$\%G_2(t) = 100 * \int_{T_C - T_{G2}}^{T_C} n(\alpha,t)d\alpha$$

These equations are true if we suppose that there is not intercell variability. That means that every cell has to spend a time T_{G1} in G_1 phase, a time T_S in S phase and a time T_{G2} in pre-mitotic phase. For a cell population which is asynchronously growing the age distribution and thus the percentage of occupation of intermitotic phases is time independent.

The growing rate of a population at the time t' is

$$b_{t'} = \frac{1}{N(t')}\left(\frac{dN}{dt}\right)_{t'}$$

the number of newborn cells in dt is 2bN(t)dt, because for each dividing cell we have two newborn cells. At the time t, the number of cells that have an age between α and $\alpha+d\alpha$ is equal to the number of cells that were born at the time $t-\alpha$ in the same interval $d\alpha$:

$2b\ N(t-\alpha)=2b\ N(t)\ \exp(-b\alpha)$.

The probability that, at a time t, a cell has an age α has the following expression:

$P(\alpha)=2b\ \exp(-b\alpha)$.

This distribution $P(\alpha)$ for a population in exponential growth is independent from the time t at which we observe the cells. This independence explains the previous sentence where we said that in an asynchronously growing cell population the percentage of occupation for each intermitotic phase is constant. Applying the equations (a) we obtain the Steel's formulae (Steel, 1977):

$$\frac{T_{G2}}{T_C} = \frac{1}{\ln 2}\ln\left[1+\frac{\%G_2}{100}\right]$$

$$\frac{T_S}{T_C} = \frac{1}{\ln 2}\ln\left[1+\frac{(\%S+\%G_2)}{100}\right]-\frac{T_{G2}}{T_C}$$

$$\frac{T_{G1}}{T_C} = 1-\frac{T_S}{T_C}-\frac{T_{G2}}{T_C}$$

From these formulae we can obtain the fraction of T_C spent in each intermitotic phase starting from the knowledge of the percentage of occupation. In this situation the data obtained from cytometric analysis are very important because we can evaluate these percentages from the study of DNA histograms.

If we suppose that there is not intercellular variation in the duration of phases and the cells can proliferate without perturbations it is quite easy to simulate the cell cycle.

The duration of cell cycle is $T_C=T_{G1}+T_S+T_{G2}$ and it can be divided in N subintervals, each one with a duration Δt, so that $T_C=N\Delta t$.

Let $G_1(k,t)$ be the number of cells laying in the k-th step of G_1, at a certain time t, similar definitions holding for $S(k,t)$ and $G_2(k,t)$. The time evolution of $G_1(k,t)$, $G_2(k,t)$ and $S(k,t)$ from t to $t+\Delta t$ is immediately obtained considering the following set of equations:

$G_1(k+1,t)=G_1(k,t-\Delta t)$

$S(1_S,t)=G_1(k_{MG1},t-\Delta t)$

$S(k+1,t)=S(k,t-\Delta t)$

$G_2(1_{G2},t)=S(k_{MS},t-\Delta t)$ (b)

$G_2(k+1,t)=G_2(k,t-\Delta t)$

$G_1(1_{G1},t)=2G_2(k_{MG2},t-\Delta t)$

Equations (b) refer to a cell cycle divided as shown in the following picture:

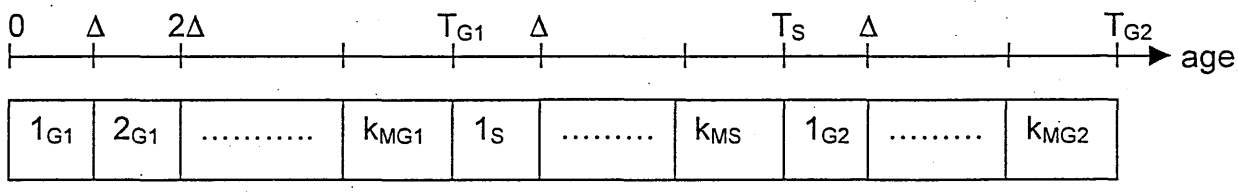

The set of equation (b) is valid for system without intercell variability and without real effects such as cell death or slowing down of cell cycle. These equations could become more realistic if we suppose that each cell spends a different time in the same phase of the cell cycle, in this case T_{ph} becomes the mean value of the time that each cell spends in a phase before leaving it. Now we can introduce a distribution function $F_{ph}(k)$ which gives us the probability that a cell, with an age k in a certain phase, leaves the same phase. For $F_{ph}(k)$ we adopted a reciprocal-normal distribution on the basis of earlier studies performed in our laboratory (Sisken and Morasca, 1965) and showing that intermitotic times can be well approximated by this function. For calculus purposes the distribution was truncated six standard deviations above its mean, assuming to include in this way

also cells with very long phase duration. Cells with longer phase duration would be considered quiescent. K_{ph} indicates the last value of k for which F_{ph} is not zero. Introducing the $D_{ph}(k)$ factor, defined in the following way:

$$D_{ph}(k) = \frac{F_{ph}(k)}{\left[1 - \sum_{j=1}^{k-1} F_{ph}(j)\right]}$$

and giving the fraction of cells completing a phase at age k, among the cells that reached age k-1, we can change the equations (b):

$$\begin{aligned}
&G_1(1_{G1}, t) = 2\sum_{k=1}^{K_{G2}} G_2(k, t-\Delta t) D_{G2}(k) \\
&G_1(k+1, t) = G_1(k, t-\Delta t)\left[1 - D_{G1}(k)\right] \\
&S(1_S, t) = \sum_{k=1}^{K_{G1}} G_1(k, t-\Delta t) D_{G1}(k) \\
&S(k+1, t) = S(k, t-\Delta t)\left[1 - D_S(k)\right] \\
&G_2(1_{G2}, t) = \sum_{k=1}^{K_S} S(k, t-\Delta t) D_S(k) \\
&G_2(k+1, t) = G_2(k, t-\Delta t)\left[1 - D_{G2}(k)\right]
\end{aligned} \qquad (c)$$

The level of complexity of these equations can be increased considering the pre-cycle phase G_0 and p_{mit}. p_{mit} is the mean number (≤ 2) of living newborn cells originating from a mitotic event. G_0 is simulated as a single compartment and bp_{G0} is the probability that a newborn cell bypass G_0 phase and enter G_1 phase. That means that G_0 cells can enter G_1 with a rate p_{G0G1}. Thus the G_1 equation in (c) becomes:

$$\begin{aligned}
&G_1(1_{G1}, t) = G_0(t-\Delta t) p_{G0G1} + bp_{G0} p_{mit} \sum_{k=1}^{K_{G2}} G_2(k, t-\Delta t) D_{G2}(k) \\
&G_0(t) = G_0(t-\Delta t)(1 - p_{G0G1}) + (1 - bp_{G0}) p_{mit} \sum_{k=1}^{K_{G2}} G_2(k, t-\Delta t) D_{G2}(k)
\end{aligned} \qquad (d)$$

For a cell population growing in vitro this is the highest level of complexity that we can consider, but at this point it is possible to introduce in the model the kinetic effects of a drug (figure 3.3 and 3.4).

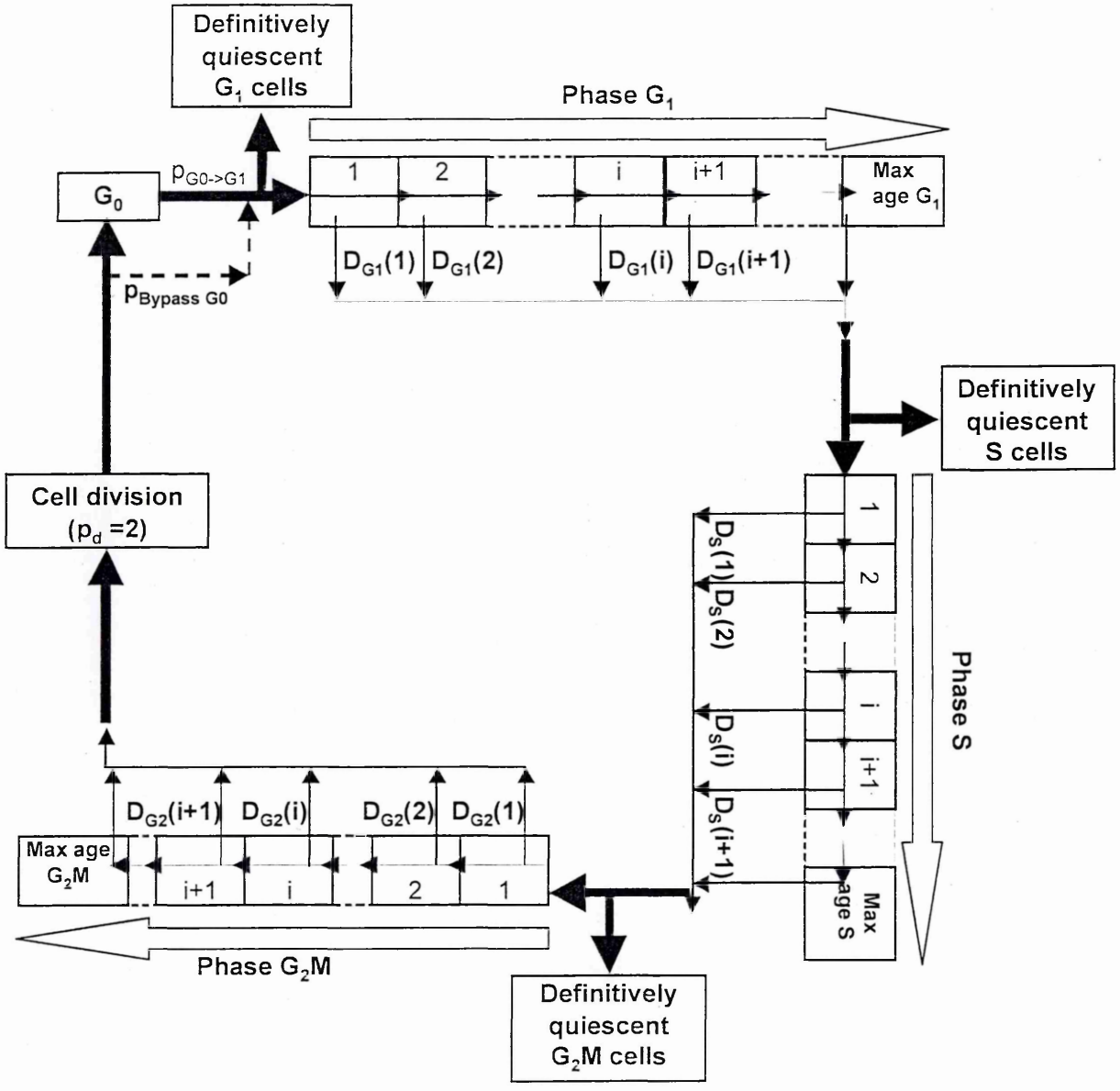

Figure 3.3: Scheme of the mathematical model, reproducing the unperturbed growth. In an asynchronously growing population, cells are distributed in every phase of the cell cycle. Each phase is divided in discrete age compartments of width Δ = 30 min, which groups cells with the same age ± 15 min.

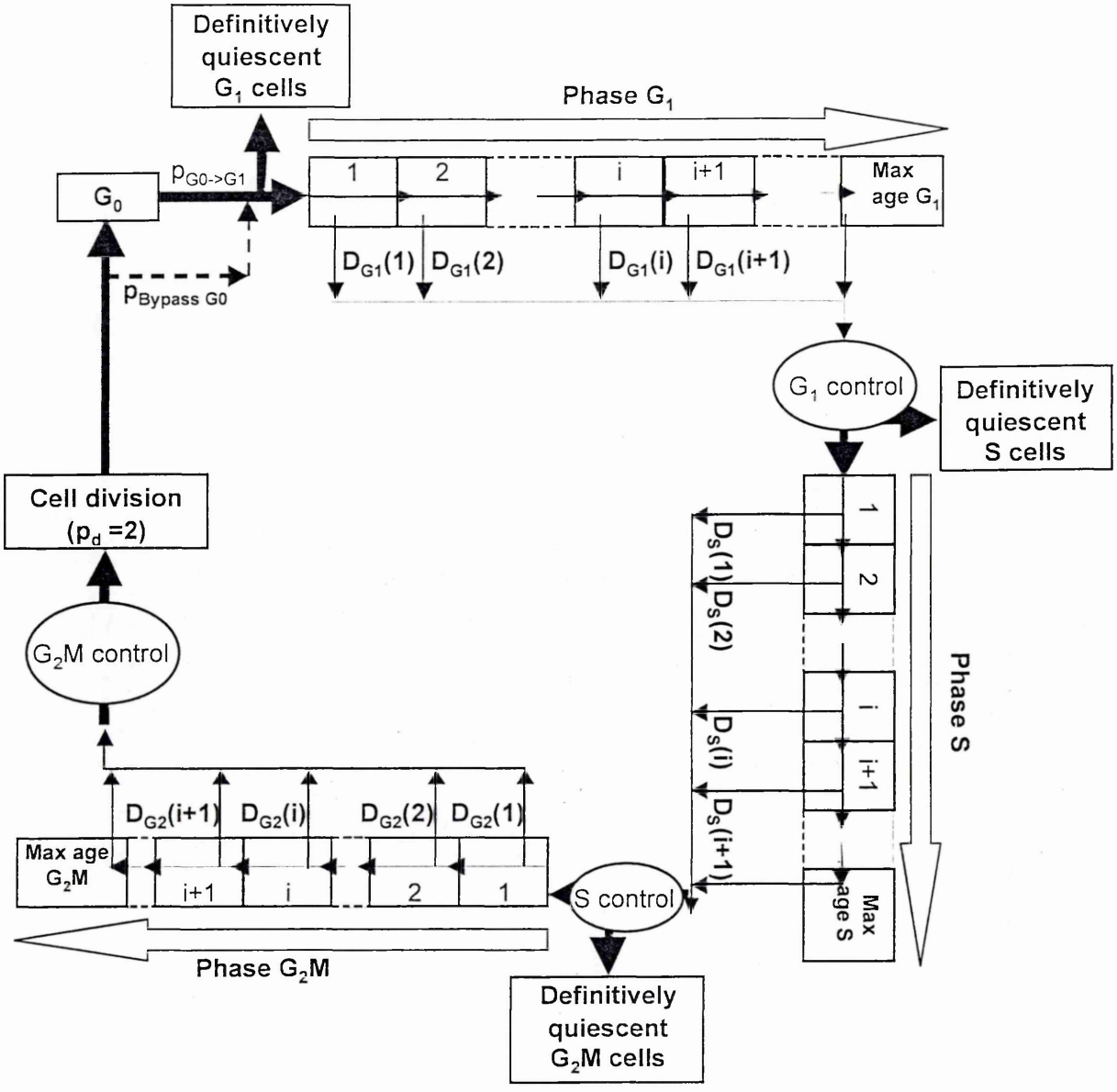

Figure 3.4: Scheme of the mathematical model, reproducing the perturbed growth. After drug treatment cells that were in G_1 phase can enter S phase as control or can remain blocked in G_1 phase, if intercepted by G_1 checkpoint. Once blocked the cells recycle, if they are able to repair their damage, or die. All these possibilities are represented in this scheme as "G_1 control".

3.6.2 Drug Perturbations

From a kinetic point of view we can briefly resume the effects of an anticancer drug. Cells can be blocked at the checkpoints at the end of G_1 or G_2M phase, or they can be slowed down in their cycle (freezing). After each time step there is a probability that the cells pass from a certain compartment to G_0 and they become definitively quiescent. The drug can kill cells that are normally cycling or cells, which are quiescent, blocked or delayed. The parameters $p_{ph}B^{in}$ represent the fraction of cells that leave their compartment and become blocked cells. There is also a probability that a blocked cell repairs the DNA damage caused by the drug and recycle. This probability can be represented by the following parameter: $p_{ph}B^{out}$, on the contrary the probability that a blocked cell dies is $p_{ph}B^{die}$.

The freezing acts in a different way from the block, because with this parameter we represent an inhibition of the age maturation of a fraction $p_{ph}F$ of non blocked cells which populates a certain phase ph at the time t. As for blocked cells there is also a probability $p_{ph}F^{die}$ that frozen cells are eliminated every time step.

Cells entering a given phase may otherwise become definitively quiescent with a probability $p_{ph}Q$. Quiescent cells accumulate in a specific compartment Q, in which death occurs with a probability $p_{ph}Q^{die}$ every step.

The last possibility is the death of a proliferating cell, that can be simulated introducing a non zero probability p^{die}_{ph} of leaving the cell population, in particular the death of a cell after mitosis can be simulated choosing for p_{mit} a value smaller than 2.

With these corrections we can compare the experimental data to the simulations obtained from this mathematical model. For instance, the evolution of the cell number in S(k) passing from t to $t+\Delta t$ can be written in the following way:

$$S(k,t+\Delta t)=S(k-1,t)(1-D_S(k))(1-p_SF(t))(1-p^{die}{}_S(t))+S(k,t)p_SF(t)(1-p_SF^{die}(t))$$

With this program it is also possible to simulate a label of BrdUrd: in practice, at a given labelling time, every cell in S phase becomes BrdUrd positive, filling the compartment $S^+(k,t)$. After that time, the evolution of positive and negative cells is followed, considering that a positive cell which doubles gives two positive cells and that the presence of BrdUrd does not change the evolution equations. Thus the program computes two parallel cycles, one describing $Ph^-(k,t)$ and the other one describing $Ph^+(k,t)$. Obviously $Ph(k,t)= Ph^-(k,t)+ Ph^+(k,t)$.

3.6.3 Simulation

This program reproduces the unperturbed growth of a cell population and its response to treatment with several drug concentrations. In particular, the task of the computer simulation is to consider all experimental data together, with a number of drug doses and recovery times, to give a complete coherent kinetic scenario based on a quantitative estimate of the time- and dose-dependence of the probabilities of cell arrest and killing.

3.6.3.a Input data

The first step towards the reconstruction of the scenario is represented by the determination of input parameters describing the baseline unperturbed growth of untreated cells:

- Mean transit times in the cell cycle phases T_{G1}, T_S and T_{G2M}
- The intercellular spread of G_1, S and G_2M transit times, measured by the respective coefficients of variation CV_{G1}, CV_S and CV_{G2M}
- Initial cell distribution through the cycle phases.

A detailed BrdUrd study of the growth of IGROV1 and HCT-116 cells led us to determine the values of these parameters. In particular, the experiments that have to be performed in order to obtain the necessary experimental data are:

- BrdUrd pulse-and-chase experiment with 20 min of labelling followed by cell count and harvesting every 3h for 48h.
- BrdUrd continuous labelling for 48h to evaluate the percentage of quiescent cells.

This part of the simulation allowed us to determine the following values:

IGROV1: T_{G1} = 9.1h; CV_{G1} = 50%; T_S = 8.7h; CV_S = 10%; T_{G2M} = 3.1h; CV_{G2M} = 10%

HCT-116: T_{G1} = 1.8h; CV_{G1} = 20%; T_S = 9.5h; CV_S = 5%; T_{G2M} = 3.2h; CV_{G2M} = 20%,

Once that we found the values of the mean transit times of different cell cycle phases, the spread of G_1, S and G_2M transit times and the initial cell distribution that reproduce the experimental data we can use them in every experiment performed with the same cell line. From an experiment to another we only have to correct the percentage of quiescent cells, keeping them in the order of 5%.

The results of the simulation of unperturbed growth of IGROV1 and HCT-116 cells are respectively reported in figure 3.5 and 3.6. The simulated data that were able to reproduce the trend of the measured data were obtained by applying the mean transit times of phases and CVs listed above. In particular, the percentage of labelled undivided cells and their fraction respect to the initial number of BrdUrd-positive cells highlighted the necessity of taking into account a certain intercell variability, even in the case of a cell population growing exponentially and without any particular perturbation (figure 3.7).

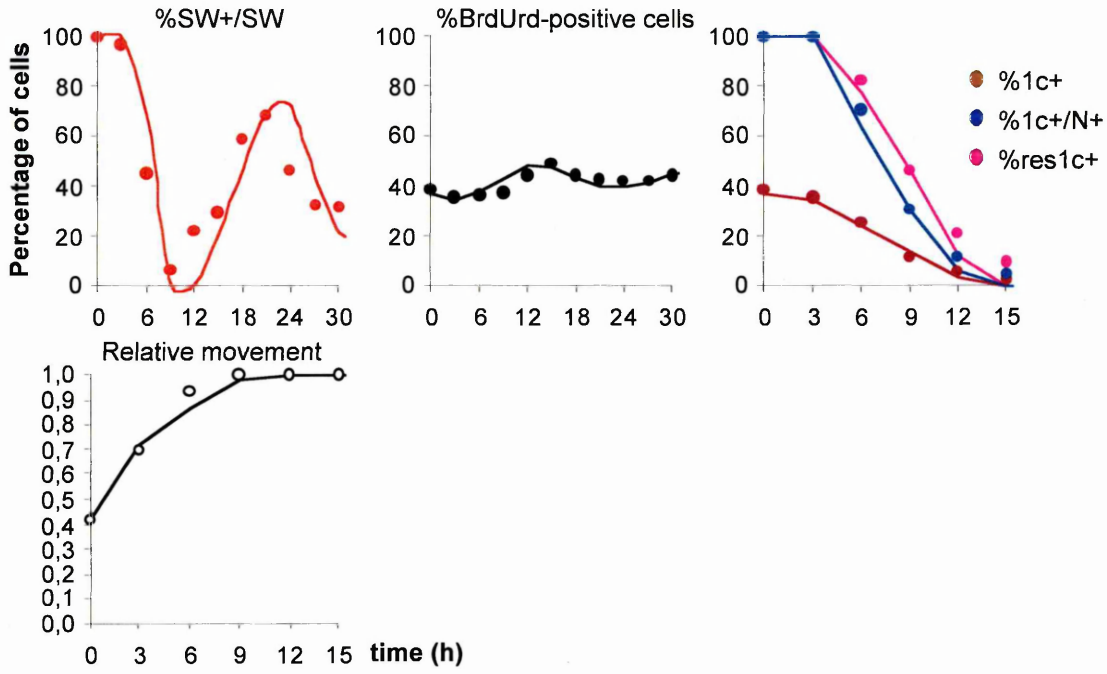

Figure 3.5: Results of the simulation of unperturbed growth of IGROV1 cells, using the parameters listed in the paragraph 3.6.3.a. The symbols represent the data obtained by the analysis of BrdUrd pulse-and-chase experiments, while the continuous line represents the result of the simulation. The considered experimental data are defined in table 3.1.

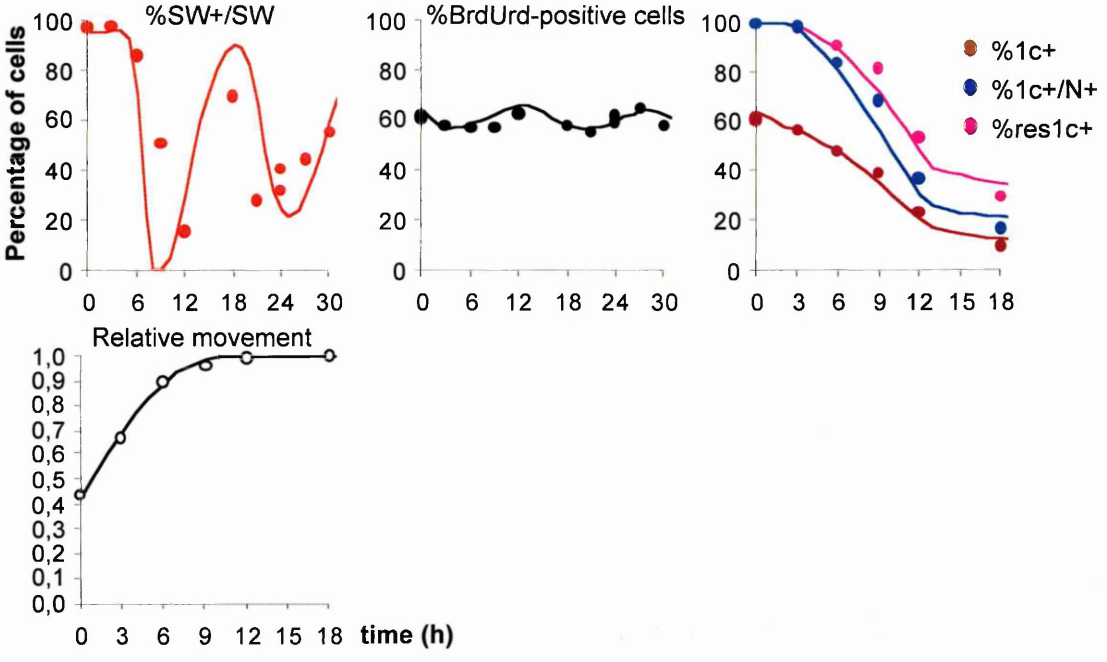

Figure 3.6: Results of the simulation of unperturbed growth of HCT-116 cells, using the parameters listed in the paragraph 3.6.3.a.

Data obtained by BrdUrd pulse-and-chase analysis	
%1c+=LU	Percentage of labelled undivided cells.
%1c+/N+=100*LU/(%$BrdUrd_+$)	Percentage of labelled undivided cells over the total percentage of BrdUrd-positive($BrdUrd_+$) cells.
%res1c+=(100*LU)/(LU+0.5($BrdUrd_+$-LU)	Percentage of labelled undivided cells over the percentage of $BrdUrd_+$ cells at the time of the labelling.
%SW	Percentage of S-phase cells included between INT(G_1+(G_2-G_1)*0.4) and INT(G_1+(G_2-G_1)*0.6), where "G_1" and "G_2" are respectively the position of G_1 and G_2 pick and INT( ) is a function that rounds a number down to the nearest integer.
%SW+	Percentage of $BrdUrd_+$ cells included between INT(G_1+(G_2-G_1)*0.4) and INT(G_1+(G_2-G_1)*0.6).
RM=(X_{mean}-G_1)/(G_2-G_1)	This number allows the quantification of the cell progression through S phase. X_{mean} is the BrdUrd mean fluorescence of labelled undivided cells.

Table 3.1: List of some of the quantities that can be calculated analysing a biparametric DNA/BrdUrd dot plot. In control samples in exponential growth these quantities depend on the mean transit time of phases and on the coefficient of variation.

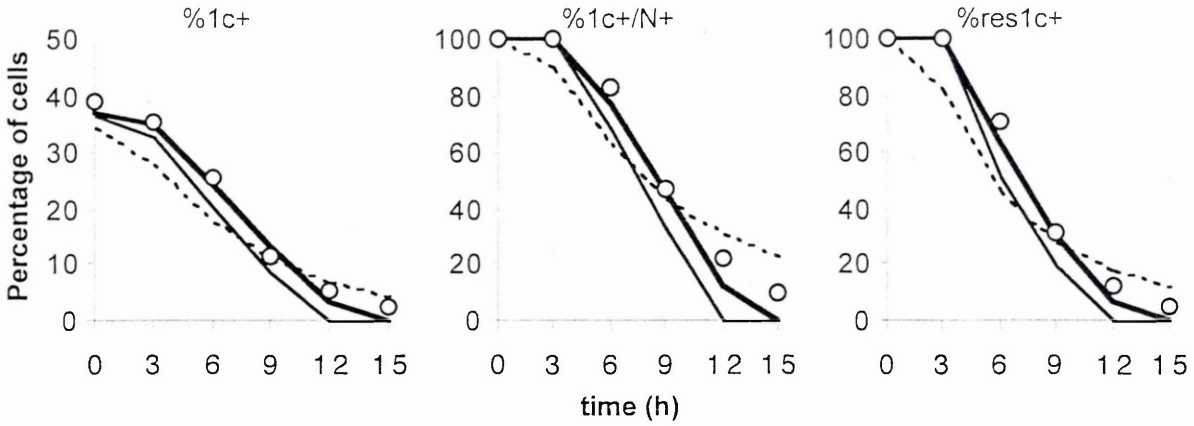

Figure 3.7: Role of the coefficient of variation (CV) in the simulation of the percentage of labelled undivided cells for IGROV1.

The symbols represent the data obtained by the analysis of BrdUrd pulse-and-chase experiment. The lines represent the results of the simulation performed with the following values of CV:

CV_{G1} = 50%; CV_S = 10%; CV_{G2M} = 10% ——————

CV_{G1} = 0.5%; CV_S = 0.5%; CV_{G2M} = 0.5% ——————

CV_{G1} = 100%; CV_S = 100%; CV_{G2M} = 100% - - - - - - - -

These graphs demonstrated that even in a cell population growing without any perturbations a certain intercell variability in the transit time of phases has to be taken into account.

Before comparing the parameters that describe the cell cycle effects induced by each drug, it was necessary to test the role of time duration and CVs in the determination of cell number and flow cytometric percentages. This kind of evaluation was done considering the scenario describing the effects of two different DDP concentrations (75 and 200 μM) and monitoring the variations of output in the correspondence of the different parameters considered (listed in table 3.2).

Base	T_{G1} (h)	T_S (h)	T_{G2M} (h)	CV_{G1} (%)	CV_S (%)	CV_{G2M} (%)
1	9.5	8.1	2.6	50	10	10
2	7.8	8.9	3.2	50	10	10
3	8.9	8.6	2.6	50	10	10
4	8.7	9.3	3.1	50	10	10
5	9.1	8.7	3.1	50	10	10
6	9.1	8.7	3.1	80	20	40
7	9.1	8.7	3.1	1	1	1
8	9.1	8.7	3.1	10	10	10
9	9.1	9.0	3.5	1	1	1

Table 3.2: The impact of the parameters describing the unperturbed growth of IGROV1 cells on the output of the simulation was tested considering the values of time duration and CVs listed above. The scenario describing the effects induced by a treatment with 75 and 200 μM DDP was that described in Montalenti et al. (1998). We defined as "Base" the set of parameters (T_{G1}, T_S, T_{G2M} and CV_{G1}, CV_S, CV_{G2M}) considered in the simulation of unperturbed growth.

The results of this study are shown in figure 3.8 where the output of the simulation was compared with the experimental data. In spite of the variation of the time duration and CVs the trend of the cell number and flow cytometric percentages was maintained with only slight variations in the absolute values of the simulated

data. This allowed us to confirm that the determination of the final scenario was not influenced by the parameters connected with the unperturbed growth.

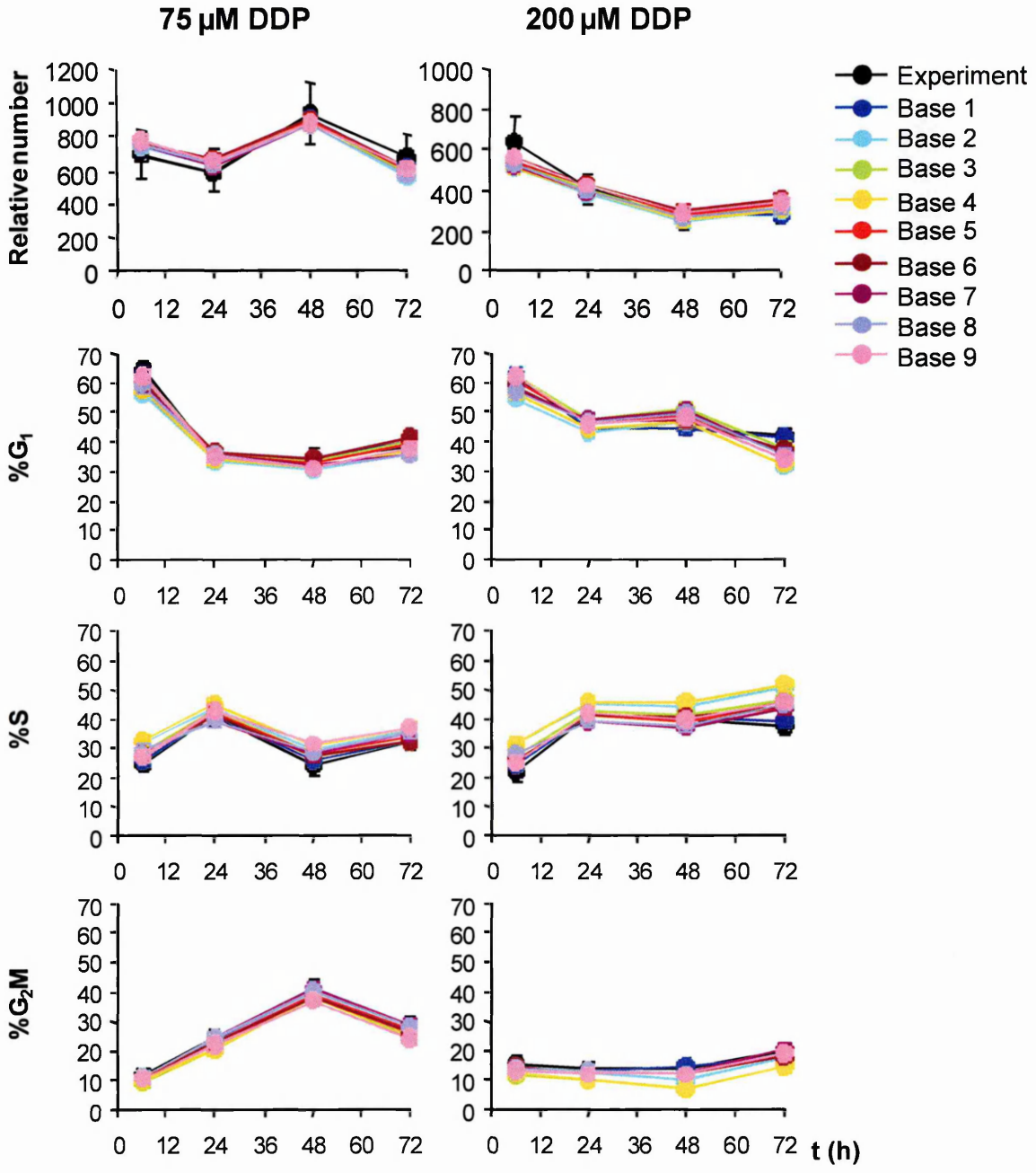

Figure 3.8: Comparison of the output obtained applying the scenario describing the effects induced by DDP treatment at different initial cell distributions described by different bases (listed in table 3.2). The experimental data are represented with the error tolerated during the simulation: 20% for the cell number and 3% for flow cytometric percentages.

In unperturbed conditions, kinetics of HCT-116 p53-/- was not different from that of wild type cells. For this reason we used the same parameters to simulate the growth of untreated cells.

Because cells were treated while in exponential growth, asynchronous initial cell distribution was chosen (i.e. cell percentages in every phase are constant over time).

To simulate all possible cell cycle perturbations, a set of additional parameters ("effect descriptors") was devised, all associated with cell cycle perturbations with a true biological significance:

- "Delay" rate (p_SF): this is the proportion of cells whose progression inside S phase is inhibited at each step, resulting in a longer mean transit time for this phase. The value of the parameter is equivalent to the fractional reduction of the DNA synthesis rate. The extreme situation (delay rate = 1) indicates complete cell "freezing" within S phase.
- "Block" probability ($p_{ph}B^{in}$): this is the proportion of cells entering a block in G_1 or G_2M phase, instead of proceeding to the next phase. In other words, "Block" represents the probability of being intercepted by a checkpoint and blocked there. Blocked cells may subsequently either re-enter the cycle or die in the block, depending on the next two parameters.
- "Recycling" rate ($p_{ph}B^{out}$): this is the proportion of blocked cells re-entering the cycle, at each time step. It is indicative of recovery in cells blocked in a particular checkpoint.
- "Death" rate ($p_{ph}B^{die}$, p_SF^{die} or $p^{die}{}_{ph}$): this is the proportion of cells removed from a group, at each time step. Independent rates can be applied to cycling, blocked or delayed cells in a phase. In the first interval of time (0-6h) the same death rate was applied on blocked and proliferating cells, because a population of blocked cells was not identifiable yet. For S phase the same death rate was

always considered on delayed and proliferating cells, because in this phase there is not a compartment for delayed cells, so that they are indistinguishable from proliferating ones.

To reduce the redundancy of descriptive parameters, drug effects in G_1 and G_2M were described only by block parameters, whereas those in S phase by freezing parameters. This choice is biologically sustainable, since G_1 and G_2 molecular checkpoints are known to be active in intercepting damaged cells, blocking them until the damage is repaired or cell death occurs, whereas there is not a definite checkpoint in the S phase. This is also coherent with DNA histogram data, which excluded the presence of a specific point in S phase where the cells accumulate. Block and recycling are probably continuous throughout S phase and the result of these two processes is described by the average delay rate considered in the model.

3.6.3.b Output data

Giving as input a set of values of the parameters describing drug effects (the "scenario" under evaluation), as output the simulation program gives the time-course of several measurable quantities consequent to this scenario. These values are compared directly with the experimental data:

- Total number of cells, reproducing the growth curve.
- Percentages of cells in G_1, S and G_2M phases.
- Output of BrdUrd experiments: percentages of G_1, S, G_2M BrdUrd unlabelled cells; percentages of "undivided" and "divided" BrdUrd-positive cells (i.e. BrdUrd-labelled cells still in the S and G_2M phases of their first simulated cycle, and in the G_1 phase of their second simulated cycle); total percentage of BrdUrd-positive cells.

Both input parameters and output data were synthetically reported in table 3.3.

INPUT PARAMETERS AND BIOLOGICAL PHENOMENA	
Unperturbed growth	
Intercell variability of phase duration	Mean time of phases T_{G1}, T_S, T_{G2}
	Coefficient of variation of the probability distribution CV_{tG1}, CV_{tS}, CV_{tG2}
Perturbed growth	
G_1 and G_2 block	Percentage of cells entering the block instead of leaving the phase $p_{ph}B^{in}$ (t,d)
Inhibition of DNA synthesis	Average reduction of DNA synthesis rate in each interval p_SF (t,d)
Cytotoxic effect	Percentage of blocked cells which dies in each interval of time $p_{ph}B^{die}$ (t,d), p_SF^{die} (t,d) or p^{die}_{ph} (t,d)
Recovery from block	Percentage of blocked cells exiting from the block and recycling in each interval of time (recycling rate) B^{out} (t,d)
OUTPUT PARAMETERS AND EXPERIMENTAL DATA	
Number of cells	N (t,d)
Percentage of cells in G_1 phase (BrdUrd positive or negative)	$\%G_1$(t,d) ($\%G_1$(t,d)+, $\%G_1$(t,d)-)
Percentage of cells in S phase (BrdUrd positive or negative)	%S(t,d) (%S(t,d)+, %S(t,d)-)
Percentage of cells in G_2 phase (BrdUrd positive or negative)	$\%G_2$(t,d) ($\%G_2$(t,d)+, $\%G_2$(t,d)-)
Fraction of BrdUrd labelled divided and undivided cells	F_{Id}(t,d) F_{Iund}(t,d)

Table 3.3: All the possible input parameters with their biological meaning are listed in this table, where "t" indicates the time after treatment and "d" the drug concentration.

3.6.3.c Optimisation

During the simulation hundreds of sets of input parameters are tested by a trial-and-error procedure. As the experimental precision of flow cytometric percentages is about 3% and for cell counts is about 20%, the fitting was considered satisfactory when all experimental data were reproduced with the same precision. Using a principle of parsimony, we start trying to reproduce the data with a few parameters, as suggested by the interpretation of flow cytometric data and adding progressively new parameters until we obtained a satisfactory reproduction of all available data. The data of each drug concentration were initially fitted independently, finding a small number of scenarios coherent with data. Then, the dose-dependence of each parameter was considered, allowing the exclusion of some biologically inconsistent scenarios that forecasted a decrease of overall blocks and cell loss when drug concentration increases.

The parameters were taken as constant in the intervals between successive experimental data (i.e. 0-6h, 6-24h, 24-48h and 48-72h). The resulting values for "Block", "Recycling" and "Death" should be considered as descriptions of average effects in those intervals. The adopted time intervals are a compromise between feasibility of the experiment and necessity to have an estimate of the time course.

We found that the hypothesis of the time-dependence of the parameters is necessary to fit the data but any detail of that time-dependence inside subsequent data points was not necessary and would not be demonstrable.

Wishing to include all basic perturbations of the cell cycle with their time-dependence, the equations of the model are too complex to be solved and we are not able to obtain cell cycle percentages as analytical functions of those perturbations. For this reason, we make simulations, solving numerically the

equations of the model. In this situation it is not necessary (and also not technically possible in our knowledge) to fit directly the data with some non-linear fitting routine and we adopt a trial-and-error procedure. This also allows us to maintain a biological comprehension of the phenomena in all phases of the analysis.

3.6.3.d Representation of the scenario

As previously described each parameter of the model represents a probability that a cell passing through a certain phase is intercepted by the checkpoint and that a blocked cell die or re-enter the cycle. From the point of view of the whole cell population this probability can also be quantified in terms of the percentage of cycling cells that remain blocked in a certain phase or that, once blocked, die or re-enter the cycle. As we demonstrated with the study of the sensitivity of the parameters (paragraphs 4.2.3, 5.2.3 and 6.2.3), there could be more than one value for each parameter that allows the reproduction of the experimental data. It is for this reason that we decided to classify the best values of the parameters in the final scenarios using interval of efficacy. For what concern the blocking activity, the categories were built using the percentage of cells that remain blocked in a particular phase, while the death and recycling rates were re-expressed in terms of the corresponding percentage of cells that would die or recycle in a group of blocked cells in the considered interval of time. Following this representation five different intervals of efficacy were hypothesized. In particular, the activity of the cell cycle control mechanisms were considered negligible when less than 5% of cells were intercepted by the checkpoint or die/recycle in a particular interval of time; thus the intervals were divided in the following way: 5-20%, 20-40%, 40-60%, 60-80 and 80-100%.

3.6.3.e Study of the sensitivity

The final scenario allowed the reproduction of all the data within the experimental precision, i.e. 3% for flow cytometric percentages and 20% for cell counts. However, a further level of evaluation is necessary to measure the uncertainty of the parameters estimation (sensitivity analysis). To study the sensitivity of each parameter in our model we started from the scenario obtained and we varied each parameter on its own to determine the impact of this variation on the output. For each parameter, a confidence band was constructed including all values enabling to simulate the data within their experimental error. A wide band means that a given parameter, at the specified time and concentration, is irrelevant for the data, while a narrow band means that the estimate is robust and the prediction of the observed data would be lost with small changes to the assumed value.

CHAPTER 4: Cell Cycle Effects of Topotecan

4.1 INTRODUCTION

4.1.1 Biochemical Mechanism of Action of Camptothecins

Camptothecin (CPT) is a potent antitumour antibiotic isolated by Wall and Wani in 1958 from extracts of *Camptotheca acuminata*, a tree native to China and Tibet which has been extensively used in traditional Chinese medicine (Wall, 1993). The structure was determined to be that of a pentacyclic alkaloid and was first reported in 1966 (Wall et al., 1966).

CPT and its derivatives, such as topotecan (TPT) and irinotecan, that are used for clinical therapy, and several novel CPT derivatives that are currently in various stages of clinical trials (Pratesi et al., 2004), show the same mechanism of action. This mechanism was elucidated about 20 years ago, when it was found that they caused DNA single-strand breaks by poisoning DNA-topoisomerase I (Hsiang et al., 1985; Holm et al., 1989). CPT binds covalently to the normally transient DNA-topoisomerase I cleavable complex and inhibits the religation step of the enzyme (Hsiang et al., 1989). As a consequence, protein-linked single-strand breaks in the DNA accumulate in the cell. These stabilised breaks are fully reversible and non-lethal (Schneider et al., 1990). However, the enzymes of the DNA synthesis machinery come up against an obstacle while processing DNA and single-strand breaks are converted to irreversible double-strand breaks. This is a crucial event for cytotoxicity (Hsiang et al., 1989) and apoptotic cell death mediated by caspase activation. On the other hand, collision with RNA polymerases produces predominantly topoisomerase I-linked single-strand breaks and the cleavable complex, located on the transcribed strand (Wu and Liu, 1997), inhibits RNA synthesis by avoiding the progression of the enzyme trough the transcribed strand itself (Zhang et al., 1990). Collision with RNA polymerases can also lead to double-strand breaks when two cleavable complexes are seated closely on the opposite strands of the DNA duplex. If CPT is removed from cells the

phenomenon reverses, probably because the topoisomerase I complex dissociates from the transcription unit, and RNA synthesis restarts (Parchment and Pessina, 1998).

Maintenance of the complex requires the presence of CPT in its active form, which is represented by the closed ring lactone. However, at neutral and alkaline pH, equilibrium favours the essentially inactive carboxy-acid from (Yao et al., 1998).

The study of different cell lines resistant to this family of compounds allowed a better comprehension of their mechanisms of action. CPT resistant cell lines are characterized by specific mutations within the gene codifying for topoisomerase I (Pommier et al., 1999). Deletion of the gene for topoisomerase I from *Saccharomyces cerevisiae* resulted in viable cells that were fully resistant to CPT. Re-expression of the yeast or human enzymes in *S. cerevisiae* restored sensitivity to CPT (Nitiss and Wang, 1988; Bjornsti et al., 1994). In general the different causes of resistance to topoisomerase I inhibitor can be grouped into three categories: (a) pre-cleavage mechanisms related to the drug metabolism and uptake; (b) topoisomerase I alterations that results in reduced levels of cleavage complexes; and (c) the post-cleavage complex mechanisms, which are related to the multiple pathways leading to cell death, cell cycle regulation and DNA repair.

4.1.2 Previous Cell Cycle Studies

The earliest studies about cell cycle effects induced by this class of compounds showed that the cytotoxicity of camptothecins is cell cycle phase specific (Li et al., 1972). In particular, it has been calculated that a cell in S phase is about 1000 times more sensitive to the cytotoxic effect of topoisomerase I inhibitors than cells in other phases of the cell cycle (Horwitz, 1975). However, if the toxicity is measured as damage produced by CPT on DNA the result is very similar either in S- and G_1-phase cells (Horwitz and Horwitz, 1973). This apparent discrepancy

suggest that the cause of cell death by CPT is probably due to the collision between the cleavage complex and the replication forks and that the entering in S phase converts a reversible damage of DNA into a lethal lesion.

The results of previous studies using synchronised cells (Li et al., 1972) have to be interpreted with caution as the synchronisation itself could modify the metabolic behaviour of the cancer cells, possibly producing artefacts (Mikulits et al., 1997). On the other side, results reported by more recent studies showed a substantial reduction of the S-phase selectivity of camptothecins (Gong et al., 1993) when cells are pretreated with DNA polymerase inhibitor as aphidicolin (Tsao et al., 1992; Wu et al., 2002). But also in this case the results might be altered because of the inhibition of DNA polymerase-dependent DNA repair processes (Moore and Randall, 1987).

More recent flow cytometric studies about cell cycle effects induced by short treatments with CPT or its derivatives add a deeper level of complexity in the comprehension of the question. In this case, accumulation or depletion of cells in G_1, S and G_2M were detected. McDonald et al. (1998) showed that, 24h after treating an ovarian cancer cell line with an IC_{80} TPT concentration, there was an accumulation of cells in G_2M phase, with reduction in G_1 and S phases, partly attributable to the block in G_2M. They also suggested that, despite the lack of significant G_1 accumulation, the depletion of the S-phase compartment observed is in part due to impaired transit across the G_1/S cell cycle checkpoint.

Some of these cell cycle effects were confirmed by Taron's study (Taron et al., 2000). They investigated the response of different cell lines to a treatment with a single concentration of TPT (identified as the IC_{50}), analysing flow cytometric DNA profiles at different times after treatment and showing a transient accumulation of cells in S and G_2M. At 24h many cells accumulated in G_2M suggesting that delay

in S was transient. In all cell lines, the authors found no difference between the cell cycle profiles of treated and control cells 48h after TPT treatment.

Experiments involving short treatments with CPT and its derivatives where more than 80% of cells were killed (O'Connor et al., 1990; O'Connor et al., 1991) suggest that the effects of these compounds are not specific to S-phase cells. The observation was confirmed in a more recent study made by Feeney et al. (2003) using time-lapse microscopy. They suggested that cells treated with TPT while in G_1 and S phase were unable to duplicate in 48h, while part of G_2M cells could divide. The proliferation of S-phase cells, unlike G_1 and G_2M cells, was inhibited even at a low TPT concentration.

This can be explained by tacking into account that topoisomerase I does not play a role only in DNA replication, but is certainly implicated in the DNA repair mechanisms as well as in the regulation of gene transcription. Both these processes occur not only during S phase but also during the other phases of the cell cycle. Thus CPT-induced DNA damage may be produced during transcription outside of S-phase as well as by DNA replication during S-phase (Mosesso et al., 2000).

4.1.3 Clinical Use

Preclinical data showing CPT activity in tumours of both colonic and gastric origin, and toxic effects of the drug to the digestive tract, led to phase I trials focusing largely on gastrointestinal malignancies. In these initial trials, myelosuppression was identified as the primary dose-limiting toxic effect. Although CPT had impressive antineoplastic activity, phase II evaluation was terminated when severe and unpredictable toxicities, including severe haemorrhagic cystitis, were observed (Eckardt et al., 1995). Poor aqueous solubility also precluded further development. Interest was then focused on the development of water-soluble

synthetic analogous, such as topotecan, which had an improved toxicity profile and broad-spectrum antitumour activity (Kingsbury et al., 1991).

Preclinical models have demonstrated that TPT is active against many tumours types, including adenocarcinomas of the ovary and colon, tumours of the central nervous systems, and sarcomas. During phase I assessment, evidence of activity was most promising when TPT was administered on an i.v. daily x5 schedule and a dose of 1.5 mg/m^2/day was selected for phase II/III evaluation (Saltz et al., 1993). This regimen, which is associated with plasma concentrations of the lacton form of about 0.1 μM (Rowinsky et al., 1992), is used against recurrent ovarian cancer, relapsed small cell lung cancer (SCLC), non-small cell lung cancer, colon cancer, and breast cancer, as well as haematological malignancies (Héron, 1998; Hochster et al., 1999). As reported by Schoemaker et al. (2002), the efficacy of this schedule of treatment could be explained by the increased topoisomerase I level observed after repeated TPT administration.

The interest about clinical role of TPT was focused also on its use in combination regimens. Reports of a number of early-phase studies in ovarian cancer and SCLC have shown activity for TPT in combination with DDP and paclitaxel (Frasci et al., 1999; Frasci et al., 2001).

4.2 RESULTS

Exponentially growing IGROV1 cells were treated for 1h with 0.05, 0.2, 1, 10, 100 μM TPT. We measured the following quantities related to the cell kinetics after treatment: overall (absolute) cell number, flow cytometric DNA histograms, biparametric DNA-BrdUrd flow cytometric histograms using two protocols (pulse-and-chase, pulse labelling).

4.2.1 Experimental Data

Figure 4.1 shows the growth curves after treatment from 0.05 μM, with almost no difference from controls, to 10 μM where cell number was stable up to 48h and then increased, and 100 μM, where no regrowth was observed up to the end of observation (96h). 1 μM would represent the IC_{50} on a 72-h growth inhibition test. Controls and 0.05-μM treated cells reached sub-confluence at 72h, while 0.2-μM treated cells continued to grow up to 96h. The 72-96h interval was included in the subsequent analyses only for 0.2 μM and higher TPT concentrations, being also 0.05 μM flow cytometric data similar to controls.

Flow cytometric DNA histograms of control and treated samples are shown in figure 4.2. Simple visual inspection of the histograms shows departures from the steady-state distribution of controls with 1-10 μM (increased percentage of cells within S at 6h, within G_2M at 24h), and 100 μM (debris and high late S and G_2M peak at 24-48h, high G_2M peak at 96h).

Short-term effects of TPT were evaluated by a pulse-and-chase experiment. Cells were exposed to BrdUrd in the last 20 min of treatment, allowing DNA-synthesizing cells to incorporate BrdUrd, becoming "BrdUrd-positive", and were collected 6h later. The resulting biparametric DNA-BrdUrd plots are shown in figure 4.3. They indicate the movement of the cells in the cell cycle in the first 6h after treatment. In untreated samples BrdUrd-positive cells that occupied S phase at 0h were distributed within late S, G_2M and G_1 phases at 6h. A dose-dependent delay was observed in treated samples. In 0.2-μM treated sample the cloud of BrdUrd-positive cells covered the middle S to G_2M part of the cell cycle with no detectable cells in G_1, after mitosis. The similarity of the 10 and 100 μM plots at 6h with controls at 0h indicates the complete freezing of the cell cycle. However DNA

synthesis was not inhibited at 0h, in fact at the end of the 1-h treatment, BrdUrd was incorporated even by 100-μM treated cells.

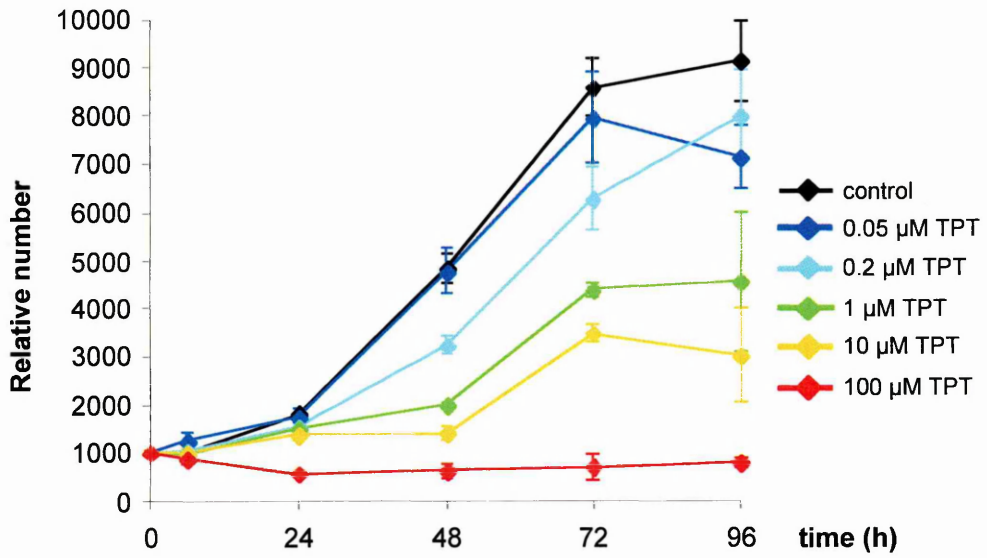

Figure 4.1: Growth curves of IGROV1 cells after 0.05, 0.2, 1, 10, 100 μM TPT for 1h, measured by Coulter Counter. Each point is an average of at least three replicate flasks.

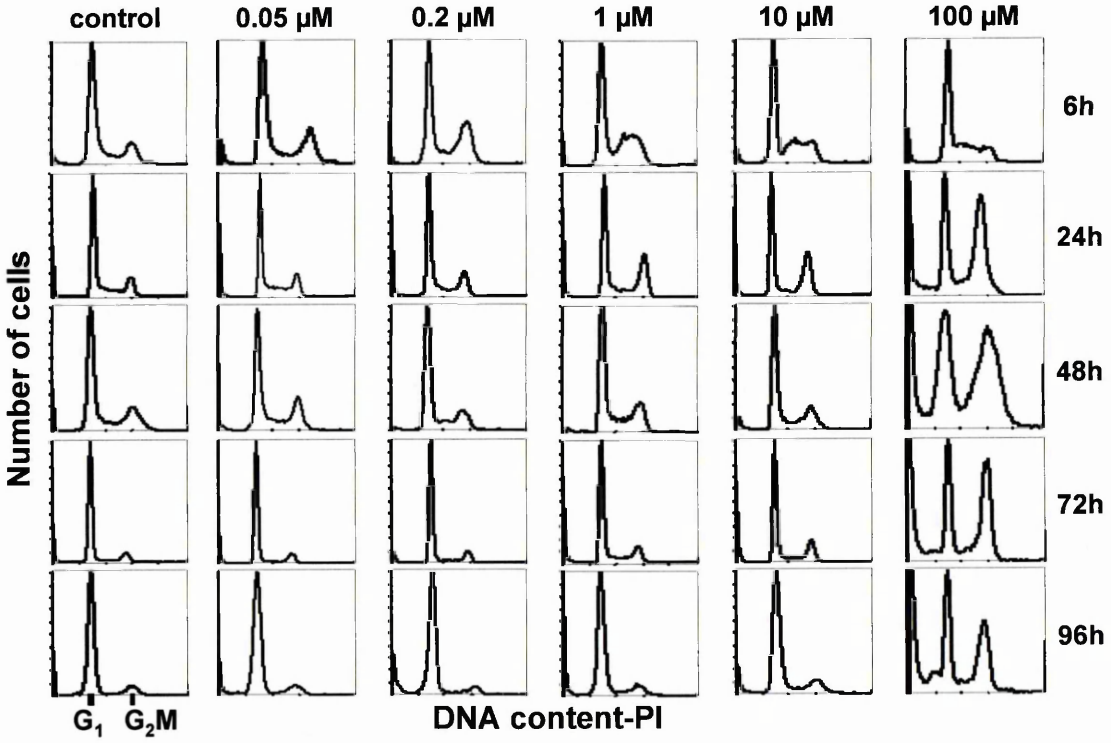

Figure 4.2: Time-course of DNA histograms after 0.05, 0.2, 1, 10 and 100 μM TPT for 1h. DNA corresponding to G_1 and G_2M cells is indicated. Persistent accumulation in the G_2M peak is particularly evident in the 100 μM histograms.

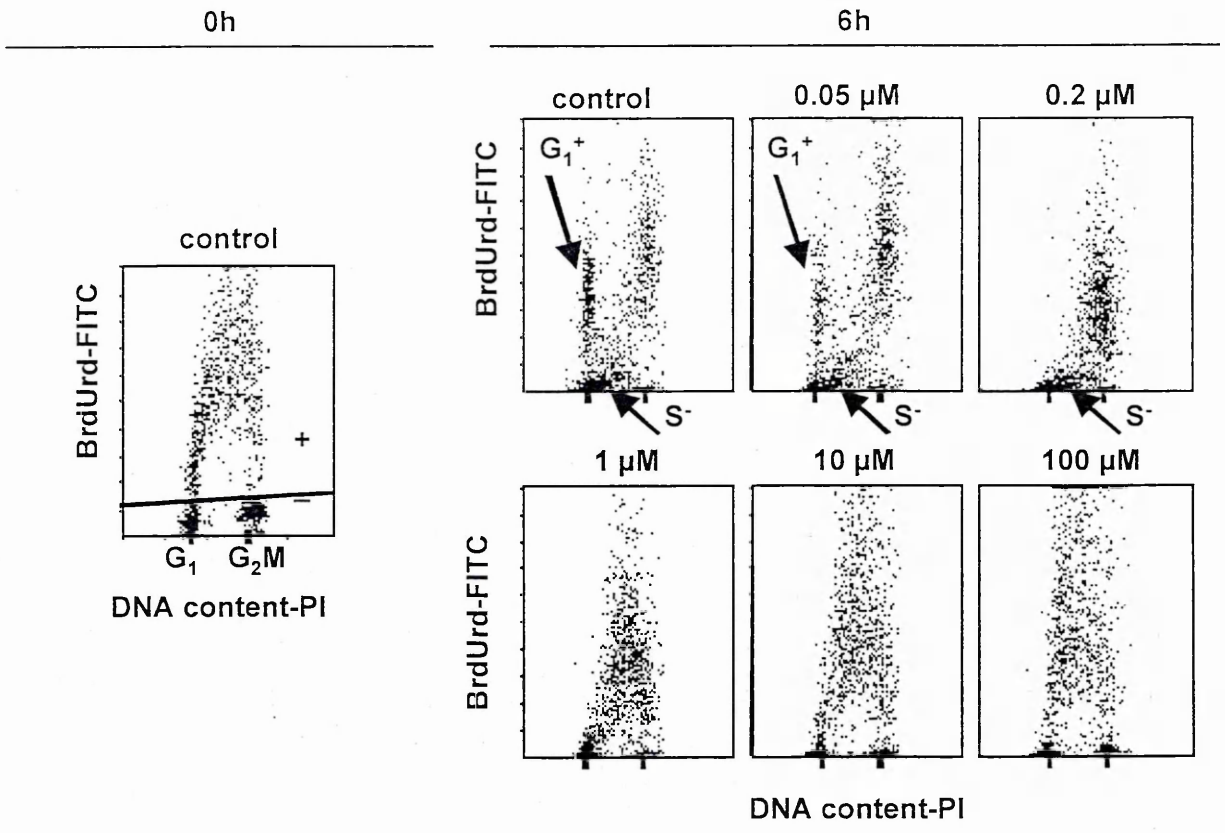

Figure 4.3: Biparametric PI-fluorescence (DNA content) and FITC-fluorescence (BrdUrd content) plots. Cells incorporated BrdUrd 20 min before the end of the 1h-treatment and were harvested 6h after the treatment (BrdUrd pulse-and-chase). Cells were considered BrdUrd-positive (in the S phase at the time of treatment, 0h) when detected above the straight line (left panel). BrdUrd-positive cells with G_1 DNA content (G_1+) at 6h were born from mitosis of cells in S phase at the time of treatment. G_1 BrdUrd-positive cells are present only in the control and in samples treated with the lowest concentration of TPT. BrdUrd-negative cells did not flow from G_1 to S in samples treated with 1 µM or higher TPT concentrations (cells were detected in the "S-" region at 6h only in controls and samples treated with 0.05 and 0.2 µM).

The mathematical model previously described (see section 3.6) becomes essential in order to combine all these experimental data and to interpret them in terms of

the underlying cell cycle effects (blocking activity in G_1 and G_2M, death rate and recycling of blocked cells, reduction of DNA synthesis rate and death rate of S-phase cells), looking for scenario(s) in which all data are coherently explained. During the simulation we tested hundreds of sets of values of blocking activity, death rate and recycling rate, looking for those that enabled us to reproduce the observation within the experimental precision.

We started the simulation testing the hypothesis that TPT had cytotoxic and cytostatic effects only on cells that were in S phase at the time of treatment (BrdUrd positive). The results are shown in figure 4.4. In the samples treated with the lowest drug concentrations this hypothesis seemed to be acceptable, in fact it was possible to reproduce the data within the experimental error, but when the drug concentration increased we were not able to fit the data any more.

Thus, the simulation falsified the hypothesis that TPT had an effect only on cells in S phase during treatment. In fact we were not able to reproduce the cell number and the flow cytometric percentages of the samples treated with TPT concentrations higher than 0.2 μM. Moreover, as shown in figure 4.3, BrdUrd-negative cells in G_1 at the time of treatment were unable to go through S phase, at least in the first 6h and with 1 μM or higher TPT concentrations.

However, the experimental data available at this point were too few to clarify whether the effects in BrdUrd-positive and BrdUrd-negative cells were different, because concurrent scenarios simulated the data within the range of the experimental error. Thus, additional experiments were run, using two different BrdUrd methods.

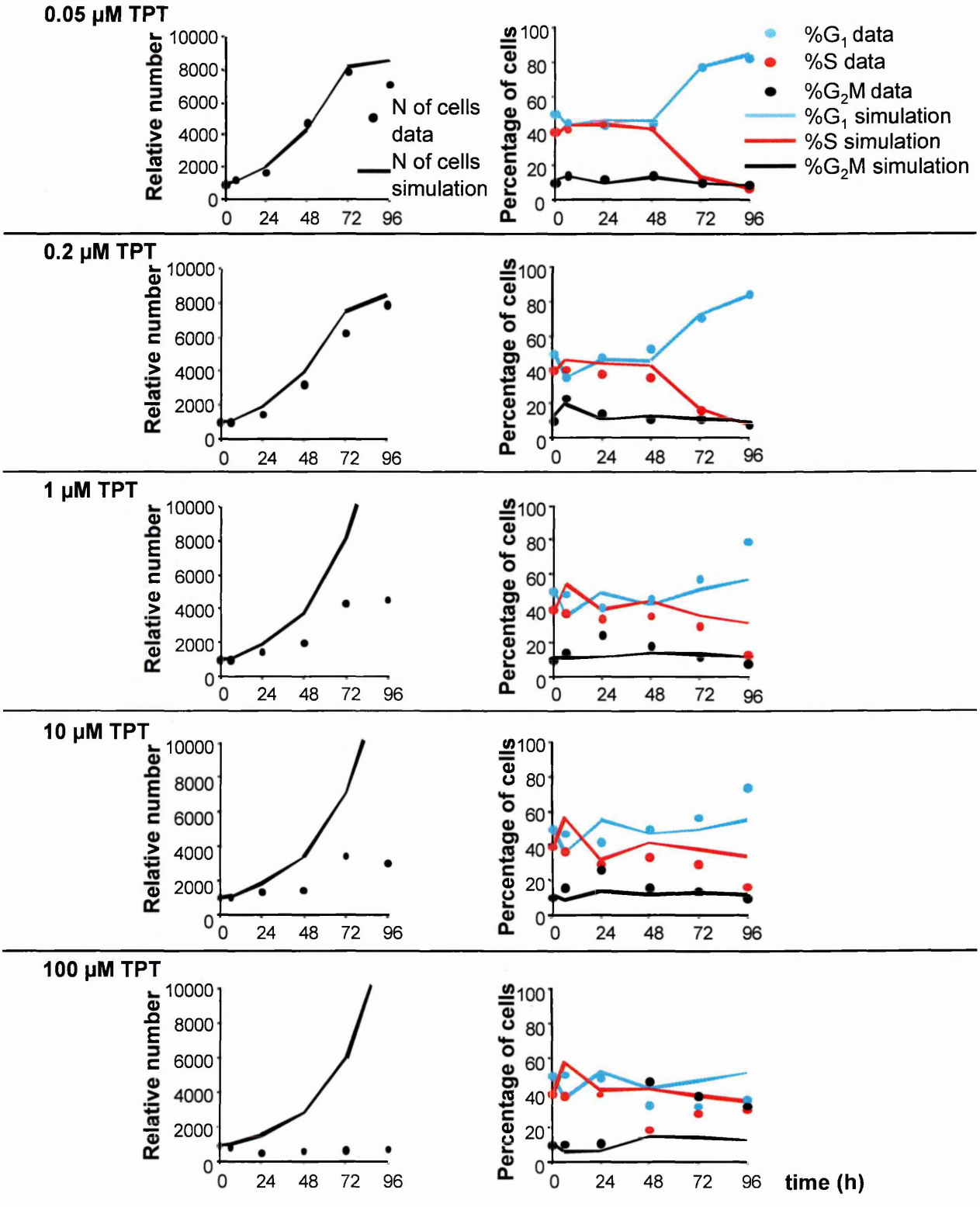

Figure 4.4: Results of the simulation obtained supposing that TPT had cytostatic and cytotoxic effects only on cells that were in S phase at the time of treatment.

The BrdUrd labelling experiment (figure 4.5a), based on exposure to BrdUrd at a given time after treatment, immediately followed by cell harvesting and fixation, serves to qualitatively monitor the DNA synthesis rate of S-phase cells. At 48h BrdUrd incorporation was similar to controls up to 1 μM, but was strongly reduced at 10 μM and only a few S-phase cells incorporated BrdUrd after treatment with 100 μM TPT. DNA synthesis was completely restored at 96h after 10 μM but was still inhibited in 100-μM treated cells.

In the BrdUrd pulse-and-chase experiment (figure 4.5b), samples were labelled with BrdUrd at the time of treatment and harvested at 72h. BrdUrd-positive cells were <10% even in the samples treated with a low TPT concentration (0.2 μM).

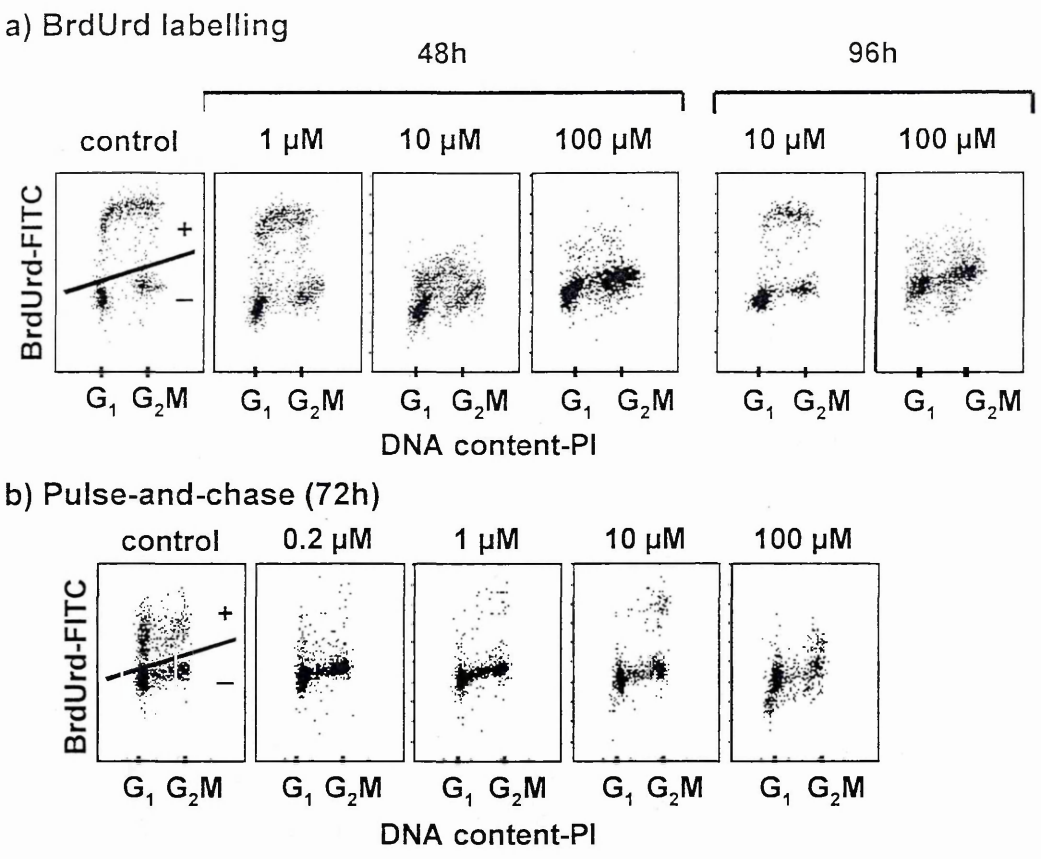

Figure 4.5: Additional BrdUrd labelling (a) and pulse-and-chase (b) experiments.

Panel a (BrdUrd labelling): 48 and 96h after treatment cells were labelled for 20 min with BrdUrd and immediately harvested and fixed, this allowed the qualitatively monitoring of DNA synthesis rate in S-phase cells. At 48h BrdUrd incorporation was similar to controls up to 1 µM, but was strongly reduced at 10 µM. The samples treated with 10 µM TPT restored their DNA synthesis activity by 96h but BrdUrd incorporation was still reduced in 100 µM-treated cells.

Panel b (pulse-and-chase): cells incorporated BrdUrd 20 min before the end of the 1h-treatment and were harvested 72h after treatment. BrdUrd-positive cells amounted to <15% even in the samples treated with 0.2 µM TPT.

4.2.2 Scenario of Cell Cycle Perturbations Underlying Experimental Data

This additional information enabled us to draw a scenario of the time course of events occurring in G_1, S and G_2M consistent with all the data for each TPT concentration. The different panels of figure 4.6 detail this scenario, whose main characteristics are the following:

4.2.2.a Events occurring in G_1 phase (figure 4.6a)

The controls of G_1 phase act during and immediately after treatment on BrdUrd-negative cells, while BrdUrd-positive cells cross G_1 checkpoint only after their first division, which may occur several hours after treatment. BrdUrd-negative cells remained blocked in this phase immediately after treatment. 1 µM TPT was the lowest concentration required to intercept almost all (80-100%) cells in transit from G_1 to S in the interval 0-6h (upper right panel). With lower TPT concentrations, less than 20% of those cells remained blocked. No more BrdUrd-negative cells were blocked after 6h.

The cytotoxic response is characterised by a substantial loss of cells in G_1 immediately after treatment (0-6h) (middle right panel). G_1 blocked BrdUrd-negative cells, that had survived the 0-6h loss, re-entered the cycle before 24h (up to 10 µM) or continued to die, recycling after 48h (100 µM) (lower right panel). BrdUrd-positive cells that could divide and reach G_1 phase were very strongly blocked, for 72h even with 0.2 µM TPT (upper left panel). G_1 block was initially not detectable in BrdUrd-positive cells, simply because no BrdUrd-positive cells were expected to come out G_1 before 24h, and for the same reason the block again became undetectable between 72-96h. There was no evidence of recycling within G_1 blocked BrdUrd-positive cells (lower left panel), meaning that the cells that were able to reach G_1 phase remained blocked there. However, they were few and it was uncertain whether they remained blocked or eventually died.

4.2.2.b Events occurring in S phase (figure 4.6b)

At low concentrations (<1 μM) there was a reduction in the DNA synthesis rate for BrdUrd-positive cells (upper left panel). Even though this effect was lower than 40% it was still well detectable for the samples treated with 0.05 μM TPT and it peaked in the 6-24h interval, where 0.2 μM was enough to almost completely inhibit DNA synthesis. The intensity was lower at the low concentrations but it remained strong at least up to 48h with the highest concentrations. Cell death was limited to BrdUrd-positive cells treated with the highest concentrations of TPT up to 24h (10 μM) or 48h (100 μM) (lower left panel). BrdUrd-negative cells were not delayed when entering S phase (upper right panel). Cells treated outside S phase were able to traverse it like controls.

4.2.2.c Events occurring in G_2M phase (figure 4.6c)

The effects of TPT in G_2M phase were stronger for cells that were in S phase at the time of treatment (left panels) than for cells initially in G_1 or in G_2M (right panels). 80-100% of the BrdUrd-positive cells expected to divide in the 0-6h interval remained blocked in G_2M even when treated with a concentration as low as 0.2 μM. Roughly half of them remained blocked in this phase when treated with 0.05 μM TPT.

The duration of that block was dose-dependent and cells arriving in G_2M continued to be blocked up to 24h (0.2 μM), 48h (1-10 μM) and at least 72h with the very high 100 μM treatment (upper left panel). Once blocked, cells were unable to recycle (not shown) and some of them eventually died (lower left panel). The pattern of the effects in G_2M of BrdUrd-negative cells was similar but with lower intensity and shorter duration (right-hand panels).

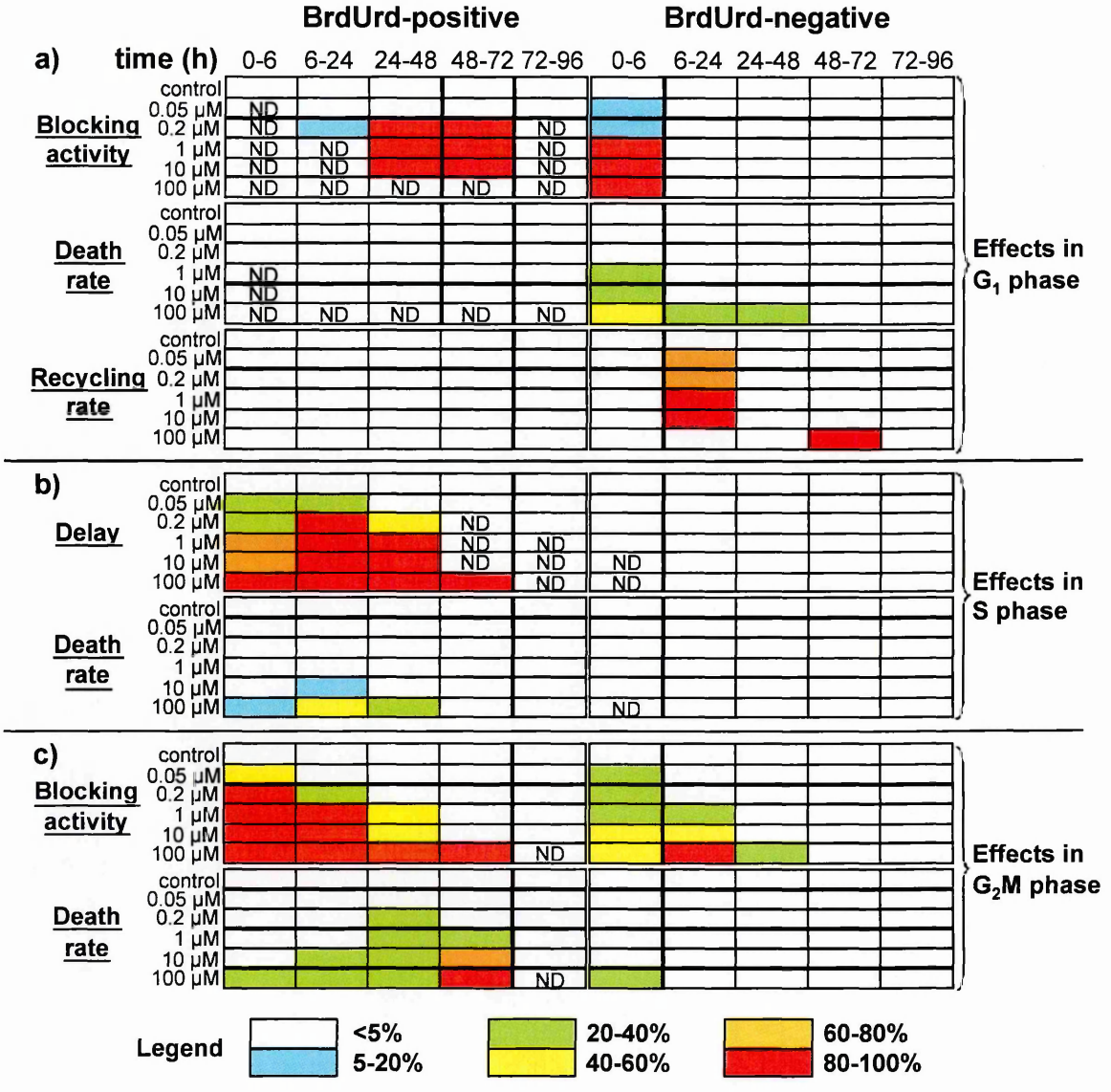

Figure 4.6: Characteristics of the response scenario for a complete reproduction of the experimental data. The blocking activity is represented as the percentage of cells that remain blocked among those traversing G_1 or G_2M in the time interval indicated. The death/recycling rates are expressed in terms of the percentages of cells that die/recycle in each time interval, within the compartment of G_1 (or G_2M) blocked cells. In the 0-6h interval the death rate in G_1 or G_2M is applied to both blocked and proliferating cells, because they cannot be distinguished. Parameters whose values are irrelevant are defined ND (non-detectable).

The S-delay rate is equivalent to the percentage reduction of the average DNA synthesis rate.

4.2.3 Sensitivity Analysis of Parameters

The results coming from the study of the sensitivity of the parameters considered in the final scenario (figure 4.6) were reported in figure 4.7. They were obtained as described in the paragraph 3.6.3.e.

This analysis confirmed that BrdUrd-negative cells treated while in G_1 phase remained blocked there for a few hours after drug washout. The high sensitivity of the parameter describing this effect confirmed its short duration. On the other side the presence of long-term blocking activity in BrdUrd-positive cells was confirmed in samples treated with low concentrations. In 100-μM treated cells the presence of a strong inhibition of DNA synthesis followed by a block in G_2M phase able to intercept almost all BrdUrd-positive cells passing through this phase avoided the formation of a population of proliferating cells. It is for this reason that the parameter describing the blocking activity in G_1 phase for BrdUrd-positive cells treated with the highest TPT concentration is not sensitive at all. At the same way the death rate in this phase was sensitive only in presence of a non-negligible subpopulation of blocked cells. However, in some non-detectable situations the dose dependence of the effects could allow the restriction of the range of possible values for each parameter. For instance the presence of a non-zero recycling probability for G_1 blocked cells in samples treated with high drug concentrations made sure the presence of a similar effect also in 0.05 and 0.2-μM treated cells.

The precision of the final estimates of the parameters of S phase delay and G_2M blocking activity resulted high by sensitivity analysis with an exception for long-term effects in BrdUrd-positive cells. In any case this study confirmed the trend illustrated in the final scenario. As observed for the death rate in G_1 phase, the parameters describing this effect in S and G_2M phase was not very sensitive, but the presence of a cell loss in these two phases was confirmed.

In order to simulate the experimental data we did not need to introduce a recycling probability for cells blocked in G_2M phase. However in the samples treated with the lowest drug concentration the small amount of cells blocked in this phase did not allow an estimation of this phenomenon, even though we could not exclude this possibility (not shown).

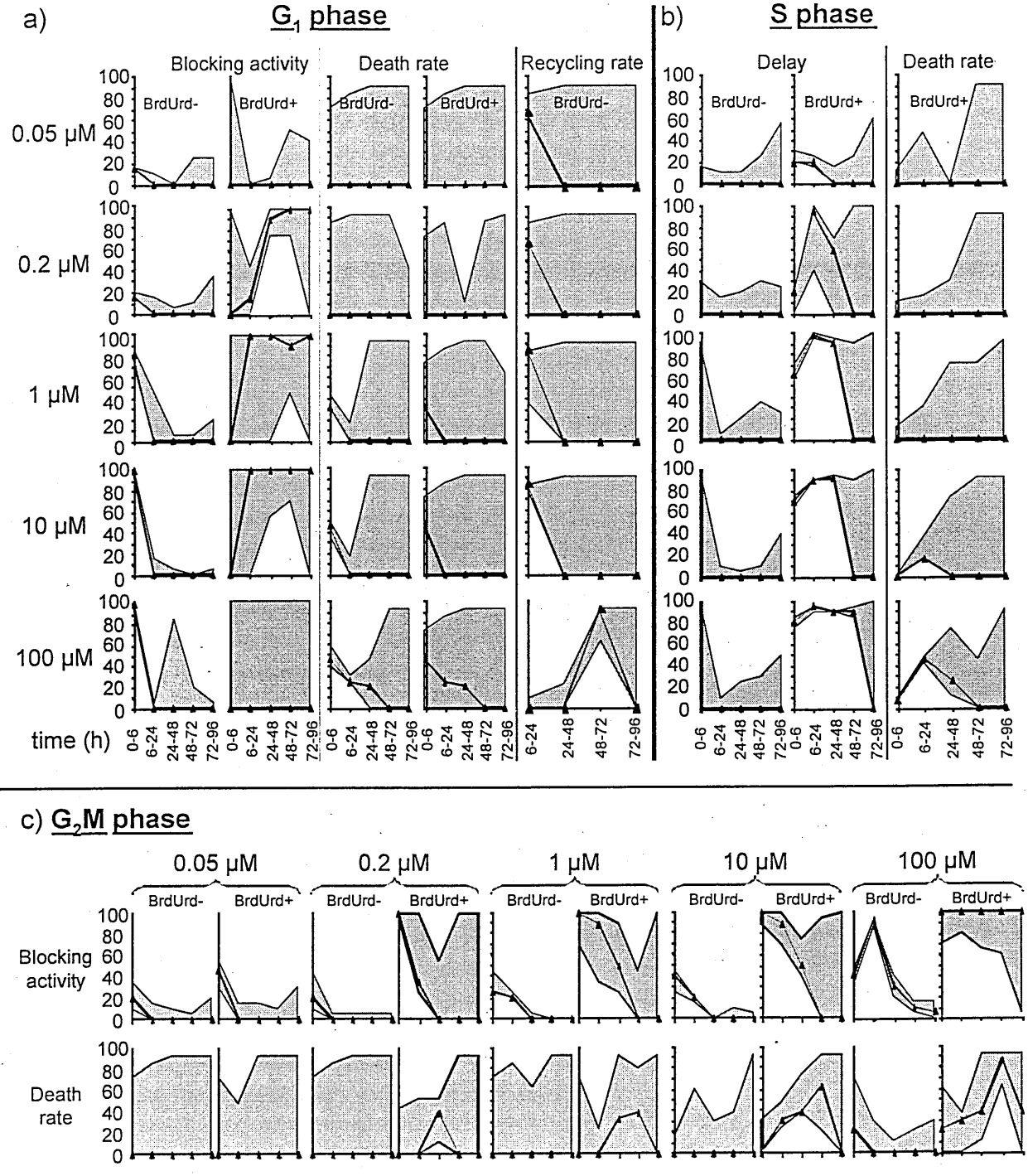

Figure 4.7: Time-course of the parameters used in the simulation. The continuous line represents the value of each parameter as obtained in the final simulation and the filled area represents the range of values of each parameter within which the simulation remained close to the experimental data.

4.2.4 Repeated Treatments

This detailed picture of the response to a single short TPT treatment can be used as a starting point for interpreting the response to more complex treatment schemes. We investigated the effects of repeated 1h TPT treatments with 0.05 or 0.2 μM TPT on three consecutive days, comparing them with single treatments.

The data for the samples treated with 0.05 μM and 0.2 μM TPT only once in this new experiment were correctly simulated with minor modifications of the values of the parameters of the scenario described in figure 4.6, confirming the previous results (not shown). As a starting working hypothesis to simulate the repeated treatments we repeatedly applied the parameters of the single-treatment simulation between 0-6 and 6-24h. As shown in figure 4.8, this led to a correct simulation of the 0.05 μM x 3 treatment (figure 4.8a), but not of 0.2 μM x 3 (figure 4.8b), failing to reproduce the cell cycle percentages at 72h and especially the cell number at 96h. Correct simulation of the 0.2 μM x 3 treatment (figure 4.8c) was obtained using the modified response scenario that differed from a simple repetition of the single treatment effect in two aspects:

- Cell loss in S phase was present after 24h (i.e. after the second treatment), while this was completely absent in the samples treated only once at concentrations lower than 10 μM. This kind of loss occurred mainly in the subset of BrdUrd-negative cells.
- BrdUrd-positive cells remained blocked for a long time in G_2M and part of them were lost after 72h, while for the samples treated only once a weaker cell loss in G_2M was present after 24h recovery.

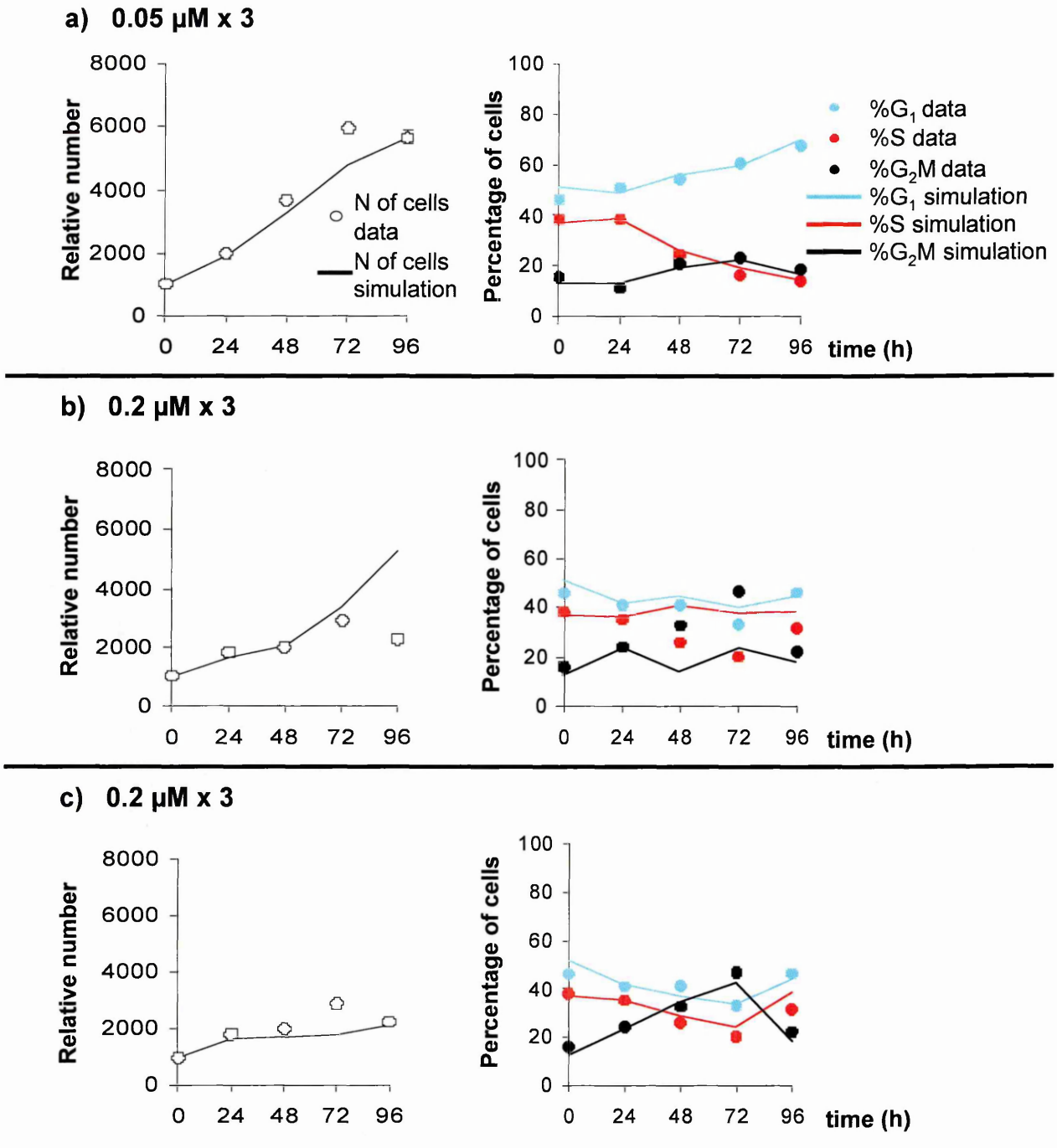

Figure 4.8: Data and simulation of repeated treatments. To reproduce the pattern of the experimental data (DNA analysis and cell count) from the samples treated three times with 0.05 µM TPT we applied three times the scenario describing a single treatment between 0-6 and 6-24h. This led to a correct simulation of the 0.05 µM x 3 treatment (figure 4.8a), but not 0.2 µM x 3 (figure 4.8b). The correct simulation of the 0.2 µM x 3 treatment (figure 4.8c) was obtained using a modified response scenario including cell loss in S phase.

4.2.5 Predictions of the Final Scenario

Once the scenario was defined the simulation gave additional information on the behaviour and heterogeneity of the cell population, that were not directly measurable from the experimental data. In particular we retrieved the percentage of cells blocked in G_1 or in G_2M at each time (figure 4.9) and the total amount of cells that died in 96h (figure 4.10). These quantities measure the impact of a specific block and killing on the growth of the whole cell population. Instead, the values of the parameters in figure 4.6 indicate the strength of the blocking or killing activity, independently of the absolute number of cells that reached that phase. Figure 4.9a reports the time course of the percentages of blocked cells in G_1 and G_2M in the single-treatment experiment. The proportion of cells blocked in G_1 was not negligible compared to the percentage of G_2M blocked. For instance, with 100 µM about 20% of the whole cell population were blocked in G_1 at 48h, despite a decrease in $\%G_1$. In the repeated-treatment experiment (figure 4.9b), the percentage of G_1 blocked cells remained low, while the percentage of G_2M blocked cells increased, reaching a peak of 30% of the whole population after the third 0.2 µM treatment.

The percentage of lost cells in 96h (figure 4.10a) indicates that 0.2 µM x 3 were more "cytotoxic" than a single treatment with 10 µM TPT and there was also a difference in the distribution of lost cells in G_1, S and G_2M phases. In 0.2-µM treated samples a cell loss was present only in G_2M phase, but the mortality was distributed between G_1 and G_2M in 1-µM treated cells. When the drug concentration increased a percentage of cells died also in S phase, this amount reached the 30% in 100-µM treated sample. Even though the cytotoxic effects of 0.2 µM x 3 treatment was higher than that achieved with a single treatment with 10

μM TPT there was not cell loss in G_1 phase, in this case the mortality was distributed between S and G_2M phase.

The information obtained with a colony assay (figure 4.10b) allowed us to confirm the data deduced with our model.

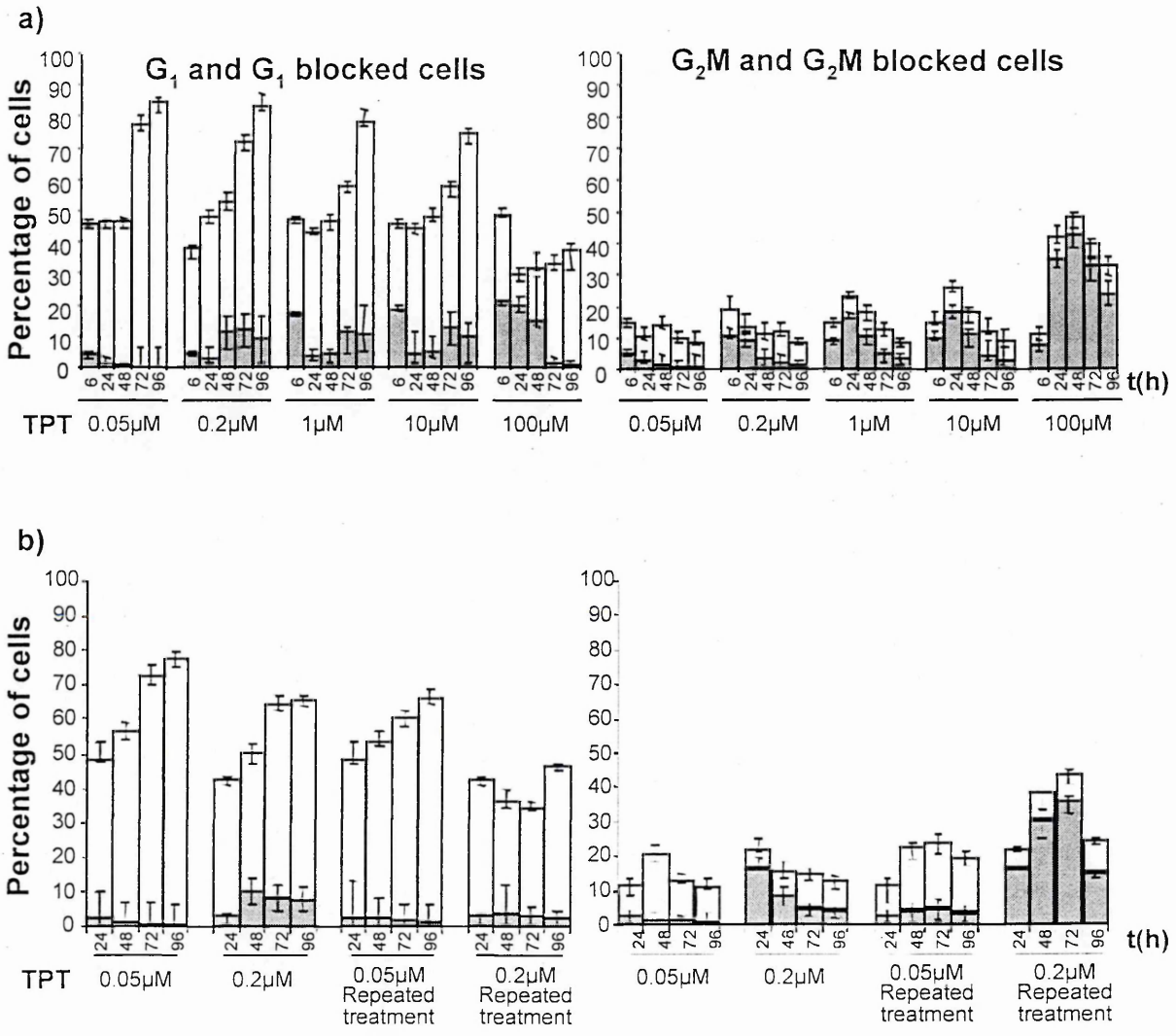

Figure 4.9: Dose- and time-dependence of the percentage of total (full height of the bars) and blocked (height of the filled area of the bars) cells in G_1 and in G_2M. This serves to evaluate the impact of the blocking effect on the cell population after treatment with 0.05, 0.2, 1, 10 and 100 μM TPT (panel a) and after repeated treatments (panel b). The error bars in the histograms indicate of the range where different simulations give predictions fitting the data within the experimental error.

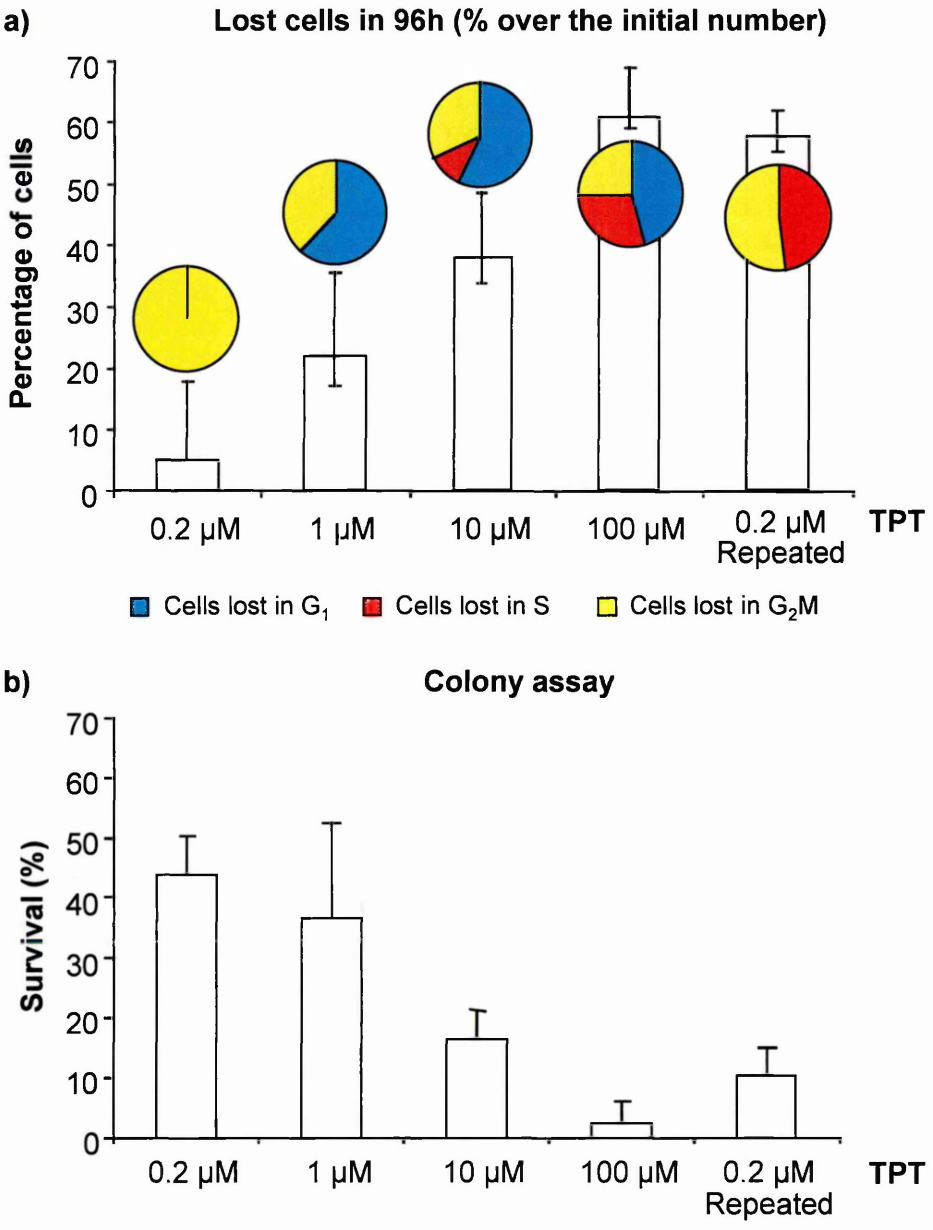

Figure 4.10: Panel a: Total percentage of dead cells in 96h obtained from the simulation. The pies above the columns of the histograms give the distribution of lost cells in the different cell cycle phases. The error bars were calculated as reported in figure 4.8. Panel b: Survival fraction measured by a colony assay. For this test every percentage is the average of four replicates.

Both the simulation and the colony assay confirmed that 0.2 µM x 3 was more "cytotoxic" than single treatment with 10 µM TPT.

4.3 DISCUSSION

In the present study we quantified the response of human ovarian cancer cells to a short TPT treatment, unravelling the complex dose- and time-dependence of the block, delay, recycling from block and death effects.

Analysis of the effect descriptors allows us to focus on a certain phase and see what happens when the cells pass through it. This analysis gave a pattern of time- and dose-dependence of the cellular response to TPT much more complex than cell cycle analyses reported in the literature. Indeed early reports of the cell cycle perturbations induced by CPT and its derivatives stressed S-phase cytotoxicity (Li et al., 1972), but in particular dose ranges and using synchronisation techniques where S-phase cells are just released from an artificial block. In these studies, G_2-enriched fractions appeared much less sensitive than S-phase cells, despite the presence of considerable S-phase contaminants. In our opinion factors other than phase specificity, like the time from release of the synchronising block, may play a role in the outcome of this kind of experiments. For instance, in repeated treatment the cells that remained blocked in G_1 phase after the first TPT treatment where more sensitive to the second treatment and many of them were killed when released from the block.

Our results are not in contradiction with these observations and with those made by further studies about cell cycle effects induced by camptothecins (McDonald and Brown, 1998; Taron et al., 2000; Feeney et al., 2003), but they introduce a much deeper level of understanding, making a clear distinction between cytotoxic and cytostatic effects and analysing their dose-dependence. Even though TPT is supposed to be S-phase specific, it was impossible to account for our experimental data assuming cytotoxic and cytostatic effects only on BrdUrd-positive cells. As shown in the final scenario (figure 4.6), both BrdUrd-positive and

BrdUrd-negative cells contributed to the overall effects, interacting with all cell cycle controls while traversing each phase.

The challenge of a short TPT treatment caused prompt activation of the G_1 block, in which the cells processed the damage rapidly, committing some cells to death or succeeding in repairing others which were able to recycle in the 6-24h interval. Roughly half the G_2M-treated cells remained blocked there but the fate of the other half is less clear, because after division they mixed with the much more numerous subpopulation of G_1 cells. Cells treated while traversing S phase follow a quite different path and their outcome was decided over a very long time. Most of them were delayed in their progression of S phase, experienced a G_2M block, and died at a low rate over a long period, up to 72h. Even with a concentration as low as 0.2 μM, less than 15% of the population present at the end of the observation (96h) were cells treated in S phase or their descendants, but this is due more to the prolonged inhibition of proliferation, while surviving BrdUrd-negative cells multiplied by subsequent divisions, than to selective cell loss.

It is important to note that the events in G_1 phase for BrdUrd-positive and BrdUrd-negative cells are quite different. The cells exposed to the drug while in G_1 (most of them) or in G_2M remained blocked in G_1 immediately after treatment, preventing them starting S phase but only for a short period (≤6h). The block was weak with low concentrations and blocked cells were able to recycle in the 6-24h interval. At higher concentrations (1-10 μM) the block was almost complete and there was some lethality within 6h. With 100 μM cell loss was more extensive, longer-lasting and residual blocked cells were able to recycle only after 48h. Few BrdUrd-positive cells could divide and reach G_1 with concentrations ≥1 μM, but they were unable to progress further to S, suggesting that, although damaged by TPT, they had bypassed the previous G_2M checkpoint. Thus the G_1 checkpoint was stricter or more sensitive to intercept and block damaged cells.

Our data were not sensitive enough to clarify at which point of G_1 these events occur and the model arbitrarily sets the G_1 block at the end of the phase. The observation that almost no cells entered S phase in the first 6h suggests that the block is at the G_1/S border (i.e. just before the onset of DNA synthesis) or throughout the phase. At least at the higher concentration block and cell loss probably occur throughout the phase, because the whole cell cycle progression is frozen and the amount of cells lost is incompatible with the (few) cells expected to reach the G_1/S border in that interval.

Simulation also allows us to evaluate the time-course of the overall cell loss, irrespective of the phase in which cells were actually lost, but still separately within the subpopulation of BrdUrd-positive and negative cells. BrdUrd-negative cells are lost mainly in G_1, immediately after treatment (from 1 µM), while BrdUrd-positive cells are lost mainly in G_2M, over a longer period, from 0 to 72h at the highest dose, 6-72h with 10 µM, 24-72h with 1 µM and 24-48h with the 0.2 µM.

In the whole 0-96h interval, although more BrdUrd-positive cells were lost, the short-term loss of BrdUrd-negative cells was not negligible at 1 µM and above. For instance, the simulation of 1 µM treatment suggested that 20% of the cells treated in G_1 (or G_2M) were killed in the 0-6h interval, against 30% of cells treated in S phase, mainly in the 24-72h interval.

These findings on cell cycle perturbations can be linked to published data at the molecular level. The primary topoisomerase I-mediated DNA lesions are single-strand breaks, but a time-dependent formation of DNA double-strand breaks is expected as a consequence of collisions between the replication fork and topoisomerase I-DNA cleavage complex (Zuco et al., 2003). As a consequence of DNA double-strand breaks, Chk2 phosphorylation occurs in an ATM-dependent manner (Chaturvedi et al., 1999). This should be in agreement with the theory that ATM activates a pathway of inhibition of DNA synthesis after double-strand

breakage (Falck et al., 2002), and is also a possible explanation of the slowing down of the BrdUrd-positive cells in S phase that we quantify in our simulation.

The block in G_2M was associated with impaired activation of CDC2-cyclin B complexes (Tsao et al., 1992). This is probably caused by ATR-induced phosphorylation of Chk1, which may play an important role in the cell cycle responses and survival after treatment with topoisomerase I poisons (Cliby et al., 2002).

The molecular origin of the G_1 block of camptothecins has not been investigated, to our knowledge. We found two kinds of G_1 block: one was strong but temporary, rapidly leading to cell death or recovery (in BrdUrd-negative cells), the other was lasting (in BrdUrd-positive cells). These findings fit with the general view of two successive waves of cell cycle checkpoint responses at G_1. The first is p53-independent and exploits a pathway where Cdc25A phosphorylation and degradation play a key role. In line with the observation that DNA single strand-breaks are rapidly reversed 1h after drug removal (Zuco et al., 2003) and that the cleavable complexes are rapidly eliminated when TPT is removed from the external medium (Feeney et al., 2003) we assume that in BrdUrd-negative cells only a single strand-break occurs, leading to the short-term response driven by the p53-independent pathway.

The second response is p53-dependent and might well be activated in our IGROV1 cells, which possess wild type p53. The p53-dependent response is expected to be sustainable for a long time (Bartek and Lukas, 2001). Agents in this pathway might also be engaged outside G_1, with a role in cell cycle delays or cell death in S and G_2M phases; these are the effects experienced by many BrdUrd-positive cells, which never had a chance to reach G_1. Feeney et al. found that after TPT treatment p53 expression increased more in S and G_2M cells than in G_1 cells

and the high level lasted a long time (Feeney et al., 2003). There is also evidence of activation of p53-dependent responses outside G_1 (Smits and Medema, 2001). Thus the G_2M effects in BrdUrd-positive cells may originate from the activation of p53-dependent pathways, and the fact that they also led to a late G_1 block is merely a consequence of the cell kinetics (these cells reached G_1 only after several hours) and not of delayed activation of the pathway.

After studying the response to a single short treatment we tested a more complicated schedule, i.e. daily repeated 0.05 or 0.2 μM TPT. These drug concentrations were similar to the plasma concentrations in patients undergoing typical TPT treatments and the schedule is closer to the clinical condition (i.e. 30 min i.v. infusion of 1.5 mg/m^2 on days 1-5 of a 21-day cycle) (Rowinsky et al., 1992; Wall et al., 1992; Schellens et al., 1996). Cell cycle effects of a single dose of 0.05 μM TPT (figure 4.6) vanished after 24h, so we can forecast the response to repeated treatment on the basis of simple 24h cycles of the values of the "effect descriptors" measured with a single treatment. In fact with the 0.05 μM x 3 schedule the data were consistent with a simple repetition of the effect of the single dose. However to fit the data with 0.2 μM x 3, we needed to introduce a loss rate for S phase cells after the second treatment, particularly within BrdUrd-negative cells, which was absent in the cells treated once with this concentration. Instead BrdUrd-positive cells died after remaining blocked for a long time in G_2M. As a result, the total percentage of cells lost in 96h indicates that 0.2 μM x 3 is more lethal than a single dose of 10 μM TPT (figure 4.10a). This was confirmed by a clonogenic assay, even though the survival figures with the two methods do not coincide numerically because of the different experimental conditions. Schoemaker et al. suggested that topoisomerase I increases after repeated

administration (Schoemaker et al., 2002) and this might explain the auto-potentiation at the molecular level.

In conclusion, our approach for analysis of cell cycle perturbations *in vitro* was to consider all the data from different tests and interpret them through a mathematical formulation of the problem. Applying the procedure after *in vitro* treatment with TPT, we found complex but biologically consistent patterns of time- and dose-dependence for each cell cycle effect descriptor, opening the way to a link to the parallel changes in the molecular pathways regulating the specific function described.

In earlier studies (Montalenti et al., 1998; Sena et al., 1999) the simulation model was always used to evaluate the cell response to a pulse-like treatment. This is a necessary step before trying to build up the effect of prolonged or more complex schedules. With the analysis of repeated TPT treatments we demonstrated that the model could be employed to explain more complex treatment schedules. In this case, the simulation clarified the origin of the auto-potentiation observed with one of these schemes.

CHAPTER 5: Cell Cycle Effects of Melphalan

5.1 INTRODUCTION

5.1.1 Biochemical Mechanism of Action of Alkylating Agents

Alkylating agents are highly reactive electrophiles that can potentially react with a large number of nucleophilic sites in mammalian cells, such as N or O atoms, with phosphate groups of DNA, or with S atoms of proteins, linking through their alkyl groups to the target molecule. In particular, the interaction of carbonium ion of these compounds with DNA is commonly considered the main cause of cell toxicity and death. The adducts formed at the N-7 and O-6 positions of guanine, the N-1 and N-3 positions of adenine, the N-3 position of cytosine interfere with DNA replication and transcription events (Ross et al., 1978a; Mattes et al., 1986). Differences in the efficiency of repair of DNA damage and the metabolic inactivation by protecting agents like glutathione partly explain the varying cell sensitivity to these drugs (Redwood and Colvin, 1980; Tew, 1994).

The nitrogen mustard derivative L-phenylalanine mustard (melphalan, L-PAM) is a typical representative of this class of drugs. It presents two chloroethylic reactive radicals of nitrogen mustards and an L-phenylalanine group bounded to the central N atom. L-PAM is actively transported into cells by the high affinity L-amino acid transport system, which also transports the amino acid glutamine and leucine. Bergel and Stock, who synthesized L-PAM in 1953, reasoned that the drug would be concentrated in tumours that actively use phenylalanine or tyrosine, such as malignant melanoma (Bergel and Stock, 1954).

L-PAM is a bifunctional (inter-strand, intra-strand) alkylating agent and its cytotoxic effects are related to its concentrations and the duration of cell exposure. The extent of DNA cross-links increases over time, implying that L-PAM quickly form monoadducts that slowly convert to cytotoxic DNA inter-strand, intra-strand or DNA-protein links (Hansson et al., 1987; O'Connor and Kohn, 1990). Although both inter- and intra-strand cross-links were effective, it was thought that in cells

the inter-strand cross-links would constitute the more effectively lethal lesion, because they are more difficult to repair and they can prevent the separation of the strands necessary for cell division (Lawley and Phillips, 1996).

In addition to the above-mentioned causes of drug resistance, in the case of L-PAM, we have also to consider alterations of the transport mechanism.

5.1.2 Previous Cell Cycle Studies

Alkylating agents such as L-PAM are considered fairly non cycle-specific drugs, being active also against resting cells (Valeriote and van Putten, 1975). In early studies, the differential sensitivity of cells treated *in vitro* in G_1, S or G_2M was studied by centrifugal elutriation or synchronisation, followed by cell survival assay.

Treatment of CHO cells subsequently separated by centrifugal elutriation and analysed by colony assay indicated that G_1 is the most sensitive phase to most alkylating agents, including L-PAM (Murray and Meyn, 1986). Similar results were obtained by synchronising DON cells by mitotic selection (Bhuyan et al., 1972) and human lymphoma cells by thymidine block (Barlogie and Drewinko, 1977). Mid to late S was found the most L-PAM resistant phase of the cell cycle, while there was a tendency for cells in G_2 phase to be more sensitive than cells in late S phase (Barlogie and Drewinko, 1977). The real sensitivity of G_2M was found higher, similar to that of G_1 cells, when a correction to the elutriation data was applied, trying to take off the (strong) contaminant of S cells in the "G_2M" fraction (Linfoot et al., 1986, using a rat brain tumour treated with nitrosoureas). In all these studies, only one or two concentrations of the drug were tested. A dose-response of cell cycle effects of L-PAM was not reported in the literature. Drewinko and Barlogie (1976), using another alkylating agent, Yoshi 864, did a study of this kind. This work suggested that inter-phase differences in sensitivity on the whole dose-

response curves were much less evident than suggested by single, particular concentrations.

Several reports indicated that the phase most affected by alkylating agents with respect to cell progression (cytostatic effect) appears to be G_2, with few reports of inhibition of DNA synthesis. Asynchronous cell populations were shown by DNA flow cytometry to accumulate in G_2M after treatment with several alkylating agents. Both the magnitude and the duration of G_2 block are dependent on the phase of treatment (Barlogie and Drewinko, 1977, using synchronised cells).

In particular, a flow cytometric study of cell cycle effects of L-PAM on an ovarian cancer cell line was supported by Erba et al. (1995) SW626 cells treated with 3.5 µg/ml L-PAM were followed at different times after treatment. At short times after drug washout DNA histograms and BrdUrd dot plots indicated a slowing down of cells through the S phase and a progressive cell accumulation in G_2M. At 18h a pronounced block in G_2 was present and the cells started to overcome the G_2M block only 36h after treatment.

5.1.3 Clinical Use

Alkylating agents are a major class of anticancer drugs with established clinical activity against a broad spectrum of human malignancies (Sarosy et al., 1988; Samuels and Bitran, 1995). In particular, alkylating agent-based chemotherapy was the treatment of choice for primary epithelial ovarian carcinomas prior to the emergence of the platinum compounds in the 1970s (Brodovsky et al., 1984; Wadler et al., 1996). Response rates to oral L-PAM ranged from 15 to 40% in advanced disease (stage III/IV). Starting from this point of view, Hasan et al. (2003) have recently investigated the effectiveness of oral L-PAM as salvage therapy in patients who progressed after platinum-based chemotherapy (Hasan et

al., 2003). But their data suggest that L-PAM has poor activity as second-line therapy agent for this kind of tumour.

However L-PAM is active against a wide spectrum of neoplasms and it is particularly used as single agent in the treatment of multiple myeloma (Selby et al., 1987).

Myelosuppression is the main side toxicity. In standard regimens it is administered orally for 4-7 consecutive days. A dose-response relationship for L-PAM in the treatment of solid tumours was demonstrated by McElwain et al. (1979), who also introduced high-dose regimens (i.v. administration) with autologous bone marrow grafting. High-dose L-PAM is used as consolidative therapy in relapsed Hodgkin's disease, breast cancer and relapsed neuroblastoma. In high-dose L-PAM regimens, after 220 mg/m^2 administration, peak plasma concentrations reach 100 μM (Reece et al., 1988)

5.2 RESULTS

5.2.1 Experimental Data

Exponentially growing IGROV1 cells were treated for 1h with 3, 10, 30, 50, 100, 300 μM of L-PAM. Then we measured the following quantities related to the cell kinetics: overall (absolute) cell number, flow cytometric DNA histograms, biparametric DNA-BrdUrd flow cytometric histograms using the pulse-and-chase protocol.

Figure 5.1 shows the growth curves after treatment. The cells treated with 3 μM L-PAM grew like controls and the number of cells treated with 10 μM decreased only after 48h. From 30 to 300 μM the behaviour of the cells was very similar, the number remaining almost constant until 48h and starting decrease between 48 and 72h.

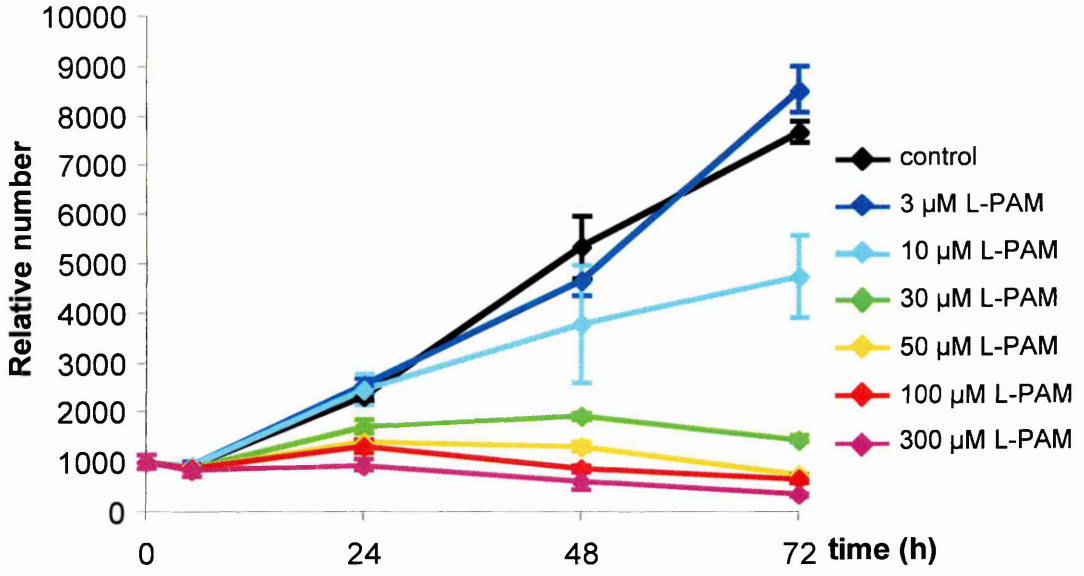

Figure 5.1: Growth curves of IGROV1 cells after 3, 10, 30, 50, 100, 300 μM L-PAM for 1h, measured by Coulter Counter. Each point is an average of at least three replicate flasks.

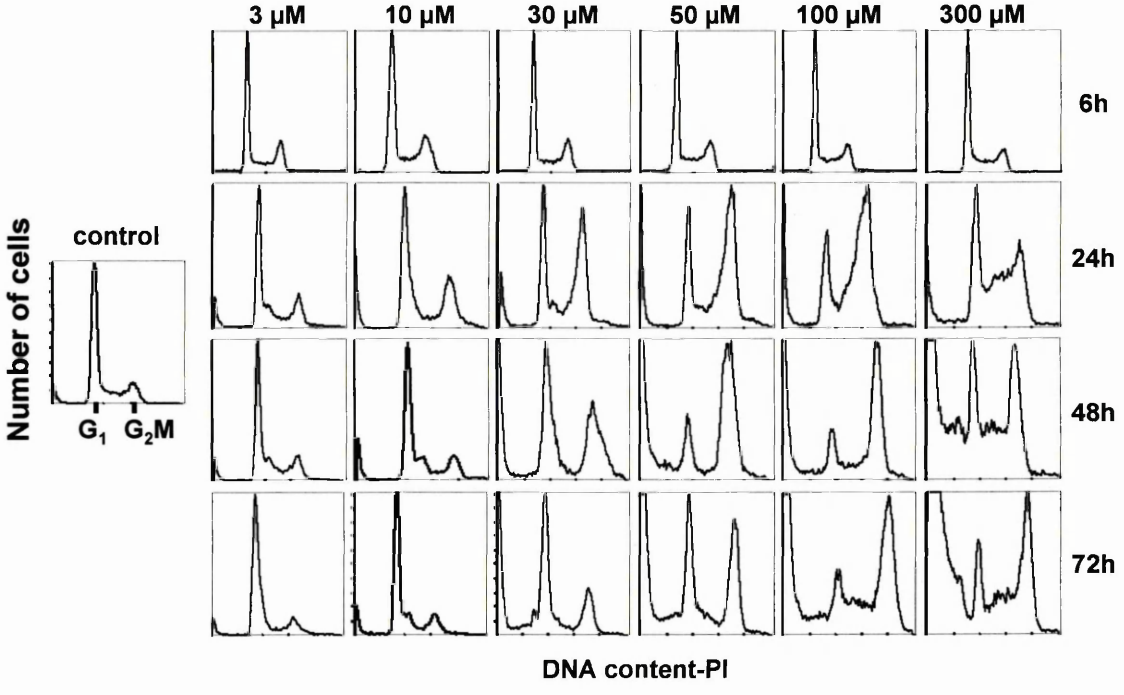

Figure 5.2: Time-course of DNA histograms after 3, 10, 30, 50, 100, 300 μM L-PAM for 1h. DNA corresponding to G_1 and G_2M cells is indicated. Persistent accumulation in the G_2M peak is particularly evident in the 50, 100 and 300 μM histograms, while a large amount of debris (in the region to the left of G_1 peak) is present at 48 and 72h in the cells treated with 300 μM L-PAM.

Flow cytometric DNA histograms of control and treated samples are shown in figure 5.2. Differences between the treated samples and the control were detectable only 24h after treatment when the cells treated with 10, 30, 50 and 100 μM L-PAM accumulated in G_2M phase. The duration of this block was apparently dose-dependent, and for the samples treated with 50 μM and higher concentrations a high percentage of G_2M cells remained blocked up to the end of observation (72h). At 48h the cells treated with the highest concentrations (100 and 300 μM) contained a large amount of debris.

Short-term effects of L-PAM were evaluated by a pulse-and-chase experiment. Cells were exposed to BrdUrd in the last 20 min of treatment, allowing DNA-synthesizing cells to incorporate BrdUrd, becoming "BrdUrd-positive", and were collected 6h later. The resulting biparametric DNA-BrdUrd plots, in figure 5.3a, indicate the movement of the cells in the cycle in the first 6h after treatment. In untreated and in 3-μM treated samples BrdUrd-positive cells that occupied S phase at 0h were distributed in late-S, G_2M and G_1 phases at 6h. In samples treated, with concentrations higher than 3 μM, the percentage of BrdUrd-positive cells in G_1 (G_1+) was lower. This was probably caused more by a block in G_2M than by a delay in S phase, because the movement of BrdUrd-positive cells towards G_2M was visibly reduced only for samples treated with 300 μM L-PAM.

Because more than one scenario of cytotoxic and cytostatic effects might explain the previous data, a BrdUrd pulse-and-chase experiment was subsequently done, collecting cells 72h after treatment and BrdUrd pulse. The BrdUrd dot plots shown in figure 5.3b revealed that more BrdUrd-positive than BrdUrd-negative cells survived 72h after treatment. When the drug concentration increased this difference decreased. The samples treated with 10 or 50 μM L-PAM presented about 80% of BrdUrd-positive cells after 72h, while after 300 μM L-PAM there was only about 55% of BrdUrd-positive cells.

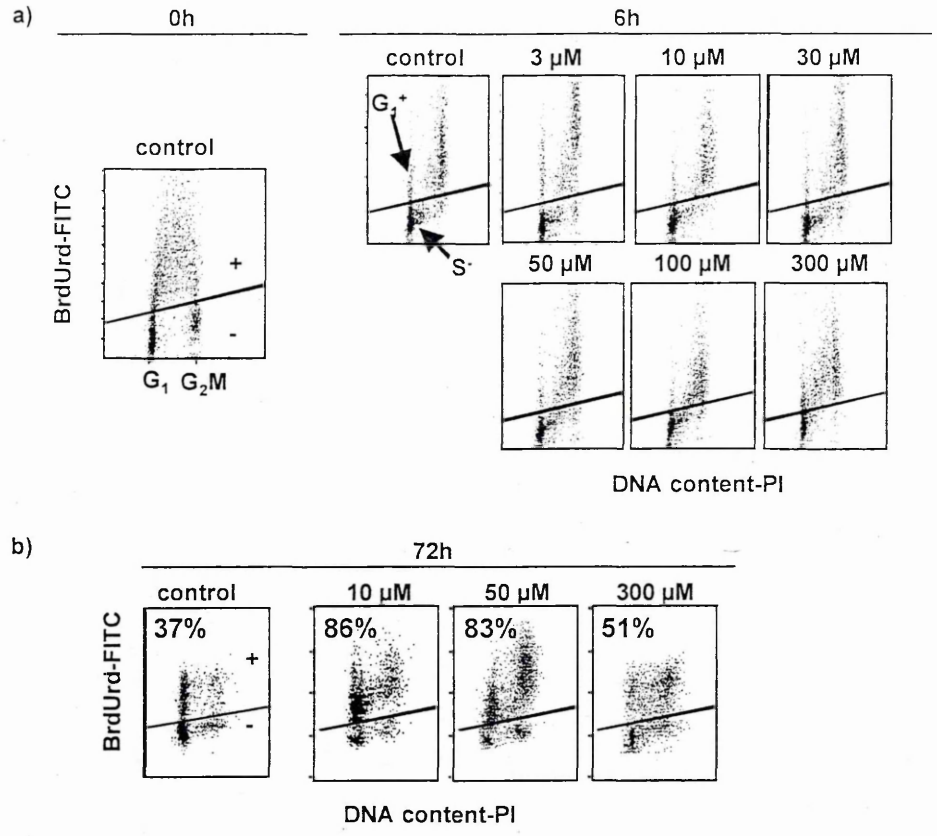

Figure 5.3: Biparametric PI-fluorescence (DNA content) and FITC-fluorescence (BrdUrd content) plots. Cells incorporated BrdUrd 20 min before the end of the 1h-treatment and were harvested after 6h (panel a) and 72h (panel b) (BrdUrd pulse-and-chase). Cells were considered BrdUrd-positive (in the S phase at the time of treatment, 0h) when detected above the line. BrdUrd-positive cells with G_1 DNA content (G_1+) at 6h were born from mitosis of cells in S phase at the time of treatment. G_1 BrdUrd-positive cells are present in the control and in samples treated with the lowest concentration of L-PAM. The percentage of G_1+ cells is lower in samples treated with L-PAM concentrations higher than 3 µM. In the BrdUrd pulse-and-chase experiment 72h after treatment the percentage of BrdUrd-positive cells is higher than that of BrdUrd-negative ones, this difference decreasing as the drug concentration increases.

Six-hour samples were detected by direct immunostaining and are thus represented with a linear BrdUrd scale; 72-h samples were detected by indirect immunostaining and are represented with a logarithmic BrdUrd scale.

Another qualitative picture of the drug effects can be obtained from figure 5.4, where the TUNEL technique confirmed the cell killing in samples treated with the highest drug concentrations. The cells treated with 300 µM L-PAM showed a substantial percentage of dUTP-FITC-positive cells from 24h; 50 and 100 µM L-PAM had cytotoxic effects after 48h.

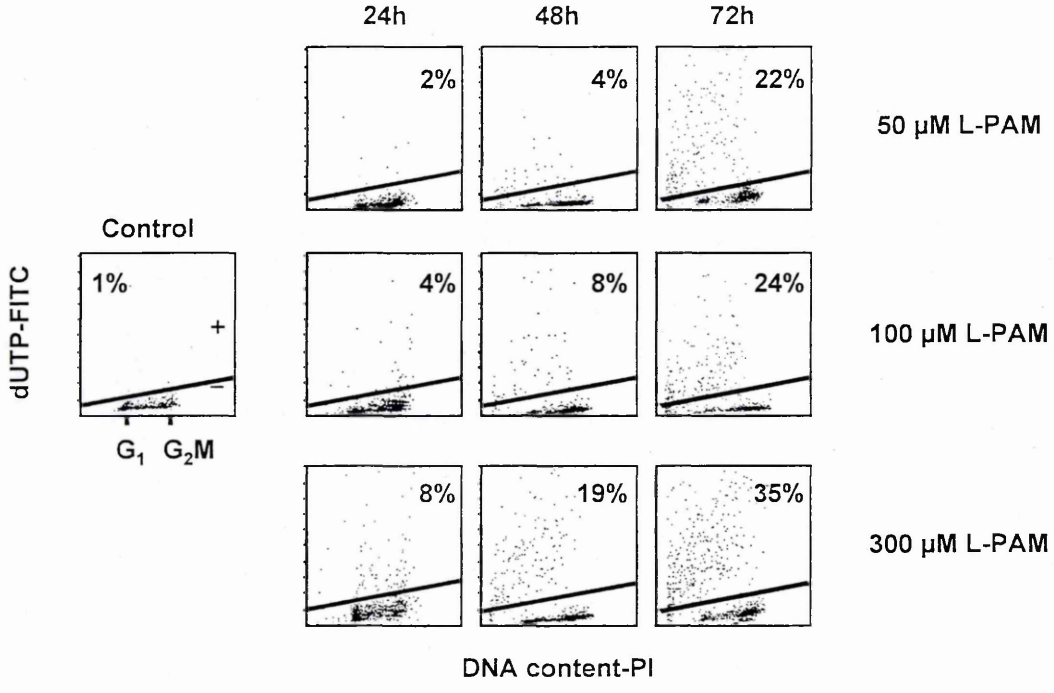

Figure 5.4: Biparametric PI-fluorescence (DNA content) and FITC-fluorescence (dUTP content). Cells with DNA fragmentation induced during apoptosis are dUTP-positive (above the straight line). For the analysis were considered only cells with a DNA content higher than 1/10 of G_1.

5.2.2 Scenario of Cell Cycle Perturbations Underlying Experimental Data

The simulation program determined a unique scenario coherent with all the experiments, taking into account the flow cytometric percentages from DNA histograms, BrdUrd dot-plots and cell count as quantitative data, and the information from the dUTP-assay as qualitative data. Figure 5.5 shows the values

of the parameters constituting the scenario. In each panel the color of a square indicates the parameter strength in a specific interval of time (column) and at a specific L-PAM concentration (row). The parameters are indicated as non-detectable (ND) when there were too few cells in a specific cell cycle phase to establish their value.

5.2.2.a Events in G_1 phase (figure 5.5a)

The molecular controls of G_1 phase act during and immediately after treatment on BrdUrd-negative cells. However the blocking activity was not strong: 5-20% for 30 to 100 μM, or 20-40% for the highest concentrations, of BrdUrd-negative cells remained blocked in this phase immediately after treatment (upper right panel). The duration of the block was dose dependent: it ended 6h after treatment with 30 μM, 24h with 30 and 100 μM, 48h with 300 μM, only at the highest concentration the same blocking activity was observed also in BrdUrd-positive cells (upper left panel).

Cells treated with at least 50 μM and blocked in G_1 died in this phase after 24h (lower panels). The highest concentration was cytotoxic for both BrdUrd-positive and BrdUrd-negative cells blocked in this phase (lower left panel). The recycling rate for cells intercepted by this checkpoint was negligible (not shown).

5.2.2.b Events in S phase (figure 5.5b)

BrdUrd-positive cells that were treated with at least 30 μM L-PAM immediately reduced their DNA synthesis rate. This reduction was either constant or, for the highest concentrations, increased with time, reaching 80-100% between 24h and 72h (top left panel). The behaviour of BrdUrd-negative cells was very similar though the effects were stronger (top right panel). At 24h after treatment both BrdUrd-positive and BrdUrd-negative cells started to die in this phase. Again, this

effect was stronger for BrdUrd-negative cells, with 60-80% of cells traversing the S phase in 24h dying (L-PAM >10 μM), compared to 20-40% of BrdUrd-positive cells (lower panels).

5.2.2.c Events in G_2M phase (figure 5.5c)

The block in G_2M was stronger for cells treated in G_1 and G_2M phase (BrdUrd-negative, top right panel) than for cells treated in S phase (BrdUrd-positive, top left panel). At the lowest concentrations (3 and 10 μM) the block ended 6h after treatment for both BrdUrd-positive and BrdUrd-negative cells, whereas it persisted until 72h for the samples treated with higher concentrations. For BrdUrd-negative cells the intensity of G_2M blocking activity increased after 6h and 60-80% of cells were intercepted by this checkpoint in the samples treated with 50, 100 and 300 μM L-PAM. As shown in the lower panels, cells blocked in G_2M phase started to die 24h after treatment, except for those treated with 3 and 10 μM, where this effect was not detectable. After 6h, 80-100% of cells treated with the highest concentration and blocked in this phase died in each interval.

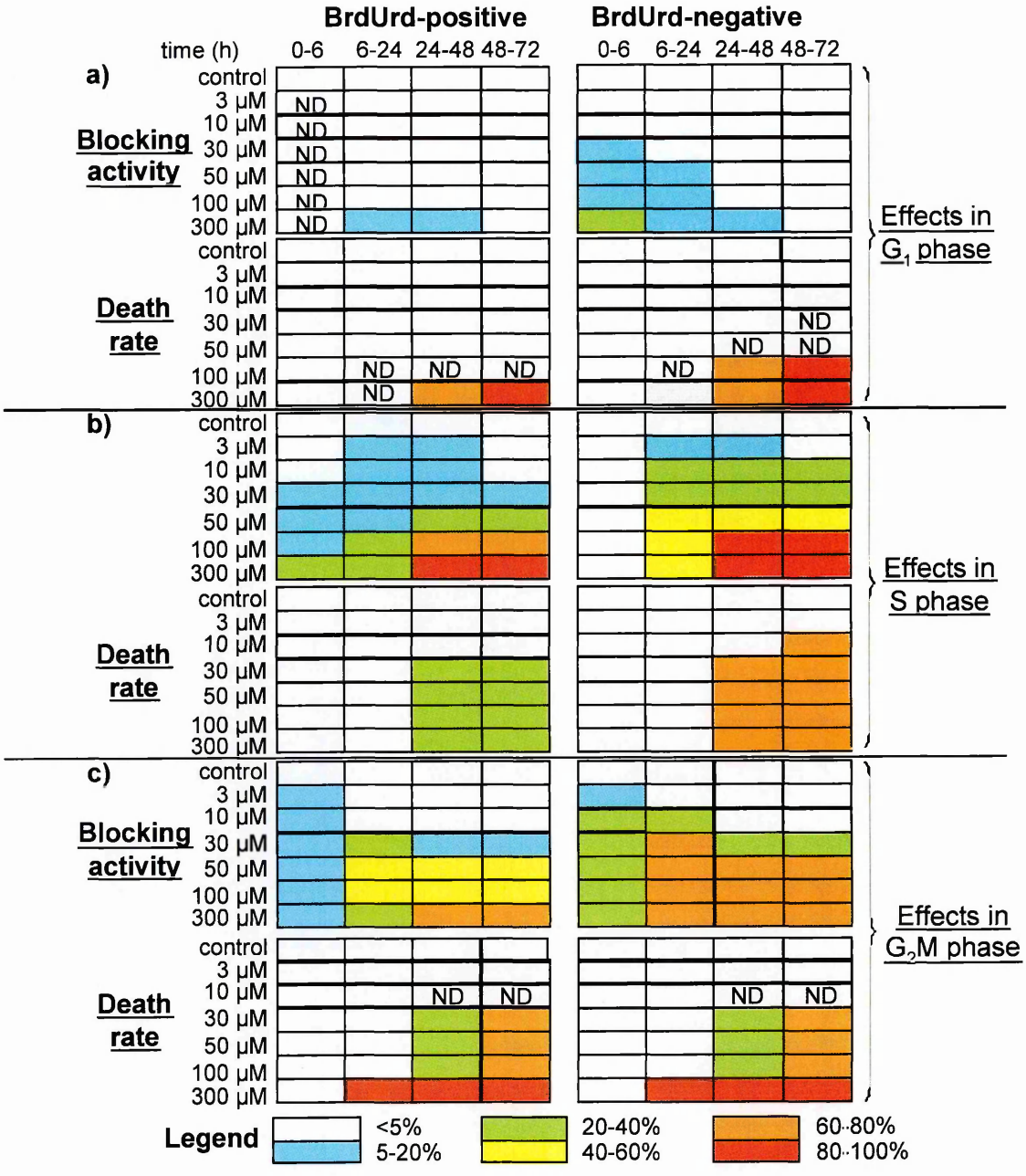

Figure 5.5: The response scenario for complete reproduction of the experimental data. Blocking activity is the percentage of cells that remain blocked among those traversing G_1 or G_2M in the interval indicated. The death/recycling rates are the percentages of cells that die/recycle in each interval, within the compartment of G_1 (or G_2M) blocked cells. In the 0-6h interval the death rate in G_1 or G_2M applies to both blocked and proliferating cells, because they cannot be distinguished. Parameters whose values are irrelevant are defined ND (non-detectable). The S-delay rate is equivalent to the percentage reduction of the average DNA synthesis rate.

5.2.3 Sensitivity Analysis of Parameters

The study of the sensitivity of the parameters considered in the final scenario was performed as described in the paragraph 3.6.3.e.

The parameter of G_1 blocking activity was very sensitive, excluding the presence of strong activity but indicating that a weak activity should necessarily be included at ≥30 μM L-PAM (figure 5.6a). The G_1 blocking activity of BrdUrd-positive cells was irrelevant for the outcome between 0 and 6h, because there was not time for these cells to reach the G_1-S transition, where the block would be detectable. Sensitivity analysis showed that in most cases the parameters of S phase delay (figure 5.6b) and G_2M blocking activity (figure 5.6c) were accurately estimated, confirming in both cases the increase in drug effects with time and drug concentration.

The parameters connected with the loss of G_1 and G_2M blocked cells became sensitive only when a subpopulation of blocked cells was not negligible, and this happened at least 24h after treatment or with high drug concentrations (panels a and c). In these instances, the need to include loss from both G_1 and G_2M was confirmed by the sensitivity analysis. In particular, to maintain the correspondence with the data, for treatment performed with concentrations higher than 100 μM a fairly high loss rate needed to be included among BrdUrd-negative cells blocked in G_1 phase after 24h. This effect could not be detected with 50 μM and at 300 μM a cell loss in G_1 was present and sensitive in both subpopulations of BrdUrd-positive and BrdUrd-negative cells. Lethality among G_2M blocked cells was proved after 24h at ≥30 μM in both BrdUrd-positive and BrdUrd-negative cells, with similar rates, while lethality in S phase was demonstrated at 48h even at 10 μM and at 24h from 30 μM (panel b).

In addition, the sensitivity analysis allowed us to conclude that the presence of recycling was compatible with our data, assuming a higher G_2M blocking activity between 6 and 24h, whereas at longer times this parameter became negligible and was replaced by a loss rate (not shown).

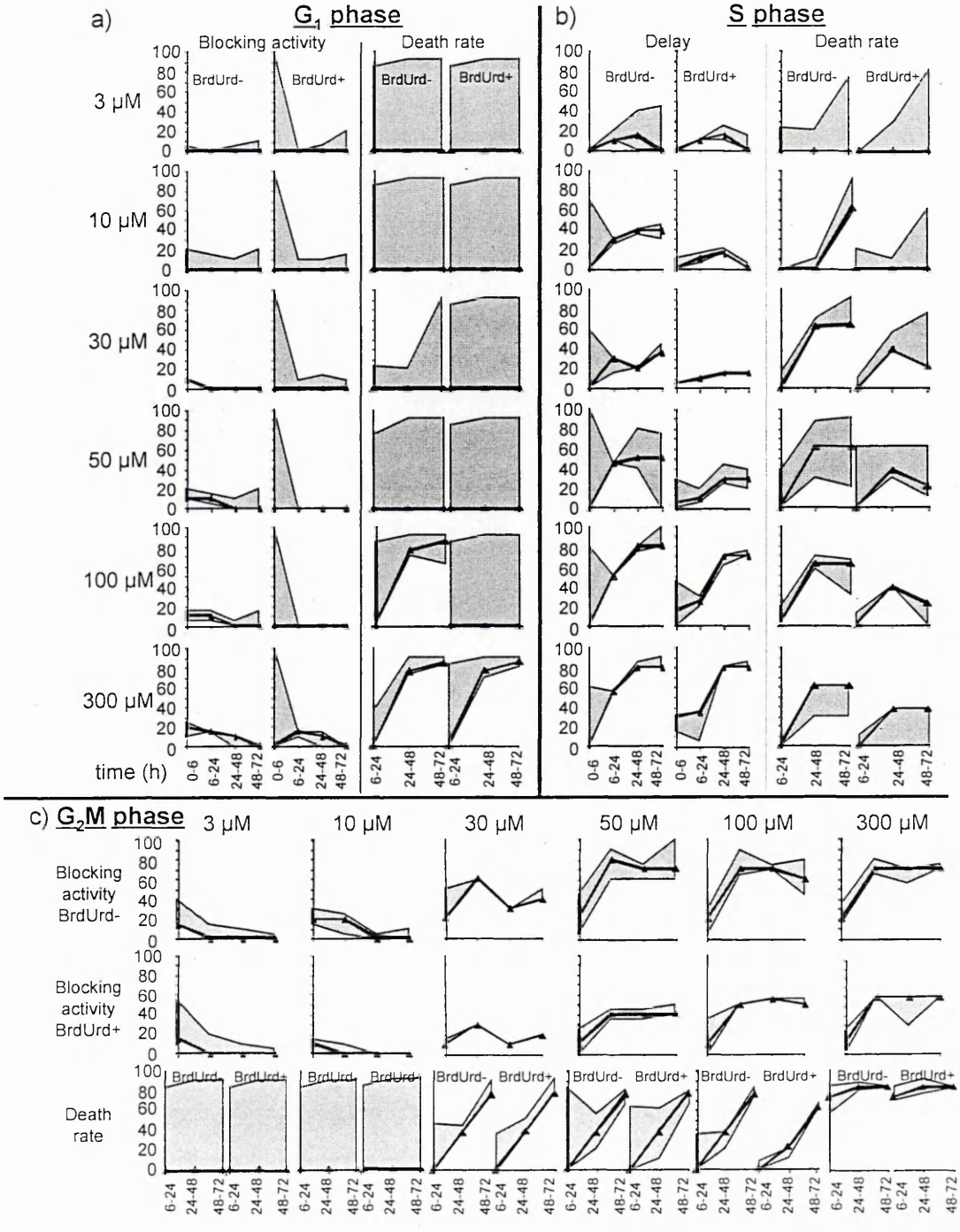

Figure 5.6: Time-course of the parameters used in the simulation. The continuous line represents the value of each parameter as obtained in the final simulation and the filled area represents the range of values of each parameter within which the simulation remained close to the experimental data.

5.2.4 Predictions of the Final Scenario

Once the final scenario is defined, its predictions can be investigated in detail by the simulation program, disclosing information on the behaviour and heterogeneity of the cell population that could not be directly measured from the experimental data. We retrieved from the simulation the percentage of cells blocked in G_1 or in G_2M at each time (figure 5.7) and the total amount of cells dying in the 72h of observation (figure 5.8). The quantities shown in these two figures help to evaluate the impact of a specific block and killing on the growth of the whole cell population. On the other side the values in figure 5.5 indicate the average strength of the blocking or killing activity within the cells that reached that phase, independently of their number.

Figure 5.7 shows the total amount of cells blocked in G_1 or in G_2M compared with the percentage of cells in the same phase. This information could not be directly obtained by flow cytometry, in fact we would not be able to distinguish blocked from cycling cells. The percentage of cells blocked in G_1 was non-zero only for the samples treated with concentrations higher than 30 μM and involved more than 10% of the whole cell population only at the highest concentration (300 μM). The percentage of blocked cells was maximum peaked in the first 24h after treatment (between 10 and 20% of all cells with 300 μM) but it decreased later on, more because of cell loss than because of proliferation of other cells.

At drug concentrations higher than 30 μM the majority of G_2M cells were blocked at 24h. The percentage of blocked G_2M cells rose until 48h, then decreased again, more because of cell loss than because of proliferation of other cells. With the highest concentration, a higher percentage of G_1 blocked cells was seen at 24h than G_2M blocked ones.

The percentage of cells lost in 72h is presented in figure 5.8. Drug concentrations higher than 30 µM had a strong cytotoxic effect, and about 65% of cells died after treatment with 30 µM L-PAM. There were almost no differences between the cytotoxicity of 50 µM and 100 µM. The pies above the columns give the distribution of cells lost in the different cell cycle phases. After 10 µM L-PAM the cytotoxic effect was explained by a loss of cells in S phase. From 30 µM, 60-70% of killed cells died in G_2M, the remainder mostly in S phase. Only at the highest concentration more than 10% of killed cells died in G_1.

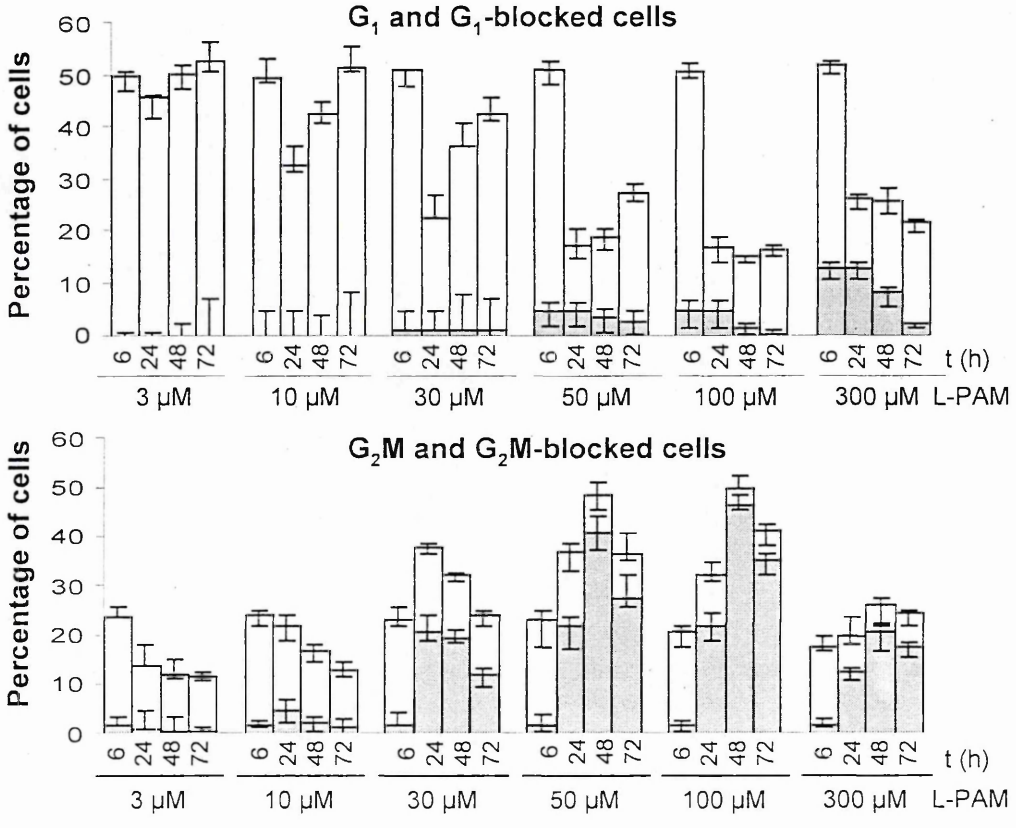

Figure 5.7: Dose-dependence and time-dependence of the percentage of total (full height of the bars) and blocked (height of the filled areas) cells in G_1 and in G_2M. This serves to evaluate the impact of the blocking effect on the cell population after treatment with 3, 10, 30, 50, 100 and 300 µM L-PAM. The error bars indicate the range where different simulations give predictions fitting the data within the experimental error.

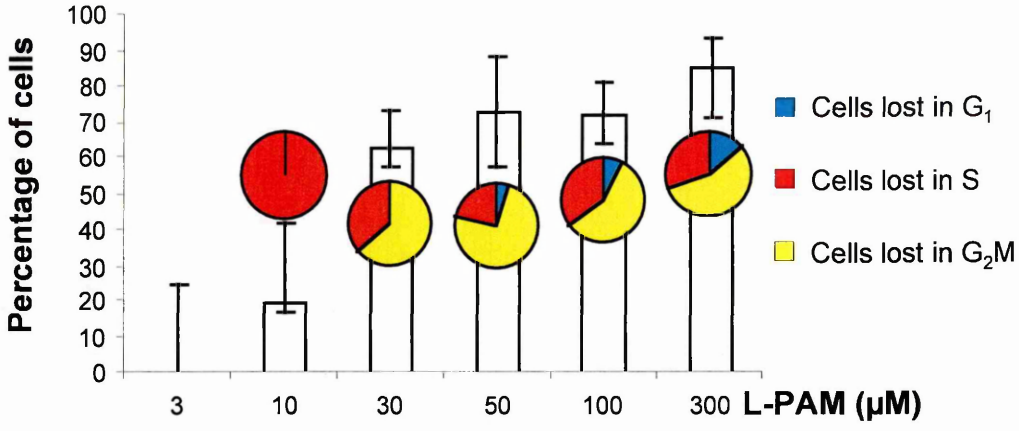

Figure 5.8: Total percentage of dead cells in 72h obtained from the simulation. The pies above the columns give the distribution of lost cells in the different phases. The error bars were calculated as reported in Figure 5.7.

5.3 DISCUSSION

Even though alkylating agents are very well known chemetherapeutic compounds we could not find in the literature a study showing a complete time- and dose-dependence of the effects induced by one of these drugs. For this reason we decided to investigate the effects induced by a short treatment with L-PAM on IGROV1 cells.

The minimal scenario of parameter values necessary to reproduce all the data (flow cytometric percentages and absolute cell number, plus the qualitative information from dUTP assay) was reported in figure 5.5. This gave a comprehensive description and quantification of the effect of L-PAM on IGROV1 cells.

The scenario was quite complex, with perturbations in each phase of the cell cycle. With low concentrations (3 or 10 μM) we detected no effects in G_1, a temporary G_2M block and a more persistent S delay. With higher concentrations (≥30 μM), cells in G_1 or in G_2M at the time of treatment were immediately blocked in the same phase. However, G_1 blocking activity was temporary and weak (only

5-20% of cells passing through this phase remained blocked there) while G_2M blocking activity increased with time.

For what concern S phase, our simulation indicated that in the first 24h there was a net delay (block + recycling) but not loss, while cell loss became evident at longer times after treatment. This suggested that the outcome of S phase block was unbalanced toward repair at short times after treatment, whereas at longer times the cells were more committed to apoptosis. This interpretation was supported by the TUNEL assay (figure 5.4).

Delay S and G_2M block were reported to be an essential step for cells to repair DNA damage (Dean and Fox, 1983). Brox et al. (1980) showed that the time at which cells overcame an L-PAM-induced G_2M block correlated with the time when DNA-protein cross-links were removed. In a resistant cell line the DNA interstrand cross-links appeared to be completely repaired in the 48h following drug removal (Erickson et al., 1978) and at the same time they were able to recover from G_2M block. In samples treated with intermediate or high L-PAM concentrations, our simulation suggested a G_2M response similar to that in S phase, with a persisting block and cell death after 24h. However additional sensitivity analysis showed that a certain low recycling rate was possible in this phase in the first 24h. At long times after treatment cell death overwhelmed any possible recycling parameter.

In samples treated with intermediate L-PAM concentrations the enrichment of BrdUrd-positive cells observed 72h after treatment (figure 5.3b) demonstrated that L-PAM had stronger effects on cells that were in G_1 and in G_2M phase at the time of treatment. The simulation interpreted this phenomenon as due especially to stronger cytostatic effects in S and G_2M in BrdUrd-negative respect to BrdUrd-positive cells, while the relatively higher mortality (in S phase) of BrdUrd-negative cells contributed less to the prevalence of BrdUrd-positive cells at 72h. At higher

concentrations, the effects of the equally strong G_2M block and mortality overwhelmed and limited the differential effect between BrdUrd-negative and BrdUrd-positive cells.

This is only partially in agreement with reports using synchronized cells, where subpopulations treated in G_1 or G_2M phase appeared more sensitive to L-PAM than cells in S phase at the time of treatment (Ludlum, 1977).

Ludlum suggested that cells alkylated during G_1-S phase might be more sensitive because they have less chance of repairing potentially lethal damage before the next phase of synthesis than in G_2M phase (Ludlum, 1977). However a study of the phase-dependent cytotoxicity of nitrogen mustard toward CHO cells concluded that the amount of initial damage and the rate of repair were constant in each phase for this drug (Clarkson and Mitchell, 1981).

As a whole, our results are not completely in keeping with current paradigms of the effects of L-PAM, pointing to a high level of complexity of the cell response to simple, short treatments. The dose-dependence of the effects and their presence at long times after treatment were also evaluated in other studies performed with different compounds (Caporali et al., 2004; Brozovic et al., 2004). Brozovic et al. (2004) observed a dose-dependent activation of proteins related with apoptosis even at very long time (120h) after 1-h treatment with DDP. We also found that cell death was still active at 72h, but we did not extend our period of observation beyond that time and we were not able to evaluate how long cell death will last.

Moreover, we observed that the percentage of cells lost in 72h (figure 5.8) reached a sort of plateau for concentrations higher than 30 μM. At lower concentrations cells were delayed in S and G_2M phases and lethality occurred in S phase. At higher L-PAM concentrations, S and G_2M delay became stronger and more persistent and a cell loss in S and in G_2M phase occurs. A cytostatic effect in G_1, without lethality, also appeared at these intermediate concentrations. At the

highest concentration the lethality in G_1 added to the other effects and the differential response of BrdUrd-positive and BrdUrd-negative cells was definitely lost.

The loss of phase specificity of the drug at the highest concentration tested and the minimal increase in overall lethality despite a ten-fold increase of the drug concentration (from 30 to 300 μM in our cell line) could be important in the design of L-PAM therapies.

CHAPTER 6: Cell Cycle Effects of Doxorubicin

6.1 INTRODUCTION

6.1.1 Biochemical Mechanism of Action of Anthracycline Antibiotics

Doxorubicin is an antitumour-antibiotic isolated from cultures of *Streptomyces peucetius var. caesius* (Arcamone et al., 1969; Di Marco et al., 1969) and with daunorubicin, another compound of the same family, has been in use for more than 30 years for the treatment of a variety of malignancies. Typical clinical DXR treatment involves bolus administration of 15-90 mg/m^2, which are associated with peak plasma concentrations in the range of 1-2 μM, rapidly declining to 25-250 nM within 1h (Speth et al., 1987; Benjamin et al., 1973).

Despite the extensive clinical use of these drugs, their mechanism of action is still uncertain and controversial. A number of different mechanisms have been proposed for the cytostatic and cytotoxic actions of these agents (Gewirtz, 1999).

6.1.1.a Inhibition of DNA and RNA synthesis

The biochemical effects first described and most often related to the cell killing effects of DXR involve intercalation into double helical DNA and inhibition of polymerases, with subsequent inhibition of DNA and RNA synthesis (Di Marco et al., 1965; Momparler et al., 1976). Di Marco et al. (1965) demonstrated inhibition of both DNA and RNA synthesis in HeLa cells over a concentration range of 0.2 through 2 μM daunorubicin. Similarly, Kim and Kim (1972) reported a pronounced effect of DXR on DNA synthesis in HeLa cells with inhibition evident at concentrations as low as 0.02 μM.

On the other side, studies by a number of investigators have failed to detect effects on DNA synthesis at the lower range of drug concentrations. Meriwether and Bachur (1972) and Wang et al. (1972) found that a concentration of at least 2 μM DXR was required for inhibition of DNA and RNA synthesis in L1210 cells. Momparler et al. (1976) also determined that elevated drug concentrations in the

range of 2 through 100 μM DXR are required for the inhibition of DNA and RNA synthesis in hamster fibrosarcoma cells.

These contradictory findings make it difficult to reach a unifying conclusion regarding the involvement of DNA and RNA synthesis inhibition in the growth-inhibitory effects of the anthracyclines. It is possible that inhibition of DNA synthesis is an early transient signalling event, that is a component of growth arrest related to the function of p53 (Kastan et al., 1991). This may relate to a cytostatic and transient component of drug action, while other effects of the anthracyclines on the tumour cell, such as the inhibition of topoisomerarse II (see 6.1.1.c), may be more closely associated with lethal effects of these compounds.

6.1.1.b Free radicals

The quinone of the anthracycline antibiotics has been shown to interfere with mitochondrial oxidative pathways. This structure permits anthracyclines to act as electron receptor in reaction mediated by oxoreductive enzymes. The addition of the free electron converts the quinones to semiquinone free radicals (Bachur et al., 1977; Bates and Winterbourn, 1982) which may induce free-radical injuries to DNA of themselves (Berlin and Haseltine, 1981; Eliot et al., 1984) or after interaction with molecular oxygen to form superoxides, hydroxyl radicals and peroxides (Bachur et al., 1978; Benchekroun et al., 1993).

However this toxicity is probably not responsible for doxorubicin-induced tumour cell killing in the *in vitro* models used for cytotoxicity evaluation. In fact Benchekroun et al. (1993) demonstrated free-radical formation only in tumour cells treated with drug concentrations which are at least ten-fold higher than those routinely achieved in the clinic. Moreover, as demonstrated by Bustamante et al. (1990), hydrogen peroxide generation is unlikely to represent a primary response to drug treatment and instead may reflect a delayed metabolic response to other

unidentified perturbations in cell function. Indeed, in this study reactive oxygen species were detected in breast tumour cells 9 days after exposure to 0.1 μM DXR.

The generation of free radical species could also lead to lipid peroxidation of the cell membrane, but again many studies related to this phenomenon have been performed using enzyme preparation, non-physiological conditions, such as high oxygen tension, or supraclinical concentrations of the anthracyclines (Kharasch and Novak, 1983; Griffin-Green et al., 1988). These approaches, using cell-free systems or elevated drug concentrations, may provide evidence for the generation of free radicals and lipid peroxidation, but they do not serve to indicate whether free radicals and lipid peroxidation play a role in anthracycline action in the intact cell. Even the increased sensitivity to DXR in cells with alterations in the level of GSH is not a key argument in support of the involvement of free radicals in DXR toxicity. Again all of the studies showing sensitization to DXR through depletion of cellular GSH do so at elevated concentrations of drug (Dusre et al., 1989; Lai et al., 1991).

If the potential involvement of free radical generation in the antitumour toxicity of the anthracyclines is still complex and controversial, it appears to be fairly well accepted that there is an association between the generation of free radicals and DXR cardiotoxicity (Myers et al., 1977).

6.1.1.c DNA adduct formation and DNA breaks

Many studies in the literature show that the dominant cellular target of anthracyclines is DNA (Myers, 1992), resulting in two major types of DNA damage: DNA adducts (Phillips et al., 1989, Cullinane and Phillips, 1990) and protein-associated single- and double-strand DNA breaks (Holm et al., 1991; Myers, 1992).

In vitro transcription assays have previously been used to clarify the nature of the interaction of DXR with DNA, and the formation of drug-induced DNA adducts was observed almost exclusively at GpC sequences (Phillips et al., 1989). A variety of experimental approaches have subsequently shown that adducts at these sites contribute to DXR-induced inter-strand cross-links at GpC sequences (Cullinane and Phillips, 1990). Potential importance of DNA cross-links is provided by the observation that fewer cross-links are present in drug-resistant cells as compared with drug-sensitive cells, even at equivalent intracellular concentrations of drug (Skladanowski and Konopa, 1994).

In the late 1970s and early 1980s Ross and coworkers (Ross et al., 1978b; Ross and Bradley, 1981) described the induction of strand breaks in the DNA of L1210 leukaemic cells treated with DXR at concentrations ranging between 0.4 and 5 μM. The strand breaks, in both single- and double-stranded DNA, were found to be protein-associated and were slowly and incompletely repaired after drug removal. In 1984, Tewey et al., using both cells and cell-free extracts, identified topoisomerase II as the target enzyme of DXR and demonstrated that subunits of the homodimeric enzyme remain locked into the 5' end of the DNA molecule after completing the cleavage reaction.

Topoisomerase II is likely to be one of the primary target sites for the activity of the anthracycline antibiotics. The strongest argument in support of this presumption may be the data indicating that tumour cells that are resistant to the anthracyclines have reduced levels or altered activity of the enzyme with a concomitant reduction in the level of drug-associated strand breaks in DNA (or a reduction in DNA-protein cross-link formation) (Capranico et al., 1987; Webb et al., 1991).

The interaction of DXR with DNA-topoisomerase II complex is a triggering event for growth arrest and cell killing through a signalling pathway leading to apoptosis.

6.1.2 Previous Cell Cycle Studies

The first studies about cell cycle effects induced by anthracycline antibiotics were performed in the early 1970s. At that time Kim and Kim (1972) showed that DXR killed HeLa cells most effectively in S phase. These results were confirmed also for human lymphoma cells (Drewinko and Gottlieb, 1973) and in CHO cells (Kimler and Cheng, 1982). In this last case a dose-dependence in cell cycle phase killing effects was observed, and the hierarchy on the sensitivity was M and early S phase (most sensitive) then G_2, with late S and G_1 phase being least sensitive.

As with the cell killing effects of DXR, the changes in cell kinetics or tumour growth are also dose-dependent. Generally, low doses or short times of treatment cause cells to progress at a slower rate through the phases of the cell cycle, intermediate doses cause a short, but reversible delay in cell cycle phase progression, and high doses can cause immediate cell cycle arrest (generally irreversible) which prevents further progression through the cell cycle.

Synchronized CHO cells were delayed in all phases of the cell cycle except mitosis by doses as low as 0.02-1 μM for 1h (Barranco et al., 1973). At these drug concentrations 30-90% of cells were killed, but the cell cycle delay was reversible in 2 or 4h and the cells continued their progression through the cell cycle for at least one more time. Using higher DXR doses (2-20 μM) Tobey et al. (1976) also demonstrated S and G_2 phase delay in CHO cells. Cells treated during G_1 phase progressed through S phase, but could not traverse G_2. Noncycling CHO cells treated with DXR were only slightly delayed in their re-entering into the cell cycle and through S and G_2 phases (Crissman et al., 1985). In general, more recent studies remark the arrest in G_2M phase as one of the most important cell cycle effects induced by DXR treatment (Bilim et al., 2000; Potter et al., 2002). If DNA repair fails, apoptosis can occur to eliminate irreparably damaged cells and there

is evidence that one consequence of treatment with DXR is the induction of apoptosis (Bellarosa et al., 2001).

Moreover, DXR is active against both proliferating and nonproliferating cells, even though proliferating cells are much more sensitive. This behaviour has been observed not only in CHO cells, but also in stimulated and nonstimulated lymphocytes (Minderman et al., 1991).

6.1.3 Clinical Use

The anthracycline group of antitumour antibiotics is used widely for cancer chemotherapy, where agents, such as doxorubicin, daunomycin, epirubicin, and idarubicin, have proved the most useful compounds. The neoplasms that the anthracyclines are effective against include acute leukaemias and solid tumours, such as carcinomas of the breast, lung, thyroid, and ovary, and soft tissue sarcomas (De Vita et al., 2001). However cardiotoxicity of DXR and tumour-cell drug resistance were considered the major problems limiting the success of chemotherapy (Bradley et al., 1988).

DXR is generally used in association with other anticancer agents such as cyclophosphamide, cisplatin and nitrosurea. In particular, a number of studies have looked at the benefit of adding DXR to the cisplatin plus cyclophosphamide combination in the therapy against ovarian cancer. Their data suggested a survival benefit for platinum-anthracyclines based combinations as compared to platinum based combinations without anthracyclines (Fanning et al., 1992; A'Hern and Gore, 1995). On the contrary, as observed by A'Hern and Gore (1995), the addition of an alkylating agent may add toxicity and lead to a dose reduction of these two drugs.

Other additional studies have been published in the late 1990s that showed second-line activity of DXR (Muggia et al., 1997) and epirubicin (Vermorken et al., 1995) in patients with ovarian cancer pretreated with platinum or paclitaxel.

6.2 RESULTS

6.2.1 Experimental Data

Exponentially growing IGROV1 cells were treated for 1h with 0.5, 1, 3, 6, 10 and 30 μM of DXR. We measured the following quantities related to the cell kinetics after treatment: overall (absolute) cell number, flow cytometric DNA histograms, biparametric DNA-BrdUrd flow cytometric histograms using pulse-and-chase protocol.

Figure 6.1 shows the growth curves after treatment. The cells treated with 0.5 μM DXR were able to growth like controls and the number of cells treated with 1 and 3 μM DXR was almost constant until 24h, when it started to increase. The behaviour of the cells treated with a concentration of DXR ranging from 6 to 30 μM was very similar, indeed the number remained almost constant until 24h, showing a slight decrease between 48 and 72h.

Flow cytometric DNA histograms of control and treated samples are shown in figure 6.2. Simple visual inspection of the histograms did not show any difference between control and treated samples at short times after treatment. Some differences started to come out 24h after treatment, when the cells treated with concentrations higher than 3 μM accumulated in G_2M phase. The duration of this effect was dose-dependent and for the samples treated with 6, 10 and 30 μM DXR a high percentage of cells remained blocked in this phase until 72h. Moreover in DNA histograms of 30-μM treated samples was possible to observe also an

accumulation of cells in late-S phase, which started 24h after treatment and was present up to the end of the observation.

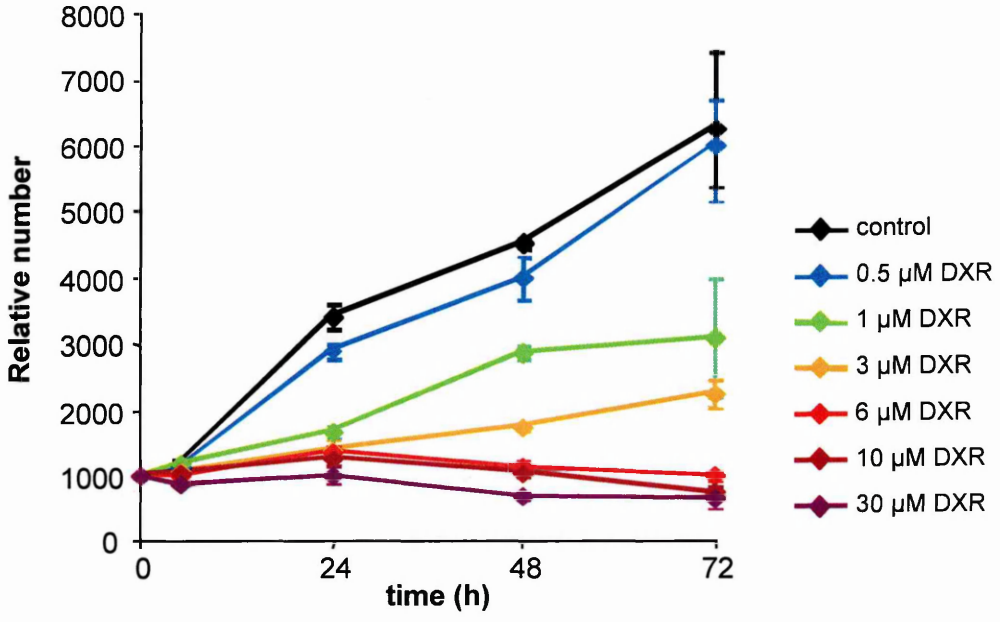

Figure 6.1: Growth curves of IGROV1 cells after 0.5, 1, 3, 6, 10 and 30 µM DXR for 1h, measured by Coulter Counter. Each point is an average of at least three replicate flasks.

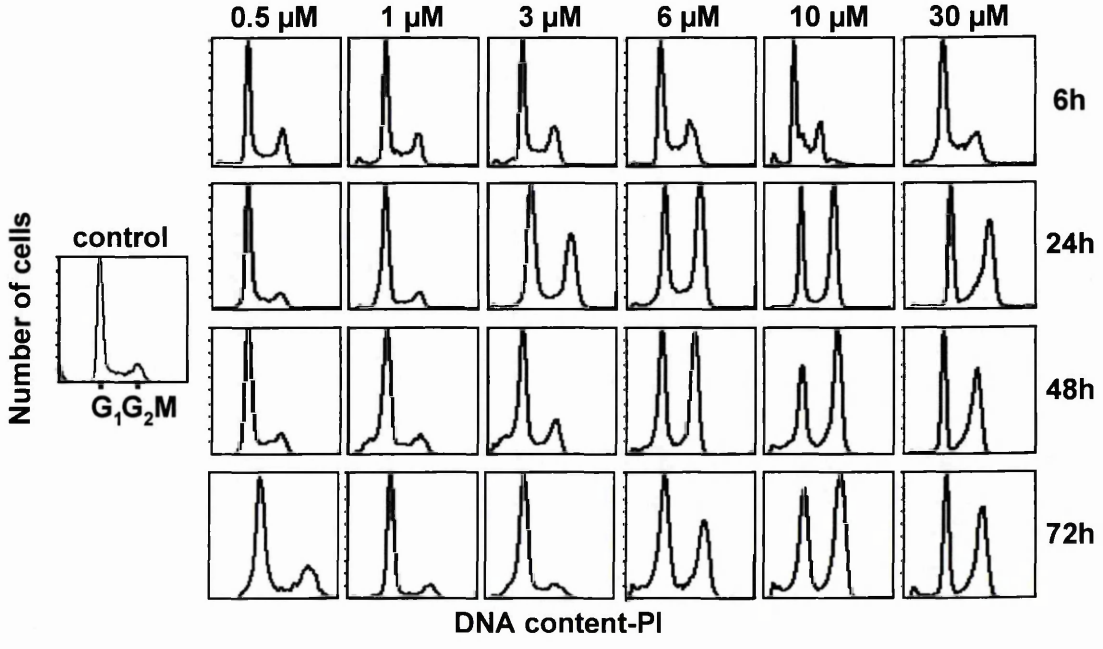

Figure 6.2: Time-course of DNA histograms after 0.5, 1, 3, 6, 10 and 30 µM DXR for 1h. DNA corresponding to G_1 and G_2M cells is indicated. Persistent accumulation in the G_2M peak is particularly evident in the 6, 10 and 30 µM histograms.

Short-term effects of DXR were evaluated by a pulse-and-chase experiment. Cells were exposed to BrdUrd in the last 20 min of treatment, allowing DNA-synthesising cells to incorporate BrdUrd, becoming "BrdUrd-positive", and were collected 6h later. The resulting biparametric DNA-BrdUrd plots are shown in figure 6.3. They indicate the movement of the cells in the cell cycle in the first 6h after treatment. In untreated samples BrdUrd-positive cells that occupied S phase at 0h were distributed within late-S, G_2M and G_1 phases at 6h. At 6h, treatments with low doses of DXR (0.5 and 1 μM) did not affect the progression of BrdUrd-positive and BrdUrd-negative cells through the different cell cycle phases, indeed treated samples presented biparametric DNA-BrdUrd plots similar to that of control sample. When the drug concentration increased the DNA synthesis became slower, and in the samples treated with 6, 10 and 30 μM DXR the cloud of BrdUrd-positive cells was distributed in middle- and late-S phase. Moreover, DNA-BrdUrd plots of these samples showed the presence of a block in G_2M phase that was not highlighted in monoparametric analysis of DNA. At 6h after treatment, a subpopulation of G_2M negative cells, that was not present in the control, was still detected in treated samples.

A quantitative analysis of biparametric plots allowed the evaluation of the duration of S phase in control and treated samples. In IGROV1 cells the mean duration of S phase in exponentially growing samples was estimated equal to 8.6h. Figure 6.4 showed the trend of this duration as function of the drug concentration. The progression of the cells through this phase became slower when the dose increased and the time that 30-μM treated cells needed to pass through S phase was estimated in about 17h, with an almost two-fold increased respect to the control.

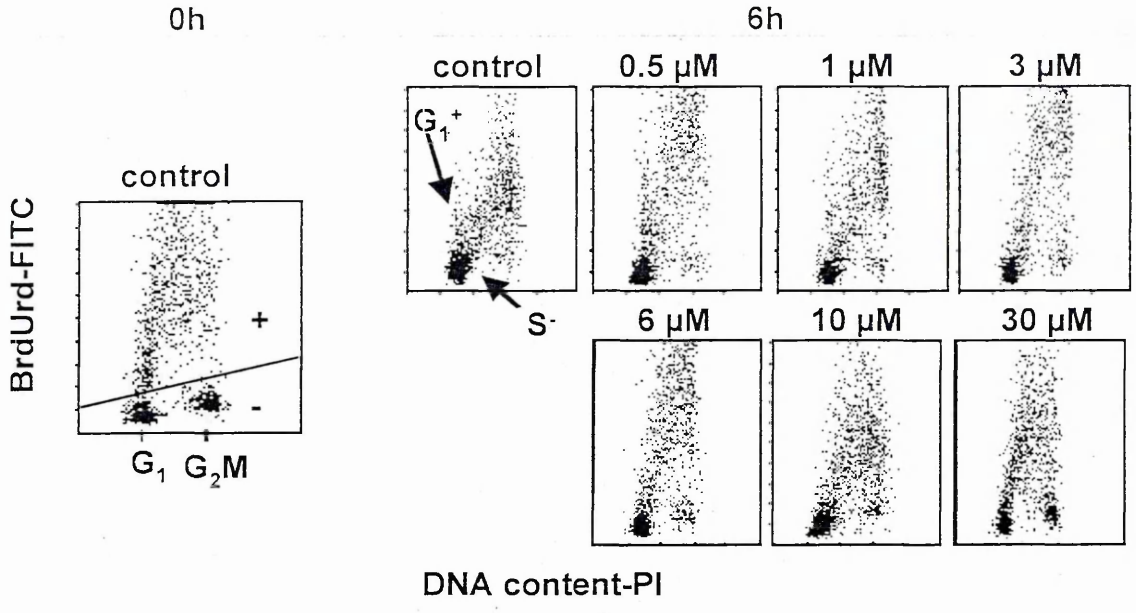

Figure 6.3: Biparametric PI-fluorescence (DNA content) and FITC-fluorescence (BrdUrd content) plots. Cells incorporated BrdUrd 20 min before the end of the 1h-treatment and were harvested 6h after treatment. Cells were considered BrdUrd-positive (in the S phase at the time of treatment, 0h) when detected above the straight line (left panel). BrdUrd-positive cells with G_1 DNA content (G_1+) at 6h were born from mitosis of cells in S phase at the time of treatment.

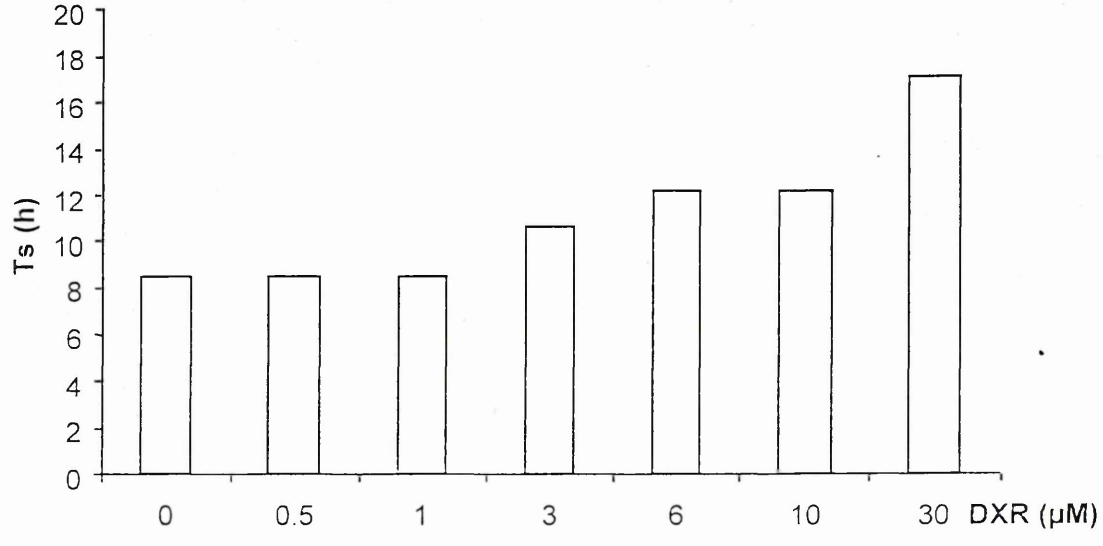

Figure 6.4: Impact of the reduction of DNA synthesis rate on the duration of S phase. Samples treated with drug concentrations higher than 3 µM needed a longer time to complete this phase.

Besides these data describing short-term effects of drug treatment, we performed also a biparametric staining DNA-dUTP, which provided at least qualitative information about the apoptosis induced by DXR (figure 6.5). Cells with fragmented DNA, because of apoptotic death, formed the dUTP-positive subpopulation. At long times after drug washout about 25% of apoptotic cells were detected in 10-μM treated samples, whereas for lower-doses treated samples we did not observe dUTP-positive cells. In IGROV1 cells treated with the highest concentration of DXR an apoptotic death process was already active 24h after treatment and the percentage of dUTP-positive cells continued to increase with the time.

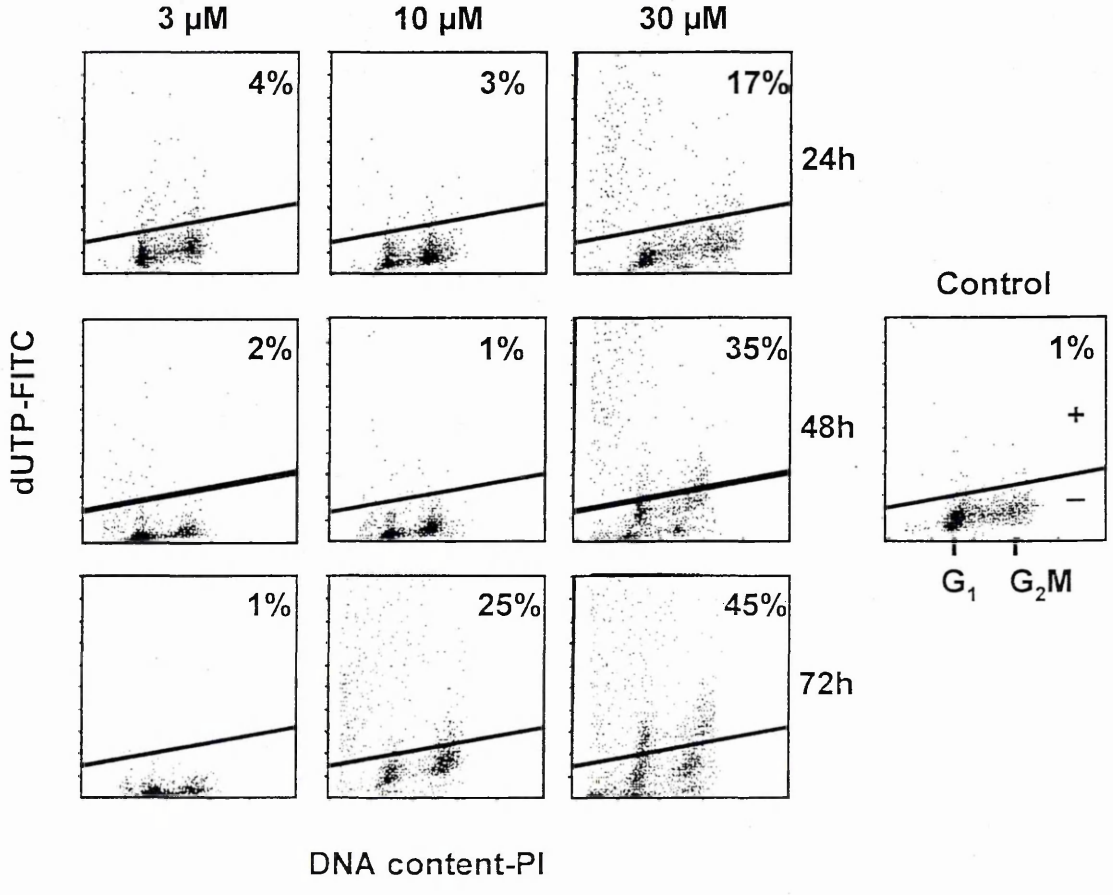

Figure 6.5: Biparametric PI-fluorescence (DNA content) and FITC-fluorescence (dUTP content) of IGROV1. Cells with DNA fragmentation induced during apoptosis are dUTP-positive, thus detected above the straight line.

At this point the simulation approach became essential to combine together all the information that came from cell count and flow cytometric analyses and to quantify the time- and dose-dependence of killing, blocking or delay and repair activity.

6.2.2 Scenario of Cell Cycle Perturbations Underlying Experimental Data

The simulation program allowed the combination of every information that came from the experimental data and the final scenario of parameters is shown in figure 6.6. Each parameter assumed different values for BrdUrd-positive and BrdUrd-negative cells only between 0 and 6h. In the following intervals of time the data could be reproduced with the same value for BrdUrd-positive and BrdUrd-negative cells. This assumption was supported by a BrdUrd pulse-and-chase experiment with cell harvesting 72h after treatment (not shown). The percentage of BrdUrd-positive cells present in the population at that time was not different from that of control samples. This indicated that DXR did not specifically affect BrdUrd-positive or BrdUrd-negative subpopulations.

6.2.2.a Events occurring in G_1 phase (figure 6.6a)

The controls of G_1 phase acted during and immediately after treatment on BrdUrd-negative cells. The blocking activity was not strong for the cells treated with the lowest doses of DXR. In fact only 5-20% of 0.5- and 1-μM treated cells were intercepted by G_1 checkpoint. The percentage of BrdUrd-negative cells that remained blocked in this phase between 0 and 6h increased in a dose-dependent way, reaching its maximum for the samples treated with the highest dose of DXR. The blocking activity in G_1 phase was persistent and only for 0.5-μM treated cells ended 24h after drug washout. For the other drug concentrations this parameter had a maximum between 6 and 24h for 1- and 3-μM treated cells, and between 24

and 48h for samples treated with higher DXR concentrations always followed by a decrease (first line panel).

The cells treated with the lowest DXR concentrations and blocked in G_1 did not die in this phase. For 1-μM treated samples only long-term cell death was present, whereas for cells treated with doses higher than 1 μM a cell loss occurred immediately after treatment and between 48 and 72h. The recycling rate for cells intercepted by this checkpoint was negligible (not shown).

6.2.2.b Events occurring in S phase (figure 6.6b)

In the samples treated with the lowest concentrations DNA synthesis was inhibited only between 6 and 24h. In the other cases the synthesis was immediately reduced and the effect was persistent and present until 72h. Moreover the intensity of this effect increased for 6-, 10- and 30-μM treated cells, reaching 80-100% between 24 and 72h (third line panel).

The cell loss in this phase occurred only at long times after treatment, except for the cells treated with the highest concentration that died immediately after treatment and between 24 and 72h. The percentage of cells that died in this phase was higher in samples treated with lower doses, 60-80% for 1-μM treated cells and 40-60% for 3-μM treated cells (fourth line panel).

6.2.2.c Events occurring in G_2M phase (figure 6.6c)

Cells treated with 0.5 μM DXR could pass through G_2M phase without any perturbation, and only 5-20% of 1-μM treated cells were intercepted by this checkpoint immediately after drug washout. In general the intensity and the duration of this blocking activity was dose-dependent, 60-80% of cells passing through G_2M remained blocked in this phase (fifth line panel).

A cell loss was present in this phase between 48 and 72h in samples treated with 6, 10 and 30 μM DXR. Moreover, 5-20% of 30-μM treated cells blocked in G_2M or passing through this phase died between 0 and 6h. The percentage of dead cells was higher at long times after treatment reaching the value of 40-60% or 60-80% for the highest dose (sixth line panel).

When the blocking activity ended, cells treated with lower dose were able to recycle, even though this behaviour was observed only in 3-μM treated cells, a recycling probability could not be excluded for 0.5- and 1-μM treated samples. For the lowest drug concentrations the number of blocked cells was too low to allow a quantification of this parameter (seventh line panel).

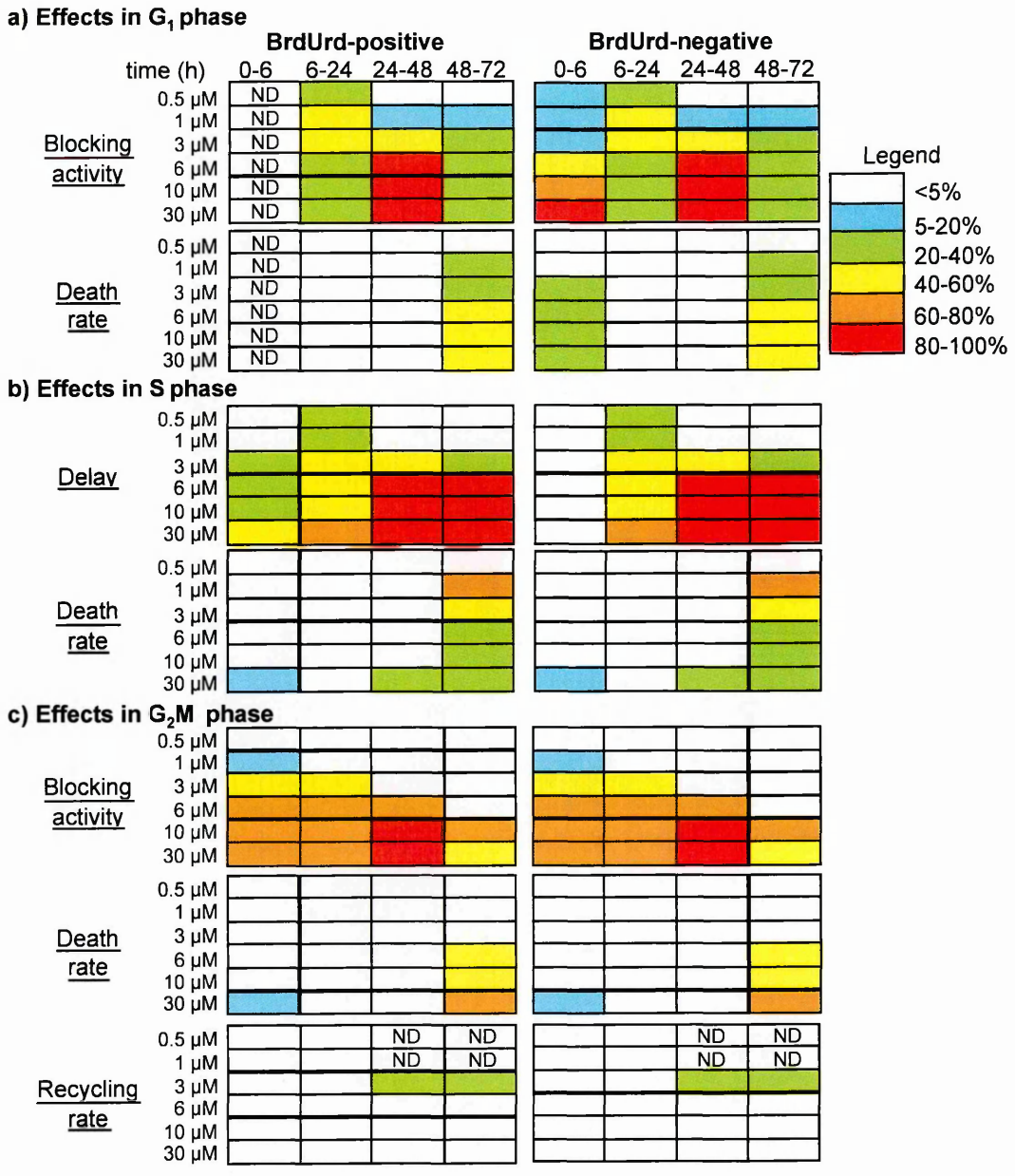

Figure 6.6: Characteristics of the response scenario for a complete reproduction of the experimental data. The blocking activity is represented as the percentage of cells that remain blocked among those traversing G_1 or G_2M in the time interval indicated. The death/recycling rates are expressed in terms of the percentages of cells that die/recycle in each time interval, within the compartment of G_1 (or G_2M) blocked cells. In the 0-6h interval the death rate in G_1 or G_2M is applied to both blocked and proliferating cells, because they cannot be distinguished. Parameters whose values are irrelevant are defined ND (non-detectable).

The S-delay rate is equivalent to the percentage reduction of the average DNA synthesis rate.

6.2.3 Sensitivity Analysis of Parameters

Once that the final scenario was obtained, a study aimed to measure the uncertainty of parameters estimation was performed as described in 3.6.3.e.

In figure 6.7 we represented the time-courses of each parameter obtained with our final simulation (represented with a continuous line) and the results that came from the study of the sensitivity. The filled area represented the range of values of each parameter within which the simulation remained close to the data as specified above.

The parameter of G_1 blocking activity was found very sensitive, confirming its oscillating trend and its persistence at long times after treatment. The behaviour of this parameter allowed the formation of a non-negligible subpopulation of blocked cells that made sensitive the parameters connected with the cell loss and the recycling probability, at least at long times after treatment. This study confirmed the presence of a cell loss in G_1 phase between 48 and 72h and between 0 and 6h, even though in this case the parameter was less sensitive. In particular the presence of a non-zero short-term death in 6-μM treated cells allowed us to confirm the presence of a cell loss also in samples treated with 10 μM DXR. On the basis of this study, a recycling probability in G_1 phase could be excluded in the samples treated at the highest concentrations, for samples treated with the lowest concentrations we could not exclude this possibility.

The precision of the final estimates of the parameters of S-phase delay and G_2M blocking activity resulted high by sensitivity analysis, confirming in both cases the trend illustrated in the final scenario. A different behaviour was observed in the recycling probability, this parameter was sensitive only in 3-μM treated cells, however its low sensitivity in lower-doses treated samples could not exclude the presence of a recycling probability also in 0.5 and 1-μM treated cells.

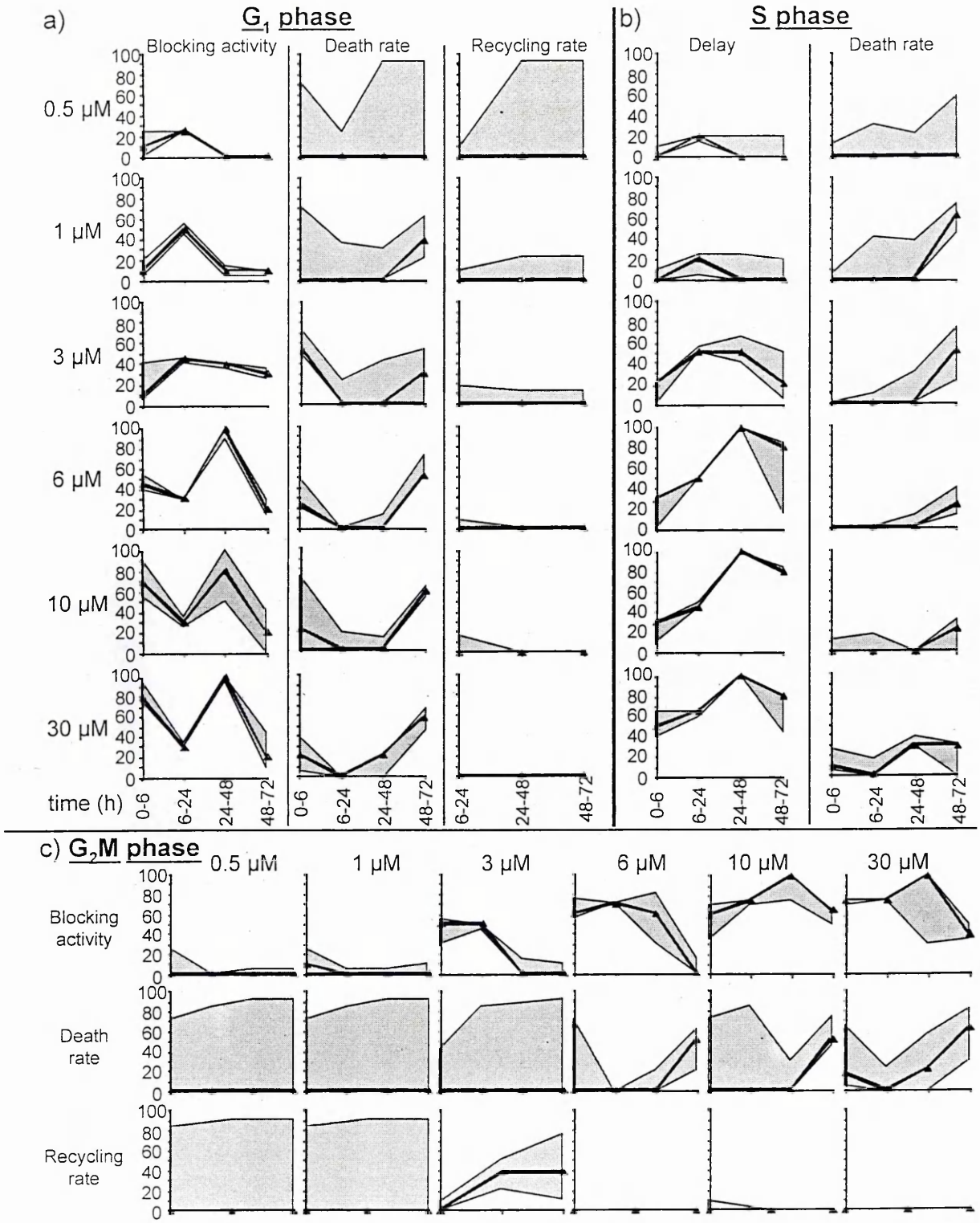

Figure 6.7: Time-course of the parameters used in the simulation. The continuous line represents the value of each parameter as obtained in the final simulation and the filled area represents the range of values of each parameter within which the simulation remained close to the experimental data.

6.2.4 Predictions of the Final Scenario

Once the final scenario was defined and confirmed by the sensitivity analysis, its predictions could be investigated in detail by the simulation program, disclosing information on the behaviour and heterogeneity of the cell population, that could not be directly measurable by the experimental data. In particular we retrieved from the simulation the percentage of cells blocked in G_1 or in G_2M at each time (figure 6.8) and the total amount of cells dying in the 72h of observation (figure 6.9). These quantities allowed the evaluation of the impact of a specific block and killing on the growth of the whole cell population. Both blocked and proliferating cells constituted the percentage of cells in G_1 and in G_2M phase, as measured by flow cytometry. Using our simulation approach, we could distinguish and appreciate these two contributions.

As shown in figure 6.8, 6h after drug washout the percentage of cells blocked in G_1 phase increased in all the samples. At the following times the percentage of G_1 cells in 0.5- and 1-μM treated samples remained almost constant but with a decrease in the percentage of blocked cells. In general, in samples treated with higher concentrations of drug, blocked cells represented the biggest part of the population in this phase.

In G_2M phase we did not observe blocked cells in the samples treated with the lowest doses of drug, but this subpopulation became detectable in cells treated with 3 μM DXR and higher concentrations. In particular, in 3-μM treated samples, G_2M blocked cells reached a maximum at 24h, followed by a decrease, but they always represented the biggest part of the population. At the same way, in samples treated with higher doses, 6h after drug washout the percentage of cells in this phase started to increase with blocked cells contributing for more than 80% to the whole population.

In figure 6.9 was illustrated the percentage of lost cells in 72h and the pies above the columns of the histograms gave the distribution of lost cells in the different cell cycle phases. From this point of view the cells treated with 1 and 3 μM DXR presented a very similar behaviour, in fact about 30% of them died in 72h and about the 65% of the lost cells died in G_1 phase. The percentage of lost cells increased in a dose-dependent way, about 70% of them died in the sample treated with the highest concentration of drug. A difference in the cell cycle phase where the cells died was observed between the samples treated with the lowest doses and those treated with 6, 10 and 30 μM DXR. In these last cases about half of the cells died in G_2M phase and the other half died in G_1.

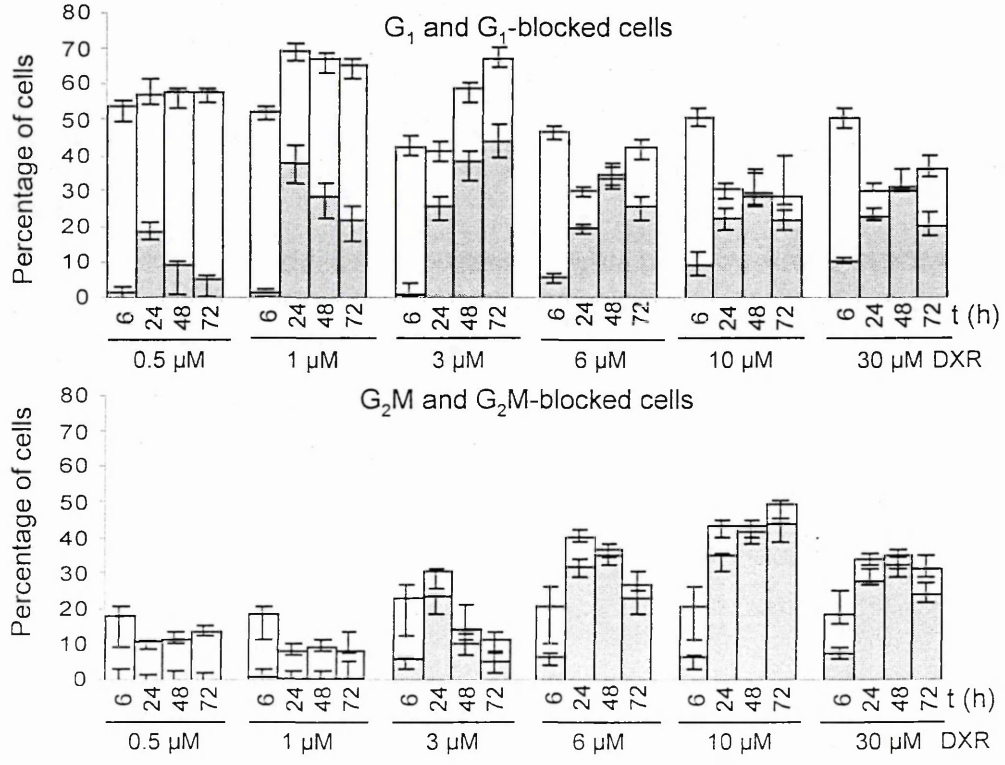

Figure 6.8: Dose-dependence and time-dependence of the percentage of total (full height of the bars) and blocked (height of the filled area of the bars) cells in G_1 and in G_2M. This serves to evaluate the impact of the blocking effect on the cell population after treatment with 0.5, 1, 3, 6, 10, and 30 μM DXR. The error bars in the histograms indicate the range where different simulations give predictions fitting the data within the experimental error.

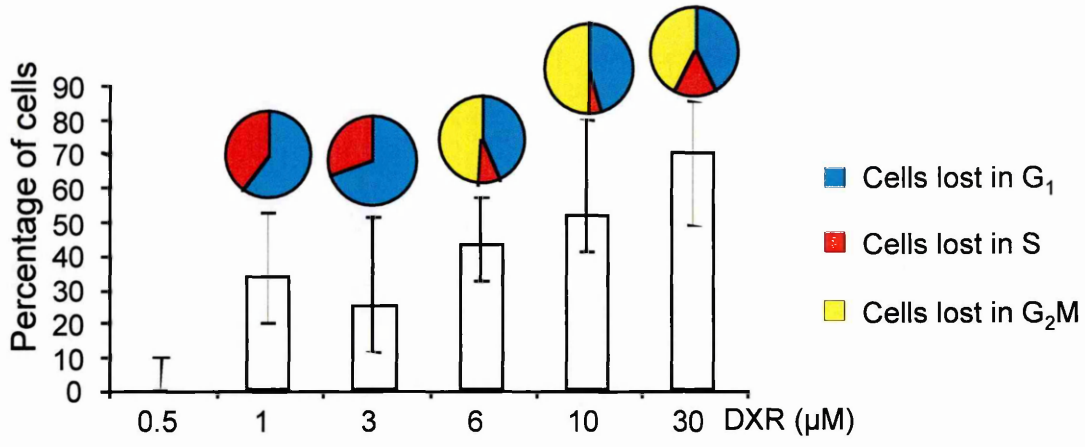

Figure 6.9: Total percentage of dead cells in 72h obtained from the simulation and calculated over the initial number of cells. The pies above the columns of the histograms give the distribution of lost cells in the different cell cycle phases. The error bars were calculated as reported in figure 6.8.

6.3 DISCUSSION

Even though DXR is a commonly utilized chemotherapeutic agent we could not find in the literature a complete study of the time- and dose-dependence of cell cycle effects induced by this drug. However we believe that a deeper knowledge of the cytokinetics of cellular events leading to treatment efficacy could be helpful in optimizing chemotherapy strategies.

The present study highlighted the complexity of the time- and dose-dependence of the effects induced by a short treatment with DXR, revealing a scenario where perturbations were present in each phase of the cell cycle. In particular, DXR affected at the same way the cell cycle progression of BrdUrd-positive and BrdUrd-negative subpopulations. This was in agreement with the conclusions made by the first studies about cytotoxic and cytostatic effects of DXR, which confirmed that DXR could not be considered a phase-specific agent (Kimler and Cheng, 1982; Tobey et al., 1976).

As we showed in figure 6.6 the cells that were in G_1 phase at the time of treatment were immediately intercepted by G_1 checkpoint. The percentage of cells that could not progress into the next phase was strongly dose-dependent. 6h after treatment BrdUrd-positive cells that could escape G_2M checkpoint arrived in G_1 and more than 20% of them remained blocked in this phase. The long duration of G_1 blocking activity excluded an active recycling at 3 μM and higher concentrations, where more than 20% of cells that were blocked in this phase died between 0 and 6h and between 48 and 72h. This cell loss was more relevant for samples treated with low concentrations.

When the dose increased the number of cells intercepted by G_2M checkpoint became higher and this made more relevant the cell loss in this phase, especially because the blocking activity in cells treated with high DXR concentrations was persistent. Only 20-40% of cells treated with low DXR concentrations and blocked in G_2M phase was able to start cycling again, otherwise blocked cells died in this phase.

The cell cycle arrest and the cell loss in G_2M phase, together with the delayed progression through S phase, were the two perturbations mainly described in the literature after short or long treatments with DXR (Tobey et al., 1976; Crissman et al., 1985; Bartkowiak et al., 1992; Bilim et al., 2000; Potter et al., 2002). In spite of its major role in the response to a treatment with low concentrations and its strength at higher concentrations the block in G_1 phase was not detected in these previous studies, probably because the percentage of G_1 cells did not increase in treated samples. As shown by our simulations, in cells treated with high DXR concentrations the percentage of G_1 cells was even decreasing because of the delayed progression of the cells through the other cell cycle phases. As shown by Waldman at al. (1995), the presence of a block in G_1 phase could be highlighted by the low percentage of S-phase cells. They used monoparametric staining of

DNA content to investigate the role of p21 protein in the activation of G_1 checkpoint after a 24-h treatment with DXR. The same idea was followed in Attardi's study (Attardi et al., 2004), but in this case a BrdUrd labelling was used to investigate the activation of G_1 checkpoint after a continuous DXR treatment. The lack of BrdUrd positive cells in S phase was interpreted as a signal of the presence of a blocking activity in G_1, which avoided the entrance of G_1 cells in S phase.

At the same time, Attardi and coworkers confirmed the presence of a block in G_2M and a delay in S phase in DXR treated samples but, whereas the block in G_1 phase seemed to be p53-dependent, the effects observed in the other cell cycle phases were p53-independent. This different behaviour could be ascribed to the ability of DXR to induce DNA damage in multiple ways. For example the ability of DXR to activate G_2M arrest responses might be consistent with the role of topoisomerase II inhibitor played by this drug. On the other hand the S phase arrest response could possibly be ascribed to the ability of DXR to intercalate into DNA and disrupt its structure, thus impeding DNA replication.

If the interpretation of cytostatic and cytotoxic effects induced by a chemoterapeutic agent is normally not easy, the situation becomes much more complex when the drug acts in multiple ways, like in the case of DXR. We demonstrated that a wide range of data collected at different times after treatment with different drug concentrations could be helpful in the analysis of the complexity of a cellular response to a treatment.

CHAPTER 7: Comparison between Cell Cycle Effects Induced by Different Anticancer Drugs

7.1 INTRODUCTION

It has been known for over 50 years that exposure of cells to chemical or physical anticancer agents delays the normal progression through the cell cycle. These cell cycle delays were initially interpreted as passive cellular responses resulting from the induction by these compounds of damage in the DNA. However, these early studies also provided circumstantial evidence that the delays actually reflect induction of cellular processes assisting the treated cell to cope with the induced damage by somehow facilitating repair (Iliakis et al., 2003). The DNA damage checkpoint pathways were originally thought to regulate only cell cycle transition, but now we know that they comprise signal transduction cascade that link the detection of DNA damage to several other processes. These include inhibition of cell cycle progression, activation of DNA repair, maintenance of genome stability and, when it is not possible to repair the damage, the initiation of permanent cell cycle block or elimination of such cells by cell death (Zhou and Elledge, 2000).

The participating proteins to this complex system can be formally divided into sensors, transducers and effectors. Sensor proteins recognize DNA damages, directly or indirectly, and function to signal the presence of these abnormalities and initiate the biochemical cascade. Transducers are typically protein kinases that relay and amplify the damage signals from the sensors by phosphorylating other kinases or downstream target proteins. Effector proteins include the ultimate downstream targets of the transducer protein kinases (reviewed by Iliakis et al., 2003). In particular ATM and ATR kinases lie upstream in the DNA damage response signal transduction network and are central to the entire response. Downstream of these proteins lie Chk1 and Chk2 kinases, which carry out subsets of the DNA damage response in mammals.

Modification of effector proteins by upstream kinases, directly or indirectly, mediates the inhibition in cell cycle progression. The effector stage is where the

DNA damage checkpoint interacts with the cell cycle machinery. The DNA damage response network consists of two parallel pathways that respond to different types of DNA damage. The ATM pathway responds to the presence of DSBs, and acts during all phases of the cell cycle. On the other side, ATR pathway responds to DSBs, but more slowly than ATM and it can respond to agents that interfere with the function of DNA replication forks (reviewed by Zhou and Bartek, 2004). DNA alkylating agents might activate both pathways.

Once that the damage has been recognized the pathways involved in cell cycle checkpoints intertwine with those regulating DNA repair processes. At least four main repair pathways operate in mammals: nucleotide-excision repair (NER), base-excision repair (BER), recombinational repair (including homologous recombination and end joining) and mismatch repair (Hoeijmakers, 2001). NER deals with the wide class of helix-distorting lesions that interfere with base pairing and generally obstruct transcription and normal replication, whereas small chemical alterations of bases are targeted by BER. Two pathways, homologous recombination and end joining were developed to face the problem of the formation of DSBs. Homologous recombination seems to dominate in S and G_2, whereas the end joining is most relevant in the G_1 phase of the cell cycle (Takata et al., 1998).

All these molecular interactions contribute to the overall cell cycle modification that can be observed in DNA flow cytometric analysis and they also contribute to the determination of growth inhibition observed measuring the absolute number of cells in a population. Due to the fact that all these molecular pathways contribute to the overall tumour response to drug treatments, the comprehension of their dynamics could become important in the optimization of the schedule of treatment. However, the molecular approach to this problem allow the identification of the molecules involved in the pathways that determine the cell response to drug

treatment, but it is generally not able to quantify the activity of cell cycle checkpoints. Cell cycle arrest, DNA repair and apoptotic death are events characterized by complex dynamics that overlap in the experimental data. It is for this reason that the separate quantification of cytostatic and cytotoxic effects is not possible by inspection of a limited data set.

In this study we performed different experiments aimed to analyse cell cycle effects induced by short treatments with TPT, DXR and L-PAM on the same cell line (IGROV1). All the collected experimental data formed a complete database reproducing the time- and dose-dependence of flow cytometric percentages and cell number, but the simple intuition of the researchers is not enough to put all available data in a coherent scenario of cell cycle perturbations. The simulation program that we normally use to analyse the experimental data allowed us to express them as a function of the blocking activity, recycling probability and cell loss that contributed to the macroscopic observation. On the base of this analysis and taking into account the results previously published by our group about cell cycle effects induced by cisplatin (Montalenti et al., 1998) and paclitaxel (Sena et al., 1999) we were able to compare the dynamics of cytostatic and cytotoxic effects of the five drugs in each cell cycle phase. The use of the same cell line and the compilation of a database for each one of the considered drugs including the time- and dose-dependence of cytostatic and cytotoxic effects allowed a better appreciation of the complexity of the cell cycle response, but also the identification of possible common features among the drugs.

From the technical point of view, even considering different experiments, we were able to reproduce the kinetics of unperturbed growth of IGROV1 cells with the parameters listed in 3.6.3.a for time duration (T_{G1}, T_S, T_{G2M}) and CVs (CV_{G1}, CV_S, CV_{G2M}). In any case, before comparing the parameters that describe the cell cycle effects, we tested the role of the estimate of duration and CVs of cell cycle phases

in unperturbed cells in the determination of cell number and flow cytometric percentages (figure 3.8) and we performed the sensitivity analysis of the parameters included in the final scenario. The results of this study have not been shown for DDP and paclitaxel, whereas for all the other drugs are reported in chapters 4, 5 and 6. The study of the sensitivity gave us all the information about the variability of each parameter connected with checkpoint activity and allowed the determination of the error bars considered in the graphs representing the values of the different parameters.

7.2 RESULTS

Once that we arrived at the determination of a scenario including all the time- and dose-dependence of the parameters that describe cytostatic and cytotoxic effects for each one of the considered drugs we went on to the comparison of the checkpoint activity in the different cell cycle phases.

7.2.1 Features of the Activity of G_1 Checkpoint

G_1 checkpoint activity was measured as the probability ($p_{G1}B^{in}$) that the cells at the end of G_1 phase were intercepted by the checkpoint and remained in G_1 instead of entering S phase. At each time step of the simulation process a fraction equal to $p_{G1}B^{in}$ within the group of cells exiting from G_1 entered a separate compartment of "G_1-blocked" cells, adding to the previously blocked ones. The cells in this compartment could both recycle and enter S phase or die with specific rates in the subsequent time steps. Thus $p_{G1}B^{in}$ indicated what was happening in G_1 phase at specific laboratory times after drug treatment, quantifying the activity of the checkpoint. A checkpoint was considered strongly active if it was able to intercept a high fraction of the cells passing through it.

As the experimental data were collected at 0, 6, 24, 48 and 72h after drug treatment, there was not information about the details of the parameter's value between subsequent data points, and we limited our analysis to the estimate of the average in each interval. For this reason, in a given interval of time, whenever a partial block was detected by a value of $p_{G1}B^{in}$ lower than 1, the value should be interpreted as a net difference between blocking and recycling effects occurring within that interval. With the available data the recycling phenomenon became detectable only in the interval of time subsequent to that where the block occurred, but only if it was not masked by a persistent blocking activity.

Nevertheless, as shown in figure 7.1, we could evaluate the time-course of checkpoint activity after treatment with the five drugs tested. Two bursts of the G_1 checkpoint activity were observed: one short-term, occurring immediately after treatment (detected in the 0-6h interval), and the second acting after 24h. We observed both kinds of G_1 block in DXR and TPT, only the short-term in DDP, only the long-term in paclitaxel, while G_1 checkpoint activity was weak in L-PAM treated cells.

Figure 7.2 shows the dose-dependence of the two kinds of G_1 block, as measured by $p_{G1}B^{in}$ between 0 and 6h (short-term block, figure 7.2a) and between 24 and 48h (long-term block, Figure 7.2b). All dose-responses were sigmoid and were fitted using a Hill function. The Hill function was characterized by the maximum value of $p_{G1}B^{in}$ (E_{max}), by the concentration producing the 50% of the maximum response (EC_{50}) and by the sigmoidicity (m) that measured the steepness of the curve. Two global non-linear fittings were made, including the values of $p_{G1}B^{in}$ of all drugs either between 0 and 6h or between 24 and 48h, and optimizing E_{max} and EC_{50} of each drug with a common sigmoidicity. Figures 7.2a and 7.2b show the results after the normalization of the concentrations to the EC_{50} values for each drug. The parameters of the best fitting are reported in table 7.1.

The fitting of the short-term block indicated that the effect rose from 0.1 x E_{max} to 0.9 x E_{max} in a 15-fold concentration range, from 0.26 x EC_{50} to 3.88 x EC_{50}. Within this range and in general whenever a block is not complete, it is also possible that $p_{G1}B^{in}$ somewhat underestimates the G_1 checkpoint activity, actually stronger but counterbalanced by repair occurring within the same interval.

An almost complete block (E_{max} close to 1) was reached with DDP, DXR, TPT, while E_{max} remained around 0.2 with L-PAM and paclitaxel. Taking into account that a detectable amount of BrdUrd-positive cells (in S phase at 0h) was not able to reach the end of the following G_1 phase in 6h, we could consider the short-term block in G_1 as mainly involving BrdUrd-negative cells, treated while in G_1 or G_2M phase. The results suggest that DDP, DXR and TPT were able to damage cells in G_1 and induce a rapid activation of G_1 checkpoint. On the contrary, G_1 cells treated with L-PAM and paclitaxel presented only a weak response and most of them were able to proceed in S phase.

The dose-response of the long-term G_1 block was very steep, suggesting the existence of a threshold-concentration. A long-term block was not observed in DDP and L-PAM treated cells, whereas in samples treated with DXR and paclitaxel it was observed in both BrdUrd-positive and BrdUrd-negative cells, whereas in TPT treated samples only BrdUrd-positive and not BrdUrd-negative cells underwent this kind of block.

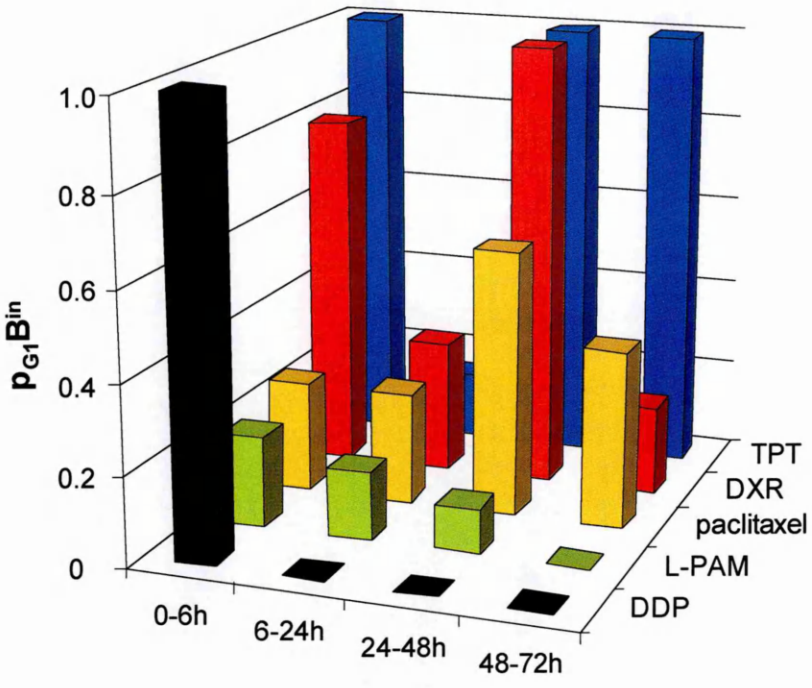

Figure 7.1: Time-course of the G_1 checkpoint activity corresponding to the drug concentration that determined the maximum of the response.

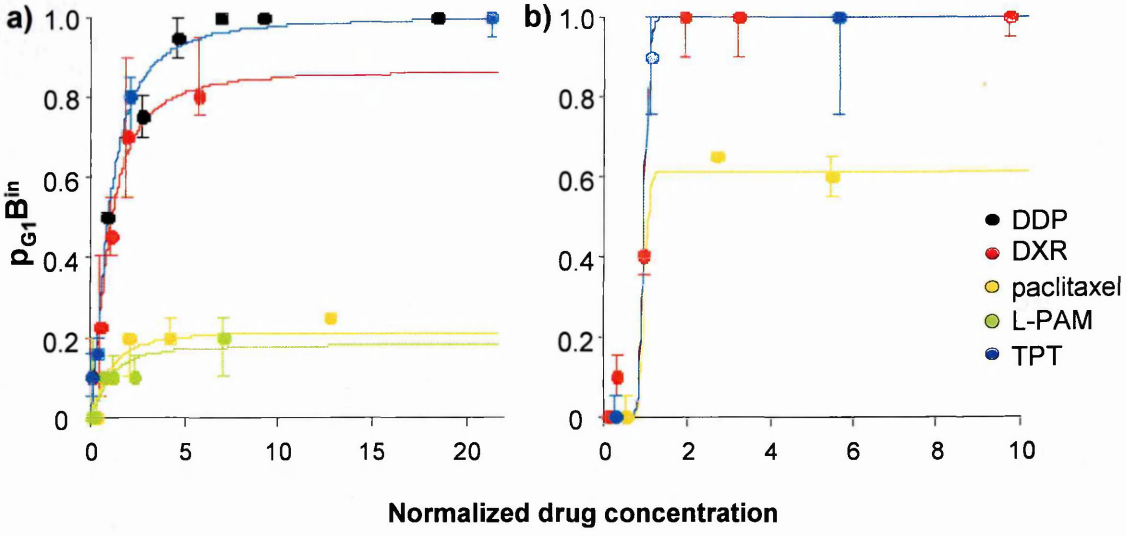

Figure 7.2: Dose-dependence of G_1 checkpoint activity detected between 0 and 6h after treatment (panel a) and between 24 and 48h after treatment (panel b). The dots represent the values of the parameters as obtained from the simulation, while the continuous line represent the fitting obtained by using the Hill function. On the horizontal axis one unit corresponds to the EC_{50} of $p_{G1}B^{in}$ for each drug. In the graphs are not represented the curves corresponding to the parameters that were null for every drug concentration.

7.2.2 Features of the Activity of G_2 Checkpoint

Figure 7.3 shows the time-dependence of probability of occurrence of G_2M block ($p_{G2}B^{in}$) in correspondence to a treatment with a drug concentration close to the EC_{50} (figure 7.3a) and at the concentration where this activity reached its maximum (figure 7.3b). In samples treated with TPT and L-PAM the experimental data required a different strength in the checkpoint activity between BrdUrd-positive and BrdUrd-negative cells, whereas for other drugs the data could be reproduced with the same strength. In any case, for cells treated with EC_{50} drug concentration G_2 blocking activity reached its maximum within 24h, then at 6h for paclitaxel and TPT or at 24h for DDP and DXR the intensity of the block declined and got exhausted. A different behaviour was observed in the case of cells treated with EC_{50} L-PAM concentration, where at short times after treatment the blocking activity in G_2M was very weak, but it increased between 6 and 24h and a residual activity was still present 72h after treatment. The longer duration of the short-term G_2 blocking activity respect to the short-term G_1 block could be explained by the fact that most of the cells are initially in S and G_1 phase and they cannot reach G_2 immediately after treatment, whereas G_1 cells immediately cross G_1 checkpoint.

When the drug concentration increases the blocking activity in this phase strengthened and lengthened (figure 7.3b), but between 0 and 6h the effect remained weak in L-PAM treated cells and relatively weak also in BrdUrd-negative cells treated with TPT. This behaviour indicated that only a low percentage of the cells crossing G_2 in that interval were intercepted by the checkpoint. This subpopulation of cells escaping the short-term G_2 block was formed by cells treated in G_2M phase in the case of TPT and by cells treated in G_2M and in middle and late S in the case of L-PAM. In spite of the weak intensity of the blocking activity this effect was persistent in L-PAM treated samples, where it remained at

its maximum up to the end of the observation. A similar continuous effect, without decreasing of intensity at longer times, was observed only in BrdUrd-positive cells treated with TPT.

Figure 7.4 shows the dose-dependence of G_2 checkpoint activity at short (panel a) and at long (panel b) times after treatment. As in the previous figure we included the distinction between BrdUrd-positive and BrdUrd-negative cells for samples treated with L-PAM and TPT, whereas with the other drugs we did not get a proof of differences between the two subpopulations. Together with the values of the parameters, as obtained by the simulation, the fitting performed with a Hill function with a common value of the sigmoidicity was also reported. The fitting of short-term G_2 blocking activity indicated that the effect rose from 0.1 x E_{max} to 0.9 x E_{max} in an 11-fold concentration range, from 0.31 x EC_{50} to 3.26 x EC_{50}, not much differently respect to the G_1 short-term block.

From this analysis it is possible to conclude that all the considered drugs were able to activate G_2 checkpoint but a strong response, as measured by E_{max}, was detected in BrdUrd-positive cells treated with TPT, in paclitaxel, DXR and DDP treated samples but not in L-PAM and BrdUrd-negative cells treated with TPT.

Figure 7.4b shows that the onset of the long-term G_2M response was sharp, with a single possible exception represented by BrdUrd-positive cells treated with TPT, where the blocking activity was relatively strong even at low concentrations. In general this trend was similar to that observed for G_1 blocking activity, even though in this case only in BrdUrd-positive cells treated with TPT and in DXR treated samples the maximum value of G_2 blocking activity was close to 1. In all the other situations its strength was intermediate, with an E_{max} included between 0.3 and 0.7.

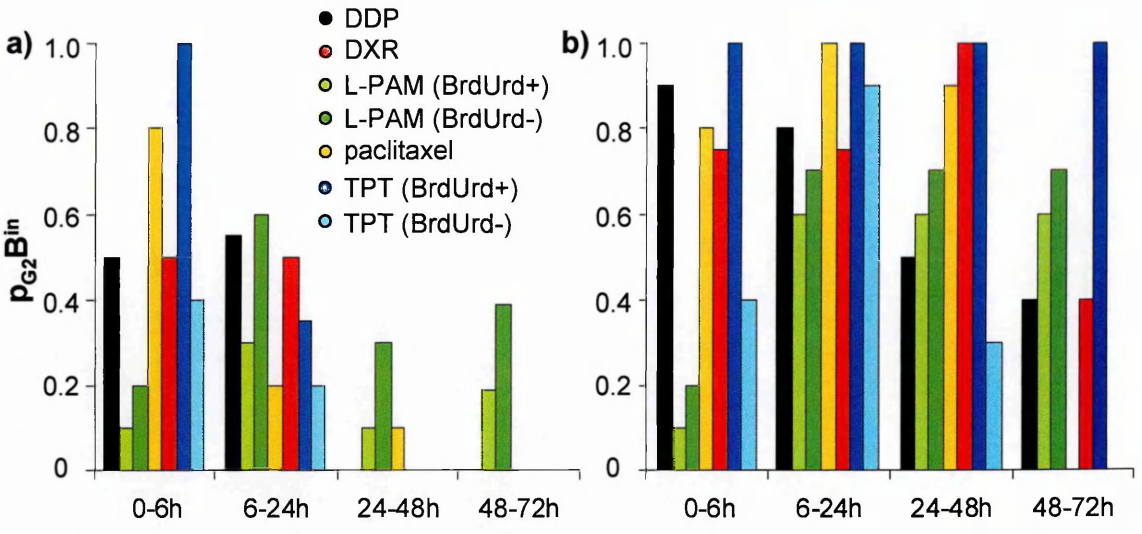

Figure 7.3: Time-course of G_2 checkpoint activity at drug concentrations close to the EC_{50} (panel a) and at its maximum (panel b).

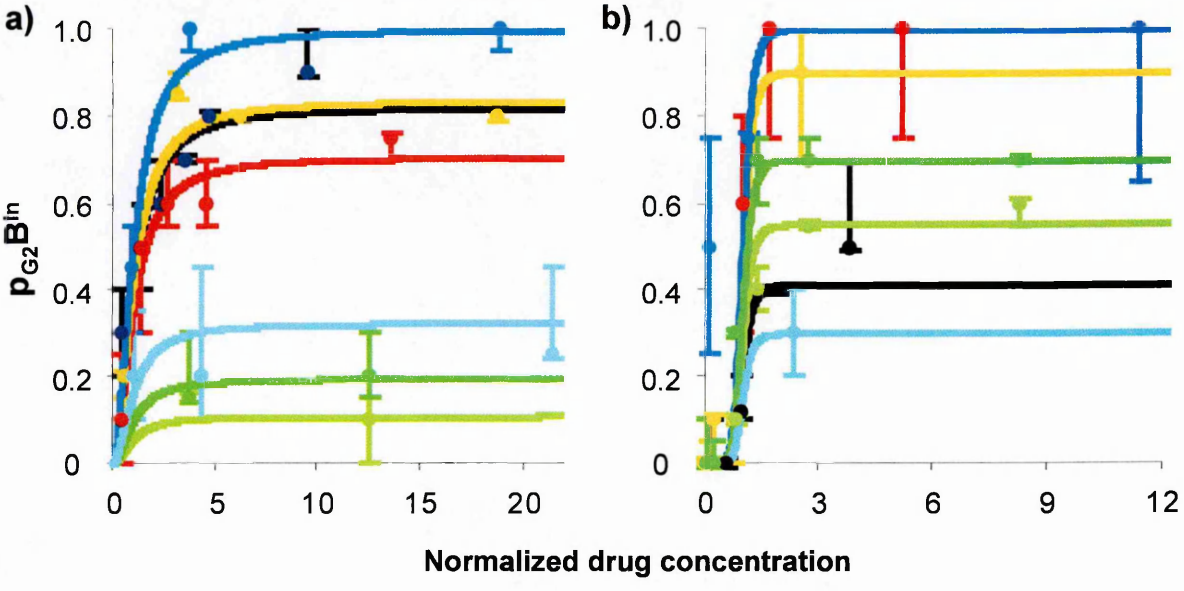

Figure 7.4: Dose-dependence of G_2 checkpoint activity detected between 0 and 6h after treatment (panel a) and between 24 and 48h (panel b). The dots represent the values of the parameters as obtained from the simulation, while the continuous line represent the fitting obtained by using the Hill function (the correspondence between the colours and the drugs was the same reported in figure 7.3).

7.2.3 Features of the Activity of S Checkpoint

The delay parameter (p_SF) was used to describe the fractional reduction of the average DNA synthesis rate, which is an effect observed in all the treated samples independently of the compound used for the treatment. Figure 7.5a shows the time-course of p_SF as obtained by the simulation of the samples treated with a drug concentration close to the EC_{50}, while figure 7.5b represents the kinetics of this parameter at the drug concentration where its value reached the maximum. This parameter showed different trends in dependence on the drug considered. For instance, between 0 and 6h, paclitaxel and L-PAM treated samples presented a low inhibition of DNA synthesis, but the effects rose 24h after treatment. On the other side, DDP induced a rapid inhibition of DNA synthesis which rapidly decreased in samples treated with low drug concentrations (panel a), whereas the parameter remained constant up to 72h in cells treated with high doses (panel b). In BrdUrd-positive cells treated with TPT and in DXR treated samples the parameter reached its maximum at intermediate times (between 6 and 48h), whereas in the case of treatment with high drug concentrations its value was almost constant and the inhibition was strong at the beginning and at the end of the observation too. The progression through S phase of BrdUrd-negative cells treated with TPT did not present any alteration, whereas the delay in S phase of BrdUrd-negative cells treated with L-PAM was not represented because considered equal to that observed in BrdUrd-positive subpopulation.

The shape of the dose-dependence of this parameter (figure 7.6) was similar to that observed for $p_{G1}B^{in}$ and $p_{G2}B^{in}$. The data obtained from the simulation were well fitted by a sigmoid curve with a common sigmoidicity for all the drugs. At short times after treatment (between 0 and 6h, figure 7.6a), the trend of the data showed a gradual increase of the effect when the drug concentration became higher,

whereas the values found between 24 and 48h (figure 7.6b) revealed a steep increase, that could be ascribed to the presence of a threshold.

Short-term delay reached fairly high values in samples treated with DDP and in BrdUrd-positive cells treated with TPT. In all the other situations the parameter was lower, in particular p_SF presented a value between 0.3 and 0.5 in DXR and L-PAM treated cells and a value lower that 0.2 in samples treated with paclitaxel. On the other side, once that the long-term delay reached the dose threshold its effect was strong in all the samples, independently of the considered anticancer compound.

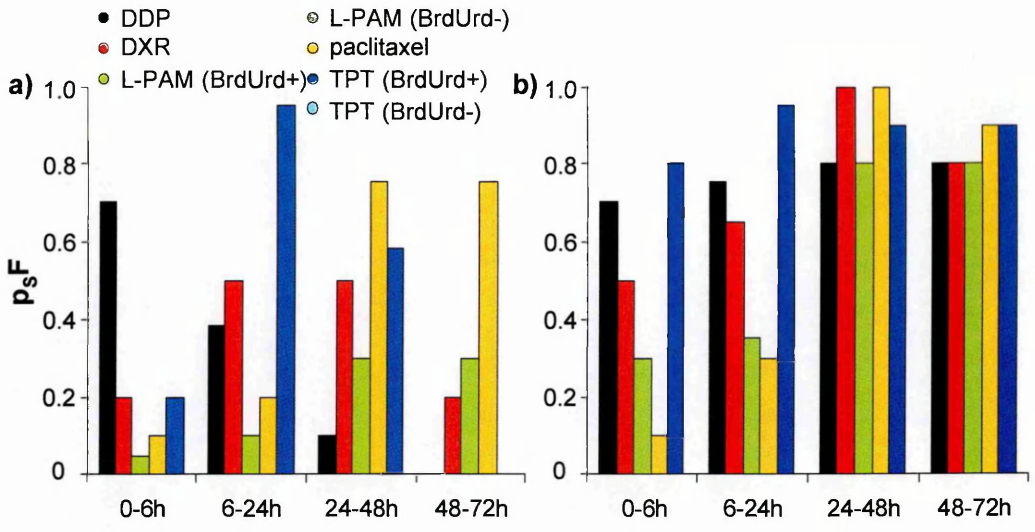

Figure 7.5: Time-course of the parameter describing the delay in S phase at the concentration closer to the EC_{50} (panel a) and at the concentration where it reached its maximum values (panel b). This effect was not present in BrdUrd-negative cells treated with TPT, while the effect produced by L-PAM treatment was equal for BrdUrd-positive and BrdUrd-negative (not shown) cells.

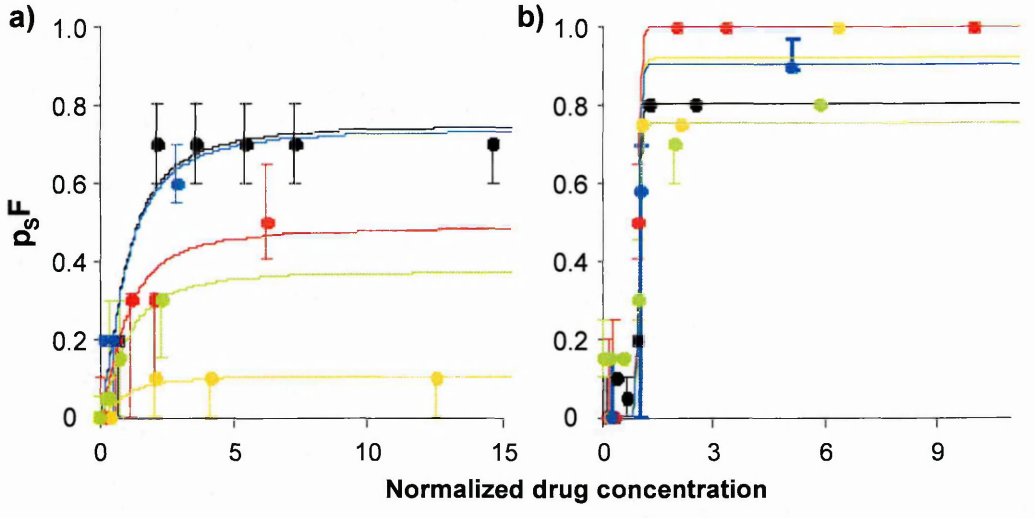

Figure 7.6: Dose-dependence of S delay detected between 0 and 6h after treatment (panel a) and between 24 and 48h after treatment (panel b). The dots represent the values of the parameters as obtained from the simulation, while the continuous line represent the fitting obtained by using the Hill function.

7.2.4 Evaluation of EC_{50}

From the fitting of the dose-response curves it was possible to obtain all the EC_{50} values for each parameter. These values are listed in table 7.1 and together with the evaluation of the E_{max} they could give an indication about the intensity of the response of each cell cycle checkpoint to DNA damage.

VALUES OF EC_{50}							
Short-term effects (0-6h)	**DDP**	**DXR**	**Paclitaxel**	**L-PAM (BrdUrd+)**	**L-PAM (BrdUrd-)**	**TPT (BrdUrd+)**	**TPT (BrdUrd-)**
G_1 block (BrdUrd-)	10.8 ***	5.2 ***	0.023 *		42.0 *		0.5 ***
S delay (BrdUrd+)	13.7 ***	4.8 ***	0.024 ***	129.2 **		0.35 ***	
G_2 block	21.1 ***	2.2 ***	0.016 *	<3 *	<3 *	0.05 ***	0.05 **
Long-term effects (24-48h)	**DDP**	**DXR**	**Paclitaxel**	**L-PAM (BrdUrd+)**	**L-PAM (BrdUrd-)**	**TPT (BrdUrd+)**	**TPT (BrdUrd-)**
G_1 block		3.1 ***	0.018 **			0.18 ***	
S delay	78.4 ***	3.0 ***	0.047 ***	50.8 ***	50.8 ***	0.2 ***	
G_2 block	52.6 **	5.7 ***	0.388 ***	36.2 **	31.1 **	8.7 ***	42.3 *

Table 7.1: All the values of the drug concentrations (μM) that determined an effect equal to the 50% of the maximum response are listed above. The stars near the EC_{50} indicate the intensity of the maximum value of each parameter. In particular: * if $E_{max} \leq 0.3$; ** if $0.3 < E_{max} \leq 0.7$; *** if $E_{max} > 0.7$.

Immediately after treatment, between 0 and 6h, G_2 checkpoint was the first (i.e. detected at the lowest drug concentrations) activated response in four of the five considered drugs, the only exception was represented by DDP. In some cases, in particular in L-PAM and in TPT treated cells a very low drug concentration was

enough to activate this response, which after TPT treatment was also able to intercept a high percentage of cells, more than 70% for BrdUrd-positive population.

The drug concentration that activated G_1 and S phase response was almost the same in all the considered drugs, only L-PAM represented an exception to this behaviour, where a very high drug concentration was necessary to activate S delay. Once that G_1 and S phase checkpoints were activated they were able to intercept a percentage of proliferating cells higher than 70%, only in paclitaxel and L-PAM treated samples less than 30% of cells passing through G_1 remained blocked in this phase.

At long times after treatment, the G_1 checkpoint was not active anymore in DDP, L-PAM and in BrdUrd-negative cells treated with TPT, whereas the effect in this phase was still present and activated by low drug concentrations in all the other considered drugs. The S and G_2 checkpoints were still active and able to reach, in most situations, an E_{max} correspondent to a percentage of intercepted cells higher than 70%. Whereas in DDP, DXR and L-PAM the EC_{50} for S and G_2 checkpoints were of the same order of magnitude, in paclitaxel and TPT treated cells they were much more different. In particular only very high drug concentrations of paclitaxel could activate a long-term G_2 response, which was in any case able to intercept a high amount of damaged cells. On the other side only a small amount of BrdUrd-negative cells treated with TPT remained blocked in G_2M phase when treated with high drug concentrations.

7.2.5 Loss and Recycling

Applying the principle of parsimony on the number of parameters, we introduced the recycling probability only at the end of a transient blocking activity. However, in samples treated with intermediate drug concentrations, when short-term blocks in

G_1 and in G_2 are not total, we could not exclude the contemporary presence of recycling. Thus, in cells treated with DXR and L-PAM, recycling was possible after short-term block in G_1, but it was not necessary to reproduce the experimental data, whereas it was unambiguously detected between 6 and 24h in cells treated with TPT, paclitaxel and DDP at low/intermediate concentrations. At high concentrations recycling was not detected, except for TPT treated cells at long times after drug washout.

For cells blocked in G_2M phase after treatment with low and intermediate concentrations of paclitaxel, DDP and DXR recycling was detected. In particular in the first case cells left G_2M phase between 6 and 24h, in the second case between 24 and 48h and in DXR treated cells the recycling was observed between 24 and 72h. Thus, in general, recycling seems to refer to short-term block, involving cells blocked in their first passage through G_1 or G_2M. Recycling from long-term block could not be detected and the steep dose-dependence of this parameter suggested the absence of repair in such a situation. Moreover, even in the presence of a recycling effect, not all the blocked cells were always able to start cycling again, some of them could remain blocked up to the end of the observation period (72h) and thus they would be probably destined to die.

Cytotoxic effects appeared when the drug concentration became higher. In table 7.2 we compared the drug concentrations that determined an overall cell loss bigger than 5% in each cell cycle phase with the doses that determined the onset of a cytostatic effect. The extent of a cytostatic only region was variable between drugs, wide in TPT, L-PAM and DDP treated samples, narrower for DXR and almost absent for paclitaxel. However, the gap between the onset of cytostatic and cytotoxic effects is further on reduced for DXR and TPT if we consider the percentage of dead cells together with the cells that were still blocked at 72h,

supposing that they are committed to die (indicated as G_1 loss* or G_2 loss* in the table 7.2).

In DDP and paclitaxel treated samples the cell killing occurred at similar drug concentrations in all cell cycle phases, whereas a very high L-PAM concentration (100 μM) and TPT concentration (10 μM) were necessary to kill the cells in G_1 and in S phase respectively.

Effect	DDP	DXR	Paclitaxel	L-PAM	TPT
G_1 block	10	0.5	0.05	30	0.2
G_1 loss	50	1	0.05	100	1
G_1 loss*	30	0.5	0.05	50	0.2
S delay	10	0.5	0.05	3	0.2
S loss	10	1	0.05	10	10
G_2 block	10	3	0.05	3	0.05
G_2 loss	50	6	0.1	10	0.2
G_2 loss*	30	3	0.1	10	0.05

Table 7.2: Drug concentrations (μM) that determined the onset of cytostatic or cytotoxic effects. In particular, for cytostatic effects, we considered the dose that determined a blocking activity higher than 0.05 in at least one interval of time, whereas for cytotoxic effects the dose that caused the death (or the permanent block) of at least 5% of cells in 72h.

The cytotoxic effects affected all cell cycle phases. In order to evaluate whether they occurred preferentially in G_1, S or G_2M we measured the distribution of cells lost in each cell cycle phase 72h after treatment with low, intermediate and high drug concentrations (table 7.3), adding to them the percentage of cells that were still blocked at that time. In samples treated with low doses of DDP and L-PAM cell loss principally occurred in S phase, while in DXR and paclitaxel treated samples the cells preferentially died in G_1 phase. Intermediate concentrations were

characterized by the onset, or strengthening of G_2 loss. G_2M was the phase where the majority of cells died at the high concentration, with the exception of DDP. The case of TPT treated cells was peculiar. For treatments performed with low/intermediate TPT doses the cell loss was mainly G_1 and G_2 phase, with some preferences for G_1. The percentage of dead cells in S phase increased with the dose, but did not reach the 25% even at the highest dose.

	DDP	DXR	Paclitaxel	L-PAM	TPT
Low Drug Concentrations					
G_1	21.4	78.3	81.3	-	59.2
S	75.3	20.0	13.4	70.8	-
G_2M	3.3	1.7	5.4	29.2	40.8
Intermediate Drug Concentrations					
G_1	19.4	42.8	62.6	2.4	59.4
S	56.6	4.5	12.4	30.3	6.2
G_2M	24.0	52.7	25.1	67.3	34.4
High Drug Concentrations					
G_1	37.1	38.4	34.9	6.5	36.6
S	37.7	13.4	9.9	29.7	22.8
G_2M	25.2	48.2	55.2	63.7	40.6

Table 7.3: The percentages of cells lost summed to those of definitively blocked in each cell cycle phase 72h after treatment with equitoxic drug concentrations were listed above. In particular the drug concentrations were classified as "low" when only 25% of cells were killed in 72h, "intermediate" when about 50% of cells were killed and "high" when 75% of cells died.

7.3 DISCUSSION

The experiments and the analysis presented in the previous chapters (4, 5 and 6) and the published studies (Montalenti et al., 1998; Sena et al., 1999) allowed the

construction of two databases. The first database includes the time-course of flow cytometric percentages and cell numbers obtained after treatments with all tested drug concentrations. This represents, in our knowledge, the first complete database that has been made with the time-course of cell cycle drug perturbations induced by short treatments at different concentrations. The second database includes all the parameters used in the model to simulate the experimental data. These parameters represent the strength of each checkpoint activity as a probabilistic quantity. From this point of view, a single cell traversing a particular cell cycle phase has a probability to be intercepted by the phase checkpoint and this probability increases with the drug concentration. The same probability, interpreted from the population point of view, corresponds to the fraction of cells that is actually intercepted by the checkpoint among those passing through it. The heterogeneity observed in the cell response to drug treatment, where some cells are intercepted by a block and other pass from one phase to another, could be explained hypothesizing the presence of a variable quantity of damage among the cells of the population. This difference can induce the activation of the checkpoints only in some cells and not in others. But the heterogeneity could also be explained by a variable response to the same damage, as a consequence of different amounts of proteins involved in the response among the cells of the same population. However, mining the parameters of the database we could highlight some common aspects of the response to DNA damage, in spite of the differences due to intercell variability and to the use of different anticancer compounds.

For all the compounds we performed short treatments (1h), even when longer schedule of treatment where suggested in consideration of the mechanism of action of the drug. In this way we could appreciate the presence of short- and long-term effects once that the drug was removed. In particular the cell response at long times after treatment revealed the existence of persistent damage into the

cells or long kinetics of response in the molecular pathways regulating the checkpoints. In fact, as known by the literature, in cells treated with alkylating agents (Hansson et al., 1987; O'Connor and Kohn, 1990) and platinum compounds (D'Incalci et al., 1985) the formation of cross-links is a slow process starting from the presence of monoadducts. On the other side, as demonstrated by Wu et al. (2002), the formation of DSBs induced by treatments with topoisomerase-inhibitors is biphasic. In particular these authors showed that a detectable amount of DSBs was already present immediately after drug washout, 8h after treatment this quantity decreased but started rising again at longer times after treatment (24-48h). All these facts, together with the failed attempts of repairing DNA damage, could justify the presence of long-term effects even in samples where the damaging agent was removed. On the contrary, the presence of short-term effects could be more due to the existence of an obstacle that avoid the normal progression through cell cycle phases, such as the presence of DNA adducts or DNA-topoisomerase-drug complexes, than to the activation of repair processes. Starting from this point of view we could explain the biphasic behaviour of some checkpoint activity, as that observed in G_1 block in TPT and DXR treated cells (figure 7.1). Moreover, this behaviour of G_1 checkpoint is also in agreement with molecular observation that hypothesized the presence of two different pathways involved in the activation of this response. The activation of the first faster response is p53-independent, whereas the pathway activated by p53 is slower, but sustainable for a long time (Bartek and Lukas, 2001).

The different time-dependence of the response to high and low doses was investigated, from a molecular point of view, by Caporali et al. (2004). In particular they studied the kinetics of activation of several proteins involved in cell cycle checkpoints after treatment with a methylating agent. In this case, the activation of ATM in cells treated with low drug concentrations was a late event and required a

functional MMR system for phosphorylation of Chk1, Chk2 and p53. On the other side, a rapid activation of ATM was detected during treatment with high doses. This could explain the different time course that was observed in the blocking activity in the samples treated with low and with high drug concentrations.

In our study the dose-response curve of the checkpoint activity at short and long times after treatment revealed two different trends, but in both cases we reached a sort of plateau in the intensity of the effect. This behaviour and the presence for long-term effects of a threshold-concentration demonstrate that the relationship among the drug concentrations, the amount of damage induced by the treatment and the cell response is not linear, but a specific amount of damage is required to activate the checkpoint activity.

If we consider the values of the EC_{50} obtained by fitting of the dose-response curve at short times after treatment we could observe that the most sensitive checkpoint is that present in G_2M phase. For four of the considered compounds it is enough a low concentration to activate this response that has to prevent damaged cells to divide. At short times after treatment only higher drug concentrations activate the response in G_1 and in S phase. This demonstrates that these two checkpoints need a bigger amount of damage to be activated and this happens in presence of treatment with higher drug concentrations or for cells that are at the second or third generation. In this case the accumulation of damage becomes able to activate even lower sensitive checkpoints. In fact the comparison of the EC_{50} between 24 and 48h reveals that the concentrations necessary to activate G_1 checkpoint were even lower than those observed for S and G_2.

Even though we considered anticancer agents with different modes of action, with this study we were able to compare all the dose-response curves of checkpoint activities and to highlight the principal similarities or differences.

CHAPTER 8: CFSE-based Approach for the Evaluation of Antiproliferative Drug Effects

8.1 INTRODUCTION

8.1.1 CFSE: Biochemical Properties

CFDASE consists of a fluorescein molecule containing two acetate moieties and a succinimidyl ester functional group. In this form, it is non-fluorescent and can spontaneously penetrate cell membranes. This compound is rapidly taken up by cells, although due to its lipophilic nature CFDASE also freely exits from cells. Once inside cells, after diffusion into the intracellular environment, endogenous esterases remove the acetate groups, rendering the molecule highly fluorescent and non-permeant to the cell membrane (CFSE). The slower exit rate prolongs the time available for CFSE to couple covalently to intracellular molecules. In addition, the succinimidyl ester reacts with free amine groups of intracellular proteins forming dye-proteins adducts. In some cases carboxyfluorescein is coupled to molecules to form conjugates that are rapidly degraded or still exit through the plasma membrane, whereas in other cases the carboxyfluorescein conjugates are stable and unable to exit from the cells (see figure 8.1). Proteins that have a low turnover rate, including some cytoskeletal components, are thought to be responsible for the very long-lived staining afforded by CFSE (Lyons, 2000).

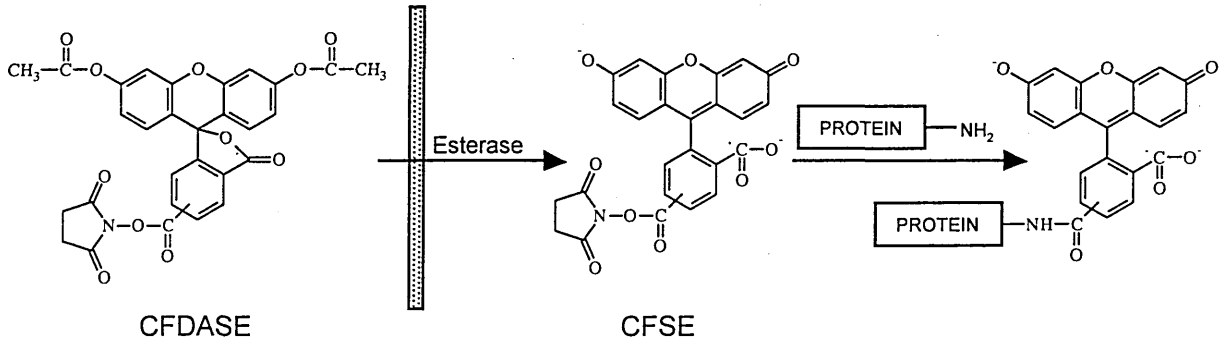

Figure 8.1: Mechanism of cellular labelling by CFDASE. CFDASE is a non-polar molecule that spontaneously penetrates cell membranes and is converted to anionic CFSE by intracellular esterases.

The spectral characteristics of fluorescent CFSE are identical to fluorescein, with optimal excitation by 488 nm argon laser light, emitting strongly at 519 nm.

When cells divide, CFSE is equally distributed between the daughter cells, which are therefore half as fluorescent as their parents, consequently, each successive generation in a population of proliferating cells is marked by specific two-fold decrease in cellular fluorescence intensity. In response to a proliferation stimulus, cells with one-half, one-fourth, one-eighth, etc. the fluorescence intensity of undivided mother cells are detected as distinct peaks in the fluorescence histogram of the entire cell population. The percentage of cells in each peak corresponds to the percentage of cells in the first (undivided mother cells), second (divided once), third (divided twice), and subsequent cell cycles, thereby providing a direct measure of the proliferating activity of the population and of the heterogeneity of that activity (León et al., 2004). The observation of multiple peaks on different days after stimulation is indicative of cell heterogeneity and highly asynchronous division, but in order to distinguish the peaks it is necessary a good resolution. Maximum resolution of division cycles is obtained when the distribution of initial cellular fluorescence intensities is narrow and autofluorescence background levels are low.

In order to make a quantitative analysis of the data obtained by CFSE histograms it is necessary to take into account two characteristics of this probe: high concentrations of CFSE may be toxic to some cell types and the majority of CFSE initially taken up by the cells it is not stably incorporated and it is lost within the first few hours (Hodgkin et al., 1996; Lyons et al., 2001; Dumitriu et al., 2001). This means that the dye concentration has to be enough to follow the cells until several days after labelling, taking into account the efflux and the fact that the fluorescence halves at each generation, without affecting exponential cell growth.

8.1.2 Applications and Previous Studies

Since its introduction in 1994 (Lyons and Parish, 1994), the flow cytometric analysis of lymphocyte proliferation by serial halving of the fluorescence intensity of the vital dye CFSE has become widely used in immunological laboratories. It has become the method of choice for investigating the division-related differentiation of lymphohemopoietic cells, as well as the kinetics of cellular expansion during an immune response. An important feature of these studies is that many biological processes in lymphocytes, such as T cell cytokine production, B cell Ig isotype switching, T cell apoptosis and cell surface molecule expression have been shown to be very division dependent. Recently a particular powerful application of CFSE-labelling has been employed to monitor T lymphocyte proliferation in response to a range of costimulatory signals (Gett and Hodgkin, 2000).

Among the cell types that have been investigated using the technique are hemopoietic stem cells (Kerre et al. 2001), T and B lymphocytes (Lyons and Parish, 1994; Hodgkin et al., 1996), natural killer cells (Warren, 1999; Cooper et al., 2002) and other cell lines (Khil et al., 1997; von Horsten et al., 2000).

As shown by Hodgkin et al. (1996) this technique allows the visualisation of eight to ten discrete cycles of cell division by flow cytometry. For its characteristics CFSE has been used not only for monitoring cell proliferation but also for tracking the migration of lymphocytes *in vivo* over several weeks (Weston and Parish, 1990).

CFSE labelling has been validated relative to standard proliferation analysis techniques such as [^{3}H]-thymidine incorporation and BrdUrd labelling. Compared with these classical techniques CFSE can provide more information, for example an entire population of cells dividing once will incorporate the same amount of [^{3}H]-thymidine as one half of the population never divided. These different division

patterns can be distinguished by CFSE labelling analysis, which allows following the division history of individual cells. At the same way BrdUrd has been extensively used to quantify *in vitro* and *in vivo* cell division. However, this method is generally unable to distinguish the progeny of cells that have undergone several divisions from those that have undergone a single division, but BrdUrd staining can be performed in combination with CFSE labelling. This biparametric staining allows the examination of the division-related proliferation rate and cell cycle profile as well as division history (Gett and Hodgkin, 1998; Hasbold et al., 1998). In addition, to being able to explore cell surface molecule changes linked to cell division, CFSE labelling has also been combined with techniques measuring production of bioactive materials such as cytokines (Gett and Hodgkin, 1998; Bird et al., 1998; Lyons 1999). Spectral characteristics of CFSE allow the use in conjunction with other fluorochromes, such as PE, PI, 7-aminoactinomycin D (Marin et al., 2003) etc.

Despite the potential usefulness of the method for investigating the antiproliferative effects of drugs, by directly measuring the time-course of the percentage of cells in each division cycle during or after treatment, the use of CFSE is still confined to immunological research. Technical reasons probably explain why it is rarely used in cancer cells. First, the easily identifiable fluorescence peaks usually obtained by labelling lymphocytes are not obtained by labelling other cell types, which have a much less homogeneous protein content. Peaks that correspond to subsequent generations are not readily distinguishable after labelling cancer cells, and this poses an apparently insurmountable obstacle to data analysis and interpretation. Additional technical problems arise with adherent cells that are eventually detached and fixed with the aim of measuring DNA content correlated with CFSE.

8.1.3 Analysis of CFSE Fluorescence Histograms

We have developed a CFSE-based method to study cell cycle effects of drugs *in vitro* and to provide the first application of it in ovarian cancer cells treated with TPT (see chapter 4).

We obtained the percentages of cells in the first, second, third and subsequent cycles ($\%C_1(t)$, $\%C_2(t)$, $\%C_3(t)$...) by fitting each histogram with a sum of gaussians, each one representing a generation of cells. Thus the average CFSE fluorescence of the second, third, etc., gaussian was assumed equal to one-half, one-fourth, etc., of the average CFSE fluorescence intensity of the first gaussian, which represented undivided cells.

Listmode data were converted as 256 channel histograms using FCS Assistant (shareware) and the analysis of the histogram profiles was made with Excel (Microsoft, Redmond, WA, USA). The spreadsheet was divided in four areas.

Area 1 included the table of the relation between channel numbers and fluorescence intensity (i.e., a column containing the channel numbers, z, and another column with the corresponding fluorescence intensity, FL(z)). The ideal relation is $FL(z) = 10^{z/64}$ for a four-decade, 256-channel scale, but analogic amplifiers may deviate from that. The correct relationship can be empirically determined, when needed, with a calibration procedure.

Area 2 included a matrix of the useful parameters of all guassians, namely, for gaussian i, the average fluorescence intensity (Mi_{FL}), average channel (Mi_{CH}), standard deviation (σi) and number of cells (Ni). Given a value of $M1_{CH}$, the corresponding $M1_{FL}$ was automatically calculated by using the relation in area 1 as a reference table and the Lookup function of Excel. The fluorescence intensity of the average of the second and subsequent gaussians was automatically generated as a function of the average of the first gaussian and of the background fluorescence (BG_{FL}; also reported in the spreadsheet) by using the formula: $Mi_{FL}=$

$(M1_{FL} - BG_{FL}) / 2^{i-1} + BG_{FL}$, accounting for subsequent halving of the CFSE-related fluorescence. Back-transformation of fluorescence intensity into channel numbers was automatically made by using area 1 as reference table, providing all updated Mi_{CH} at each recalculation of the spreadsheet.

Area 3 included the histograms of data, of each gaussian and of the fitted curve in separate columns. The formulas of each gaussian used the parameters of the matrix in area 2 and the formula of the fitting function was simply the point-by-point sum of gaussians.

Area 4 included additional quantities, in particular the objective function (the sum of square errors), the reduced chi-square and the value of the background fluorescence level.

In addition, the plot of data and fitting is automatically generated in the spreadsheet.

The constrained non-linear fitting was accomplished with the Solver function associated with the Excel spreadsheet. The fitting routine used a sum of squares error criterion to optimize the following parameters: (a) average channel of the first gaussian (the average of the others being automatically calculated as specified above), (b) standard error (assumed equal) of all gaussians and (c) the number of cells in each gaussian (constrained to be positive).

The initial estimate of the average of the first gaussian (undivided cells) at each experimental time was provided by the parallel calculation of the efflux (see 8.2.2). Then the optimization was made by constraining this parameter in a small range (three channels) around that initial value.

Once that we have obtained the percentage of cells in the different cycles at time t, it is possible to calculate the fraction of the starting population that at a given time t remained blocked without dividing, $f_1(t)$ or the fraction of cells that were able to

proliferate by dividing once ($f_2(t)$), twice ($f_3(t)$), etc. This leads to an approximate, "average", result because descendants do not divide in a synchronized way, and an "original" cell may actually, at a given time, have some descendants in the second generation, some in the third, and so on.

Within this approximation, the proportion of the original cells that divided zero, one, two or more times can be calculated by correcting the $\%C_i(t)$ values for the amplification due to divisions, as it is done in immunological studies to evaluate the frequency of precursors cells able or unable to proliferate (Givan et al. 1999). Among cells present at time t, any cell in the first generation is still a cell (undivided) of the starting population, two cells in the second generation come from a single "starting" cell, like any four in the third generation and so on. Thus $f_i(t)$ and $\%C_i(t)$ values are related through the following formula:

$$f_i(t) = (\%C_i(t)/2^{i-1})/[\%C_1(t) + \%C_2(t)/2 + \%C_3(t)/4 +...]. \quad \text{(equation 1)}$$

These fractions are based on the cells still detected at time t and do not contain any information on the amount of cell loss. However, an estimate of the fraction of survival, Fs(t), within the starting cell population can be obtained by joining the $f_i(t)$ values with the absolute number of cells at the same time, N(t), independently measured with a Coulter Counter. In this simplified proliferation model,

$N(t) = N(0) \times Fs(t) \times [f_1(t) + f_2(t) \times 2 + f_3(t) \times 4 +...]$, so Fs(t) is given by the following equation:

$$Fs(t) = N(t)/[N(0) \times (f_1(t) + f_2(t) \times 2 + f_3(t) \times 4 +...)]$$

$$= [N(t)/N(0)] \times [\%C_1(t) + \%C_2(t)/2 + \%C_3(t)/4 +...]/100. \quad \text{(equation 2)}$$

The absolute number of surviving cells reported in figure 8.11 is then calculated as $N(0) \times Fs(t)$.

Conversely, if the fraction of survival is known, the relative growth, N(t)/N(0), can be directly calculated by using only percentages of cells after reverting equation 2. In particular, when cell loss is negligible, the relative growth curve is given by:

$$N(t)/N(0) = 100/[\%C_1(t) + \%C_2(t)/2 + \%C_3(t)/4+...]. \quad \text{(equation 3)}$$

8.2 RESULTS

8.2.1 CFSE Labelling and Toxicity

Cells were labelled in suspension just before seeding the culture. No advantages were obtained, in terms of the width of the CFSE fluorescence histogram, by labelling cells in adherence some time after seeding or by seeding synchronized cells. The start of the experiment with the drug, usually 24h after seeding, was adopted as time zero; thus, CFSE-loading and seeding occurred at "-24h". The main advantage of this protocol is that, at the start of the experiment, CFSE is stably incorporated into the cells, thereby avoiding the pitfalls associated with rapid efflux after labelling. In addition, any residual CFSE in solution is washed away by the change of the medium in all samples at the time of treatment.

High CFSE concentrations are toxic to the cells, particularly when they are labelled in the absence of serum proteins. However, CFSE is sequestered by serum protein and with too low concentrations the fluorescence intensity comes too close to background fluorescence to be reliable. A valuable compromise was to use 1 μM CFSE for 15 min of labelling in PBS under gentle agitation. The growth curve of cells labelled in this way does not perfectly overlap the growth curve of unlabeled cells, but the cells have the same doubling time when in exponential growth (figure 8.2) and the CFSE fluorescence intensity of proliferating IGROV1 cells remains well above the background fluorescence level for several days (figure 8.3).

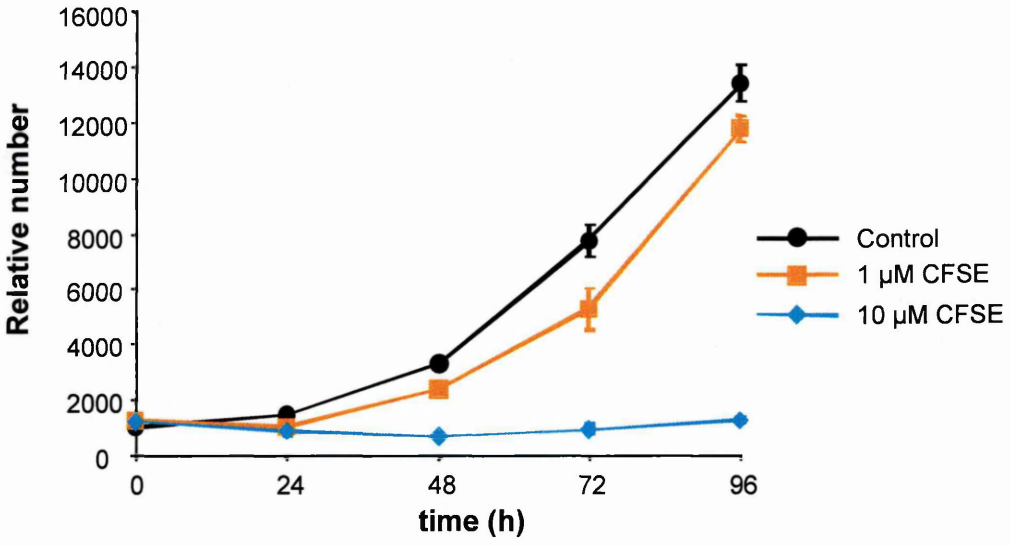

Figure 8.2: Growth curves of IGROV1 cells after labelling with 0, 1 and 10 µM CFSE. The cells were labelled at 0h in the absence of serum. Even though the growth curve of 1-µM labelled cells does not overlap the growth curve of the control they have the same doubling time when in exponential growth.

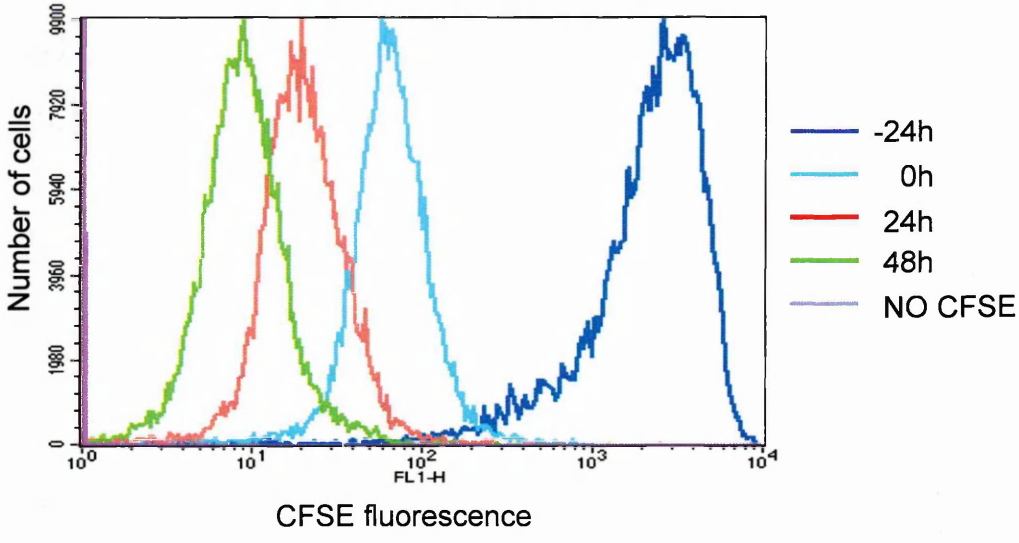

Figure 8.3: Time-course of fluorescence histograms of IGROV1 cells labelled with 1 µM CFSE just before seeding (-24h, in the time scale adopted). Cells were harvested and directly analyzed (without fixation) at -24h (a few minutes after labelling) and 0, 24 and 48 h. With the chosen amplification, the –24-h histogram was detected within the scale in the fourth decade, but the background fluorescence of cells without CFSE was barely detectable.

8.2.2 CFSE efflux

Figure 8.3 shows a more than 10-fold decrease of CFSE fluorescence between -24 and 0h. This decrease obviously cannot be ascribed to a rapid proliferation of our cells because: (a) doubling time would be about 6h to account for such a decrease (and the doubling time of exponentially growing IGROV1 cells is 22h), and (b) a parallel Coulter Counter cell count indicated only a small increase in cell number (as usual in just-seeded cell cultures). Thus, the fluorescence is not completely retained by the cells, and this contributes to the decrease besides the halving at each division. We also used quiescent lymphocytes in order to evaluate properly the decrease of CFSE fluorescence unrelated to cell proliferation.

CFSE efflux in quiescent lymphocytes showed a biphasic pattern (figure 8.4a). A huge decrease in fluorescence in the first hours after labelling was followed by a continuous small decrease for up to 8 days thereafter. In the same experiment, some cells were fixed in ethanol at the same times and analyzed all together at the end of the time course. Fluorescence was weaker in fixed than fresh cells, but after the first 24h the difference was smaller and the rate of decline was very similar. This suggested that the fluorescence intensity of fixed cells was proportional to that of fresh cells from 24h post-labelling and thus a valid measure of CFSE content relative to that time. This finding was important with a view to using CFSE in multiparametric tests in fixed cells. As the actual experiments started at 0h (at the beginning of treatment, at least 24h after labelling), the first phase of fluorescence decrease did not affect the results and was not further investigated. We focused instead on correcting the data for efflux in the second phase, from 0h onward. The same relative fluorescence decrease from 0h was observed in formaldehyde plus ethanol-fixed cells and ethanol-fixed cells.

Evaluation of the efflux was complicated in proliferating cells by the halving of the fluorescence at each division. Nevertheless, the decrease in fluorescence intensity of undivided cells at different times must be estimated to avoid misinterpreting them as divided cells, which would lead to a completely wrong evaluation of the proliferating activity of the population. Once established, the position of undivided cells in the fluorescence scale at each time would constrain the positions of cells in the subsequent generations by halving the fluorescence of the previous, taking into account background fluorescence and the log scale calibration (if needed).

We estimated the efflux outline of proliferating cells from the equation:

$$CFSEfl(t) = N(t) \times Avfl(t)$$

where CFSEfl(t) represents a measurement of the overall integrated fluorescence intensity of the entire population, N(t) is the absolute number of cells independently evaluated by Coulter Counter, and Avfl(t) is the average fluorescence intensity per cell measured on the flow cytometric histogram. CFSEfl(t) is proportional to the overall amount of CFSE inside the cells, thus, in control samples, with negligible cell loss, the ratio of CFSEfl(t) to CFSEfl(0) enabled us to estimate the decrease in fluorescence from 0h due to efflux. This decrease corresponds to the fluorescence decrease that would be detected in undivided cells, so we can track their average position (channel number) in the logarithmic scale, with respect to their position at 0h. In IGROV1 cells, the outline of fluorescence efflux from 0h, calculated using the equation above, was similar to that calculated directly in quiescent lymphocytes, with fairly good reproducibility between independent experiments.

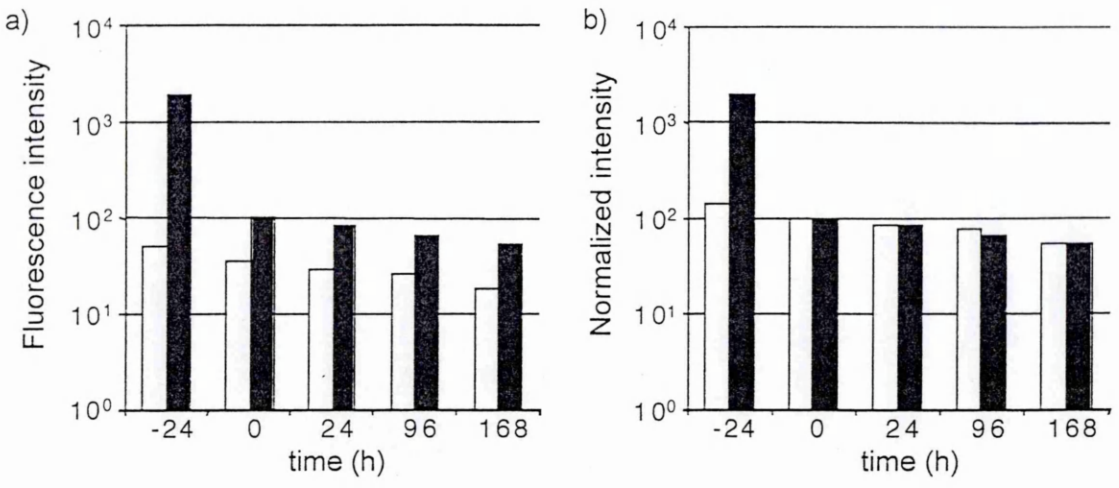

Figure 8.4: Time-course of the decrease of fluorescence intensity in CFSE-labelled quiescent lymphocytes. Cells were analyzed directly at the times indicated (solid columns) or fixed and then analyzed at the end of the experiment (open columns). Each value was the average of two replicated samples.

Panel a: Average fluorescence intensity in the same unit of measurement (average background fluorescence was about 1 fluorescence unit). Panel b: Fluorescence intensity relative to the respective 0-h value (24h after seeding).

8.2.3 Biparametric DNA/CFSE in TPT-treated cells

On the basis of previous methodological studies, we examined data from an experiment in which IGROV1 cells, loaded with CFSE, were either treated for 1h with TPT or kept as untreated controls. Figure 8.5 shows biparametric DNA/CFSE dot plots of control and treated samples at 72h and the 0-h control sample. The drug effect was barely detectable in monoparametric DNA histograms (almost overlapping untreated controls after 24h, as will be shown in figure 8.6) but became evident at simple visual inspection of the biparametric plots. With 10 μM TPT we observed cells with CFSE fluorescence in the range of 72-h control cells (inside the lower box) and cells with higher CFSE content. The latter were delayed because they divided fewer times than controls, and some remained in the range of first cycle cells (inside the upper box). Percentages of cells in the two boxes

provide a first glance at the antiproliferative effect of the drug and its dose dependence. In addition, the biparametric histograms of treated cells showed that few of delayed cells were in S phase, compared with the regularly proliferating cells in the lower box, suggesting that they were at least partly blocked in G_1 and G_2M at 72h.

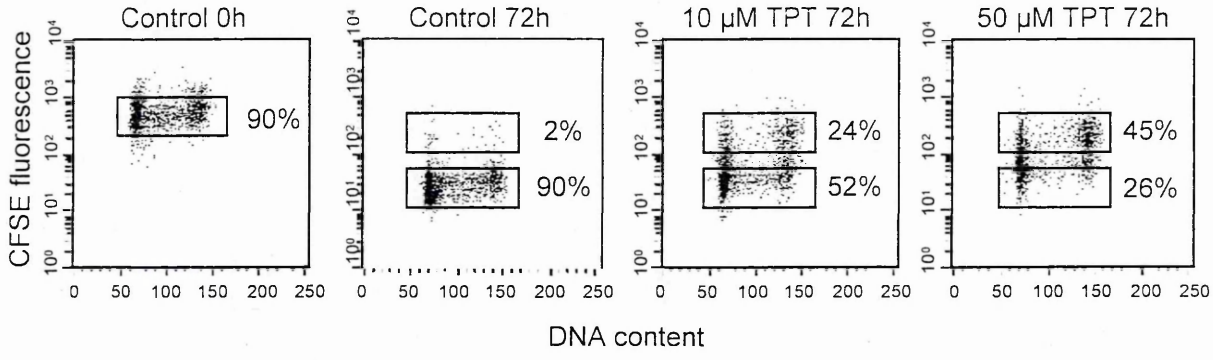

Figure 8.5: DNA/CFSE dot plots of controls and cells treated with 10 or 50 µM TPT 72h after treatment (96h from CFSE loading, right) and 0-h control (left). Most control cells divided several times within 72h and were detected in the lower rectangular box, whereas most treated cells had higher CFSE content with fewer divisions. As a reference, the upper box approximately indicates the range of cells in the first cycle and was drawn in the 72-h plots by taking calculated efflux into account.

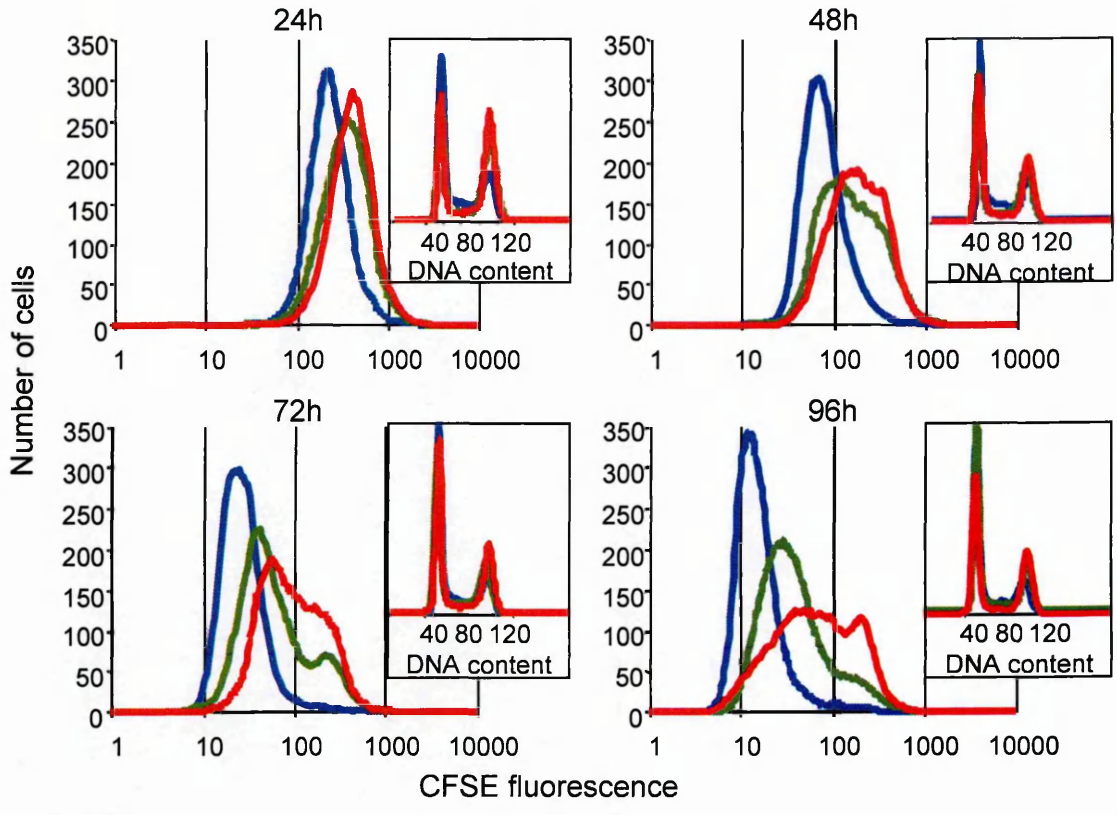

Figure 8.6: Time-course of CFSE histograms in controls and treated cells (logarithmic scale). The peak of controls (blue line) shifts progressively towards lower CFSE content due to subsequent divisions and CFSE efflux. The fluorescence of treated cells (10 μM, green line; 50 μM, red line) remains spread over a wider range on the right side of control peaks, suggesting the contemporary presence of cells from several generations before the one reached by untreated cells. DNA histograms are shown in insets.

8.2.4 Time-Course

To make a quantitative interpretation of the proliferation delays caused by TPT, we analyzed the cells at various times to obtain the time course of CFSE histograms shown in figure 8.6. The average CFSE content of controls decreased as time went on, due to halving at each generation and CFSE efflux, whereas CFSE histograms of treated cells tend to spread, as expected for delayed cells. Each histogram was formed by the point-by-point sum of the distributions of cells in

each generation, which in turn depended on the percentages of cells in cycle 1 (undivided), 2 (divided once), 3, etc. These percentages were found by fitting each histogram with an envelope of gaussians in the X-scale of channel numbers. Histograms of controls and treated samples at the same time were fitted with almost the same value of the average of the first gaussian, with one channel tolerance and within three channels from the value suggested by the estimate of the efflux described above. The channel number of the average of the other gaussians was automatically generated as a function of the average of the first, of the background and of the calibration of the logarithmic scale. The standard deviation of all gaussians of a sample was assumed as equal, as expected with logarithmic amplification when changing the fluorescence intensity of all cells by the same factor. In a few samples (e.g., 10-μM sample in figure 8.7) a visual discrimination of the peak of first cycle cells was possible, allowing a preliminary estimate of the standard deviation. After examination of these cases, we assumed that the standard deviation in our data set was between 8 and 10 channels. Then a non-linear fit was done of each histogram by changing the mean of the first gaussian, the standard deviation within the specific boundaries, and the number of cells (i.e., area) of each gaussian. This area is proportional to the percentage of cells in the corresponding generation. The resulting fittings (figure 8.7) were always satisfactory (reduced chi-square < 3). However, satisfactory fittings were also obtained without correcting the position of the gaussians for CFSE efflux. Thus we challenged the results obtained with and without efflux correction by calculating the predicted growth curve in controls using equation 3 and assuming negligible cell loss. The outline predicted, which took efflux into account, was in keeping with the Coulter Counter measurement; without correction, we had a much higher growth rate (figure 8.8). For instance, at 72h, the peak interpreted as

first cycle with the correction would be interpreted as second cycle without correction.

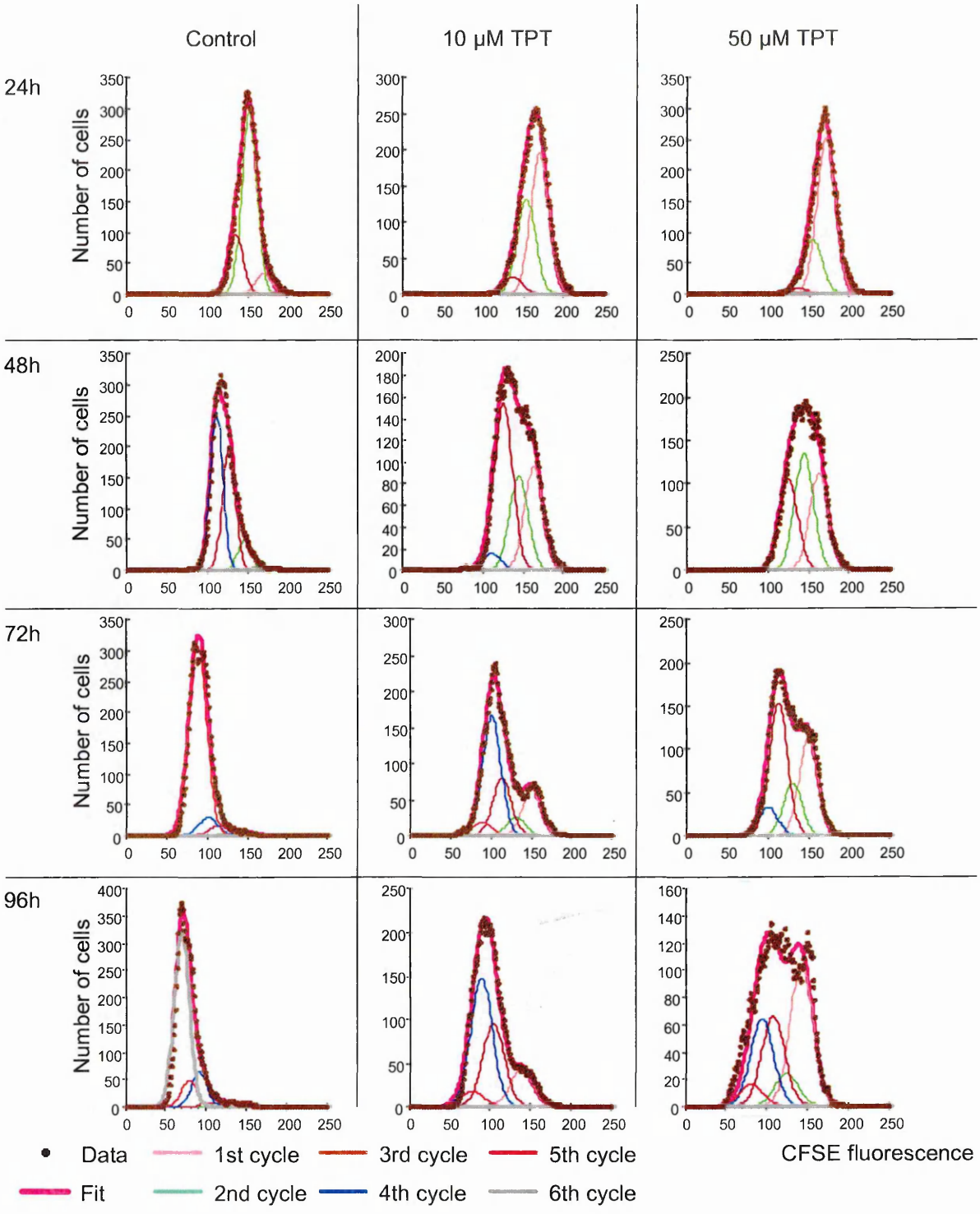

Figure 8.7: Best fitting of CFSE histograms of controls (left) and cells treated with 10 µM TPT (middle) or 50 µM TPT (right) at different times after treatment. Panels show data points with overall fit (magenta line) and the underlying gaussians that represent cells in subsequent generations.

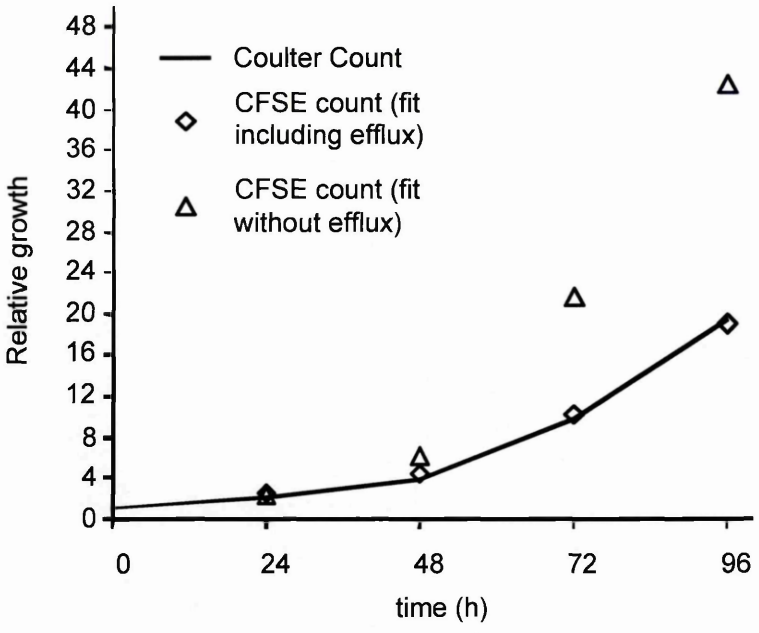

Figure 8.8: Calculation of the relative growth in untreated cells taking CFSE efflux into account (diamonds) or neglecting that correction (triangles). The continuous line represents the actual growth as measured with a Coulter Counter.

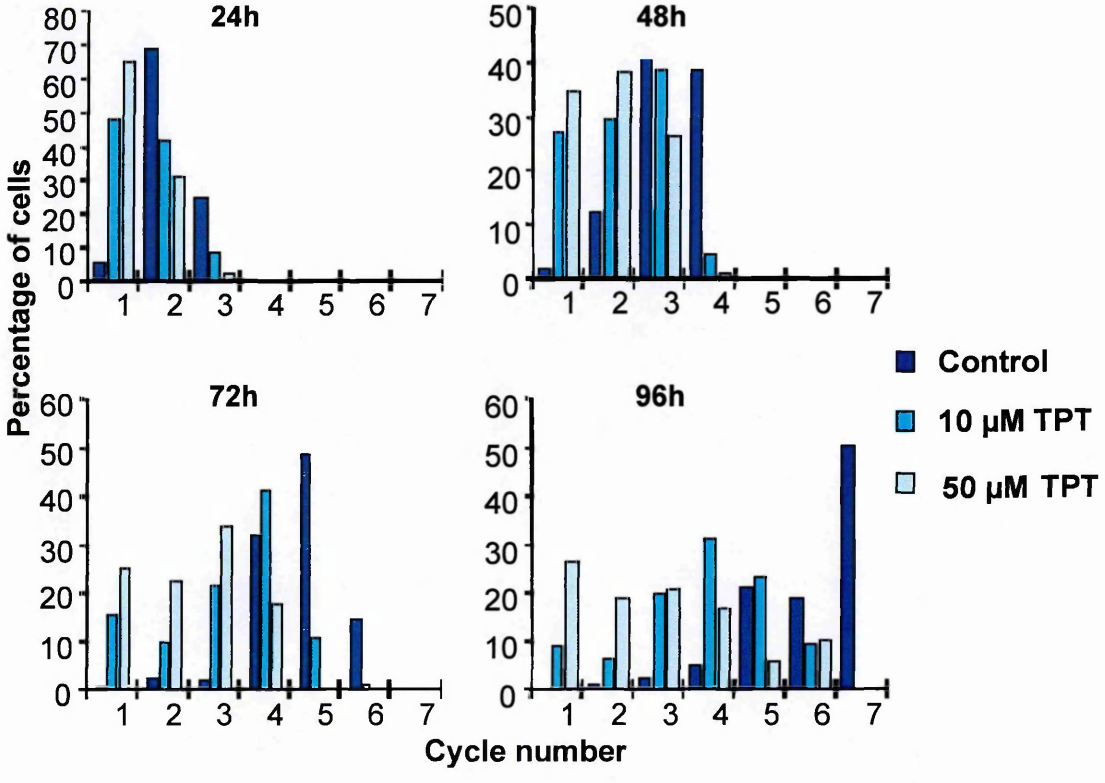

Figure 8.9: Time-course of the distribution of cells within generations, corresponding to the best fit of the data.

Figure 8.9 shows the resulting distribution of cells within the generations. 24h after treatment two-thirds (50 μM) or one-half (10 μM) of cells remained undivided, whereas most untreated controls were in the second and third cycles. Later, whereas controls progressively entered subsequent generations, treated cells remained in the first cycle or progressed more slowly. Eventually, at 96h, treated cells were spread over several cycles. In particular the 50 μM treated cells were almost equally split across the first (26%), second (19%), third (21%), fourth (17%), fifth and sixth (16%) cycles. This suggests that, even if treated cells succeed in dividing once, some of them are then arrested in later cycles.

The same data of the 50-μM treatment can also be expressed in terms of the outcome of the "original" cell population (i.e., of the cells present at time of treatment). On average, for every 26 cells that were still undivided at 96h, 9.5 divided once and generated 19 descendants, 5.25 divided twice and generated 21 descendants, 2 divided three times and generated 17 descendants, and only one was able to divide at least four times and produce 16 descendants. Thus, for every 26 cells that remained undivided (and detected at 96h), only 18 divided at least once.

The analysis was further improved by taking account of the parallel measure of the absolute number of cells. By combining the overall cell number with the flow cytometric percentage of first cycle cells, we calculated the number of cells per flask that were blocked immediately and did not divide (figure 8.10). At 24h 85% of control cells divided, compared with 30% of those treated with 10 μM TPT and only 5% of cell treated with 50 μM. Then the number of undivided cells decreased to 50% of the original population at 48 and 72h and reached 30% at 96h, similarly in cells treated with 10 and 50 μM. This was due to cell division and cell death.

The simple analysis presented in the paragraph 8.1.3 describes the contributions of these two drug effects (figure 8.11). The pie plots in figure 8.11 show the 96-h outcome of 1.1 $x10^5$ cells per flask treated with TPT for 1h. The two TPT concentrations caused a similar long-term block for about one-fourth of the cells with dose dependence in cell kill (55% of cells were dead at 50 μM vs. 40% at 10 μM).

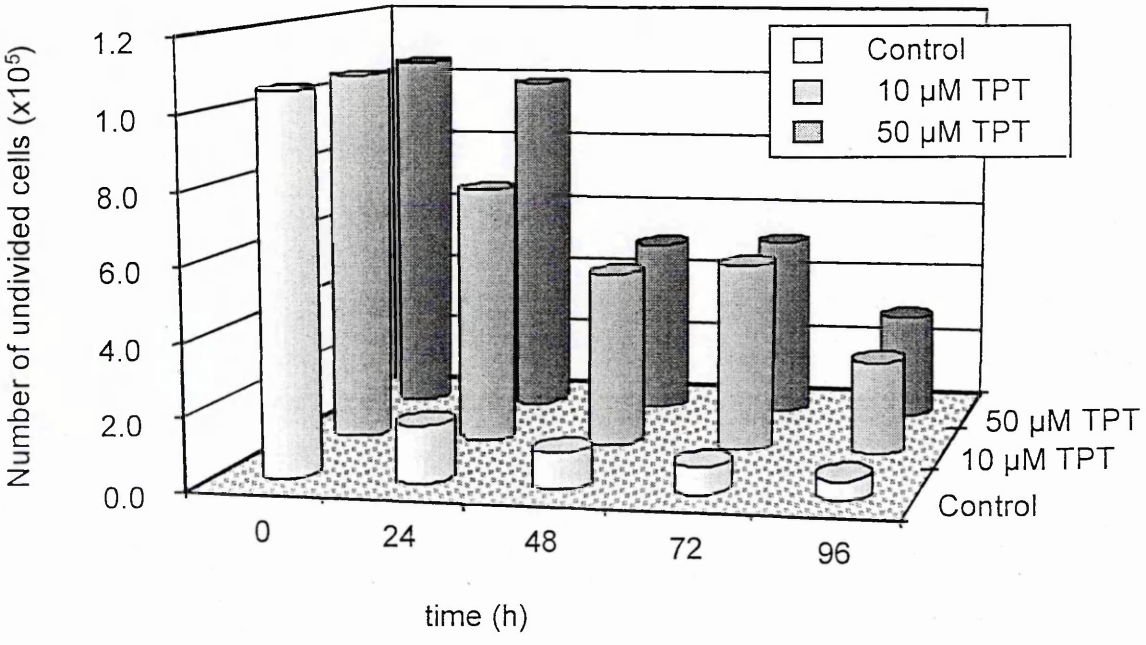

Figure 8.10: Time-course of the number of cells that remained blocked in the first cycle. This number was obtained by multiplying the percentages of the first-generation cells by overall cell number, which was independently calculated with a Coulter Counter.

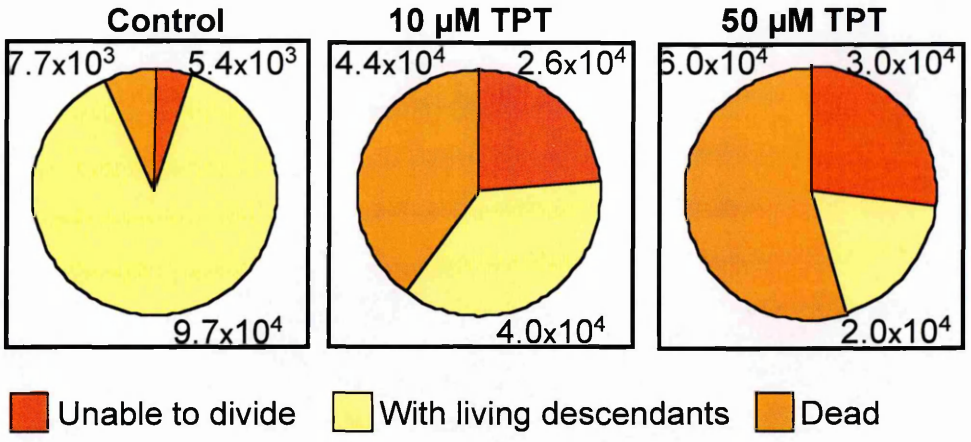

Figure 8.11: Outcome of the starting population of 1.1 x 10^5 cells that were untreated (left) and treated with 10 µM TPT (middle) and 50 µM TPT (right) at the end of the experiment (96h). The number of cells that remained undivided comes from figure 8.10. The number of cells that divided at least once was calculated by summing the "clones" present in each generation (i.e., 100 cells in the second cycle at 96h originating from 50 starting cells, 100 cells in the third cycle from 25 starting cells, etc.). The number of cells lost (dead and disrupted) at 96h was calculated as the difference.

8.2.5 Triparametric DNA/BrdUrd/CFSE in TPT-treated cells

As shown in chapter 4, cytotoxic and cytostatic effects induced by TPT are dependent on the phase where the cells were at the time of treatment. S-phase cells were the most affected by the drug, even though blocking activity and cell death were present also in the subpopulation of cells treated during G_1 and G_2M phase. However with the classical flow cytometric measurements we were not able to distinguish in which generation the cells remained blocked and if they died before or after generating descendants. With BrdUrd pulse-and-chase of CFSE-labelled cells we could obtain this information.

At different times after treatment it was possible to measure and analyze CFSE histograms of BrdUrd-positive and BrdUrd-negative cells. Biparametric dot plot of BrdUrd content versus DNA content in a 10-µM treated sample at 24h is reported

in figure 8.12 (panel a, left), by gating BrdUrd-positive cells we could obtain the CFSE histograms of the two subpopulations (figure 8.12, panel a, right). Also in this case the results could be quantified by analysing each histogram as previously explained (see 8.1.3) and figure 8.12 (panel b) shows the time course of the distribution of BrdUrd-positive and BrdUrd-negative cells within generations. In control samples the cells were proliferating and at 72h they could reach the fourth and the fifth generation, on the contrary the cell proliferation in treated samples was slower. At 72h BrdUrd-negative cells treated with 10 μM TPT could divide four times, whereas the cells treated with the highest concentration could reach only the third generation. A different behaviour was observed in BrdUrd-positive cells, only a small percentage of 10-μM treated cells were able to divide and to reach the third generation at 72h the most part of this subpopulation remained in the first generation, especially in 100-μM treated samples. Moreover BrdUrd-positive cells were affected by cell loss whose presence was highlighted by the decreasing of cell percentage. If we consider only living cells we can calculate the relative percentage of cells that were able to proliferate at each time (figure 8.13). At 72h 76% of BrdUrd-positive cells treated with 10 μM TPT were unable to divide and this percentage reached the 86% in cells treated with the highest concentration of drug. Only 9% of cells treated with 10 μM TPT while in S phase were able to divide twice. On the contrary the subpopulation formed by BrdUrd-negative cells was much more heterogeneous. 72h after treatment with 10 or 100 μM TPT there were respectively 18% and 44% of BrdUrd-negative cells still undivided but there were also 31% and 36% of cells that divided once and 28% and 21% of cell that divided twice.

All the information obtained by the analysis of CFSE histograms in biparametric and triparametric staining can be used to integrate the set of experimental data generally compared with the output of the simulation. In figure 8.14 we reported

the results of this comparison for cells treated with 100 μM TPT. The scenario used to reproduce the data was very similar to that described in figure 4.6 for the cells treated with the same drug concentration and the good agreement between experimental and simulated data confirmed, once more, the effects described in that occasion.

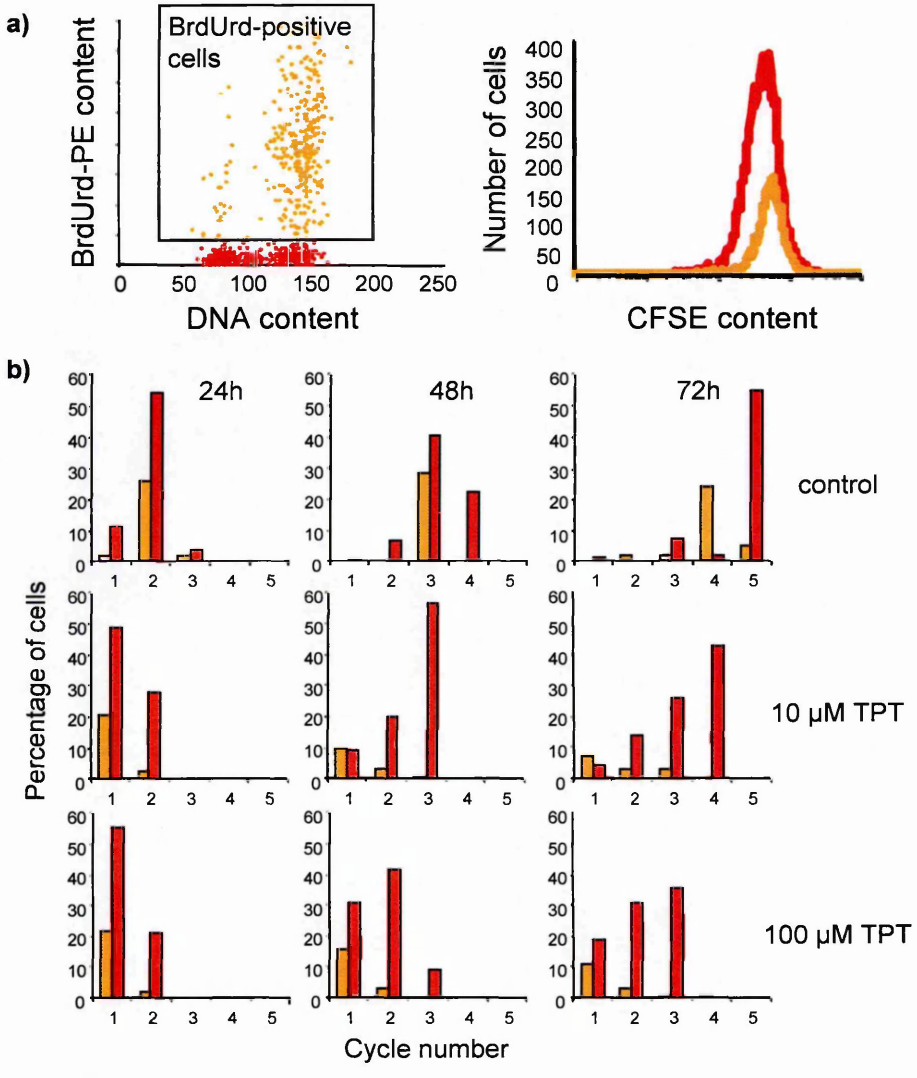

Figure 8.12: Triparametric staining of IGROV1 cells. Just before seeding cells were labelled with CFSE and at the time of treatment S-phase cells incorporated BrdUrd. The samples were fixed at different times after treatment. Panel a: DNA/BrdUrd dot plot of 10-μM treated sample at 24h (left). BrdUrd labelling allows the distinction of CFSE content in BrdUrd-positive and BrdUrd-negative subpopulation (right). Panel b: Time course of the distribution of BrdUrd-positive (orange columns) and BrdUrd-negative cells (red columns) within generations.

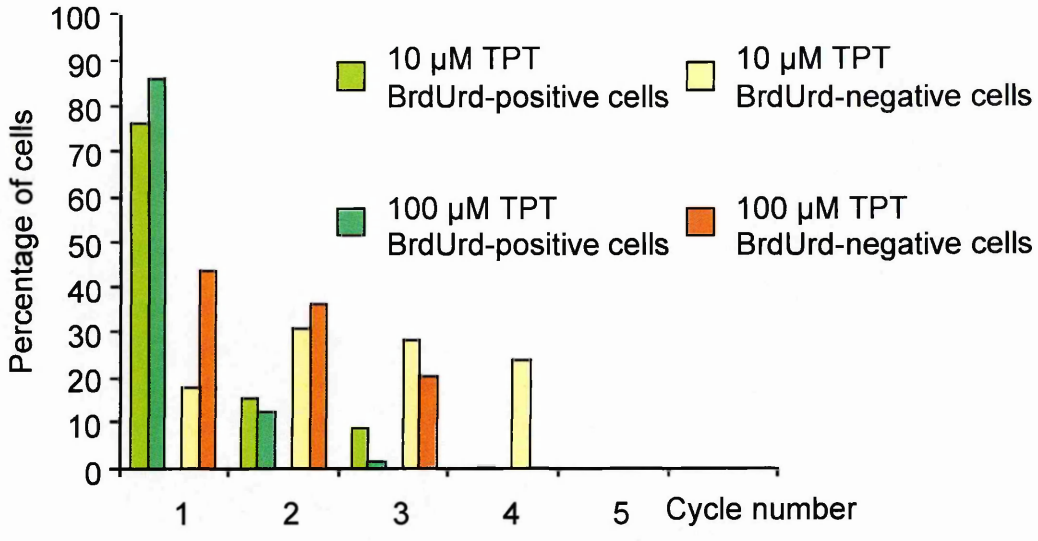

Figure 8.13: Ability of generating descendant at 72h after treatment.

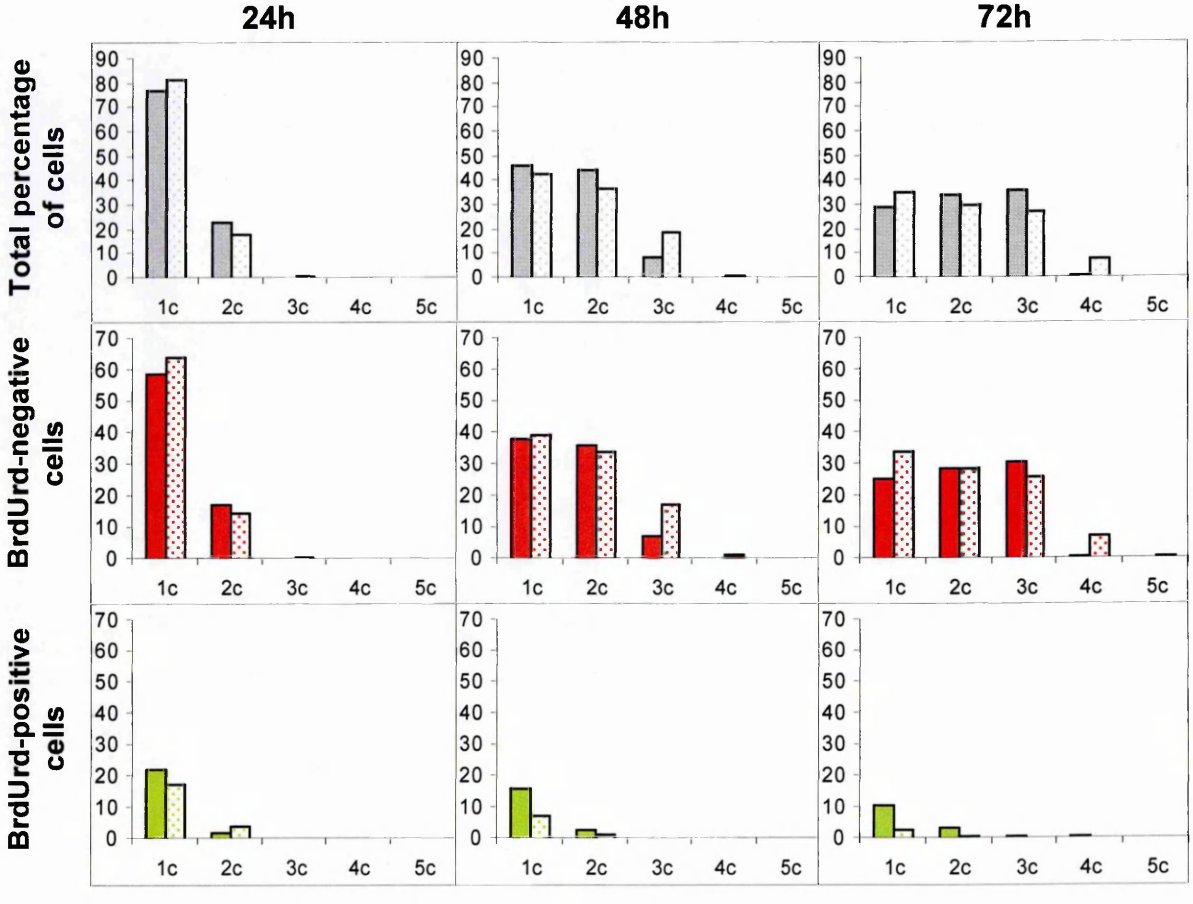

Figure 8.14: Comparison between the experimental data obtained by the analysis of CFSE histograms in triparametric staining (full column) and the data obtained by the simulation (dotted column). In particular we represented here the cell distribution in different generations for cell treated with 100 µM TPT. The simulation was obtained by applying the scenario reported in figure 4.6.

8.3 DISCUSSION

As far, the use of CFSE to test the effects of antiproliferative drugs *in vitro* has been limited in leukaemic cells (Plate et al., 2000; Holtz et al., 2002) and has not been attempted, to our knowledge, with non-haematological mammalian cell lines, probably because of methodological problems. The CFSE method for immunological studies has been illustrated in detail (Lyons et al., 2001), with evidence of possible toxicity, incomplete retention of the substance, and the need for robust identification of the CFSE fluorescence intensity of undivided cells. Standard protocols (Lyons et al., 2001) overcame these limitations, at least in the case of lymphocytes, by optimizing the loading with quiescent cells, running controls of undivided (unstimulated) and unloaded (without CFSE) cell populations, and supporting the analysis by visual identification of the histogram peaks.

With other cell types, in particular non-haematological cancer cells, the problems were similar, but further more complicated by the higher intercell variability of loading (possibly a direct consequence of intercell variability of protein content), resulting in broader, overlapping peaks. In such conditions, to analyze the data on a solid ground, we had to evaluate critically all the steps of the procedure, identify possible pitfalls, and devise methods to overcome them.

We initially tested different loading procedures by comparing CFSE treatment in adherent cells or suspension with synchronized or unsynchronized cells. Selection by sorting a subpopulation of cells in a narrow gate of fluorescence intensity (Nordon et al., 1999; Holtz et al., 2002) was considered impractical for our purposes, because we wanted a test for drug evaluation, where a number of treatments and replicated flasks could be used with adherent cell populations. In addition, we felt that the sorting procedure was prone to the risk of selecting a

particular subpopulation of cells, e.g., partially and unpredictably synchronized, and thus potentially losing the true intercell variability of the entire population's response to the drug challenge. Eventually, we adopted a short CFSE exposure of unsynchronized cells in suspension at the time of seeding.

Most of the strong fluorescence signal detected just after loading was lost in the first hours because of the efflux of non-protein-bound dye and catabolism of CFSE-bound proteins in the cells (Lyons et al., 2001; Nordon et al., 1999; Hasbold et al., 1999; Dumitriu et al., 2001). CFSE that remained at 24h was more stably incorporated, decreasing slowly over the next few days, and the fluorescence intensity remained strong enough to detect at least five divisions before the signal became confounded with background fluorescence (measured in controls without CFSE). Thus, by setting drug treatment at least 24h after seeding, the pitfalls related to the strong initial decrease in fluorescence were overcome, and the cell population received the drug at the beginning of the asynchronous exponential phase of growth. Attempts at using higher CFSE concentrations failed because CFSE itself caused some growth inhibition, which was clearly unacceptable in a test aimed at evaluating the antiproliferative effects of drugs.

At the time of treatment and daily thereafter, cells were fixed to allow multiparametric analysis. Good DNA/CFSE biparametric histograms were obtained with ethanol fixation, and were no better (in terms of peak sharpness) using formaldehyde plus ethanol. Relative efflux from 0h was also superimposable in ethanol-fixed and formaldehyde plus ethanol-fixed samples.

CFSE fluorescence was detected in the optical path FL1 by using a four-decade logarithmic amplifier. We found that amplifier's distortions were present but negligible for our analysis except for very low or very high fluorescence intensities (roughly in the first and fourth decades). Thus the need for that correction was avoided with a suitable choice of the photomultiplier tube amplifier, so that the

channel range of all histograms of the time course was in the second and third decades. Two decades account for six divisions with a moderate efflux, thereby allowing a thorough study of the antiproliferative drug effects.

The CFSE fluorescence distribution is then fitted with a series of gaussians (using channel numbers as abscissa), with each representative of a cell generation. Any good program for non-linear fitting can be used, but care should be made in selecting the position of the first peak (e.g. by separate analysis of the efflux), excluding relevant distortions of the logarithmic amplifier (or account for them) in the range of the measure, and setting appropriate constraints.

For fitting purposes, the standard deviation of all gaussians was assumed to be constant. This assumption is theoretically correct only if at each division the two sibling cells would inherit exactly half the CFSE fluorescence of the mother cell. Because cytokinesis is not perfect, we would expect an increase of the standard deviation as generation number increases. However, an increase was not observed between the best-fit standard deviations measured in populations at the beginning of our experiments (when the first generations prevail) and subsequently.

Another problem in the analysis of CFSE is represented by the fact that the fluorescence of cells in the sixth and seventh generation, detected in controls at 96h, was about three and two times, respectively, the average fluorescence of negative controls, making it unreliable to distinguish such generations. This is less of a problem in treated samples, where only a few cells divide for so many generations.

The position of the gaussian of undivided cells cannot be easily found simply by keeping a non-stimulated control of quiescent cells, as in most immunological studies, because cancer cells naturally divide. One alternative is to use controls whose proliferation is inhibited by exogenous treatment, e.g., with a low

concentration of Colcemid (Holtz et al., 2002). However, we preferred to estimate the efflux directly by calculating the overall CFSE content retained by control cells (Fazekas de St Groth et al., 1999), using the absolute cell number measured independently with a Coulter Counter. This procedure is also applicable in cell lines where a simple and exact antiproliferative response to Colcemid or other antiproliferative drugs cannot be achieved, such as the line used in this study. In this way we obtained a consistent prediction (within a few channels) of the position of the highest fluorescence peak of cells in treated samples. The best fit of this position is then done by the fitting routine.

Our data showed that the CFSE method is useful to evaluate the antiproliferative effects of TPT. In chapter 4 we presented the results obtained with classical flow cytometric analysis and with the simulation program that we used to interpret experimental data, but CFSE labelling adds a new complexity by evaluating the flux of cells through subsequent generations. In particular, BrdUrd pulse-and-chase of CFSE labelled cells confirmed that cells in S phase at the time of treatment were the most affected by the drug, in fact about the 90% of BrdUrd-positive cells remained unable to proliferate at least until 72 h after treatment (see figure 8.13). Moreover the output of the simulation program used to interpret cell cycle effects induced by drug treatment was modified in order to include the percentage of cells at the different generations. As demonstrated in figure 8.14, these data could be directly compared with the data obtained from the analysis of CFSE histograms. The addition of experimental information could be helpful in the restriction of the number of scenarios consistent with the data.

CHAPTER 9: Role of p53 in Cell Cycle Perturbations Induced by Cisplatin

9.1 INTRODUCTION

9.1.1 p53

p53 was the first described (De Leo et al., 1979) and one of the most studied tumour-suppressor genes. Although p53 is dispensable for normal development, it has a key role in the cellular response to DNA damage from both endogenous and exogenous sources providing the maintenance of genomic integrity and a protective effect against tumorigenesis.

The p53 protein has a short half-life and it is normally maintained at low levels in unstressed mammalian cells by continuous ubiquitination and subsequent degradation proteasoma-mediated. The Mdm2 protein is one of the enzymes involved in labelling p53 with ubiquitin (Momand et al., 2000), Mdm2 protein binds p53 and stimulates the addition of ubiquitin groups to the carboxy terminus of p53, which is degraded. This lowers the concentration of p53 and reduces transcription of the *Mdm2* gene, closing the feedback loop and allowing p53 levels to rise again. After genotoxic stress, p53 ubiquitination is suppressed and the wild-type p53 protein is stabilized and accumulates in the nucleus and transactivates several downstream genes (Amundson et al., 1998).

The activation of p53 in response to DNA damage is a multifactorial process, where DNA damage or aberrant growth signals trigger different pathways of activation of p53. Many different kinase families phosphorylate p53, including DNA-PK, the casein kinase family, MAP kinase and CDKs (Meek, 1998). ATM and ATR are two of the major upstream regulators of the p53 response to DNA damage. Whereas ATM and DNA-PK primarily respond to DSBs (Carr, 2000), ATR responds to both ultraviolet light DNA damage (Unsal-Kacmaz et al., 2002) and DNA DSBs, and it also responds to other kind of damage induced by stalled replication forks, hypoxia (Hammond et al., 2002) and protein-kinase inhibitors.

p53 is upstream of several pathways in which genes regulated by this protein are involved, among its target genes there are *p21* and *14-3-3σ*. They represent the major mediators of p53-induced cell cycle arrest (Vogelstein et al., 2000). As already explained in paragraph 1.1, p53 protein directly stimulates the expression of $p21^{WAF1/CIP1}$, an inhibitor of cyclin-dependent kinases (CDKs). Through its negative effects on various CDKs, $p21^{WAF1/CIP1}$ can arrest the cells in G_1 (Brugarolas et al., 1999) and in G_2 (Innocente et al., 1999; Bunz et al., 1998).

In addition to playing a role in cell-cycle checkpoint response, the activation of p53 can lead to apoptosis, in fact the activation of several p53 downstream genes has been shown to trigger this death process (El Deiry, 1998; Vousden and Lu, 2002). The mechanisms underlying p53-induced apoptosis likely involve reactive oxygen species generation (Johnson et al., 1996) and mitochondrial dysfunction, including that caused by the induction of *Bax* (Green and Reed, 1998). A very large number of genes have been identified as potential downstream targets of p53 activation or suppression, but only two pro-apoptotic genes, *Noxa* and *Puma* (Jeffers et al., 2003; Villunger et al., 2003), have been established as being of critical importance *in vivo*.

Even though the mechanisms are not clearly understood, p53 also participates in DNA damage repair. p53 may transcribe target genes that are important in the regulation of nucleotide-excision repair of DNA, chromosomal recombination and chromosome segregation (Vogelstein et al., 2000). Two examples of p53 target genes that participate in DNA damage repair are *GADD45* (Smith et al., 1994) and *p53R2* (Tanaka et al., 2000). Additionally, it has been suggested that p53 itself plays a role in genetic stability with the C-terminus of p53 binding to different forms of DNA damage including single-stranded DNA, ends of DNA stranded breaks and bulges caused by insertions or deletions (Balint and Vousden, 2001). It has been shown that cells lacking in p53 do not display a completely efficient NER (Wani et

al., 1999) or BER (Offer et al., 2001) thus demonstrating the importance of p53 and its products in DNA damage repair.

9.1.1.a Inactivation of p53 in human tumours

Wild-type p53 function can be lost by mutation and the p53 protein does not correctly function in most human cancer (Hollstein et al., 1991). In about half of these tumours, p53 is inactivated directly as a result of mutation in the coding region of the *p53* gene. The mutations occur at many sites within the gene but the most common class of mutation is a point mis-sense mutation in the central DNA binding domain of the protein. These mutant proteins can accumulate to high levels in tumour cells and the mutations act as dominant negative as the full-length mutant protein forms mixed inactive oligomers with the wild type protein (Lane, 2004).

On the other side half of all human tumours retain wild type p53, but its tumour suppressor function is bypassed by inactivation of upstream signalling pathways or indirectly inactivated binding to viral proteins (Levine et al., 1991).

Although the interest in the tumour suppressor p53 and the studies about the complexity of its function and regulation in carcinogenesis, the problem regarding the role of p53 modifications in cancer chemotherapy and cancer prevention is still open. In spite of the effort that has been done to determine the effects of p53 inactivation on the response of cancer cells to therapeutic agents, the results are conflicting, with some studies indicating enhanced sensitivity and others indicating increased resistance to the same compounds (Blandino et al., 1999).

9.1.2 Biochemical Mechanism of Action of Cisplatin

We believed that in this situation of complex molecular interactions, with redundant pathways involved in different mechanisms of cell cycle controls, a correct

understanding of the role of p53 should pass through a quantitative evaluation of its function in blocking activity, DNA repair and apoptosis.

In particular, in this study we decided to focus our attention on the role of p53 in the cell response to a DDP pulse-like treatment. We evaluated the perturbations induced by this drug on two isogenic cell lines, one expressing wild type p53 and the other lacking for the gene coding for this protein.

DDP is a platinum co-ordination complex that was first synthesized in 1845. Interest in DDP was revised in 1965 by the discovery of its biological activity in a bacterial culture, where this compound was able to inhibit cell division and induce filamentous cell growth (Rosenberg and Camp, 1965).

In general the mechanism of action of DDP is not too far from that observed for alkylating agents. Within the nucleus DDP may react rapidly with electrophylic sites on the DNA, forming monoadducts, which can be converted to cross-links by a slower reaction with the second DNA strand (D'Incalci et al., 1985). The adducts can take the form of intra- or inter-strand cross-links, which may cause major local distortions of DNA structure, involving both bending and unwinding of the double helix. The intra-strand cross-links are the most abundant products of the interaction (Fichtinger-Schepman et al., 1985). On the other side, inter-strand cross-links represent a small amount of the total DDP lesions, but several studies have suggested that they can also be responsible for the cytotoxicity of the drug (Ducore et al., 1982; Plooy et al., 1984). As the monoadducts can be converted to cross-links by a slower reaction with the second DNA strand, it has been proposed that the low sensitivity of some cells to the cytotoxic action of DDP could be due to a fast removal of drug-DNA monoadducts before they are converted to lethal inter-strand cross-links (Micetich et al., 1983).

The distortion of DNA caused by the drug stabilizes the interactions between DNA and its binding proteins. These trapped proteins contribute not only to enforce

architectural changes, but they might mask DNA lesions, such as cisplatin-DNA adducts, from the NER machinery, or simply deplete important proteins that are involved in transcription (Hurley, 2002).

The affinity of DDP for nitrogen and sulphur atoms allows the drug to bind different proteins affecting their function, for instance in DDP sensitive cells there are alterations in mitochondrial enzymes, cytoskeleton proteins and transmembrane transport systems.

As a result DDP treatment inhibits DNA replication, RNA transcription, arrests at the G_2 phase and/or promotes programmed cell death (Sorenson et al., 1990).

Although DDP is widely used for treatment of a variety of solid tumours, the efficacy of treatment is often limited by the onset of resistance mechanisms. Resistance to DDP is multifactorial (Kartalou and Essigmann, 2001). Reduced intracellular accumulation of this compound, caused by alteration in the drug transport through the cell membrane, is frequently observed in DDP resistant cell lines (Parker et al., 1991). Other mechanisms involve sulphur-containing molecules, as glutathione (GSH). In this case GSH covalently links DDP and the complex may be transported out of the cell by an ATP-dependent pump (Ishikawa and Ali-Osman, 1993). Conjugation with GSH also inhibits the conversion of monoadducts to cross-links, thereby reducing the cytotoxic potential of the adducts.

Alterations in the expression of oncogenes, tumour suppressor genes (including p53) and genes coding for proteins involved in DNA repair have also been implicated in the cellular resistance to DDP. For instance, different studies have shown that resistance to DDP can also be related to MMR deficiency both *in vitro* and *in vivo* (Fink et al., 1996; Fink et al., 1997). As the most abundant lesions produced by DDP in DNA are intra-strand cross-links, loss of MMR produces drug

resistance by impairing the ability of the cells to detect adducts in its DNA and thus to activate a pathway leading to apoptosis (Nehmè et al., 1997).

9.1.3 Clinical Use of Platinum Compounds

DDP is one of the most efficacious anticancer drugs. It displayed a significant antitumour activity against several types of tumour. DDP is used as single agent in the treatment of testis, bladder, ovary, cervix, head, neck and lung cancer, but its efficacy in combination with other compounds, such as bleomycin, etoposide and vinblastin, was also tested (Einhorn, 1986). In particular, the reason for the very high sensitivity of testicular cancer to DDP is not fully elucidated even though Lutzker and Levine (1996) suggested that one of the possible reasons might be related to the fact that this kind of tumour very rarely shows p53 mutation.

DDP or its analogue carboplatin are two effective agents against ovarian cancer, used alone or in combination with paclitaxel, cyclophosphamide, or doxorubicin (Omura and Brady, 1993). Moreover the drug increased cell sensitivity to radiation therapy (Pearson and Raghavan, 1985).

9.1.4 Background and Rationale of the Study

Due to the complexity of the mechanism of cellular responses to DDP-induced damage it is not surprising that the published data are not all consistent in relation to the role of p53 and MMR on DDP cytotoxic effects.

Lymphoma cells, ovarian cancer cells, and lung cancer cells mutated in p53 were less sensitive to DDP than wild type cells (Fan et al., 1994; Eliopoulos et al., 1995; Perego et al., 1996), and the suggested cause was that p53-dependent apoptotic response was inactivated. Consistent with these findings are the studies by Sansom and Clarke (2002) that investigated the response to DDP *in vivo* in the murine intestinal epithelium, showing that p53 deficiency caused an abrogation of

the apoptotic pathways. Moreover cells derived from p53-/- mice and from mice defecting both for *p53* and *Msh2*, a gene coding for a protein involved in MMR, treated with DDP, showed an increased clonogenic survival compared to wild type cells.

In contrast, as shown by Hawkins et al. (1996), p53-/- mouse fibroblasts were more sensitive to DDP than wild type cells. Similarly, inactivation of p53 in human foreskin cells, breast cancer cells and colon cancer cells sensitized them to DDP (Fan et al., 1995), presumably because wild type cells were not susceptible to apoptosis and p53 could facilitate repair and extend the time available for it.

In such a situation we believe that the use of a wide range of drug concentrations together with a method enabling a clear distinction between cytostatic and cytotoxic effects should help to clarify the phenomena.

The choice of the cell line is also crucial. As reported by Pestell et al. (2000) conflicting results were obtained even using the same cell line. They studied the response of an ovarian cancer cell line A2780 to a treatment with DDP and they compared the results with the same line transfected with the human papillome virus protein HPV-16 E6, which stimulates the degradation of p53 through an ubiquitin pathway. In A2780/E6 cells the disrupted p53 function determined an increased sensitivity to drug treatment. In this cell line, and similarly in HCT-116/E6 (Lin et al., 2001), the loss of G_1/S checkpoint and decreased cisplatin-DNA adduct repair were considered the principal causes of the increased cytotoxicity of DDP. However they cited another study in which the same cell line transfected with a dominant negative mutant p53 showed a higher resistance to DDP, compared with the parental cell line (Herod et al., 1996). Also Brown et al. (1993) performed some experiments transfecting A2780 cells with mutant p53 which acted as a dominant negative and they showed that the presence of this form of the protein did not affect the response of this cell line to DDP treatment. This

behaviour could derive from interaction of the mutant protein with the environment or from the presence of a residual functional wild-type p53. All that seems to indicate that a p53-/- cell line is the best system to investigate the role of this protein in the response to a drug treatment. For this reason we chose to use the colon carcinoma cell line HCT-116 and its isogenic cell line with p53 disrupted by homologous recombination.

A recent study performed by Lin et al. (2004) revealed that wild type cells HCT-116 exhibited greater sensitivity to a 72h treatment with different anticancer agents, including DDP, compared to the sensitivity shown by HCT-116 p53-/- cells. They found a possible explanation of this result in a paper published by Yamaguchi et al. (2001), which demonstrated that lack of p53 function in HCT-116 p53-/- cells might avoid the activation of p53-dependent apoptosis, generating an increased resistance to chemotherapeutic agent-induced DNA damage.

It should also be taken into consideration that in colon carcinoma cell line HCT-116 a constitutive mutation in mismatch repair gene *hMLH1* is present. Loss of MMR because of mutation of *Msh2* or *MLH1* underlies the majority of cases of hereditary nonpolyposis colon cancer and contributes to the resistance of this kind of cancer to DDP (Fishel et al., 1993). In this case loss of DNA mismatch repair activity and the p53 status both contribute to the cell response to DNA damage. In addition, as shown by Vikhanskaya et al. (1999), the absence of DNA mismatch repair due to loss of *hMLH1* led to an increase in p53 stability after DNA damage.

9.2 RESULTS

9.2.1 Experimental Data

Using the experimental plan already explained in the previous chapters, exponentially growing colon carcinoma cells HCT-116 and HCT-116 p53-/- were treated for 1h with 0, 10, 30 and 100 μM DDP. After treatment the cells were

counted in order to obtain the overall cell number and then fixed to perform different flow cytometric analyses. In this way we could obtain monoparametric DNA histograms, biparametric DNA/BrdUrd dot plots, using BrdUrd pulse-and-chase and BrdUrd-labelling protocols, detection of apoptosis by TUNEL assay and detection of cytostatic effects by CFSE histograms.

Figure 9.1 shows the growth curves of HCT-116 and HCT-116 p53-/- obtained calculating the mean values of cell number coming from, at least, three different experiments. The growth curves of the controls indicated that HCT-116 and HCT-116 p53-/- had the same doubling time and, considering the similarity of cell cycle percentages, we could also suppose that they had the same kinetics in unperturbed conditions. The comparison of the growth curves after treatment with the same DDP concentration did not reveal striking differences between the two cell lines.

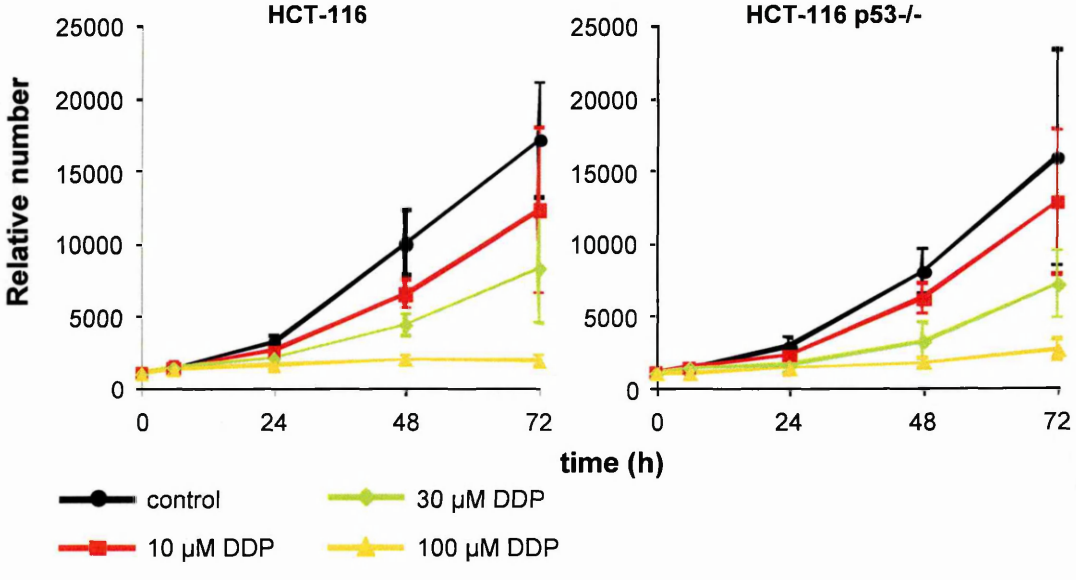

Figure 9.1: Growth curves of HCT-116 and HCT-116 p53-/- cells after 10, 30, 100 µM DDP for 1h, measured by Coulter Counter. Each point is an average of at least three different experiments represented with its standard deviation.

Flow cytometric DNA histograms of control and treated samples are shown in figure 9.2. In both cell lines DDP induced an accumulation of cells in G_2M phase which was dose-dependent. In the samples treated with the highest drug concentration the effect was still present 72h after treatment. At this time in p53-/- cells (figure 9.2b) a decreasing in G_2M peak and a high amount of debris were detected, on the contrary wild type cells (figure 9.2a) showed a DNA histogram very similar to that observed 24h earlier with a strong accumulation in G_2M phase. DNA percentages of the two cell lines, obtained as mean value of at least three different experiments, were plotted in the same graph (figure 9.3). This representation highlighted the differences between HCT-116 and HCT-116 p53-/-. For 10-μM treated samples the percentage of G_1 population in HCT-116 cells increased with the time, particularly in wild type cells. However, as demonstrated by the wide error bars, this behaviour of wild type cells was variable in the different experiments, and this determined a partial overlapping with the percentage of G_1 cells calculated for the controls, where a smaller increase was also present. An opposite behaviour characterised the population in S phase. 24h and 48h after drug washout HCT-116 p53-/- treated with the lowest DDP concentration presented a higher percentage of cells in S phase. The main feature of the cells treated with 30 μM DDP was an increase in the percentage of G_2M cells at 24h, confirming the smaller increase observed in the same subpopulation of cells for the lowest dose. This trend was similar in wild type and p53-/- cells. Some differences between the two cell lines were present in the percentage of cells in G_1 and S phase. In particular, 48h after treatment the percentage of S-phase cells was higher in HCT-116 p53-/-. This trend was already present in 10- and 30-μM treated samples, but it became clear in the cells treated with the highest drug concentration. Moreover in 100-μM treated samples the percentage of cells in G_2M

phase remained constant in HCT-116, whereas in p53-/- cells there was a decrease between 48h and 72h.

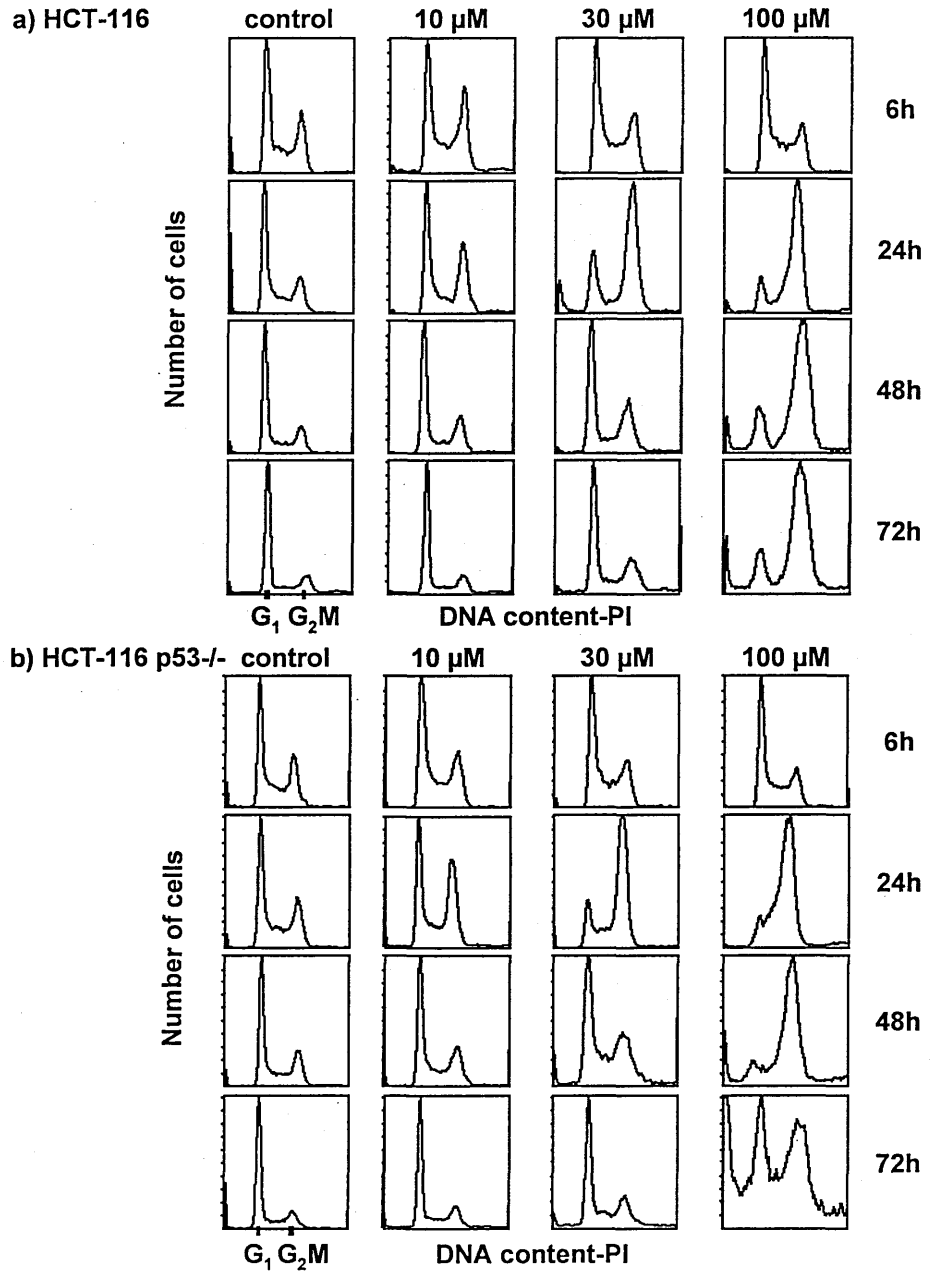

Figure 9.2: Time-course of DNA histograms of wild type cells (panel a) and p53-deficient cells (panel b) after 10, 30, 100 µM DDP for 1h. The data come from one typical experiment, but DNA profiles were similar in all the experiments. In particular, persistent accumulation in the G_2M peak is evident in the 100-µM histograms of wild type cells, whereas a high amount of debris is present at 72h in the p53-deficient cells treated with 100 µM DDP. The time-course of DNA distribution of control samples were similar for HCT-116 and HCT-116 p53-/-.

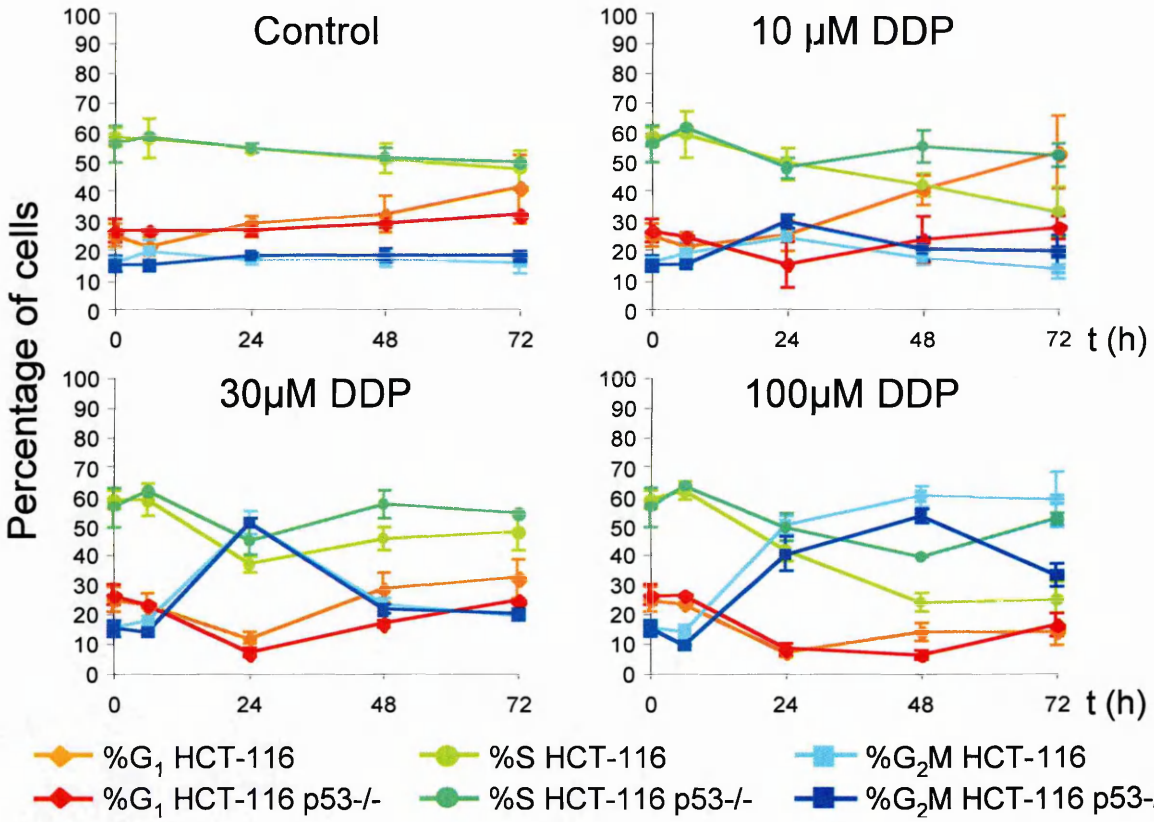

Figure 9.3: Time-course of DNA percentages of the two cell lines. Each point is the average of the percentages of cells in the different cell cycle phases as obtained analysing DNA distributions of at least three different experiments. The data are represented with their standard deviation.

Short-term effects of DDP on HCT-116 and HCT-116 p53-/- were evaluated by a pulse-and-chase experiment. As previously explained (paragraph 3.4.2), cells were exposed to BrdUrd in the last 20 min of treatment, allowing DNA-synthesising cells to incorporate BrdUrd, becoming "BrdUrd-positive", and were collected 6h later. The resulting biparametric DNA-BrdUrd plots are shown in figure 9.4. In control samples 6h after BrdUrd labelling BrdUrd-positive cells were distributed within late-S, G_2M and G_1 phases. In treated samples of both cell lines a dose dependent delay was observed, especially for treatment with 30 and 100 µM DDP, where the cloud of BrdUrd-positive cells was still detected in middle-S and G_2M phase. Moreover in the samples treated with 100 µM DDP BrdUrd-

positive cells did not reach G_1 phase suggesting that this subpopulation was slowed down in its progression through S phase and then intercepted by G_2M checkpoint. Although, at short time after treatment, BrdUrd pulse-and-chase experiment did not show strong differences between the behaviour of wild type and p53-/- cells, the progression of BrdUrd-positive cells through S phase was more delayed in HCT-116 p53-/-, especially for the samples treated with 10 and 30 μM DDP.

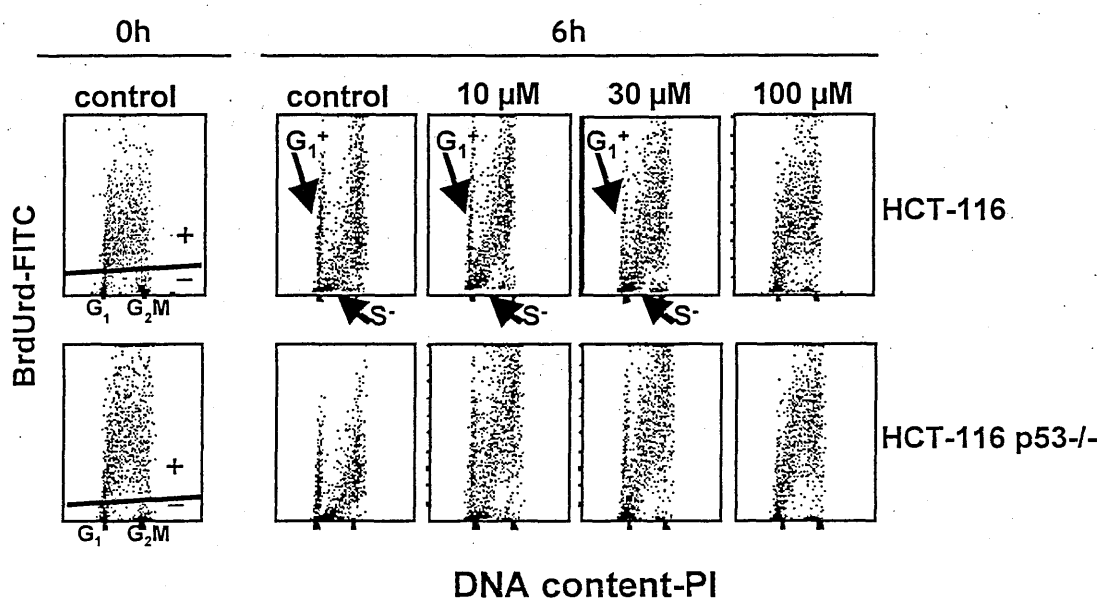

Figure 9.4: Biparametric PI-fluorescence (DNA content) and FITC-fluorescence (BrdUrd content) plots. Cells incorporated BrdUrd 20 min before the end of the 1h-treatment and were harvested 6h after treatment. Cells were considered BrdUrd-positive (in the S phase at the time of treatment, 0h) when detected above the straight line (left panels). BrdUrd-positive cells with G_1 DNA content (G_1+) at 6h were born from mitosis of cells in S phase at the time of treatment. G_1 BrdUrd-positive cells are present in the control and in samples treated with 10 and 30 μM DDP for both cell lines. BrdUrd-negative cells with S DNA content (S-) at 6h originated from G_1 phase at the time of treatment.

Other qualitative information could be derived from BrdUrd labelling 24 and 48h after treatment and from BrdUrd pulse-and-chase at 72h. In the first case (figure 9.5) cells were labelled with BrdUrd and immediately harvested and fixed, this allowed to distinguish DNA synthesizing cells from cells that were not cycling or that were delayed in their progression through S phase. 24h after treatment biparametric dot plots of 10-μM treated cells were very similar to the controls and in general, also for cells treated with higher doses, the DNA synthesis was not completely inhibited by the drug. Even in 100-μM treated samples a small amount of BrdUrd-positive cells was present. The comparison between the biparametric dot plots of wild type (9.5a) and p53-/- cells (9.5b) 24h after treatment highlighted some differences in the behaviour of the two cell lines. In 30-μM treated samples the amount of cells detected in S-late phase with low BrdUrd-fluorescence was higher in HCT-116 p53-/- than in wild type cells. Moreover, in p53-/- cells treated with the highest dose of DDP, a high percentage of BrdUrd-negative S-phase cells (i.e. not cycling) was detected. These observations indicate that the reduction of DNA synthesis was stronger in HCT-116 p53-/-.

48h after treatment, the biparametric dot plot of wild type cells treated with 10 μM DDP was similar to the control, whereas BrdUrd-positive cells in HCT-116 p53-/- were characterized by a lower level of fluorescence. This sample and also the others treated with higher doses confirmed the presence of a reduction in DNA synthesis rate. Moreover in samples treated with the highest concentration we were almost unable to detect BrdUrd-positive cells.

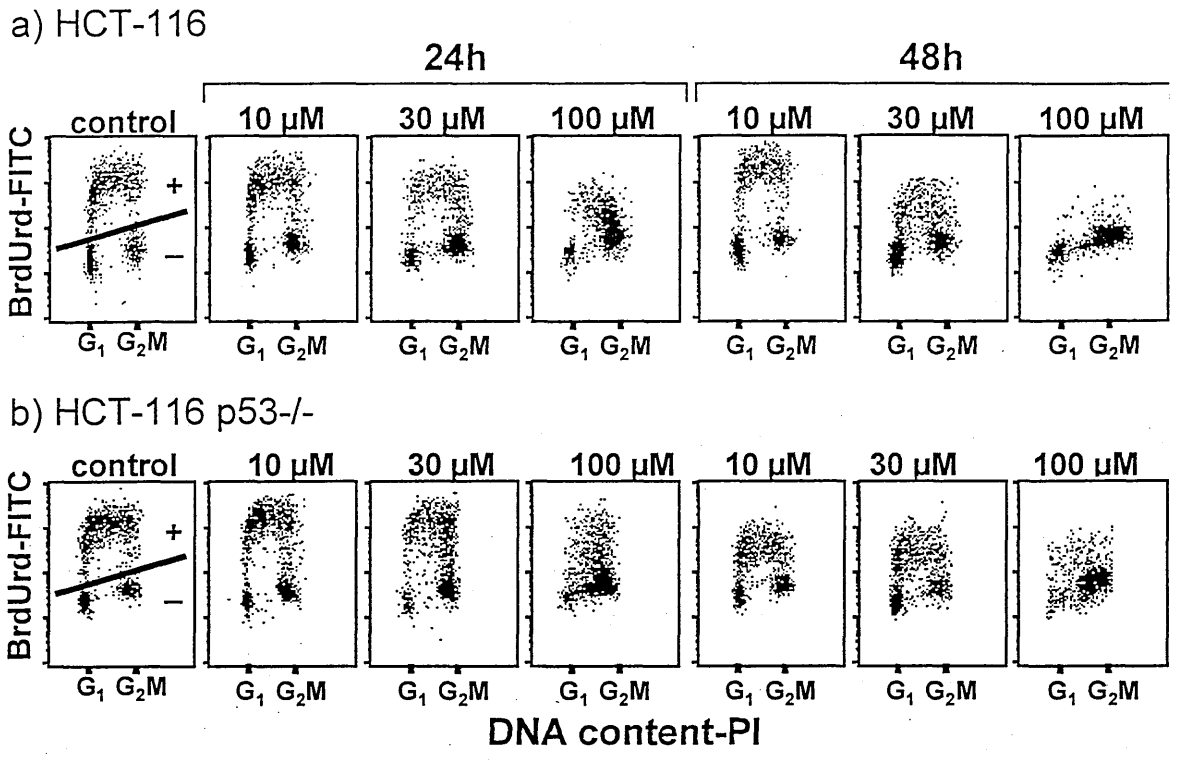

Figure 9.5: Biparametric DNA-BrdUrd dot plots of HCT-116 (panel a) and HCT-116 p53-/- (panel b). 24h and 48h after treatment cells were labelled with BrdUrd and immediately harvested and fixed. The cells that are detected above that straight line were synthesizing DNA ant thus incorporated BrdUrd.

In figure 9.6 we represented the other information that could be derived from BrdUrd pulse-and-chase experiment at 72h. The similarity of the percentage of BrdUrd-positive cells of treated and control samples indicated that in both the cell lines DDP did not specifically affect BrdUrd-positive or BrdUrd-negative subpopulations. In the case of a selective killing, e.g. of cells treated while in S phase, we would have observed a strong decrease in the percentage of BrdUrd-positive cells.

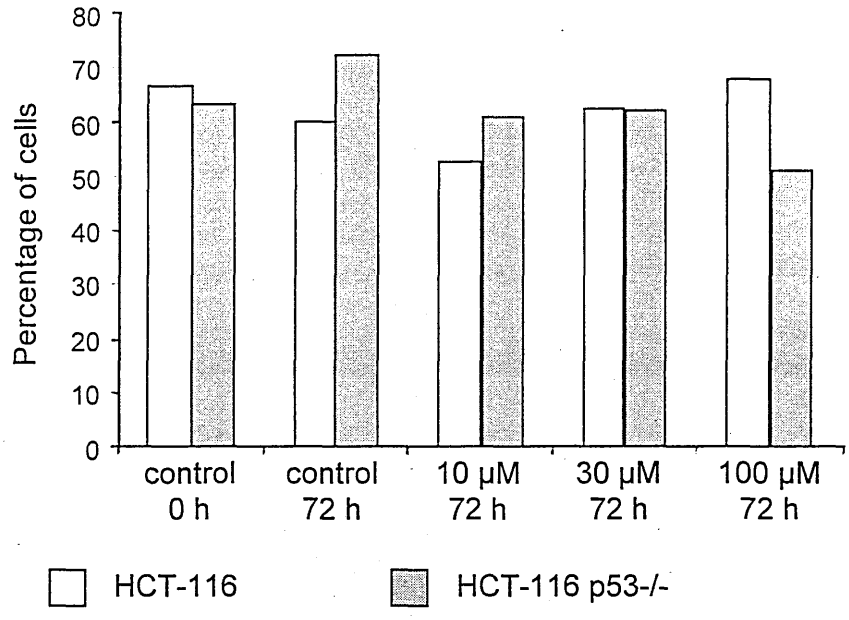

Figure 9.6: Comparison between the percentage of BrdUrd-positive cells in HCT-116 and HCT-116 p53-/- as detected with BrdUrd pulse-and-chase experiment at 72h after treatment.

Figure 9.7a and 9.7b show the biparametric dot plots DNA/dUTP, which provide at least qualitative information about the apoptosis induced by drug treatment. Cells with fragmented DNA, because of apoptotic death, formed the dUTP-FITC-positive subpopulation. In HCT-116 and HCT-116 p53-/- only cells treated with the highest DDP concentration presented more than 4% of cells in this status. A high percentage of dUTP-FITC-positive cells were already detected 48h after treatment in HCT-116 cells, whereas a low amount of apoptotic cells was present in p53-/- cells at 72h.

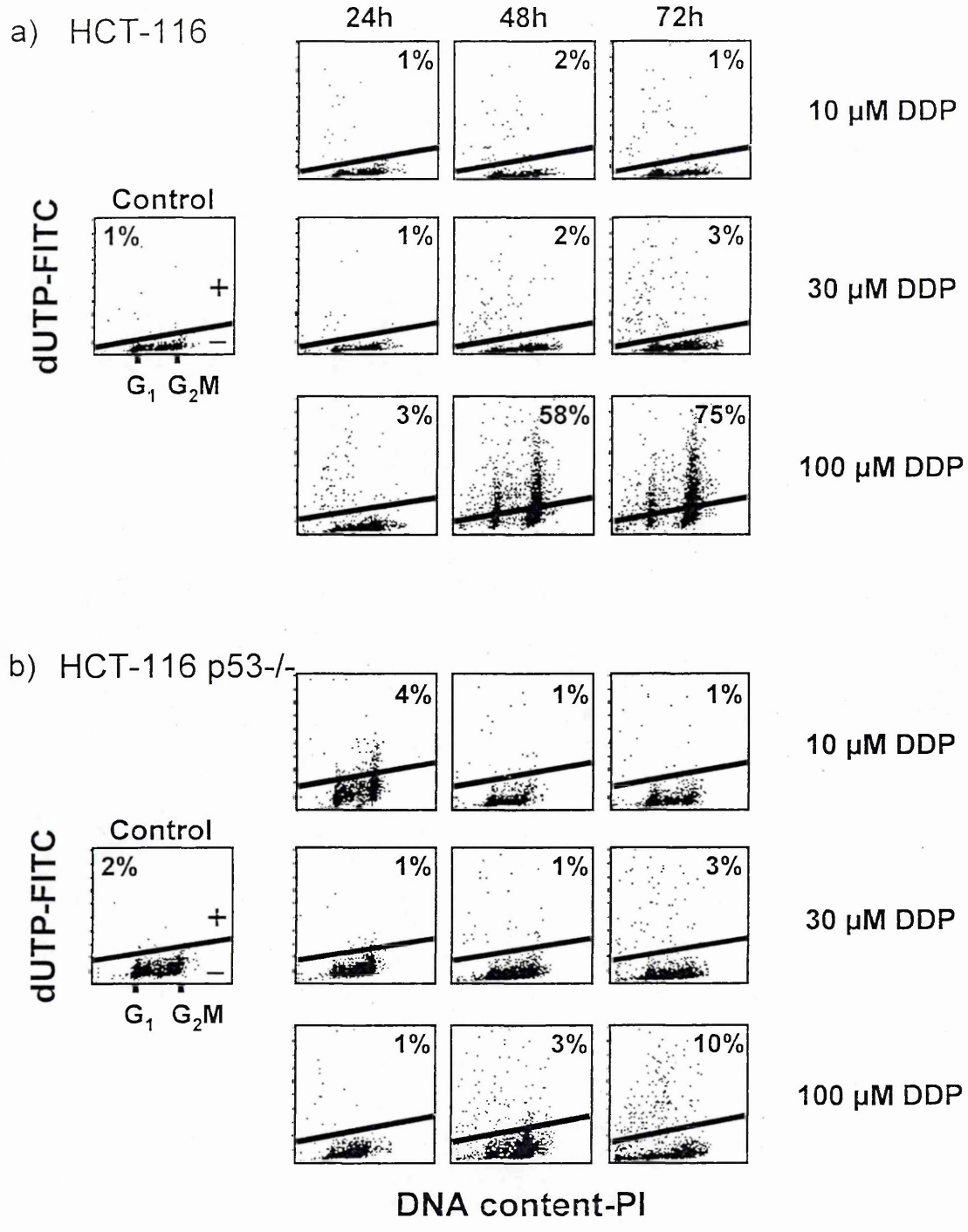

Figure 9.7: Biparametric PI-fluorescence (DNA content) and FITC-fluorescence (dUTP content) of HCT-116 (panel a) and HCT-116 p53-/- (panel b). Cells with DNA fragmentation induced during apoptosis are dUTP-positive, thus detected above the straight line.

At this point the simulation approach was applied to combine together all the information that came from cell count and flow cytometric analyses and to quantify the time- and dose-dependence of killing, blocking or delay and repair activity.

9.2.2 Scenario of Cell Cycle Perturbations Underlying Experimental Data

Several simulation runs were performed with the aim of fitting the data in figure 9.1 and 9.3 and taking into account the qualitative information reported in figure 9.5, 9.6 and 9.7. The scenario of parameter values enabling to reproduce all the data is shown in figure 9.8.

The twelve panels represent the time- and dose-dependence of blocking activity (1^{st} and 4^{th} line), death rate (2^{nd} and 5^{th} line) and recycling rate (3^{rd} and 6^{th} line) in HCT-116 (1^{st}, 2^{nd} and 3^{rd} line) and in HCT-116 p53-/- (4^{th}, 5^{th} and 6^{th} line). The effects occurred in BrdUrd-positive cells (left column) were also separated from those occurred in the BrdUrd-negative ones (right column).

9.2.2.a Events occurring in G_1 phase (figure 9.8a)

In the samples treated with 30 and 100 μM DDP cells remained blocked in this phase only between 0h and 6h (first line panel). Between 6h and 24h almost all the cells treated with the highest concentrations and blocked in G_1 could repair their damage and start cycling again (third line panel), this behaviour was similar in both cell lines.

The most evident difference between wild type and p53-/- cells was observed in the samples treated with the lowest drug concentration. Some of HCT-116 cells (5-20%) treated with 10 μM DDP were intercepted by G_1 block. The effect was persistent and still present 72h after treatment. Instead, in HCT-116 p53-/- G_1 block lasted 6h after treatment (fourth line panel).

9.2.2.b Events occurring in S phase (figure 9.8b)

The passage through S phase of BrdUrd-positive and BrdUrd-negative cells was affected in the same way by the treatment, but differently in the two cell lines.

Wild type cells immediately reduced their DNA synthesis but this effect lasted for 24h in 10- and 30-μM treated samples, whereas it was persistent in the cells treated with 100 μM DDP. For cells treated with the highest DDP concentration the delay rate remained constant up to 72h (first line panel). 5-20% of S-phase cells, or 20-40% for the samples treated respectively with 30 and 100 μM, died in this phase just after treatment. In cells treated with 100 μM DDP a cell loss between 24h and 72h added to the cell loss present at short time after treatment (second line panel).

In HCT-116 p53-/- DNA synthesis was more delayed than in wild type cells. Even in the samples treated with the lowest concentration a 20-40% of reduction of DNA synthesis rate was observed and the delay was still present 72h after treatment (third line panel). However, cell death was limited to cells treated with 30 and 100 μM DDP and it occurred only immediately after treatment (fourth line panel).

9.2.2.c Events occurring in G_2M phase (figure 9.8c).

G_2M checkpoint in wild type cells intercepted BrdUrd-positive and BrdUrd-negative cells just after treatment. The percentage of cells that remained blocked during their passage through this phase increased in a dose dependent way, and they reached a peak 24h after treatment. After 24h the percentage of cells entering the G_2M block decreased, even though for the samples treated with the highest concentration a residual effect was present 72h after treatment (first line panel). Between 0h and 6h, 5-20% of cells treated with 30 μM DDP and 20-40% of cells treated with 100 μM DDP died in this phase (second line panel). Only 20-40% of

cells treated with 30 μM DDP and blocked in G_2M could start cycling again between 24h and 48h (third line panel).

HCT-116 p53-/- cells were more strongly blocked in G_2M phase. In the samples treated with 30 μM DDP almost all the cells passing through G_2M between 24h and 48h were intercepted by the checkpoint. However, in the samples treated with the highest concentration, this effect lasted 48h after treatment and it was followed by the death of 20-40% of blocked cells. This behaviour was different from that observed in HCT-116, where the cells continued to be blocked up the end of the experiment and cell loss was not present.

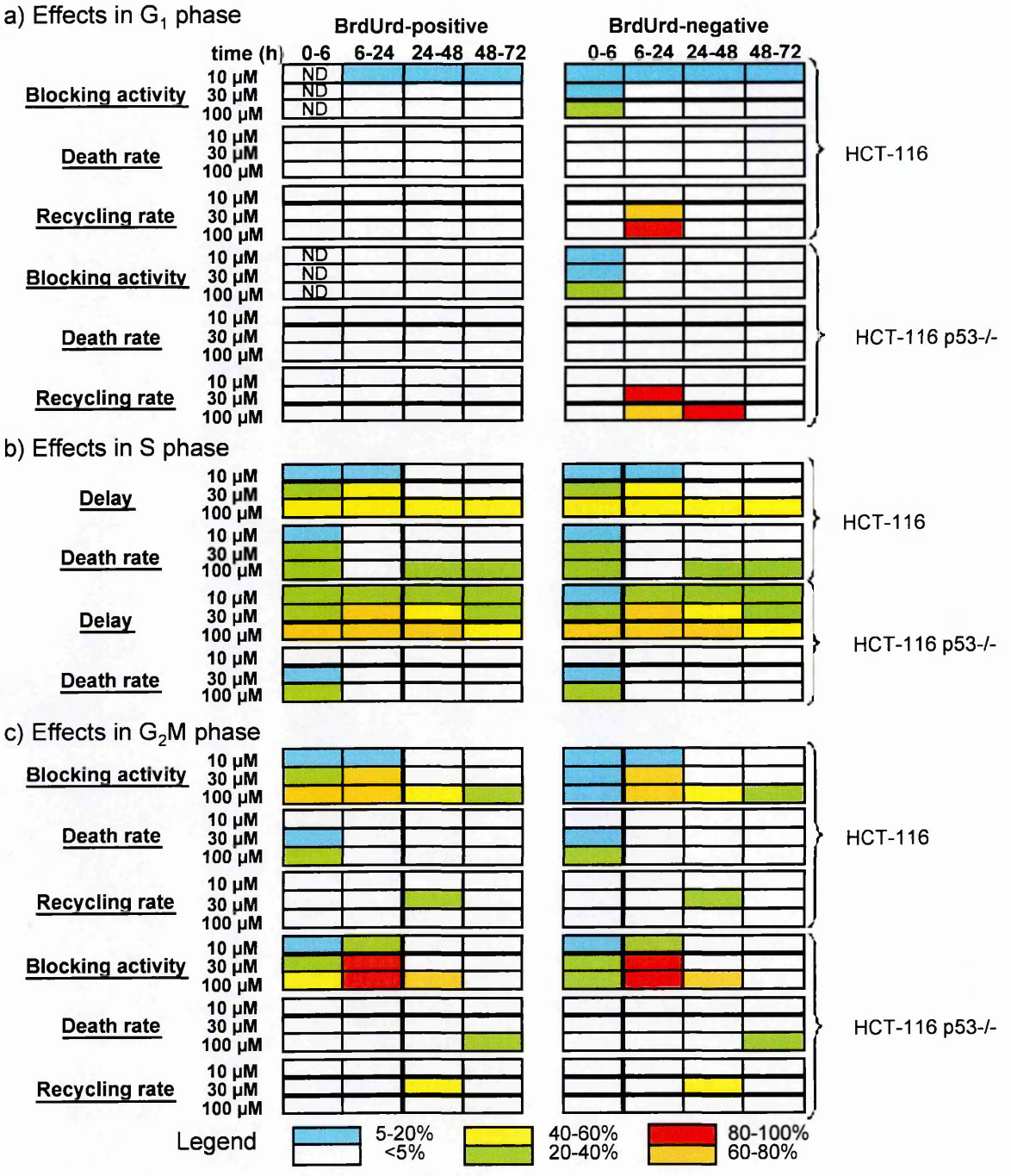

Figure 9.8: Characteristics of the response scenario for a complete reproduction of the experimental data. The blocking activity is represented as the percentage of cells that remain blocked among those traversing G_1 or G_2M in the time interval indicated. The death/recycling rates are expressed in terms of the percentages of cells that die/recycle in each time interval, within the compartment of G_1 (or G_2M) blocked cells.

9.2.3 Sensitivity Analysis

As we previously explained (paragraph 3.6.3.e) the final scenario shown in figure 9.8 allowed the reproduction of the data within the experimental precision, i.e. 3% for flow cytometric percentages and 20% for cell counts. Once that the final scenario was found it was necessary a further level of evaluation to measure the uncertainty of parameters estimation (sensitivity analysis). This study was done measuring how much the values obtained for each single parameter are allowed to vary maintaining the reproduction of data within their experimental error as in the adopted final scenario. In figures 9.9 and 9.10 we respectively represented the results of this study for HCT-116 and for HCT-116 p53-/-. The time course of each parameter obtained from the final simulation (represented with a continuous line) was compared with the results that came from the study of the sensitivity. The dashed area represented the range of values of each parameter within which the simulation remained close to the data as specified above. A wide band means that a given parameter, at the specified time and concentration, is irrelevant for the data, while a narrow band means that the estimate is robust and the prediction of the observed data would be lost by small alterations of the assumed value.

In wild type cells the parameter of G_1 blocking activity was found very sensitive, confirming the presence of a block in this phase for BrdUrd-negative cells in the first 6h after treatment (figure 9.9a). The presence of a blocking activity at long times in 10-μM treated cells was confirmed by this study in both BrdUrd-positive and BrdUrd-negative cells. At this drug concentration a recycling of G_1 blocked cells could not be excluded, especially because this effect was observed at higher concentration after 6h, when the blocking activity ended. 24h after treatment with 30 and 100 μM DDP the recycling rate became undetectable because there were not blocked cells any more. The sensitivity of cell loss of G_1 blocked cells was not

tested because this parameter was not relevant and always considered equal to zero in our simulation.

The precision of the final estimates of the parameters of S phase delay and cell loss resulted high by sensitivity analysis. The study confirmed the presence of a cell loss between 24h and 72h for cells treated with the highest drug concentration and a trend of increase with drug concentration for the parameter describing the delay in S phase (figure 9.9b).

The parameters connected with the blocking activity in G_2M phase were very sensitive to the data (figure 9.9c), confirming an increase in the block's strength between 6h and 24h. For the cells treated with 10 and 30 μM DDP the blocking activity lasted 24h after treatment leaving place to the presence of recycling. Sensitivity analysis confirmed the presence of a recycling activity in 30-μM treated cells blocked in G_2M and it also revealed that a non-zero recycling rate in 10-μM treated cells was compatible with our data. In wild type cells treated with 30 μM DDP the presence of a cell loss in G_2M phase between 0h and 6h was confirmed by the sensitivity analysis. Even though the cell loss in the same interval of time in 100-μM treated cells was not sensitive, the dose-dependence of the effects allowed us to consider non-zero this parameter.

As shown in figure 9.10 also the parameters used in the simulation of p53-/- cells were highly sensitive. The presence of G_1 blocking activity on BrdUrd-negative cells at short times after treatment was confirmed (figure 9.10a). Also the presence of a recycling probability was confirmed at short times after treatment in 30 and 100-μM treated samples, whereas this parameter was not sensitive in the cells treated with the lowest drug concentration (figure 9.10a). This could be ascribed to the small amount of cells that remained blocked in this phase.

As the sensitivity of the parameter connected with the delay in S phase was high (figure 9.10b) we could conclude that DNA synthesis in p53-/- cells were more

delayed than in wild type cells. The presence of cell loss was confirmed only in the first 6h after treatment in samples treated with 30 and 100 μM DDP.

The time-dependent trend of the parameters connected with the effects in G_2M phase was very similar for the two cell lines (figure 9.9c and 9.10c). The most important difference was observed in the parameter describing the cell loss in G_2M phase. In HCT-116 p53-/- only the cells treated with the highest drug concentration died in G_2M phase 48h after treatment and this behaviour was confirmed with good sensitivity by this analysis.

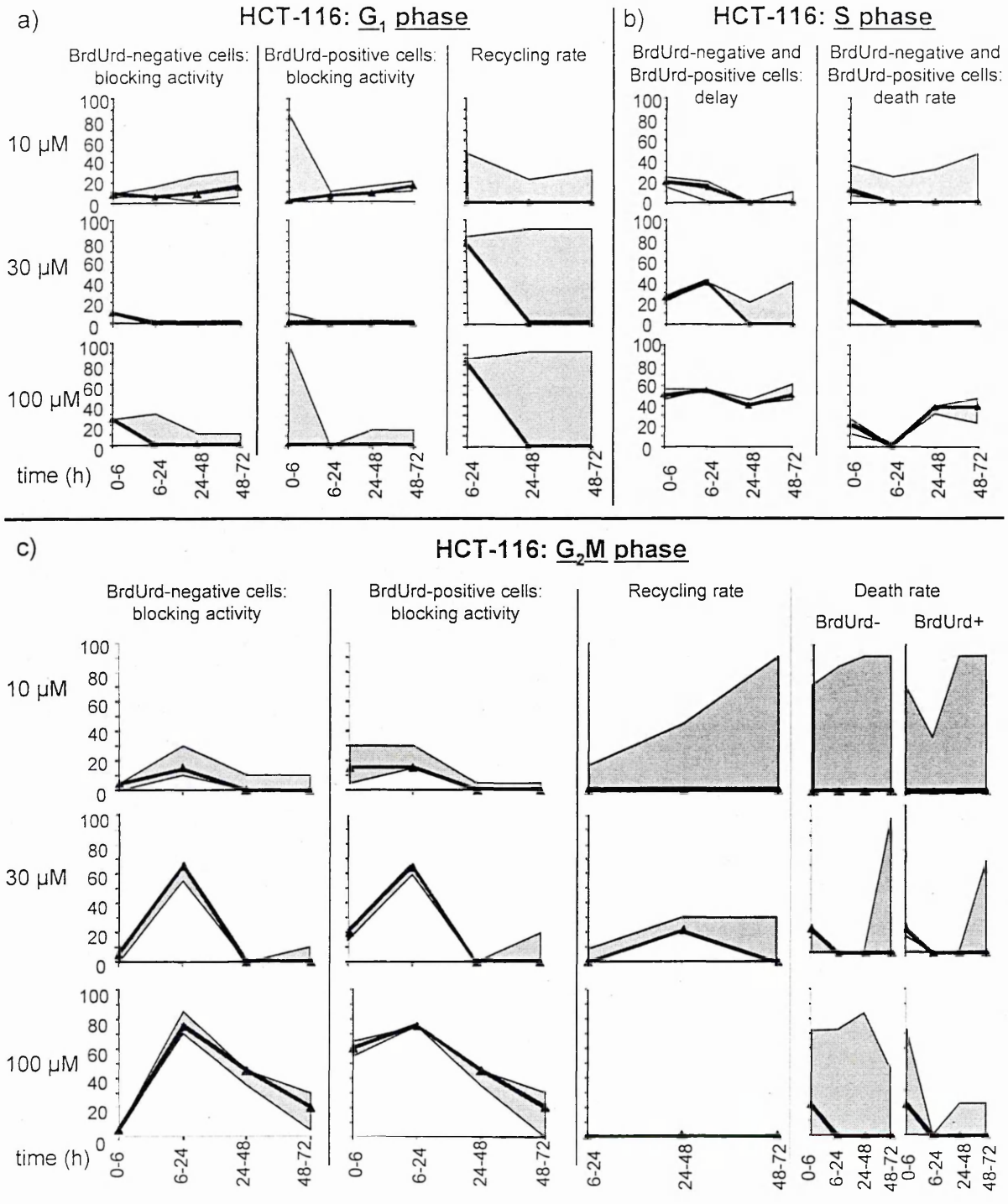

Figure 9.9: Time-course of the parameters used in the simulation. The continuous line represents the value of each parameter as obtained in the final simulation and the filled area represents the range of values of each parameter within which the simulation remained close to the experimental data. Panels a, b and c respectively represent the sensitivity of the parameters describing the effects in G_1, S and G_2M phase for wild type cells.

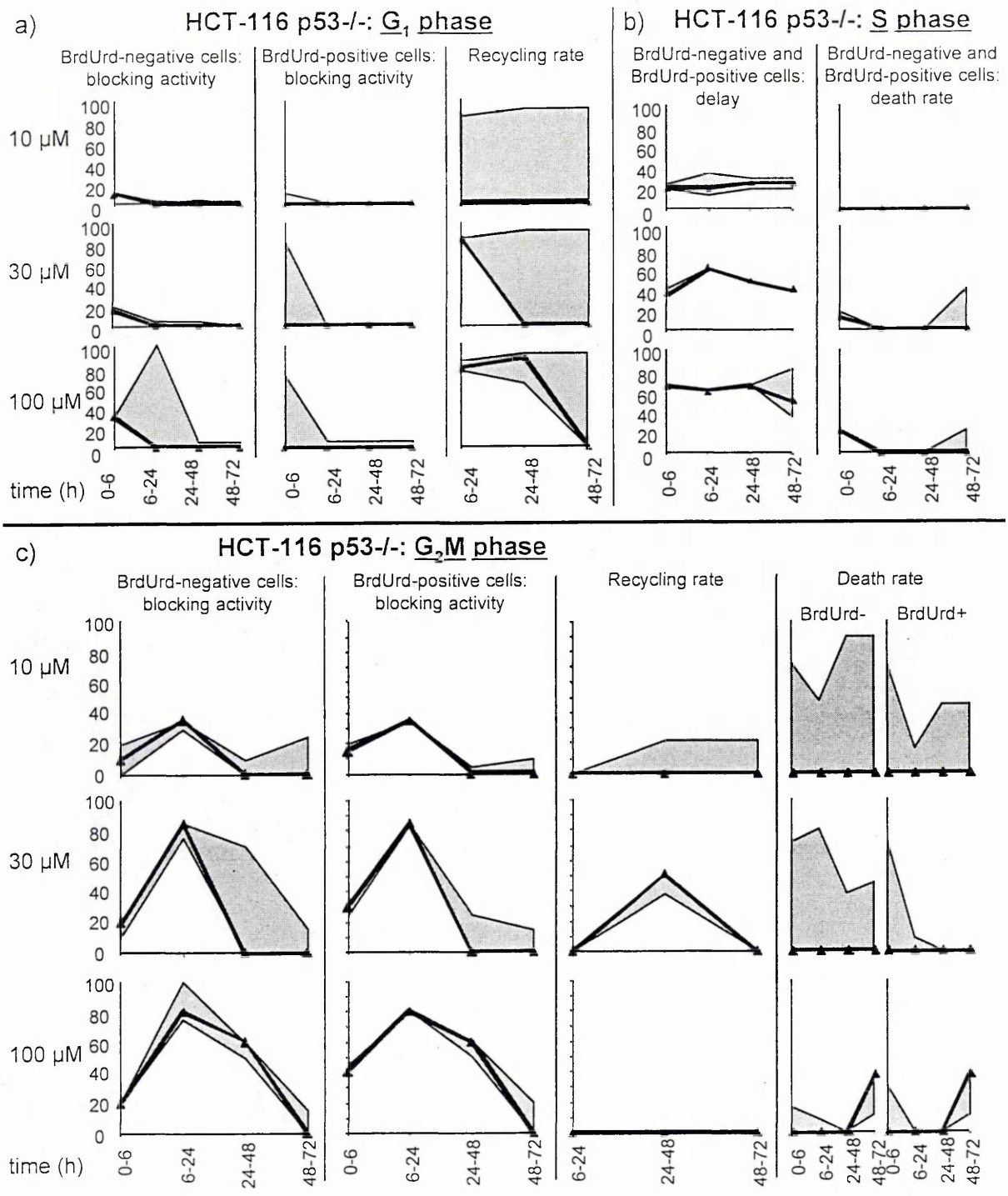

Figure 9.10: Sensitivity of the parameters describing the effects in G_1 (panel a), S (panel b) and G_2M phase (panel c) for p53-deficient cells.

9.2.4 Predictions of the Final Scenario

As already shown in the previous chapters, the final scenario could be used to obtain information on the behaviour and heterogeneity of the cell population that could not be measured otherwise. These predictions allowed an evaluation of the impact of a specific cell cycle effect (block, killing or recycling) on the growth of the whole cell population.

In figure 9.11 we represented the total amount of cells blocked in G_1 or in G_2M compared with the total amount of cells in the same phase. $\%G_1$ and $\%G_2M$ were obtained calculating the mean values of different experiments, whereas the percentage of blocked cells was calculated using the simulation. Only a small proportion of cells in G_1 phase was blocked and the most evident differences between wild type and p53-/- cells were detectable in the samples treated with 10 μM DDP. In this case, 72h after treatment, about 18% of HCT-116 cells in G_1 were blocked. At the same time there were not blocked p53-/- cells in this phase.

After treatment many cells accumulated in G_2M and from figure 9.11 we could appreciate that a big proportion of G_2M cells was constituted by blocked cells. In 10-μM treated cells the highest amount of G_2M blocked cells was reached 24h after treatment. In this case about 10% of wild type cells over a total amount of 20% were blocked in G_2M, whereas for p53-/- cells the amount of blocked cells reached the 20% over a total amount of 30% of G_2M cells. Also in 30-μM treated samples the amount of G_2M blocked cells reached its maximum 24h after treatment with a similar behaviour for the two cell lines. The decrease in the percentage of G_2M cells at 48h could be explained with the presence of a recycling probability in both the cell lines. In the samples treated with the highest drug concentration the amount of G_2M blocked cells reached its maximum 48h after treatment. Whereas in wild type cells this amount remained constant also at

72h, in p53-/- cells there was a decrease in G_2M blocked cells that could be ascribed to the presence of cell loss.

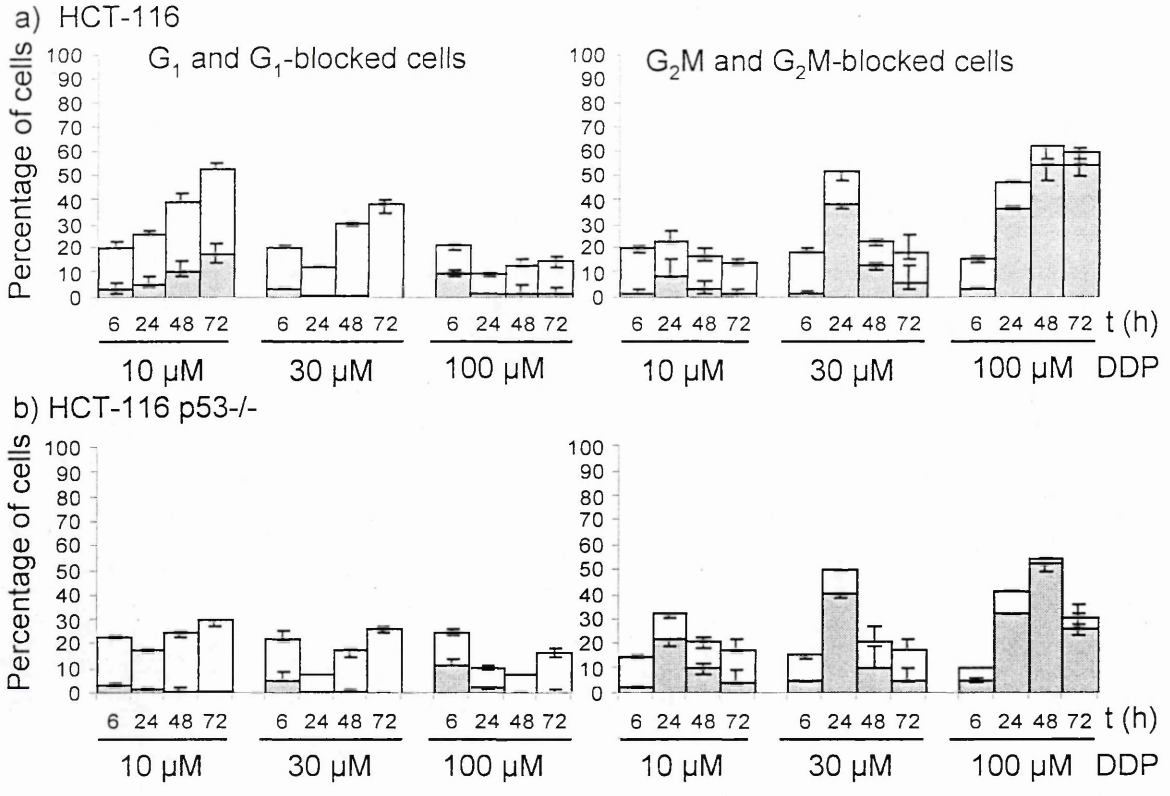

Figure 9.11: Dose-dependence and time-dependence of the percentage of total (full height of the bars) and blocked (height of the filled area of the bars) cells in G_1 and in G_2M for wild type and p53-deficient cells. This serves to evaluate the impact of the blocking effect on the cell population after treatment with 10, 30, 100 µM DDP. The error bars in the histograms indicate of the range where different simulations give predictions fitting the data within the experimental error.

From the simulation it was also possible to obtain the percentage of cells lost immediately after treatment and in 72h. In figure 9.12 the cytotoxic effect of DDP on HCT-116 and HCT-116 p53-/- was compared. Treatment with 10 µM and 30 µM DDP were more cytotoxic for wild type cells that preferably died in S phase, between 0h and 6h after treatment. The bigger proportion of cells lost in S phase was represented by the BrdUrd-positive subpopulation. 17% of HCT-116 cells

treated with 30 μM DDP died in 6h and 88% of them was lost in S phase. On the contrary, for samples treated with the highest DDP concentration the mortality was higher in p53-/- cells. 37% of HCT-116 p53-/- cells was lost in 72h, compared to 25% of wild type cells, and the difference was due to cell loss at long times after treatment, in fact the percentage of lost cells in 6h was similar for wild type and p53-/- cells. In HCT-116 p53-/- 60% of cells died in G_2M phase, while 91% of wild type cells died in S phase. For wild type cells about 60% of the cells dead in S phase were BrdUrd-positive, at the same way for HCT-116 p53-/- the biggest part of the cells lost in S and in G_2M phase were BrdUrd-positive.

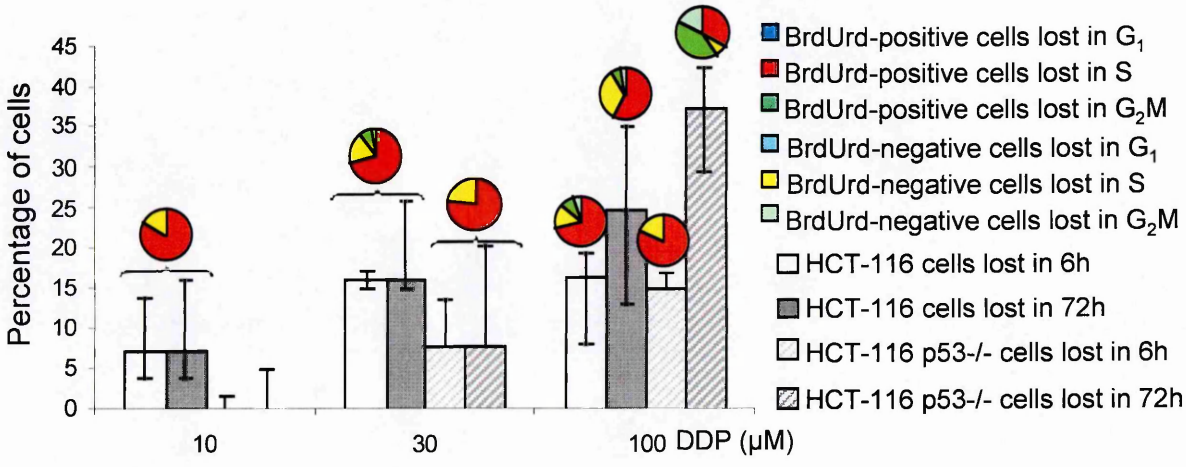

Figure 9.12: Comparison between the total percentage of dead cells in 6h and in 72h obtained from the simulation for HCT-116 and HCT-116 p53-/-. The pies above the columns of the histograms give the distribution of the cells lost in the different cell cycle phases. The error bars were calculated as reported in figure 9.11.

9.2.5 CFSE Labelling of HCT-116 and HCT-116 p53-/-

In order to deepen the interpretation of the proliferation delays caused by DDP, we labelled HCT-116 and HCT-116 p53-/- cells with CFSE and we treated them with 30 and 100 μM DDP. A time-course of CFSE histograms was obtained fixing the

cells at different times after treatment. In figure 9.13 the data coming from one typical experiment were represented.

As explained in chapter 8, CFSE fluorescence intensity of control cells shifted toward lower values of fluorescence because of cell division, whereas CFSE histograms of treated cells tend to spread, as expected for delayed cells. Analysing each histogram as sum of gaussians, each one representing a cell generation, it was possible to obtain the percentage of cells that at a certain time after treatment remained undivided, those that were able to divide once, twice, etc. Comparing the results, the most important differences between the two considered cell lines could be observed at 72h, even though some differences in the controls should be taken into account. In fact at this time HCT-116 treated with 30 μM DDP reached the 6^{th} generation, whereas p53-/- cells treated with the same concentration reached the 5^{th} generation, but also their control was slowed down in comparison with wild type control. On the contrary the difference between the two cell lines treated with 100 μM DDP were much more evident and thus not conditioned by the different behaviour of the controls. In this case the majority of wild type cells remained blocked at the 1^{st} and 2^{nd} generation, whereas a big proportion of surviving p53-/- cells where in 3^{rd} or subsequent generations. This suggested that some p53-/- cells were able to escape the block and survive better than wild type cells.

These experimental data could also be compared with the output of the simulation that results from the application of the final scenario. This comparison might give a contribution to the discrimination between different possible scenarios. In figure 9.14 the cell distribution at 72h obtained from experimental and simulated data was compared.

In general the trend of the cell percentages in the different generation was respected. The differences could be explained taking into account that the

simulated data were obtained as mean value of different experiments, whereas the data of CFSE came only from one of them. Moreover our model could not differentiate in a specific phase the effects that occurred at the cells in the first generation from those that occurred in the latter generations.

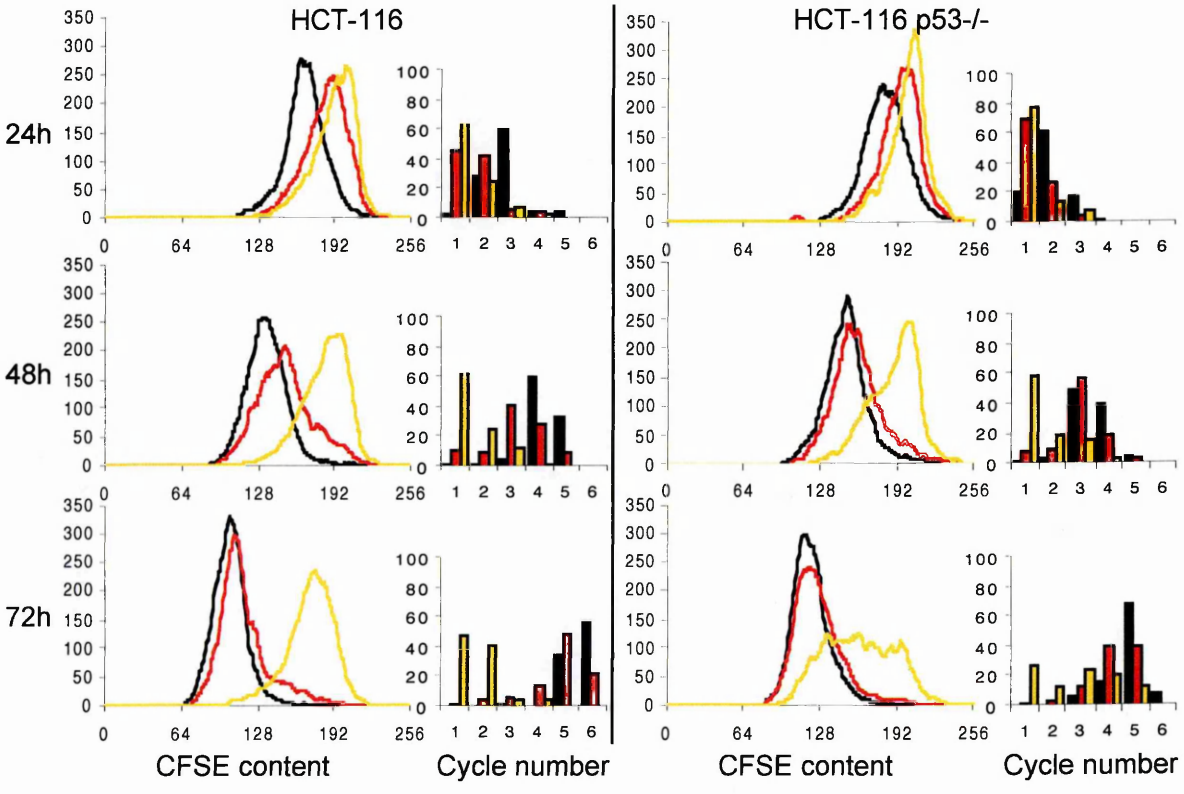

Figure 9.13: Time-course of CFSE histograms of HCT-116 and HCT-116 p53-/- after 1h-treatment with DDP. In CFSE profiles the controls are represented with the black line, the samples treated with 30 μM DDP with the red line and the samples treated with 100 μM DDP with the yellow one. The histograms beside CFSE profiles represent the percentage of cells in each generation as obtained by the analysis of flow cytometric data. All the data shown in this figure come from one typical experiment.

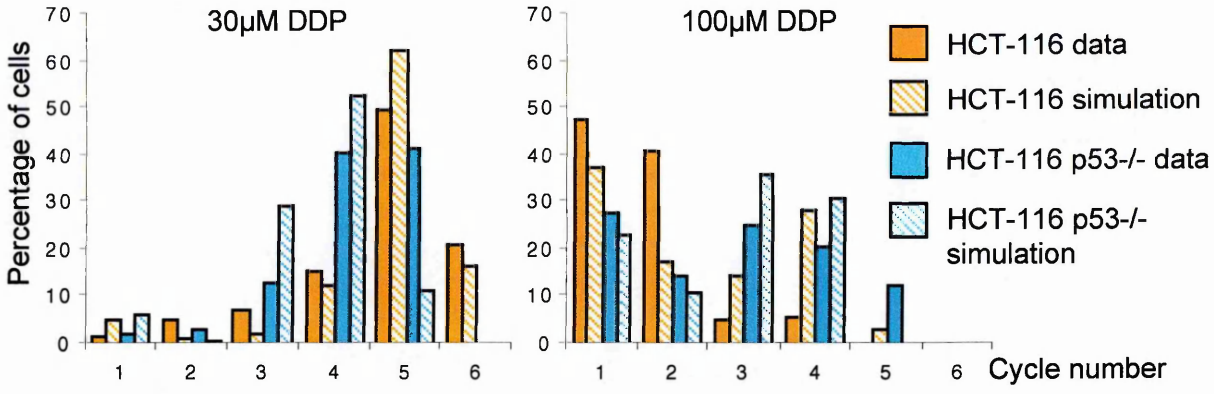

Figure 9.14: Comparison between the cell distribution at 72h obtained with the analysis of CFSE histograms and those obtained as output of the simulation, for samples treated with 30 and 100μM DDP. The differences between the experimental data and the result of the simulation could be ascribed to the fact that the simulated experiment was different from that performed with CFSE. Moreover our model could not differentiate the effects that occurred at the cells at the first generation to those that occurred in the last generation.

9.3 DISCUSSION

We demonstrated that short DDP treatments induced complex cytostatic and cytotoxic responses in each cell cycle phase, and each effect presented a peculiar time- and dose-dependence.

In wild type cells a blocking activity was observed in G_1 and in G_2M phase immediately after treatment and, at the same time, the cell progression through S phase was delayed. Most cytostatic effects ended within 24h after treatment, except for the samples treated with the highest dose, where a blocking activity in G_2M and a delay in S phase were still present at 72h. The end of the blocking activity in G_1 and in G_2M phase left place to recycling, observed between 6h and 24h in G_1 phase for 30- and 100-μM treated cells and between 24h and 48h in G_2M phase for 30-μM treated cells. Cell loss, particularly in S-phase cells, was

observed between 0h and 6h, even at low and intermediate concentration, whereas at the highest concentration a second wave of loss occurred after 24h.

These results could be compared with those reported for IGROV1 cells (Montalenti et al., 1998) treated with the same DDP concentrations. In general the perturbations induced by DDP on the cell cycle of HCT-116 were not too different from those found for IGROV1 cells. In particular, after a short block in G_1 or in G_2M phase, IGROV1 cells treated with low doses started cycling again. A blocking activity and a cell loss were simultaneously present in the first 6h after treatment. The long-term death characterized the treatment performed with higher doses. In IGROV1 cells, like in HCT-116, the cell progression through S phase was delayed by the treatment and the duration of this effect was strongly dose-dependent. However, if the kinetics of these phenomena looked similar in the two cell lines, their intensity was different, in fact IGROV1 cells resulted much more sensitive to this drug. This is coherent with the hypothesis that cells lacking for proteins related to MMR, as HCT-116, are more resistant to DDP, although a role of other genes differently expressed in the two cell lines cannot be excluded. Instead, the differences observed in the kinetics of the blocking activity, cell loss and recycling in the isogenic HCT-116 and HCT-116 p53-/- cell lines could be unambiguously ascribed only to the presence or absence of p53.

Qualitative inspection of cell counts, TUNEL assay, DNA histograms and DNA/BrdUrd dot plots, obtained in parallel for HCT-116 and HCT-116 p53-/-, evidenced several, but not strong, differences in the response between the two cell lines. Our findings were not in agreement with other studies comparing HCT-116 and HCT-116/E6 cell lines (Lin et al., 2001; Vikhanskaya et al., 1999) and reporting a much higher sensitivity of the HCT-116/E6 clone with disrupted p53 function. However the use of papilloma virus-derived E6 to inactivate p53 is reported to cause major effects on cells other than those just mediated by p53

inhibition (Klingelhutz et al., 1996; Bunz et al., 1999). Instead, our data are in keeping with those of Carrassa et al. (2004) and of Lin et al. (2004) who performed experiments using HCT-116 p53-/-. In the first case they demonstrated that wild type and p53-/- cells had a similar sensitivity to short DDP treatment. In Lin's study the cells were continuously treated for 72h, but also in this case they found at the most a two-fold increased sensitivity to this drug for cells with wild type p53. However, in both these studies the contribution of p53 in distinct cell cycle control mechanisms of block, recycling and death was not quantified. This analysis was attempted in the present study, examining a complete time- and dose-series of experimental data with the previously described mathematical method (see section 3.6). This procedure proved successful in the explanation of phenomena which were apparently contradictory confirming, once again, the complexity of the role of p53 in the response to a drug treatment.

In treatments with low DDP concentration (10 μM) the absence of p53 seemed to prevent the cells from a limited short-term death, occurring in cells traversing S phase. Cytostatic effects were detected in all cell cycle phases but in S and in G_2M phase they were relatively stronger if p53 was absent. Thus, damaged cells with wild type p53 died, whereas p53-/- cells were able to survive but they were more impaired than surviving HCT-116 in the subsequent progression through S and G_2M phase. Moreover, some wild type cells were continuously intercepted by G_1 checkpoint. This effect was not present in HCT-116 p53-/-, suggesting an impairment of G_1 checkpoint in this cell line, even though this checkpoint showed to have a minor role in the overall response of HCT-116 to treatment with low DDP concentrations.

Similar effects were observed at short time after treatment with intermediate concentration (30 μM), even though with a stronger intensity, confirming the differences found in 10-μM treated samples. As for the lowest concentration, short-term cytotoxicity was higher in wild type cells, while the progression through S and G_2M phase was slower in p53-/- cells. Between 6h and 24h, 90% of the HCT-116 p53-/- passing through G_2M remained blocked in this phase compared to the 65% of wild type cells. Then, both G_2M-blocked p53-/- and wild type cells started cycling again between 24h and 48h and there was not long-lasting cell death. For what concerns the G_1 response, a low short-term block was common to both wild type and p53-/- cells, followed by recycling in the subsequent interval of time (between 6h and 24h). This effect was associated to cells originally in G_1 phase (BrdUrd-negative), whereas BrdUrd-positive cells, that could divide and reach G_1 phase, were not blocked there. This behaviour differed from that observed at the lowest concentration, were G_1 checkpoint was activated in some BrdUrd-positive wild type cells, but in this case the delay in S phase and the blocking activity in G_2M phase were less efficient. Moreover, several p53-/- cells that divide once and went out from G_1 after 24h were delayed in traversing S phase, suggesting that repair was not completed in the checkpoints previously traversed. These findings are consistent with the hypothesis of a less efficient repair in p53-/- cells, and with the hypothesis of a long-term G_1 block not functioning when p53 is absent. On the contrary the effects observed in G_1 phase in 30- and 100-μM treated samples were equivalent in wild type and p53-/- cells, with a short-term block followed by a recycling between 6h and 24h.

The situation changed in cells treated with a relatively high concentration of DDP, such as 100 μM, where the presence of long-term cytotoxic effects was relevant, whereas the cytostatic effects in all phases reproduced and confirmed those observed in 30-μM treated cells. At short times after treatment a cell loss was

observed in S-phase cells of both cell lines whereas only HCT-116 blocked in G_2M phase died there. The absence of a killing activity in G_2M confirmed the behaviour observed at 30 μM, suggesting an involvement of p53 in shifting towards death the fate of G_2M blocked cells at short times after treatment. On the other side G_2M-blocked HCT-116 p53-/- collapsed between 48h and 72h, the presence of a non-apoptotic cell death was confirmed by the high amount of debris (figure 9.2a) and the low percentage of dUTP-positive cells detected at 72h (figure 9.7b). Long-term death in HCT-116 involved cells that, 24h after treatment, reached S phase after dividing once. This fact could explain the absence of wild type cells in the 3rd and subsequent generations at 72h whereas some p53-/- cells were still present (figure 9.13, lower panels). The ability of these cells to bypass G_1 checkpoint had two possible explanations. The first hypothesis is that at such a high level of damage the p53-dependent G_1 block was not functioning, because some of the proteins involved in this molecular pathway could not be properly produced. The second hypothesis is that the trigger towards apoptosis was given while cells were in G_1 but they did not remain blocked in that phase.

The reconstruction of this scenario was possible by integrating data obtained with different techniques and with a complete experimental plan including the monitoring of the cells treated with several drug concentrations at different times after drug washout. The use of computer simulation allowed that integration. We believe that part of the contradictory results reported in the literature could be explained as shortcut interpretations of piece of information obtained with incomplete experimental plans.

For instance, from a simple analysis of flow cytometric histograms the disappearance of accumulation of cells in G_2M at 72h in p53-/- cells could be interpreted as a consequence of a shorter duration in G_2M blocking activity. This

interpretation would have supported the hypothesis that p53 was important not only in the occurrence of G_2M arrest but especially in the duration of the effect (Bunz et al., 1998; Hirose et al., 2001). However our deeper investigation induced to suppose that the situation was more complex, with a blocking activity overlapped to a cell loss, so that these two contributions determined the overall percentage of cells in this phase.

However, due to the low blocking activity induced in G_1 phase by DDP, even in wild type cells, the role of p53 in this checkpoint should be further investigated with a compound inducing a stronger block in this phase.

CHAPTER 10: General Discussion

The efficacy of many treatments with anticancer agents could be limited by wrong knowledge about the cytokinetic properties of the cell population and, on the other side, by an incomplete knowledge of the effects induced by the considered compounds. In fact we demonstrated in this thesis that even low concentrations of agents believed to be rather phase-specific could induce effects in each cell cycle phase. Thus the appreciation and the quantification of these effects provide an important contribution to the comprehension of the mode of action of a particular anticancer agent. Very often also clinically used drugs are not completely understood from the point of view of the time- and dose-dependence of the effects induced in the cell cycle and many published reports catch only partial aspects of them. It is for this reason that we decided to make a complete study of the cell cycle response to treatments with a set of drugs belonging to different classes of chemotherapeutic agents. As far as we know, a study of this kind, producing a database of data with the same methods and with the same biological model, is lacking in the scientific literature. Thus we decided to approach the problem focusing our attention on a biological model represented by an ovarian cancer cell line. The choice was driven by the fact that our laboratory has been interested since many years in the study of this kind of tumour and its therapies. As a consequence the choice of the drugs considered in this project (cisplatin, doxorubicin, melphalan, paclitaxel and topotecan) fell on compounds that are in use, or were used in the past, for the treatment of the ovarian cancer as single or combined agent, in first line therapy or for relapsed tumours.

As a model of ovarian cancer we decided to use a cell line stabilised *in vitro* and we chose IGROV1 for the following reasons:

i. This cell line is one of the ovarian cancer lines considered by NCI for the project of drug screening (http://dtp.nci.nih.gov/branches/btb/ivclsp.html).

ii. IGROV1 shows a response to the drug treatment with the compounds considered in this project not too far from the average response showed by the group of ovarian cancer cell lines considered in the NCI panel.

iii. Culture conditions of IGROV1 were previously optimised in our laboratory (Chiorino et al., 2001), obtaining a good reproducibility of cell growth.

iv. From the molecular point of view IGROV1 have p53 wild type and the other cell cycle relevant genes are not exceptionally expressed respect to the other ovarian cell lines in the NCI panel.

On the other side, from the point of view of the schedule of treatment, we decided to perform pulse-like treatment for all the considered drugs. In our opinion, the choice of investigating the cell cycle effects induced by 1-h treatments represents the first necessary step before tackling the problem of building the effect upon prolonged or more complex schedules. Moreover the extent of the observation period was 72h because, as previous experience indicated, cytostatic and cytotoxic effects are still present at long times after drug washout.

The data collected with all drugs were analysed with the mathematical approach developed by our group. This method allows the simulation of the fluxes of cells through the cell cycle in unperturbed conditions and in the presence of specific hypotheses concerning the post-treatment dynamics of the activity of G_1, S and G_2M checkpoints. In this way we were able to reproduce all the data retrieved at different times and drug concentrations and with different techniques. Moreover, with the simulation approach, we could overcome many limitations deriving from other experimental methods that are not able to quantify separately cytostatic and cytotoxic effects (for further details see section 1.3). The application of a mathematical model reproducing the cell cycle before and after drug treatment allowed the appreciation of the heterogeneity of the cell response to DNA damage

induced by anticancer agents, evaluating the percentage of cells intercepted by each checkpoint.

A remarkable aspect of this approach was the strong connection between experiments and theory. In fact, differently from many "theoretical" mathematical models, the simulation was used to reproduce a huge amount of experimental data. On the other hand the simulation was also crucial in the recognition of different combinations of G_1, S and G_2M perturbations coherent with the data and in the design of additional experiments to test concurrent hypotheses.

As the model is a simplification of the complex cell response to a drug treatment, our aim was not to use it for a precise measure of the parameters but to obtain an estimate of the strength of the corresponding phenomenon, enabling to explain the available data. On the other side, wishing to include all basic perturbations of the cell cycle with their time-dependence, the equations of the model are too complex to be solved and we are not able to obtain cell cycle percentages as analytical functions of those perturbations. For this reason, we made simulations, solving numerically the equations of the model. In this situation it was not necessary (and also not technically possible in our knowledge) to fit directly the data with some non-linear fitting routine and we adopted a trial-and-error procedure. This also allowed us to maintain a biological comprehension of the phenomena in all phases of the analysis.

At the end, with our analysis we were able to determine a set of parameters (scenario) that describe and quantify the cytostatic and cytotoxic effects induced by the treatment with each one of the considered drugs. Eventually, the work done for this project produced two complete databases, one including the data (flow cytometric percentages and cell numbers at different times after treatment with several drug concentrations - appendix 1) and the second including the time- and

dose-dependence of the parameters used in the model and associated to blocking activity and repair or killing in G_1, S and G_2M.

In this way we were not only able to separate cytostatic from cytotoxic effects, but we could also evaluate in which phase of the cell cycle they occurred. In addition, using BrdUrd labelling and pulse-and-chase, a distinction between cells that were in S phase at the time of treatment and cells that were in G_1 and G_2M was possible without any synchronization. Thus we could follow the fate of the two subpopulations through the different cell cycle phases and quantify separately the impact of the drug on BrdUrd-positive and BrdUrd-negative cells.

The possibility of using other flow cytometric information was also tested in this project. In particular, CFSE staining allowed the distinction between cells in the first, second or other cycles after treatment. We applied this new approach to the case of IGROV1 cells treated with different concentrations of topotecan and we followed the cell proliferation until 72h after treatment. Moreover the setting up of a triparametric staining with CFSE, BrdUrd-PE and PI for DNA content enabled us to monitor the effect of topotecan on proliferation of cells that were in S phase at the time of treatment. The results of this study (chapter 8) highlighted the heterogeneity of drug effects: some cells die, some do not proliferate at all, and some divide once, twice or even three times in the 72-h observation period. This issue is often overlooked, particularly in studies based on cell extracts, where researchers examine changes in average molecular quantities, thus averaging the response of the time- and dose-dependent fraction of cells that remain healthy with that of the cells that try to repair the damage and even with dying cells. However, strong intercell variability of the response is not surprising because of the potential differences in the protein content at the time of treatment and in cellular drug exposure (Evans et al., 2004). In fact, on the first point, the amount of each protein at the time of treatment is the result of many complex interactions,

each one with its own statistical variability, and therefore is likely to vary widely among individual cells. Many combinations of these amounts are probably compatible with normal cell life and proliferation. Concerning drug exposure, other reports (Feeney et al., 2003; Errington et al., 2005) suggested that the actual drug concentration widely varies inside the cells even in the strictly controlled environment of *in vitro* culture. However, with our model we were able to face this complexity and the data coming from CFSE could be correctly simulated. As we have demonstrated in chapters 8 and 9 this was possible even though in the model we did not differentiate the effects that occurred at the cells in the different generations.

The model was not only able to explain the data obtained with CFSE staining but it was also used to analyse the information connected with more complex schedules of treatment. We considered the case of repeated TPT treatments on IGROV1 cells demonstrating that the model is self-consistent and it can be applied to investigate the origin of an auto-potentiation phenomenon that was observed with a fractionated scheme.

Moreover, additional and extensive studies were done in order to test the results obtained with the simulation. In particular the study of the sensitivity of the parameters considered in the model allowed an estimation of the possible range of error of the scenario that was obtained for each drug. This represented a necessary step towards the comparison of the cell response activated by different anticancer agents. Despite the belonging of the five compounds to different classes of chemotherapeutic agents, inducing different types of damage, this part of the study leaded to the recognition of the existence of common trends in the response to drug treatments.

As far, we focused our attention on the same cell line, but with a similar approach, it is possible to analyse the similarity and the differences between the response of

different cell lines to the treatment with the same anticancer agent. With this kind of experiments it is possible to answer two different questions: are cell cycle effects induced by drug treatment independent of the employed cell line? What is the role of a particular protein in the cell response to drug treatment?

We addressed the issue of the reproducibility of the scenario with different cell lines, performing a treatment with L-PAM on another ovarian cancer cell line (A2780) and a colon carcinoma cell line (HCT-116) and we confirmed most of the features observed with IGROV1. However, the same effects observed in IGROV1 cells were also detected in A2780 treated with a lower concentration and in HCt-116 treated with a higher concentration. This difference of sensitivity between the three cell lines might also be caused by events upstream cell cycle response, like different drug transport across cell membrane or different amounts of DNA lesions produced during exposure to L-PAM. The results of this study are not shown in this thesis, but have been published on Lupi et al. (in press).

The last part of the project was addressed to answer the second question. In particular we investigated the role of p53 in the response to a treatment with DDP. In this case we used two isogenic cell lines differing only for the expression of p53 and we compared the scenarios describing the effects induced by DDP in the two systems. Many studies has been done about this topic (see references in chapter 9), but they generally lack in the quantification of the contribution of p53 in different cell cycle control pathways and their results are not always in agreement. Our contribution to this subject was represented by a complete description of the time- and dose-dependence of the role of p53 in the response to DNA damage. In particular we confirmed the role of p53 in the activation of the apoptotic pathway, making an observation similar to that reported by Zamble et al. (1998) in teratocarcinoma cells treated with DDP. The presence of p53 induces a more rapid apoptotic response, even though its absence does not alter the cellular

sensitivity. On the other side, the role ascribed to p53 in the maintenance of G_2M blocking activity (Bunz et al., 1998; Hirose et al., 2001) was not confirmed by our study, which instead pointed on different kinetics of loss between G_2M blocked cells in HCT-116 and HCT-116 p53-/-.

These studies open new perspectives for future projects. For instance, a deeper investigation of the role of p53 in the response to other anticancer agents could be done focusing a particular attention on its role in the induction of G_1 checkpoint activity that has not been further investigated in the case of DDP, because of its low effect in this phase in the considered cell line. Besides the role of p53, it would be also interesting to study the role of other key proteins in the activation of cell cycle checkpoints after drug treatment.

On the other side the study of more complicated schedules of treatment or the investigation of the origin of the potentiation deriving from the use of drug combination or fractionation would be helpful in the design of new tests aimed to find treatments with more efficacious outcome.

APPENDIX 1

We reported in table A.1 the time course of the experimental data obtained from the study of the response of IGROV1 cells to 1-h treatments with cisplatin, doxorubicin, melphalan, paclitaxel and topotecan applying the basic experimental plan (see Materials and Methods). Besides the flow cytometric percentages calculated from DNA histograms or from biparametric DNA/BrdUrd dot plots we listed the relative number of cells: N_R = N(t)*1000/N(0) where N(t) is the datum obtained from the count made with Coulter Counter and N(0) is the number of cells at the time of treatment (0h). The cell numbers listed in the table were obtained as the average of at least three replicated samples. These replicated samples were then pooled for flow cytometric analysis.

DNA histograms were analysed on the basis of a program developed in our laboratory that uses a sum-of-gaussian method to obtain the percentages of cells in G_1, S and G_2M (figure A.1) (Ubezio, 1985). At short times after treatments, together with DNA histograms, a flow cytometric measure of DNA/BrdUrd was performed. The obtained cytogram is generally very similar to that shown in figure A.2. On this plot we drew four regions of interest and we calculated the percentage of cell in each one of these regions.

%1c+: percentage of labelled undivided cells (i.e. cells that are at the first cycle) in the upper right window (LU).

%BrdUrd+: percentage of all labelled cells, including the undivided and divided ones.

%G_1S-: percentage of unlabelled G_1 and S cells, in the lower left window.

%G_2M-: percentage of unlabeled G_2M cells, in the lower right window.

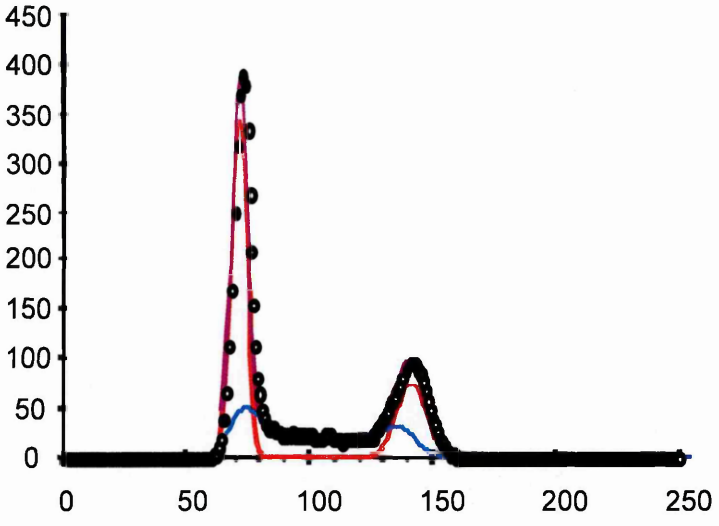

Figure A.1: Example of DNA histogram analysed as sum of gaussians. The open circles represent the experimental data, the red line represents the G_1 and G_2M gaussians and the blue line represents the S gaussians. The sum of all these contributions gives the fitting of the data (continuous line above the circles).

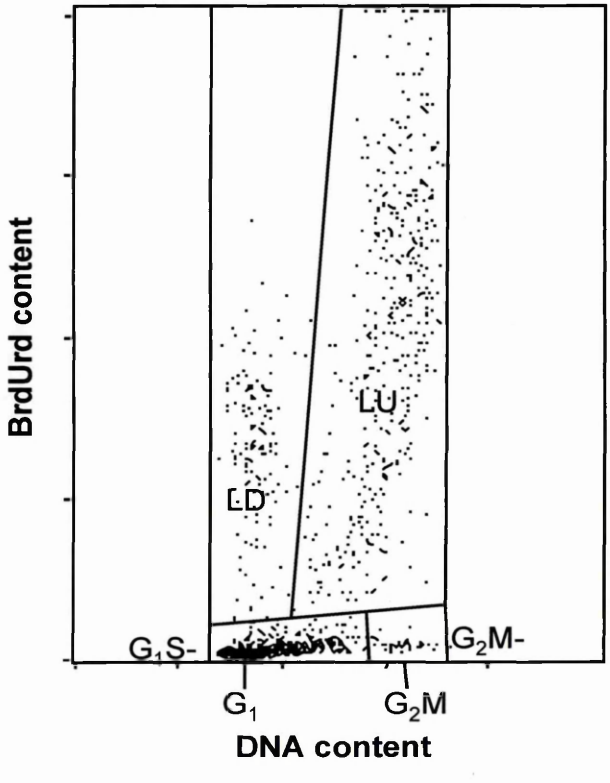

Figure A.2: Example of flow cytometric DNA/BrdUrd biparametric distribution. Four windows are set, separating labelled divided (LD), labelled undivided (LU), unlabelled G_1S (G_1S-), and unlabelled G_2M (G_2M-) cells.

The four-listed "observables" are the main quantities that can be obtained by biparametric DNA/BrdUrd distribution. The partition of the cytogram that has been chosen is probably as much robust as possible, because it exploits the gaps between BrdUrd+ and BrdUrd- cells and between divided and undivided cells to distinguish the different subpopulations. The distinction between G_2M- and G_1S-cells is also clear, at least until cells exiting G_1 arrive in G_2M phase, but, for the cell lines that have been considered during this project, the choice of performing this kind of measurement at 6h after BrdUrd labelling excludes this possibility.

In some instances additional measures of BrdUrd pulse-and-chase at 72h after treatment were performed. However, in this case, only the window of BrdUrd+ cells could be drawn because the partial overlap of BrdUrd+ cells divided several times with BrdUrd- cells renders somewhat uncertain the positioning of this window. For this reason we sometimes considered of limited precision the estimate of the percentage of BrdUrd+ cells and we decided to indicate only a range instead of a precise value. In any case the addition of this measure to the panel of the experimental data supported the exclusion or inclusion of scenarios with strong differential effects between BrdUrd+ and BrdUrd- cells.

Together with quantitative data other qualitative information was also reported. In particular we indicated with "Y" the presence of apoptotic cells, detected by TUNEL assay and the presence of debris highlighted by DNA histograms. For some samples TUNEL assay was not performed, in this case dUTP in the table was identified by "NM" (standing for "not measured").

Table A.1: Time-course of experimental data obtained treating IGROV1 cells with DDP, DXR, L-PAM, paclitaxel and TPT.

DRUG	CONCENTRATION (μM)	TIME (h)	RELATIVE NUMBER	%G_1	%S	%G_2M	%BrdUrd+	%1c+	%G_1S-	%G_2-	dUTP+	DEBRIS
DDP	0	0	1000±50	52.3	41.6	6.1						
		6	1164±40	52.7	37.0	10.0	38.0	20.0	62.0	1.0		
		24	2133±9	59.0	32.0	9.0						
		48	5212±65	56.0	35.0	9.0						
		72	9002±920	64.0	29.1	6.9						
	10	6	1130±60	51.4	34.8	13.8	37.0	24.0	64.0	1.0	NM	
		24	1390±210	52.0	29.0	19.0					NM	
		48	2960±450	60.0	30.0	9.0					NM	
		72	6480±810	57.0	35.0	8.0					NM	
	30	6	910±80	51.6	36.0	12.4	32.0	26.0	65.0	3.0	NM	
		24	1070±120	35.0	30.0	36.0					NM	
		48	1920±80	51.0	31.0	19.0					NM	
		72	2100±130	57.0	28.0	15.0					NM	
	50	6	800±60	54.4	33.9	11.7	36.0	32.0	61.0	3.0	NM	
		24	960±110	31.0	31.0	38.0					Y	Y
		48	1200±20	43.0	19.0	38.0					Y	Y
		72	840±70	46.0	36.0	18.0					Y	Y
	75	6	700±80	51.4	37.0	11.6	35.0	31.0	62.0	3.0	NM	
		24	600±150	35.0	41.0	24.0					Y	Y
		48	940±20	35.0	24.0	41.0					Y	Y
		72	680±20	39.0	32.0	29.0					Y	Y
	100	6	600±90	54.7	36.3	9.0	28.0	25.0	68.0	4.0	NM	
		24	540±40	35.0	39.0	26.0					Y	Y
		48	600±20	40.0	28.0	32.0					Y	Y
		72	490±40	32.0	36.0	32.0					Y	Y
	200	6	640±60	58.2	30.3	11.5	32.0	31.0	63.0	6.0	NM	
		24	410±40	45.0	41.0	14.0					Y	Y
		48	260±70	45.0	40.0	15.0					Y	Y
		72	300±50	42.0	38.0	20.0					Y	Y

DRUG	CONCENTRATION (μM)	TIME (h)	RELATIVE NUMBER	%G_1	%S	%G_2M	%BrdUrd+	%1c+	%G_1S-	%G_2-	dUTP+	DEBRIS
DXR	0	0	1000±27	47.5	41.3	11.2	39.7					
		6	1190±46	51.6	38.6	9.8	37.5	31.0	58.9	3.6		
		24	2204±197	50.4	38.9	10.7						
		48	4473±81									
		72	6649±1148									
	0.5	6	1080±113	44.2	38.2	17.6	40.7	34.6	56.8	2.5	NM	
		24	1800±118	59.2	32.5	8.3					NM	
		48	3805±333	55.6	33.3	11.1					NM	
		72	5990±656	56.5	29.7	13.8					NM	
	1	6	1185±45	47.1	36.2	16.7	35.8	33.0	60.6	3.6	NM	
		24	1679±86	69.5	21.9	8.6					NM	
		48	2860±99	66.4	24.5	9.1					NM	
		72	3341±897	64.0	25.4	10.6	~40				NM	
	3	6	1056±32	43.6	37.6	18.8	42.2	40.4	53.5	4.3	NM	
		24	1355±57	41.4	30.0	28.6						
		48	1722±57	57.7	27.6	14.7						
		72	2100±208	67.8	21.3	10.9						
	6	6	975±107	41.4	38.8	19.8	41.1	39.6	53.0	5.9	NM	
		24	1373±212	29.3	29.8	40.9					NM	
		48	1088±99	35.1	27.7	37.2					NM	
		72	952±80	42.2	29.5	28.3	30-50				NM	
	10	6	1009±26	36.2	45.4	18.4	39.5	37.2	51.6	5.9	NM	
		24	1255±99	31.2	25.7	43.1						
		48	1003±65	29.0	27.8	43.2						
		72	720±94	29.5	23.0	47.5					Y	
	30	6	865±19	49.1	38.7	12.2	35.9	34.1	52.3	11.8	NM	
		24	1058±129	29.7	34.7	35.6					Y	
		48	698±78	33.9	31.9	34.2					Y	
		72	567±157	37.1	30.8	32.1	30-50				Y	

DRUG	CONCENTRATION (μM)	TIME (h)	RELATIVE NUMBER	%G_1	%S	%G_2M	%BrdUrd+	%1c+	%G_1S-	%G_2-	dUTP+	DEBRIS
L-PAM	0	0	1000±119	48.5	40.4	11.1						
		6	1104±28	50.7	30.1	19.2	39.6	31.0	58.2	2.3		
		24	2325±74	47.2	40.0	12.8						
		48	5327±621	48.0	41.4	10.6						
		72	7668±226	60.8	29.1	10.1						
	3	6	1229±66	50.2	26.8	23.0	37.5	29.4	59.7	2.8	NM	
		24	2523±136	43.7	39.3	17.0					NM	
		48	4657±316	48.9	38.8	12.3					NM	
		72	8526±470	53.4	35.8	10.8					NM	
	10	6	1229±34	49.3	25.9	24.8	39.8	31.4	59.6	2.8	NM	
		24	2443±320	34.7	44.0	21.3					NM	
		48	4101±1171	43.4	41.6	15.0					NM	
		72	5113±817	53.2	34.9	11.9	>80				NM	
	30	6	1168±40	51.6	26.4	22.0	39.4	32.3	57.2	3.4	NM	
		24	1709±125	24.0	37.3	38.7					NM	
		48	1923±59	39.4	28.8	31.8					NM	Y
		72	1451±66	44.5	33.3	22.2					NM	Y
	50	6	1168±78	51.2	26.4	22.4	39.5	32.5	57.3	3.2	NM	
		24	1381±28	17.7	46.2	36.1						
		48	1322±84	17.9	33.8	48.3						Y
		72	750±11	26.2	35.6	38.2	>80				Y	Y
	100	6	1168±76	50.9	28.9	20.1	36.2	29.8	59.6	4.2	NM	
		24	1330±134	16.9	50.4	32.7						
		48	869±35	12.6	34.8	52.6					Y	Y
		72	665±97	14.4	44.1	41.5					Y	Y
	300	6	1118±130	51.5	30.8	17.7	34.9	28.9	59.8	4.2	NM	
		24	930±104	26.4	52.7	20.9					Y	
		48	611±167	25.7	49.7	24.6					Y	Y
		72	330±30	19.0	56.3	24.7	~50				Y	Y

DRUG	CONCENTRATION (μM)	TIME (h)	RELATIVE NUMBER	%G_1	%S	%G_2M	%BrdUrd+	%1c+	%G_1S-	%G_2-	dUTP+	DEBRIS
Paclitaxel	0	0	1000±54	52.4	36.3	11.3						
		6	1278±32	52.8	32.3	14.9	42.2	22.4	56.5	1.3		
		24	2084±24	54.0	31.0	15.0						
		48	4582±21	60.0	29.0	11.0						
		72	9844±35	65.0	28.0	7.0						
	0.01	6	1176±72	48.5	32.5	19.0	40.2	24.2	59.6	2.9	NM	
		24	1770±78	52.0	34.0	14.0					NM	
		48	4434±5	59.0	30.0	11.0					NM	
		72	7054±51	66.0	27.0	7.0					NM	
	0.05	6	880±174	35.8	27.7	35.5	33.2	29.7	57.8	9.1	NM	
		24	1633±30	55.0	35.0	10.0						
		48	1768±153	66.0	30.0	4.0						
		72	2125±92	60.0	33.3	7.0						Y
	0.1	6	791±34	41.1	30.7	28.2	35.1	31.6	59.8	5.1	NM	
		24	1196±104	55.0	28.0	17.0					Y	Y
		48	1158±64	49.0	38.0	13.0					Y	Y
		72	895±85	52.0	38.0	10.0					Y	Y
	0.3	6	783±55	36.3	28.3	35.4	38.8	37.0	53.3	7.9	NM	
		24	1038±32	29.0	16.0	55.0					Y	Y
		48	737±52	20.0	33.0	47.0					Y	Y
		72	564±45	21.0	41.0	38.0					Y	Y
	1	6	786±42	32.7	32.1	35.2	37.5	36.6	55.7	6.8	NM	
		24	814±85	8.0	12.0	80.0					NM	Y
		48	495±175	6.0	20.0	74.0					NM	Y
		72	571±201	18.0	21.0	61.0					NM	Y

DRUG	CONCENTRATION (μM)	TIME (h)	RELATIVE NUMBER	%G_1	%S	%G_2M	%BrdUrd+	%1c+	%G_1-	%G_2-	dUTP+	DEBRIS
TPT	0	0	1000±40	50.2	39.8	10.1	38.9	38.9	51.1	10.1		
		6	999±80	51.5	38.5	10.0	37.7	20.7	58.7	3.6		
		24	1785±54	53.4	35.6	11.0						
		48	4823±311	48.7	38.1	13.1						
		72	8580±607	78.6	12.1	9.3						
		96	9109±832	83.2	7.7	9.1						
	0.05	6	1241±172	44.7	41.4	13.9	37.9	29.2	58.1	4.0		
		24	1744±139	44.3	43.3	12.4						
		48	4771±461	44.8	41.1	14.1						
		72	7949±933	78.1	11.5	10.4						
		96	7142±661	83.3	7.3	9.4						
	0.2	6	1037±90	36.1	40.5	23.5	36.6	35.9	58.9	4.5		
		24	1509±21	47.3	38.2	14.5	35.5					
		48	3232±180	52.8	35.7	11.5	13.7					
		72	6277±676	71.5	16.7	11.8	7.8					
		96	7968±948	84.4	8.0	7.5						
	1	6	981±112	48.9	37.1	14.0	41.5	41.5	54.2	4.3		
		24	1468±180	40.9	34.2	24.9	39.1					
		48	1992±33	45.7	36.1	18.2	10.2					
		72		58.3	30.3	11.5	9.9					
		96	4548±1458	79.6	12.7	7.8						
	10	6	1011±90	46.9	37.2	16.0	48.1	48.1	47.7	4.2		
		24	1354±128	42.8	30.1	27.1	35.3					
		48	1395±145	49.5	34.2	16.3	13.8					
		72		56.6	29.6	13.8	8.7					
		96	3009±998	73.9	16.6	9.5						
	100	6	874±126	50.9	38.6	10.5	43.9	43.9	51.2	4.9		
		24	640±28	29.4	28.1	42.5	35.3					
		48	628±144	33.4	19.3	47.4	13.8					Y
		72	685±267	32.8	28.7	38.6	8.7				Y	Y
		96	782±105	36.6	30.6	32.8					Y	Y

REFERENCES

Agarwal ML, Taylor WR, Chernov MV, Chernova OB, Stark GR (1998) The p53 network. *J Biol Chem* **273:** 1-4.

A'Hern RP, Gore ME (1995) Impact of doxorubicin on survival in advanced ovarian cancer. *J Clin Oncol* **13:** 726-732.

Albert R (2005) Scale-free networks in cell biology. *J Cell Sci* **118:** 4947-4957.

Amundson SA, Myers TG and Fornace AJ (1998) Roles for P53 in growth arrest and apoptosis: Putting on the brakes after genotoxic stress. *Oncogene* **17:** 3287-3299.

Anderson AR, Chaplain MA (1998) Continuous and discrete mathematical models of tumor-induced angiogenesis. *Bull Math Biol* **60:** 857-899.

Arcamone F, Franceschi G, Penco S, Selva A (1969) Adriamycin (14-hydroxydaunomycin), a novel antitumor antibiotic. *Tetrahedron Lett* **13:** 1007-1010.

Arellano M, Moreno S (1997) Regulation of CDK/cyclin complexes during the cell cycle. *Int J Biochem Cell Biol* **29:** 559-573.

Armitage P, Doll R (1954) The age distribution of cancer and a multi-stage theory of carcinogenesis. *Br J Cancer* **8:** 1-12.

Armitage P, Doll R (1957) A two-stage theory of carcinogenesis in relation to the age distribution of human cancer. *Br J Cancer* **11:** 161-169.

Assoian RK, Zhu X (1997) Cell anchorage and the cytoskeleton as partners in growth factor dependent cell cycle progression. *Curr Opin Cell Biol* **9:** 93-98.

Attardi LD, de Vries A, Jacks T (2004) Activation of the p53-dependent G1 checkpoint response in mouse embryo fibroblasts depends on the specific DNA damage inducer. *Oncogene* **23:** 973-980.

Bachur NR, Gordon SL, Gee MV (1977) Anthracycline antibiotic augmentation of microsomal electron transport and free radical formation. *Mol Pharmacol* **13:** 901-910.

Bachur NR, Gordon SL, Gee MV (1978) A general mechanism for microsomal activation of quinone anticancer agents. *Cancer Res* **38:** 1745-1750.

Balint E, Vousden KH (2001) Activation and activities of the p53 tumour suppressor protein. *Br J Cancer* **85:** 1813-1823.

Bao S, Tibbetts RS, Brumbaugh KM, Fang Y, Richardson DA, Ali A, Chen SM, Abraham RT, Wang XF (2001) ATR/ATM-mediated phosphorylation of human Rad17 is required for genotoxic stress responses. *Nature* **411:** 969-974.

Barlogie B, Drewinko B (1977) Lethal and kinetic response of cultured human lymphoid cells to melphalan. *Cancer Treat Rep* **61:** 425-436.

Barranco SC, Gerner EW, Burk KH, Humphrey RM (1973) Survival and cell kinetics effects of adriamycin on mammalian cells. *Cancer Res* **33:** 11-16.

Bartek J, Lukas J (2001) Pathways governing G1/S transition and their response to DNA damage. *FEBS Letters* **490:** 117-122.

Bartkowiak D, Hemmer J, Röttinger E (1992) Dose dependence of the cytokinetic and cytotoxic effects of epirubicin in vitro. *Cancer Chemother and Pharmacol* **30:** 189-192.

Basse B, Baguley BC, Marshall ES, Joseph WR, van Brunt B, Wake G, Wall DJ (2003) A mathematical model for analysis of the cell cycle in cell lines derived from human tumors. *J Math Biol* **47:** 295-312.

Bates DA, Winterbourn CC (1982) Deoxyribose breakdown by the adriamycin semiquinone and H2O2: Evidence for hydroxyl radical participation. *FEBS Lett* **145:** 137-142.

Bellamy CO (1997) p53 and apoptosis. *Br Med Bull* **53:** 522-538.

Bellamy WT (1992) Prediction of response to drug therapy of cancer. A review of *in vitro* assays. *Drugs* **44:** 690-708.

Bellarosa D, Ciucci A, Bullo A, Nardelli F, Manzini S, Maggi CA, Goso C (2001) Apoptotic events in a human ovarian cancer cell line exposed to anthracyclines. *J Pharmacol Exp Ther* **296:** 276-283.

Benard J, Da Silva J, De Blois MC, Boyer P, Duvillard P, Chiric E, Riou G (1985) Characterization of a human ovarian adenocarcinoma line, IGROV1, in tissue culture and in nude mice. *Cancer Res* **45:** 4970-4979.

Benchekroun MN, Sinha BK, Robert J (1993) Doxorubicin-induced oxygen free radical formation in sensitive and doxorubicin-resistant variants of rat glioblastoma cell lines. *FEBS Lett* **326:** 302-305.

Benjamin RS, Riggs CE and Bachur NR (1973) Pharmacokinetics and metabolism of adriamycin in man. *Clin Pahrmacol Ther* **14:** 592-600.

Bergel F, Stock JA (1954) Cyto-active amino-acid and peptide derivatives. Part I. Substituted phenylalanines. *J Chem Soc* 2409-2417.

Berlin V, Haseltine WA (1981) Reduction of adriamycin to a semiquinone free radical by NADPH cytochrome P-450 reductase produces DNA cleavage in a reaction mediated by molecular oxygen. *J Biol Chem* **256:** 4747-4756.

Bertuzzi A, Gandolfi A, Giovenco MA (1981) Mathematical models of the cell cycle with a view to tumor studies. *Math Biosci* **53:** 159-188.

Bertuzzi A, Gandolfi A, Sinisgalli C, Iacoviello D (1997) Steel's potential doubling time and its estimation in cell populations affected by nonuniform cell loss. *Math Biosci* **143:** 61-89.

Bhuyan BK, Scheidt LG, Fraser TJ (1972) Cell cycle phase specificity of antitumor agents. *Cancer Res* **32:** 398-407.

Bignami M, Casorelli I, Karran P (2003) Mismatch repair and response to DNA-damaging antitumour therapies. *Eur J Cancer* **39:** 2142-2149.

Bilim V, Kawasaki T, Takahashi K, Tomita Y (2000) Adriamycin induced G_2/M cell cycle arrest in transitional cell cancer cells with wt p53 and p21(WAF1/CIP1) genes. *J Exp Clin Cancer Res* **19:** 483-488.

Bird JJ, Brown DR, Mullen AC, Moskowitz NH, Mahowald MA, Sider JR, Gajewski TF, Wang CR, Reiner SL (1998) Helper T cell differentiation is controlled by the cell cycle. *Immunity* **9:** 229-237.

Bjornsti MA, Knab AM, Benedetti P (1994) Yeast Saccharomyces cerevisiae as a model system to study the cytotoxic activity of the antitumor drug camptothecin. *Cancer Chemother Pharmacol* **34** Suppl: S1-5.

Black SM, Wolf CR (1991) The role of glutathione-dependent enzymes in drug resistance. *Pharmacol Ther* **51:** 139-154.

Blandino G, Levine AJ, Oren M (1999) Mutant p 53 gain of function: differential effects of different p53 mutants on resistance of cultured cells to chemotherapy. *Oncogene* **18:** 477-485.

Bradley G, Juranka PF, Ling V (1988) Mechanisms of multidrug resistance. *Biochim Biophys Acta* **948:** 87-128.

Brattain MG, Fine WD, Khaled FM, Thompson J, Brattain DE (1981) Heterogeneity of malignant cells from a human colonic carcinoma. *Cancer Res* **41:** 1751-1756.

Breward CJ, Byrne HM, Lewis CE (2003) A multiphase model describing vascular tumour growth. *Bull Math Biol* **65:** 609-640.

Brodovsky HS, Bauer M, Horton J, Elson PJ (1984) Comparison of melphalan with cyclophosphamide, methotrexate and 5-fluorouracil in patients with ovarian cancer. *Cancer* **53:** 844-852.

Brown R, Clugston C, Burns P, Edlin A, Vasey P, Vojtesek B, Kaye SB (1993) Increased accumulation of p53 protein in cisplatin-resistant ovarian cell lines. *Int J Cancer* **55:** 678-684.

Brox LW, Gowans B, Belch A (1980) L-phenylalanine mustard (melphalan) uptake and cross-linking in the RPMI 6410 human lymphoblastoid cell line. *Cancer Res* **40:** 1169-1172.

Brozovic A, Fritz G, Christmann M, Zisowsky J, Jaehde U, Osmak M, Kaina B (2004) Long-term activation of SAPK/JNK, P38 kinase and FAS-L expression by cisplatin is attenuated in human carcinoma cells that acquired drug resistance. *Int J Cancer* **112:** 974-985.

Brugarolas J, Moberg K, Boyd SD, Taya Y, Jacks T, Lees AJ (1999) Inhibition of cyclin-dependent kinase 2 by p21 is necessary for retinoblastoma protein-mediated G_1 arrest after gamma-irradiation. *Proc Natl Acad Sci USA* **96:** 1002-1007.

Buchkovich K, Duffy LA, Harlow E (1989) The retinoblastoma protein is phosphorylated during specific phases of the cell cycle. *Cell* **58:** 1097-1105.

Bunz F, Dutriaux A, Lengauer C, Waldman T, Zhou S, Brown JP, Sedivy JM, Kinzler KW, Vogelstein B (1998) Requirement for p53 and p21 to sustain G_2 arrest after DNA damage. *Science* **282:** 1497-1501.

Bunz F, Hwang PM, Torrance C, Waldman T, Zhang Y, Dillehay L, Williams J, Lengauer C, Kinzler KW, Vogelstein B (1999) Disruption of p53 in human cancer cells alters the responses to therapeutic agents. *J Clin Invest* **104:** 263-269.

Bustamante J, Galleano M, Medrano EE, Boveris A (1990) Adriamycin effects on hydroperoxide metabolism and growth of human breast tumor cells. *Breast Cancer Res Treat* **17:** 145-153.

Byrne H, Preziosi L (2003) Modelling solid tumour growth using the theory of mixtures. *Math Med Biol* **20:** 341-366.

Caporali S, Falcinelli S, Starace G, Russo MT, Bonmassar E, Jiricny J, D'Atri S (2004) DNA damage induced by temozolomide signals to both ATM and ATR: role of the mistmatch repair system. *Mol Pharmacol* **66:** 478-491.

Capranico G, Riva A, Tinelli S, Dasdia T, Zunino F (1987) Markedly reduced levels of anthracycline-induced DNA strand breaks in resistant P388 leukemia cells and isolated nuclei. *Cancer Res* **47:** 3752-3756.

Carmichael J, DeGraff WG, Gazdar AF, Minna JD, Mitchell JB (1987) Evaluation of a tetrazolium-based semiautomated colorimetric assay: assessment of radiosensitivity. *Cancer Res* **47:** 943-946.

Carr AM (2000) Cell cycle. Piecing together the p53 puzzle. *Science* **287:** 1765-1766.

Carrassa L, Broggini M, Erba E, Damia G (2004) Chk1 but not Chk2, is Involved in the Cellular Response to DNA Damaging Agents: Differential Activity in Cells Expressing or not p53. *Cell Cycle* **3:** 1177-1181.

Chabner BA, Roberts TG Jr (2005) Timeline: Chemotherapy and the war on cancer. *Nat Rev Cancer* **5:** 65-72.

Chang S, Khoo C, DePinho RA (2001) Modeling chromosomal instability and epithelial carcinogenesis in the telomerase-deficient mouse. *Semin Cancer Biol* **11:** 227-239.

Chaplain M, Anderson A (2004) Mathematical modelling of tumour-induced angiogenesis: network growth and structure. *Cancer Treat Res* **117:** 51-75.

Chaturvedi P, Eng WK, Zhu Y, Mattern MR, Mishra R, Hurle MR, Zang X, Annan RS, Lu Q, Faucette LF, Scott GF, Li X, Carr SA, Johnson RK, Winkler JD, Zhou BB (1999) Mammalian Chk2 is a downstream effector of the ATM-dependent DNA damage checkpoint pathway. *Oncogene* **18:** 4047-4054.

Chiorino G, Metz JA, Tomasoni D, Ubezio P (2001) Desynchronization rate in cell populations: mathematical modeling and experimental data. *J Theor Biol* **208:** 185-199.

Chu E, DeVita VT (1997) Principles of cancer management: chemotherapy. In: Cancer: principles and practice of oncology 6th edition. DeVita VT, Hellman S, Rosenberg SA (eds.), JB Lippincott, Philadelphia 17: 289-306.

Clarkson JM, Mitchell DL (1981) The importance of DNA damage and repair in the cell cycle sensitivity of CHO cells to nitrogen mustard. *Radiat Res* **88:** 587-596.

Cliby WA, Lewis KA, Lilly KK, Kaufmann SH (2002) S phase and G_2 arrest induced by topoisomerase I poisons are dependent on ATR kinase function. *J Biol Chem* **277:** 1599-1606.

Cook JA, Mitchell JB (1989) Viability measurements in mammalian cell systems. *Anal Biochem* **179:** 1-7.

Cooper MA, Bush JE, Fehniger TA, VanDeusen JB, Waite RE, Liu Y, Aguila HL, Caligiuri MA (2002) In vivo evidence for a dependence on interleukin 15 for survival of natural killer cells. *Blood* **100:** 3633-3638.

Costanzo V, Robertson K, Ying CY, Kim E, Avvedimento E, Gottesman M, Grieco D, Gautier J (2000) Reconstitution of an ATM-dependent checkpoint that inhibits chromosomal DNA replication following DNA damage. *Mol Cell* **6:** 649-659.

Crissman HA, Darzynkiewicz Z, Tobey RA, Steinkamp JA (1985) Normal and perturbed Chinese hamster ovary cells: correlation of DNA, RNA, and protein content by flow cytometry. *J Cell Biol* **101:** 141-147.

Cullinane C, Phillips DR (1990) Induction of stable transcriptional blockage sites by adriamycin: GpC specificity of apparent adriamycin-DNA adducts and dependence on iron(III) ions. *Biochemistry* **29:** 5638-5646.

De Leo AB, Jay G, Appella E, Dubois GC, Law LW, Old LJ (1979) Detection of a transformation-related antigen in chemically induced sarcomas and other transformed cells of the mouse. *Proc Natl Acad Sci USA* **76:** 2420-2424.

De Vita VT, Hellman S, Rosenberg SA (2001). Principles and Practice of Oncology, Ed. 6. Lippincott Williams and Wilkins, Philadelphia.

Dean SW, Fox M (1983) Investigation of the cell cycle response of normal and Fanconi's anaemia fibroblasts to nitrogen mustard using flow cytometry. *J Cell Sci* **64:** 265-279.

Di Marco A, Gaetani M, Scarpinato B (1969) Adriamycin (NSC-123,127): a new antibiotic with antitumor activity. *Cancer Chemother Rep* **53:** 33-37.

Di Marco A, Silverstrini R, Di Marco D, Dasdia T (1965) Inhibiting effect of the new cytotoxic antibiotic daunomycin on nucleic acids and mitotic activity of HeLa cells. *J Cell Biol* **27:** 545-550.

D'Incalci M, Szmigiero L, Erickson LC, Hartley JA, Kohn KW (1985) A filter incubation method for the determination of potentially crosslinkable sites in DNA in mammalian cells. *Anal Biochem* **150:** 161-165.

Dole M, Nunez G, Merchant AK, Maybaum J, Rode CK, Bloch CA, Castle VP (1994) Bcl-2 inhibits chemotherapy-induced apoptosis in neuroblastoma. *Cancer Res* **54:** 3253-3259.

Drewinko B, Barlogie B (1976) Age-dependent survival and cell-cycle progression of cultured cells exposed to chemotherapeutic drugs. *Cancer Treat Rep* **60:** 1707-1717.

Drewinko B, Gottlieb JA (1973) Survival kinetics of cultured lymphoma cells exposed to adriamycin. *Cancer Res* **33:** 1141-1146.

Druker BJ, Tamura S, Buchdunger E, Ohno S, Segal GM, Fanning S, Zimmermann J, Lydon NB (1996) Effects of a selective inhibitor of the Abl tyrosine kinase on the growth of Bcr-Abl positive cells. *Nat Med* **2:** 561-566.

Ducore JM, Erickson LC, Zwelling LA, Laurent G, Kohn KW (1982) Comparative studies of DNA cross-linking and cytotoxicity in Burkitt's lymphoma cell lines treated with cis-diamminedichloroplatinum(II) and L-phenylalanine mustard. *Cancer Res* **42:** 897-902.

Dumitriu IE, Mohr W, Kolowos W, Kern P, Kalden JR, Herrmann M (2001) 5,6-carboxyfluorescein diacetate succinimidyl ester-labeled apoptotic and necrotic as well as detergent-treated cells can be traced in composite cell samples. *Anal Biochem* **299:** 247-52.

Durham JP, Ives DH (1969) Deoxycytidine kinase I. Distribution in normal and neoplastic tissue and interrelationship of deoxycytidine and 1-β-D-arabinofuranosylcytosine phosphorilation. *Molec Pharmac* **5:** 358-375.

Dusre L, Mimnaugh EG, Myers CE, Sinha BK (1989) Potentiation of doxorubicin cytotoxicity by buthionine sulfoximine in multidrug-resistant human breast tumor cells. *Cancer Res* **49:** 511-515.

Eastman A (1987) Cross-linking of glutathione to DNA by cancer chemotherapeutic platinum coordination complexes. *Chem Biol Interact* **61:** 241-248.

Easton J, Wei T, Lahti JM, Kidd VJ (1998) Disruption of the cyclin D/cyclin-dependent kinase/INK4/retinoblastoma protein regulatory pathway in human neuroblastoma. *Cancer Res* **58:** 2624-2632.

Eckardt J, Eckhardt G, Villalona-Calero M, Drengler R, Von Hoff D (1995) New anticancer agents in clinical development. *Oncology* **9:** 1321-1334.

Einhorn LH (1986) Have new aggressive chemotherapy regimens improved results in advanced germ cell tumors? *Eur J Cancer Clin Oncol* **22:** 1289-1293.

El Deiry WS (1998) Regulation of p53 downstream genes. *Semin Cancer Biol* **8:** 345-357.

El Deiry WS, Tokino T, Velculescu VE, Levy DB, Parsons R, Trent JM, Lin D, Mercer WE, Kinzler KW, Vogelstein B (1993) WAF1, a potential mediator of p53 tumor suppression. *Cell* **75:** 817-825.

El-Rayes BF, Lo Russo PM (2004) Targeting the epidermal growth factor receptor. *Br J Cancer* **91:** 418-424.

Eliopoulos AG, Kerr DJ, Herod J, Hodgkins L, Krajewski S, Reed JC, Young LS (1995) The control of apoptosis and drug resistance in ovarian cancer: influence of p53 and Bcl-2. *Oncogene* **11:** 1217-1228.

Eliot H, Gianni L, Myers C (1984) Oxidative destruction of DNA by the adriamycin–iron complex. *Biochemistry* **23:** 928-936.

Erba E, Mascellani E, Pifferi A, D'Incalci M (1995) Comparison of cell-cycle phase perturbations induced by the DNA-minor-groove alkylator tallimustine and by melphalan in the SW626 cell line. *Int J Cancer* **62:** 170-175.

Erickson LC, Osieka R, Kohn KW (1978) Differential repair of 1-(2-chloroethyl)-3-(4-methylcyclohexyl)-1-nitrosourea-induced DNA damage in two human colon tumour cell lines. *Cancer Res* **38:** 802-808.

Errington RJ, Ameer-beg SM, Vojnovic B, Patterson LH, Zloh M, Smith PJ (2005) Advanced microscopy solutions for monitoring the kinetics and dynamics of drug-DNA targeting in living cells. *Adv Drug Deliver Rev* **57:** 153-167.

Evans ND, Errington RJ, Shelley M, Feeney GP, Chapman MJ, Godfrey KR, Smith PJ, Chappell MJ (2004) A mathematical model for the in vitro kinetics of the anti-cancer agent topotecan. *Math Biosci* **189:** 185-217.

Evans T, Rosenthal ET, Youngblom J, Distel D, Hunt T (1983) Cyclin: a protein specified by maternal mRNA in sea urchin eggs that is destroyed at each cleavage division. *Cell* **33:** 389-396.

Falck J, Mailand N, Syljuasen RG, Bartek J, Lukas J (2001) The ATM-Chk2-Cdc25A checkpoint pathway guards against radioresistant DNA synthesis. *Nature* **410:** 842-847.

Falck J, Petrini JHJ, Williams BR, Lukas J, Bartek J (2002) The DNA damage-dependent intra-S phase checkpoint is regulated by parallel pathways. *Nature Genetics* **30:** 290-294.

Fan S, El-Deiry S, Bae I, Freeman J, Jondle D, Bhatia K, Fornace AJ, magrath I, Kohn KW, O'Connor PM (1994) *p53* gene mutations are associated with decreased sensitivity of human lymphoma cells to DNA-damaging agents. *Cancer Res* **54:** 5824-5830.

Fan S, Smith ML, Rivet DJ, Duba D, Zhan Q, Kohn KW, O'Connor AJPM (1995) Disruption of p53 function sensitizes breats cancer MCF-7 cells to cispaltin and pentoxifyliine. *Cancer Res* **55:** 1649-1654.

Fanning J, Bennet TZ, Hilgers RD (1992) Meta-analysis of cisplatin, doxorubicin, and cyclophosphamide versus cisplatin and cyclophosphamide chemotherapy of ovarian cancer. *Obstet Gynecol* **80:** 954-969.

Farber S, Diamond LK, Mercer RD, Sylvester RRF, Wolff JA (1948) Temporary remissions in acute leukemia in children produced by folic antagonist, 4-aminopteroylglutamic acid (aminopterin). *N Engl J Med* **138:** 787-793.

Fazekas de St Groth B, Smith AL, Koh WP, Girgis L, Cook MC, Bertolino P (1999) Carboxyfluorescein diacetate succinimidyl ester and the virgin lymphocytes: a marriage made in haeven. *Immunol Cell Biol* **77:** 530-538.

Feeney GP, Errington RJ, Wiltshire M, Marquez N, Chappell SC, Smith PJ (2003) Tracking the cell cycle origins for escape from topotecan action by breast cancer cells. *Br J Cancer* **88:** 1310-1317.

Fichtinger-Schepman AMJ, van der Veer JL, den Hertog JHJ, Lohman PHM, Reedijk J (1985) Adducts of the antitumor drug cis-diamminedichloroplatinum(II) with DNA: formation, identification and quantitation. *Biochemistry* **24:** 707-713.

Fink D, Nebel S, Aebi S, Zheng H, Cenni B, Nehmè A, Christen RD, Howell SB (1996) The role of DNA mismatch repair in platinum drug resistance. *Cancer Res* **56:** 4881-4886.

Fink D, Zheng H, Nebel S, Norris PS, Aebi S, Lin TP, Nehmè A, Christen RD, Haas M, MacLeod CI, Howell SB (1997) *In vitro* and *in vivo* resistance to cisplatin in cells that have lost DNA mismatch repair. *Cancer Res* **57:** 1841-1845.

Fishel R, Lescoe MK, Rao MRS, Copeland NG, jenkins NA, Garber J, Kane M, Kolodner R (1993) The human mutator gene homolog MSH2 and its association with hereditary nonpolyposis colon cancer. *Cell* **75:** 1027-1038.

Fisher JC (1958) Multiple-mutation theory of carcinogenesis. *Nature* **181:** 651-652.

Fisher JM, Naujokaitis AS, Uehara Y, Rabinovitz M (1983) Evidence for a membrane sulphydryl associated with resistance to melphalan in a murine L1210 leukemia line. *Biochem Biophys Res Commun* **117:** 670-676.

Franks SJ, Byrne HM, King JR, Underwood JC, Lewis CE (2003) Modelling the early growth of ductal carcinoma in situ of the breast. *J Math Biol* **47:** 424-452.

Frasci G, Nicolella G, Comella P, Carreca I, DeCataldis G, Muci D, Brunetti C, Natale M, Piantedosi F, Russo A, Palmeri S, Comella G, Panza N (2001) A weekly regimen of cisplatin, paclitaxel and topotecan with granulocyte-colony stimulating factor support for patients with extensive disease small cell lung cancer: a phase II study. *Br J Cancer* **84:** 1166-1171.

Frasci G, Panza N, Comella P, Carteni G, Guida T, Nicolella GP, Natale M, Lombardi R, Apicella A, Pacilio C, Gravina A, Lapenta L, Comella G (1999) Cisplatin-topotecan-paclitaxel weekly administration with G-CSF support for ovarian and small-cell lung cancer patients: a dose-finding study. *Ann Oncol* **10:** 355-358.

Frei E (1972) Combination cancer therapy. *Cancer Res* **32:** 2593-2607.

Frei E (1985) Curative cancer chemotherapy. *Cancer Res* **45:** 6523-6537.

Galmarini CM, Mackey JR, Dumontet C (2002) Nucleoside analogues and nucleobases in cancer treatment. *Lancet Oncol* **3:** 415-424.

Gett AV, Hodgkin PD (1998) Cell division regulates the T cell cytokine repertoire, revealing a mechanism underlying immune class regulation. *Proc Natl Acad Sci USA* **95:** 9488-9493.

Gett AV, Hodgkin PD (2000) A cellular calculus for signal integration by T cells. *Nature Immunol* **1:** 239-244.

Gewirtz DA (1999) A critical evaluation of the mechanisms of action proposed for the antitumor effects of the anthracycline antibiotics adriamycin and daunorubicin. *Biochem Pharmacol* **57:** 727-741.

Gianni L, Sessa C, Capri G, Grasselli G, Spataro V, Bonadonna G (1999) Farmaci chemioterapici distruzione e resistenza. In: Medicina oncologica, Ed. 6. Bonadonna G and Robustelli della Cuna G (eds.), Masson, Milano 31: 535.

Gilman A (1963) The initial clinical trial of nitrogen mustard. *Am J Surg* **105:** 574-578.

Gilman A, Phillips FS (1946) The biological actions and therapeutic applications of β-chloroethyl amines and sulfides. *Science* **103:** 409-415.

Girard F, Strausfeld U, Fernandez A, Lamb NJ (1991) Cyclin A is required for the onset of DNA replication in mammalian fibroblasts. *Cell* **67:** 1169-1179.

Givan AL, Fisher JL, Waugh M, Ernstoff MS, Wallace PK (1999) A flow cytometric method to estimate the precursor frequencies of cells proliferating in response to specific antigens. *J Immunol Methods* **230:** 99-112. Erratum in *J Immunol Methods* 237: 207 (1999).

Goldie JH, Coldman AJ (1979) A mathematical model for relating the drug sensitivity of tumors to their spontaneous mutation rate. *Cancer Treat Rep* **63:** 1727-1733.

Goldie JH, Coldman AJ (1983) Quantitative model for multiple levels of drug resistance in clinical tumors. *Cancer Treat Rep* **67:** 923-931.

Goldie JH, Coldman AJ (1985) A model for tumor response to chemotherapy: an integration of the stem cell and somatic mutation hypotheses. *Cancer Invest* **3:** 553-564.

Gong J, Li X, Darzynkiewicz Z (1993) Different patterns of apoptosis of HL-60 induced by cyclohexamide and camptothecin. *J Cell Physiol* **157:** 263-270.

Grant DF, Bessho T, Reardon JT (1998) Nucleotide excision repair of melphalan monoadducts. *Cancer Res* **58:** 5196-5200.

Green DR, Reed JC (1998) Mitochondria and apoptosis. *Science* **281:** 1309-1312.

Greenblatt MS, Bennett WP, Hollstein M, Harris CC (1994) Mutations in the p53 tumor suppressor gene: clues to cancer etiology and molecular pathogenesis. *Cancer Res* **54:** 4855-4878.

Griffin-Green EA, Zaleska MM, Erecinska M (1988) Adriamycin-induced lipid peroxidation in mitochondria and microsomes. *Biochem Pharmacol* **37:** 3071-3077.

Guo CY, D'Anna JA, Li R, Larner JM (1999) The radiation-induced S-phase checkpoint is independent of CDKN1A. *Radiat Res* **151:** 125-132.

Hall M, Peters G (1996) Genetic alterations of cyclins, cyclin-dependent kinases, and Cdk inhibitors in human cancer. *Adv Cancer Res* **68:** 67-108.

Hammond EM, Denko NC, Dorie MJ, Abraham RT, Giaccia AJ (2002) Hypoxia links ATR and p53 through replication arrest. *Mol Cell Biol* **22:** 1834-1843.

Hansson J, Lewensohn R, Ringborg U, Nilsson B (1987) Formation and removal of DNA cross-links induced by melphalan and nitrogen mustard in relation to drug-induced cytotoxicity in human melanoma cells. *Cancer Res* **47:** 2631-2637.

Hartwell LH, Weinert TA (1989) Checkpoints: controls that ensure the order of cell cycle events. *Science* **246:** 629-634.

Hasan J, Jayson GC (2003) Oral melphalan as a treatment for platinum-resistant ovarian cancer. *Br J Cancer* **88:** 1828-1830.

Hasbold J, Gett AV, Rush JS Deenick E, Avery D, Jun J, Hodgkin PD (1999) Quantitative analysis of lymphocyte diffrentiation and proliferation in vitro using carboxyfluorescein succinimidyl ester. *Immunol Cell Biol* **77:** 516-522.

Hasbold J, Lyons AB, Kehry MR, Hodgkin PD (1998) Cell division number regulates IgG1 and IgE switching of B cells following stimulation by CD40 ligand and IL-4. *Eur J Immunol* **28:** 1040-1051.

Hawkins DS, Demers GW, Galloway DA (1996) Inactivation of p53 enhances sensitivity to multiple chemotherapeutic agents. *Cancer Res* **56:** 892-898.

Herod JJ, Eliopoulus AG, Warwick J, Niedobitek G, Young LS, Kerr DJ (1996) The prognostic significance of Bcl-2 and p53 expression in ovarian carcinoma. *Cancer Res* **56:** 2178-2184.

Héron JF (1998) Topotecan: an oncologist's view. *Oncologist* **3:** 390-402.

Hinds PW, Mittnacht S, Dulic V, Arnold A, Reed SI, Weinberg RA (1992) Regulation of retinoblastoma protein functions by ectopic expression of human cyclins. *Cell* **70:** 993-1006.

Hirose Y, Berger MS, Pieper RO (2001) p53 affects both the duration of G_2/M arrest and the fate of temozolomide-treated human glioblastoma cells. *Cancer Res* **61:** 1957-1963.

Hochster H, Wadler S, Runowicz C, Liebes L, Cohen H, Wallach R, Sorich J, Taubes B, Speyer J (1999) Activity and pharmacodynamics of 21-Day topotecan infusion in patients with ovarian cancer previously treated with platinum-based chemotherapy. New York Gynecologic Oncology Group. *J Clin Oncol* **17:** 2553-2561.

Hodgkin PD, Lee JH, Lyons AB (1996) B cell differentiation and isotype switching is related to division cycle number. *J Exp Med* **184:** 277-281.

Hoeijmakers JH (2001) Genome maintenance mechanisms for preventing cancer. *Nature* **411:** 366-374.

Hollstein M, Sidransky D, Vogelstein B and Harris CC (1991) p53 mutations in human cancers. *Science (Wash DC)* **253:** 49-53.

Holm C, Covey D, Kerrigan KW, Pommier Y (1991) DNA topoisomerases in cancer. In Pomesil M and Kohn K (eds). Oxford University Press, New York, pp. 161-171.

Holm C, Covey J, Kerrigan D, Pommier Y (1989) Differential requirement of DNA replication for the cytotoxicity of DNA topoisomerase I and II inhibitors in Chinese hamster DC3F cells. *Cancer Res* **49:** 6365-6368.

Holtz MS, Slovak ML, Zhang F, Sawyers CL, Forman SJ, Bhatia R (2002) Imatinib mesylate (STI571) inhibits growth of primitive malignant progenitors in chronic myelogenous leukemia through reversal of abnormally incresed proliferation. *Blood* **99:** 3792-3800.

Horwitz SB (1975) Antibiotics In: Mechanism of action of antimicrobial and antitumor agents. Corcoran W and Hahn FE (eds), Springer Verlag, NY, Vol III: 48-75.

Horwitz SB, Horwitz MS (1973) Effects of camptothecin on the breakage and repair of DNA during the cell cycle. *Cancer Res* **33:** 2834-2836.

Howard A and Pelc SR (1953) Synthesis of DNA in normal and irradiated cells and its relation to chromosome breakage. *Heredity* **6:** 261-273.

Hsiang YH, HErtzberg R, Hecht S, Liu LF (1985) Camptothecin induces protein-linked DNA breaks via mammalian DNA topoisomerase I. *J Biol Chem* **260:** 14873-14878.

Hsiang YH, Lihou MG, Liu LF (1989) Arrest of replication forks by drug-stabilized topoisomerase I-DNA cleavable complexes as a mechanism of cell killing by camptothecin. *Cancer Res* **49:** 5077-5082.

Hurley LH (2002) DNA and its associated processes as targets for cancer therapy. *Nat Rev Cancer* **2:** 188-200.

Iida H, Towatari M, Tanimoto M, Morishita Y, Kodera Y, Saito H (1997) Overexpression of cyclin E in acute myelogenous leukemia. *Blood* **90:** 3707-3713.

Iliakis G, Wang Y, Guan J, Wang H (2003) DNA damage checkpoint control in cells exposed to ionizing radiation. *Oncogene* **22:** 5834-5847.

Innocente SA, Abrahamson JLA, Cogswell JP, Lee JM (1999) p53 regulates a G_2 checkpoint through cyclin B1. *Proc Natl Acad Sci USA* **96:** 2147-2152.

Ishikawa T, Ali-Osman F (1993) Glutathione-associated *cis*-diamminedichloroplatinum(II) metabolism and ATP-dependent efflux from leukemia cells. Molecular characterization of glutathione-platinum complex and its biological significance. *J Biol Chem* **268:** 20116-20125.

Jeffers JR, Parganas E, Lee Y, Yang C, Wang J, Brennan J, MacLean KH, Han J, Chittenden T, Ihle JN, McKinnon PJ, Cleveland JL, Zambetti GP (2003) Puma is an essential mediator of p53-dependent and -independent apoptotic pathways. *Cancer Cell* **4:** 321-328.

Ji C, Marnett LJ, Pietenpol JA (1997) Cell cycle re-entry following chemically-induced cell cycle synchronization leads to elevated p53 and p21 protein levels. *Oncogene* **15:** 2749-2753.

Johnson TM, Yu Z-X, Ferrans VJ, Lowenstein RA, Finkel T (1996) Reactive oxygen species are downstream mediators of p53-dendent apoptosis. *Proc Natl Acad Sci USA* **93:** 11848-11852.

Kamb A (2005) What's wrong with our cancer models? *Nat Rev Drug Discov* **4:** 161-165.

Kartalou M, Essigmann JM (2001) Mechanisms of resistance to cisplatin. *Mutat Res* **478:** 23-43.

Kastan MB, Onyekwere O, Sidransky D, Vogelstein B, Craig RW (1991) Participation of p53 protein in the cellular response to DNA damage. *Cancer Res* **51:** 6304-6311.

Kato J, Matsushime H, Hiebert SW, Ewen ME, Sherr CJ (1993) Direct binding of cyclin D to the retinoblastoma gene product (pRb) and pRb phosphorylation by the cyclin D-dependent kinase CDK4. *Genes Dev* **7:** 331-342.

Keepers YP, Pizao PE, Peters GJ, van Ark-Otte J, Winograd B, Pinedo HM (1991) Comparison of the sulforhodamine B protein and tetrazolium (MTT) assays for in vitro chemosensitivity testing. *Eur J Cancer* **27:** 897-900. Erratum in: Eur J Cancer 27: 1717.

Kerre TC, De Smet G, De Smedt M, Offner F, De Bosscher J, Plum J, Vandekerckhove B (2001) Both CD34+38+ and CD34+38- cells home specifically to the bone marrow of NOD/LtSZ scid/scid mice but show different kinetics in expansion. *J Immunol* **167:** 3692-3698.

Keyomarsi K, Conte D Jr, Toyofuku W, Fox MP (1995) Deregulation of cyclin E in breast cancer. *Oncogene* **11:** 941-950.

Kharasch ED, Novak RF (1983) Inhibitory effects of anthracenedione antineoplastic agents on hepatic and cardiac lipid peroxidation. *J Pharmacol Exp Ther* **226:** 500-506.

Khil LY, Kim JY, Yoon JB, Kim JM, Keum WK, Kim ST, Yoon Y, Yoon MY, Moon CK, Lee JH, Ha J, Kim SS, Kang I (1997) Insulin has a limited effect on the cell cycle progression in 3T3 L1 fibroblasts. *Mol Cells* **7:** 742-748.

Kim SH, Kim JH (1972) Lethal effects of adriamycin on the division cycle of HeLa cells. *Cancer Res* **32:** 323-325.

Kimler BF, Cheng CC (1982) Comparison of the effects of dihydroxyanthraquinone and adriamycin on the survival of cultured Chinese hamster cells. *Cancer Res* **42:** 3631-3636.

King RW, Jackson PK, Kirschner MW (1994) Mitosis in transition. *Cell* **79:** 563-571.

Kingsbury WD, Boehm JC, Jakas DR, Holden KG, Hecht SM, Gallagher G, Caranfa MJ, McCabe FL, Faucette LF, Johnson RK, et al. (1991) Synthesis of water-soluble (aminoalkyl)camptothecin analogues: inhibition of topoisomerase I and antitumor activity. *J Med Chem* **34:** 98-107.

Klingelhutz AJ, Foster SA, McDougall JK (1996) telomerase activation by the *E6* gene product of human papillomavirus type 16. *Nature* **380:** 79-82.

Knehr M, Poppe M, Enulescu M, Eickelbaum W, Stoehr M, Schroeter D, Paweletz NA (1995) Critical appraisal of synchronization methods applied to achieve maximal enrichment of HeLa cells in specific cell cycle phases. *Exp Cell Res* **217:** 546-553.

Knudson AG (1971) Mutation and cancer: statistical study of retinoblastoma. *Proc Natl Acad Sci USA* **68:** 820-823.

Ko LJ, Prives C (1996) p53: puzzle and paradigm. *Genes Dev* **10:** 1054-1072.

Koberle B, Masters JRW, Hartley JA, Wood RD (1999). Defective repair of cisplatin-induced DNA damage caused by reduced XPA protein in testicular germ cell tumours. *Curr Biol* **9:** 273-276.

Kohn KW (1998) Functional capabilities of molecular network components controlling the mammalian G1/S cell cycle phase transition. *Oncogene* **16:** 1065-1075.

Komarova NL (2005) Mathematical modeling of tumorigenesis: mission possible. *Curr Opin Oncol* **17:** 39-43.

Kozusko F, Chen P, Grant SG, Day BW, Panetta JC (2001) A mathematical model of in vitro cancer cell growth and treatment with the antimitotic agent curacin A. *Math Biosci* **170:** 1-16.

Lai G-M, Moscow JA, Alvarez MG, Fojo AT, Bates SE (1991) Contribution of glutathione and glutathione-dependent enzymes in the reversal of adriamycin resistance in colon carcinoma cell lines. *Int J Cancer* **49:** 688-695.

Lamb JR, Friend SH (1997) Which guesstimate is the best guesstimate? Predicting chemotherapeutic outcomes. *Nat Med* **3:** 962-963.

Lane D (2004) p53 from pathway to therapy. *Carcinogenesis* **25:** 1077-1081.

Larner JM, Lee H, Hamlin JL (1997) S phase damage sensing checkpoints in mammalian cells. *Cancer Surv* **29:** 25-45.

Lawley PD, Phillips DH (1996) DNA adducts from chemotherapeutic agents. *Mutat Res* **355:** 13-40.

Leach FS, Elledge SJ, Sherr CJ, Willson JK, Markowitz S, Kinzler KW, Vogelstein B (1993) Amplification of cyclin genes in colorectal carcinomas. *Cancer Res* **53:** 1986-1989.

Lee H, Larner JM, Hamlin JL (1997) A p53-independent damage-sensing mechanism that functions as a checkpoint at the G1/S transition in Chinese hamster ovary cells. *Proc Natl Acad Sci USA* **94:** 526-531.

León K, Faro J, Carneiro J (2004) A general mathematical framework to model generation structure in a population of asynchronously dividing cells. *J Theor Biol* **229:** 455-476.

Levine AJ, Momand J and Finlay CA (1991) The p53 tumour suppressor gene. *Nature* **351:** 453-456.

Li LH, Fraser TJ, Olin EJ, Bhuyan BK (1972) Action of campothecin on mammalian cells in culture. *Cancer Res* **32:** 2643-2650.

Lin X, Ramamurthi K, Mishima M, Kondo A, Christen RD, Howell SB (2001) p53 modulates the effects of loss of DNA mismatch repair on the sensitivity of human colon cancer cells to the cytotoxic and mutagenic effects of cisplatin. *Cancer Res* **61:** 1508-1516.

Lin ZP, Belcourt MF, Cory JG, Sartorelli AC (2004) Stable suppression of the R2 subunit of ribonucleotide reductase by R2-target short interference RNA sensitizes p53(-/-) HCT-116 colon cancer cells to DNA-damaging agents and ribonucleotide reductase inhibitors. *J Biol Chem* **279:** 27030-27038.

Linfoot PA, Gray JW, Dean PN, Marton LJ, Deen DF (1986) Effect of cell cycle position on the survival of 9L cells treated with nitrosoureas that alkylate, cross-link, and carbomoylate. *Cancer Res* **46:** 2402-2406.

Ludlum DB (1977) Alkylating agents and the nitrosoureas. In: Cancer, a comprehensive treatise, Becker FF (eds). Plenum Press, New York, pp. 285-307.

Lukas C, Bartkova J, Latella L, Falck J, Mailand N, Schroeder T, Sehested M, Lukas J, Bartek J (2001) DNA damage-activated kinase Chk2 is independent of proliferation or differentiation yet correlates with tissue biology. *Cancer Res* **61:** 4990-4993.

Lupi M, Cappella P, Matera G, Natoli C, Ubezio P (2005) Interpreting cell cycle effects of drugs: the case of melphalan. *Cancer Chemother Pharmacol* in press.

Lupi M, Matera G, Branduardi D, D'Incalci M, Ubezio P (2004) Cytostatic and cytotoxic effects of topotecan decoded by a novel mathematical simulation approach. *Cancer Res* **64:** 2825-2832.

Luria SE, Delbruck M (1943) Mutations of bacteria from virus sensitivity to virus resistance. *Genetics* **28:** 491-511.

Lutzker SG, Levine AJ (1996) A functionally inactive p53 protein in teratocarcinoma cells is activated by either DNA damage or cellular differentiation. *Nat Med* **2:** 804-810.

Lyons AB (1999) Divided we stand: tracking cell proliferation with carboxyfluorescein diacetate succinimidyl ester. *Immunol Cell Biol* **77:** 509-515.

Lyons AB (2000) Analysing cell division in vivo and in vitro using flow cytometric measurement of CFSE dye dilution. *J Immunol Methods* **243:** 147-154.

Lyons AB, Hasbold J, Hodgkin PD (2001) Flow cytometric analysis of cell division history using dilution of carboxyfluorescein diacetate succinimidyl ester, a stably integrated fluorescent probe. *Methods Cell Biol* **63:** 375-398.

Lyons AB, Parish CR (1994) Determination of lymphocyte division by flow cytometry. *J Immunol Methods* **171:** 131-137.

Manfredi JJ, Horwitz SB (1986) Taxol: an antimitotic agent with a new mechanism of action. In: Cell cycle effects of drugs. Dethlefsen LA (eds), Pergamon press, Oxford 11: 287.

Mansury Y, Deisboeck TS (2003) The impact of "search precision" in an agentbased tumor model. *J Theor Biol* **224:** 325-337.

Marin L, Minguela A, Torio A, Moya-Quiles MR, Muro M, Montes-Ares O, Parrado A, Alvarez-Lopez DM, Garcia-Alonso AM (2003) Flow cytometric quantification of apoptosis and proliferation in mixed lymphocyte culture. *Cytometry A* **51:**107-118.

Matsuoka S, Huang M, Elledge SJ (1998) Linkage of ATM to cell cycle regulation by the Chk2 protein kinase. *Science* **282:** 1893-1897.

Matsuoka S, Rotman G, Ogawa A, Shiloh Y, Tamai K, Elledge SJ (2000) Ataxia telangiectasia-mutated phosphorylates Chk2 in vivo and in vitro. *Proc Natl Acad Sci USA* **97:** 10389-10394.

Mattes WB, Hartley JA, Kohn KW (1986) DNA-sequence selectivity of guanine-N7 alkylation by nitrogen mustard. *Nucleic Acid Res* **14:** 2971-2987.

Mauro F, Gohde W, Schumann J, Teodori L, Spanò M (1986) Considerations in the design of possible cell cycle effective drugs. *Int J Radiat Biol Relat Stud Phys Chem Med* **49:** 307-333.

McDonald AC, Brown R (1998) Induction of p53-dependent and p53-independent cellular responses by topoisomerase I inhibitors. *Br J Cancer* **78:** 745-751.

McDonald ER 3rd, El Deiry WS (2000) Cell cycle control as a basis for cancer drug development (Review). *Int J Oncol* **16:** 871-886.

McElwain TJ, Hedley DW, Burton G, Clink HM, Gordon MY, Jarman M, Juttner CA, Millar JL, Milsted RA, Prentice G, Smith IE, Spence D, Woods M (1979). Marrow autotransplantation accelerates haematological recovery in patients with malignant melanoma treated with high-dose melphalan. *Br J Cancer* **40:** 72-80.

Meek DW (1998) Multisite phosphorylation and the integration of stress signals at p53. *Cell Signal* **10:** 159-166.

Meriwether WD, Bachur NR (1972) Inhibition of DNA and RNA metabolism by daunorubicin and adriamycin in L1210 mouse leukemia. *Cancer Res* **32:** 1137-1142.

Micetich K, Zwelling LA, Kohn KW (1983) Quenching of DNA:platinum(II) monoadducts as a possible mechanism of resistance to cis-diamminedichloroplatinum(II) in L1210 cells. *Cancer Res* **43:** 3609-3613.

Mikulits W, Dolznig H, Edelmann H, Sauer T, Deiner EM, Ballou L, Beug H, Mullner EW (1997) Dynamics of cell cycle regulators: artifact-free analysis by recultivation of cells synchronized by centrifugal elutriation. *DNA Cell Biol* **16:** 849-859.

Miller C, Koeffler HP (1993) P53 mutations in human cancer. *Leukemia* **2:** S18-21.

Minderman H, Linssen PC, Wessels JM, Haanen C (1991) Doxorubicin toxicity in relation to the proliferative state of human hematopoietic cells. *Exp Hematol* **19:** 110-114.

Minocha A, Long BH (1984) Inhibition of the DNA catenation activity of type II topoisomerase by VP16-213 and VM26. *Biochem Biophys Res Commun* **122:** 165-170.

Miyake H, Hara I, Yamanaka K, Arakawa S, Kamidono S (1999) Synergistic enhancement of resistance to cisplatin in human bladder cancer cells by overexpression of mutant-type p53 and Bcl-2. *J Urol* **162:** 2176-2181.

Moller MB, Ino Y, Gerdes AM, Skjodt K, Louis DN, Pedersen N (1999) Aberrations of the p53 pathway components p53, MDM2 and CDKN2A appear independent in diffuse large B cell lymphoma. *Leukemia* **13:** 453-459.

Momand J, Wu HH, Dasgupta G (2000) MDM2--master regulator of the p53 tumor suppressor protein. *Gene* **242:** 15-29.

Momparler RL, Karon M, Siegel SE, Avila F (1976) effect of adriamycin on DNA, RNA and protein synthesis in cell-free systems and intact cells. *Cancer Res* **36:** 2891-2895.

Montagnoli A, Fiore F, Eytan E, Carrano AC, Draetta GF, Hershko A, Pagano M (1999) Ubiquitination of p27 is regulated by Cdk-dependent phosphorylation and trimeric complex formation. *Genes Dev* **13:** 1181-1189.

Montalenti F, Sena G, Cappella P, Ubezio P (1998) Simulating cancer-cell kinetics after drug treatment: application to cisplatin on ovarian carcinoma. *Physical Rev E* **57:** 5877-5887.

Moore RC, Randall C (1987) Different effects of 1-beta-D-arabinofuranosylcytosine and aphidicolin in S-phase cells - chromosome aberrations, cell-cycle delay and cytotoxicity. *Mutat Res* **178:** 73-80.

Morrow CS, Cowan KH (1990) Glutathione S-transferases and drug resistance. *Cancer Cells* **2:** 15-22.

Mosesso P, Pichierri P, Franchitto A, Palitti F (2000) Evidence that camptothecin-induced aberrations in the G2 phase of cell cycle of Chinese hamster ovary (CHO) cell lines is associated with transcription. *Mutat Res* **452:** 189-195.

Muggia FM, Hainsworth JD, Jeffers S, Miller P, Groshen S, Tan M, Roman L, Uziely B, Muderspach L, Garcia A, Burnett A, Greco FA, Morrow CP, Paradiso LJ, Liang LJ (1997) Phase II study of liposomal doxorubicin in refractory ovarian cancer: antitumor activity and toxicity modification by liposomal encapsulation. *J Clin Oncol* **15:** 987-993.

Murray D, Meyn RE (1986) Cell cycle-dependent cytotoxicity of alkylating agents: determination of nitrogen mustard-induced DNA cross-links and their repair in Chinese hamster ovary cells synchronized by centrifugal elutriation. *Cancer Res* **46:** 2324-2329.

Myers CE (1992) Anthracyclines. *Cancer Chemother Biol Resp Modif* **13:** 45-52.

Myers CE, McGuire WP, Liss RH, Ifrim I, Grotzinger K, Young RC (1977) Adriamycin: the role of lipid peroxidation in cardiac toxicity and tumor response. *Science* **197:** 165-167.

Nehmè A, Baskaran R, Aebi S, Fink D, Nebel S, Cenni B, Wang JYJ, Howell SB, Christen RD (1997) Differential induction of c-jun NH_2-terminal kinase and c-abl kinase in DNA mismatch repair-proficient and deficient cells exposed to cisplatin. *Cancer Res* **57:** 3253-3257.

Nitiss J, Wang JC (1988) DNA topoisomerase-targeting antitumor drugs can be studied in yeast. *Proc Natl Acad Sci USA* **85:** 7501-7505.

Norbury C, Nurse P (1992) Animal cell cycles and their control. *Annu Rev Biochem* **61:** 441-470.

Nordling CO (1953) A new theory on cancer-inducing mechanism. *Br J Cancer* **7:** 68-72.

Nordon RE, Nakamura M, Ramirez C, Odell R (1999) Analysis of growth kinetics by division tracking. *Immunol Cell Biol* **77:** 523-529.

Norton L, Simon R (1977) Tumor size, sensitivity to therapy, and design of treatment schedules. *Cancer Treat Rep* **61:** 1307-1317.

O'Connor PM, Kerrigan D, Bertrand R, Kohn KW, Pommier Y (1990) 10,11-Methylenedioxycamptothecin, a topoisomerase I inhibitor of increased potency: DNA damage and correlation to cytotoxicity in human colon carcinoma (HT-29) cells. *Cancer Commun* **2:** 395-400.

O'Connor PM, Kohn KW (1990) Comparative pharmacokinetics of DNA lesion formation and removal following treatment of L1210 cells with nitrogen mustards. *Cancer Commun* **2:** 387-394.

O'Connor PM, Nieves-Neira W, Kerrigan D, Bertrand R, Goldman J, Kohn KW, Pommier Y (1991) S-phase population analysis does not correlate with the cytotoxicity of camptothecin and 10,11-methylenedioxycamptothecin in human colon carcinoma HT-29 cells. *Cancer Commun* **3:** 233-240.

Offer H, Zurer I, Banfalvi G, Reha'k M, Falcovitz A, Milyavsky M, Goldfinger N, Rotter V (2001) p53 modulates base excision repair activity in a cell cycle-specific manner after genotoxic stress. *Cancer Res* **61:** 88-96.

Ohtsubo M, Theodoras AM, Schumacher J, Roberts JM, Pagano M (1995) Human cyclin E, a nuclear protein essential for the G1-to-S phase transition. *Mol Cell Biol* **15:** 2612-2624.

Omura GA, Brady MF (1993) Meta-analysis of cisplatin, doxorubicin, and cyclophosphamide versus cisplatin and cyclophosphamide chemotherapy of ovarian carcinoma. *Obstet Gynecol* **81:** 641-642.

Oren M (1999) Regulation of the p53 tumor suppressor protein. *J Biol Chem* **274:** 36031-36034.

Owen MR, Sherratt JA (1999) Mathematical modeling of macrophage dynamics in tumors. *Math Models Methods Appl Biol Chem* **377:** 675-684.

Pan ZQ, Reardon JT, Li L, Flores-Rozas H, Legerski R, Sancar A, Hurwitz J (1995) Inhibition of nucleotide excision repair by the cyclin-dependent kinase inhibitor p21. *J Biol Chem* **270:** 22008-22016.

Parchment RE, Pessina A (1998) Topoisomerase I inhibitors and drug resistance. *Cytotechnology* **27:** 149-164.

Parker RJ, Eastman A, Bostick-Bruton F, Reed E (1991) Acquired cisplatin resistance in human ovarian cancer cells is associated with enhanced repair of cisplatin-DNA lesions and reduced drug accumulation. *J Clin Invest* **87:** 772-777.

Pauwels B, Korst AE, de Pooter CM, Pattyn GG, Lambrechts HA, Baay MF, Lardon F, Vermorken JB (2003) Comparison of the sulforhodamine B assay and the clonogenic assay for in vitro chemoradiation studies. *Cancer Chemother Pharmacol* **51:** 221-226.

Pearson BS, Raghavan D (1985) First-line intravenous cisplatin for deeply invasive bladder cancer: update on 70 cases. *Br J Urol* **57:** 690-693.

Perego P, Giarola M, Righetti SC, Supino R, Caserini C, Delia D, Pierotti MA, Miyashita T, Reed JC, Zunino F (1996) Association between cisplatin resistance

and mutation of p53 gene and reduced bax expression in ovarian carcinoma cell systems. *Cancer Res* **56:** 556-562.

Pestell KE, Hobbs SM, Titley JC, Kelland LR, Walton MI (2000) Effect of p53 status to platinum complexes in a human ovarian cancer cell line. *Mol Pharmacol* **57:** 503-511.

Phillips DR, White RJ, Cullinane C (1989) DNA sequence-specific adducts of adriamycin and mitomycin C. *FEBS Lett* **246:** 233-240.

Pines J (1991) Cyclins: wheels within wheels. *Cell Growth Differ* **2:** 305-310.

Plate J, Petersen KS, Buckingham L, Shahidi H, Schofield CM (2000) Gene expression in chronic lymphocytic leukemia B cells and changes during induction of apoptosis. *Exp Hematol* **28:** 1214-1224.

Plooy AC, van Dijk M, Lohman PHM (1984) Induction and repair of DNA cross-links in chinese hamster ovary cells treated with various platinum coordination compounds in relation to platinum binding to DNA, cytotoxicity, mutagenicity, and antitumor activity. *Cancer Res* **44:** 2043-2061.

Pommier Y, Pourquier P, Urasaki Y, Wu J, Laco GS (1999) Topoisomerase I inhibitors: selectivity and cellular resistance. *Drug Resist Updat* **2:** 307-318.

Potter AJ, Gollahon KA, Palanca BJA, Harbert MJ, Choi YM, Moskovitz AH, Potter JD, Rabinovitch PS (2002) Flow cytometric analysis of the cell cycle phase specificity of DNA damage induced by radiation, hydrogen peroxide and doxorubicin. *Carcinogenesis* **23:** 389-401.

Pratesi G, Beretta GL, Zunino F (2004) Gimatecan, a novel camptothecin with a promising preclinical profile. *Anticancer Drugs* **15:** 545-552.

Qi AS, Zheng X, Du CY, An BS (1993) A cellular automaton model of cancerous growth. *J Theor Biol* **161:** 1-12.

Qu Z, MacLellan WR, Weiss JN (2003) Dynamics of the cell cycle: checkpoints, sizers, and timers. *Biophys J* **85:** 3600-3611.

Redwood WR, Colvin M (1980) Transport of melphalan by sensitive and resistant L1210 cells. *Cancer Res* **40:** 1144-1149.

Reece PA, Hill HS, Green RM, Morris RG, Dale BM, Kotasek D, Sage RE (1988) Renal clearance and protein binding of melphalan in patients with cancer. *Cancer Chemother Pharmacol* **22:** 348-352.

Rogers AM, Hill R, Lehmann AR, Arlett CF, Burns VW (1980) The induction and characterization of mouse lymphoma L5178Y cell lines resistant to 1-β-D-arabinofuranosylcytosine. *Mutat Res* **69:** 139-148.

Rosenberg B, Camp LV (1965) Inhibition of cell division in Escherichia coli by electrolysis products from a platinum electrode. *Nature* **205:** 698-699.

Ross WE, Bradley MO (1981) DNA double-stranded breaks in mammalian cells after exposure to intercalating agents. *Biochim Biophys Acta* **654:** 129-134.

Ross WE, Ewig RAG, Kohn KW (1978a) Differences between melphalan and nitrogen mustard in the formation and removal of DNA cross-links. *Cancer Res* **38:** 1502-1506.

Ross WE, Glaubiger DL, Kohn KW (1978b) Protein-associated DNA breaks in cells treated with adriamycin or ellipticine. *Biochim Biophys Acta* **519:** 23-30.

Rowinsky EK, Grochow LB, Hendricks CB, Ettinger DS, Forastiere AA, Hurowitz LA, McGuire WP, Sartorius SE, Lubejko BG, Kaufmann SH, Donehower RC (1992) Phase I and pharmacologic study of topotecan: a novel topoisomerase I inhibitor. *J Clin Oncol* **10:** 647-656.

Rubinstein LV, Shoemaker RH, Paull KD, Simon RM, Tosini S, Skehan P, Scudiero DA, Monks A, Boyd MR (1990) Comparison of in vitro anticancer-drug-screening data generated with a tetrazolium assay versus a protein assay against a diverse panel of human tumor cell lines. *J Natl Cancer Inst* **82:** 1113-1118.

Saltz L, Sirott M, Young C, Tong W, Niedzwiecki D, Tzy-Jyun Y, Tao Y, Trochanowski B, Wright P, Barbosa K, et al. (1993) Phase I clinical and pharmacology study of topotecan given daily for 5 consecutive days to patients with advanced solid tumors, with attempt at dose intensification using recombinant granulocyte colony-stimulating factor. *J Natl Cancer Inst* **85:** 1499-1507. Erratum in: J Natl Cancer Inst 85: 1777 (1993).

Samuels BL, Bitran JD (1995) High-dose intravenous melphalan: a review. *J Clin Oncology* **13:** 1786-1799.

Sansom OJ, Clarke AR (2002) The ability to engage enterocyte apoptosis does not predict long-term crypt survival in *p53* and *Msh2* deficient mice. *Oncogene* **21:** 5934-5939.

Sarosy G, Leyland-Jones B, Soochan P, Cheson BD (1988) The systemic administration of intravenous melphalan. *J Clin Oncol* **6:** 1768-1782.

Schellens JH, Creemers GJ, Beijnen JH, Rosing H, de Boer-Dennert M, McDonald M, Davies B, Verweij J (1996) Bioavailability and pharmacokinetics of oral topotecan: a new topoisomerase I inhibitor. *Br J Cancer* **73:** 1268-1271.

Schneider E, Hsiang YH, Liu LF (1990) DNA topoisomerases as anticancer drug targets. *Adv Pharmacol* **21:** 149-183.

Schoemaker NE, Herben VMM, De Jong LA, van Waardenburg R, Pluim D, Huinink WW, Beijnen JH, Schellens JHM (2002) Topoisomerase I levels in white blood cells of patients with ovarian cancer treated with paclitaxel-cisplatin-topotecan in a phase I study. *Anticancer Drugs* **13:** 87-91.

Selby PJ, McElwain TJ, Nandi AC, Perren TJ, Powles RL, Tillyer CR, Osborne RJ, Slevin ML, Malpas JS (1987) Multiple myeloma treated with high dose intravenous melphalan. *Br J Haematol* **66:** 55-62.

Sena G, Onado C, Cappella P, Montalenti F, Ubezio P (1999) Measuring the complexity of cell cycle arrest and killing of drugs: kinetics of phase-specific effects induced by taxol. *Cytometry* **37:** 113-124.

Senderowicz AM (2004) Targeting cell cycle and apoptosis for the treatment of human malignancies. *Curr Opin Cell Biol* **16:** 670-678.

Shah MA, Schwartz GK (2001) Cell cycle-mediated drug resistance: an emerging concept in cancer therapy. *Clin Cancer Res* **7:** 2168-2181.

Sherr CJ (1994) G1 phase progression: cycling on cue. *Cell* **79:** 551-555.

Sherr CJ (1996) Cancer cell cycles. *Science* **274:** 1672-1677.

Sherr CJ, Roberts JM (1995) Inhibitors of mammalian G1 cyclin-dependent kinases. *Genes Dev* **9:** 1149-1163.

Simeoni M, Magni P, Cammia C, De Nicolao G, Croci V, Pesenti E, Germani M, Poggesi I, Rocchetti M (2004) Predictive pharmacokinetic-permacodynamic modeling of tumor growth kinetics in xenograft models after administration of anticancer agents. *Cancer Res* **64:** 1094-1101.

Sisken JE, Morasca L (1965) Intrapopulation kinetics of the mitotic cycle. *J Cell Biol* **25:** 179-189.

Skipper HE, Schabel FM Jr, Wilcox WS (1964) Experimental evaluation of potential anticancer agents, XIII. On the criteria and kinetics associated with "curability" of experimental leukemias. *Cancer Chemother Rep* **35:** 1-111.

Skladanowski A, Konopa J (1994) Relevance of interstrand DNA crosslinking induced by anthracyclines for their biologic activity. *Biochem Pharmacol* **47:** 2279-2287.

Smith ML, Chen IT, Zhan Q, Bae I, Chen CY, Gilmer TM, Kastan MB, O'Connor PM, Fornace AJ (1994) Interaction of the p53-regulated protein Gadd45 with proliferating cell nuclear antigen. *Science* **266:** 1376-1380.

Smits VA, Medema RH (2001) Checking out the G_2/M transition. *Biochim Biophys Acta* **1519:** 1-12.

Sorenson CM, Barry MA, Eastman A (1990) Analysis of events associated with cell cycle arrest at G_2 phase and cell death induced by cisplatin. *J Natl Cancer Inst* **82:** 749-755.

Speth PA, Linssen PCM, Boezeman JBM, Wessels HMC, Haanen C (1987) Cellular and plasma adriamycin concentrations in long-term infusion therapy of leukemia patients. *Cancer Chemother Pharmacol* **20:** 305-310.

Steel GG (1977) Growth kinetics of tumours. Clarendon press, Oxford.

Swanson KR, Bridge C, Murray JD, Alvord EC Jr (2003) Virtual and real brain tumors: using mathematical modeling to quantify glioma growth and invasion. *J Neurol Sci* **216:** 1-10.

Takata M, Sasaki MS, Sonoda E, Morrison C, Hashimoto M, Utsumi H, Yamaguchi-Iwai Y, Shinohara A, Takeda S (1998) Homologous recombination and non-homologous end-joining pathways of DNA double-strand break repair have overlapping roles in the maintenance of chromosomal integrity in vertebrate cells. *EMBO J* **17:** 5497-5508.

Tanaka H, Arakawa H, Yamaguchi T, Shiraishi K, Fukuda S, Matsui K, Takei Y, Nakamura Y (2000) A ribonucleotide reductase gene involved in a p53-dependent cell-cycle checkpoint for DNA damage. *Nature* **404:** 42-49.

Taron M, Plasencia C, Abad A, Martin C, Guillot M (2000) Cytotoxic effects of topotecan combined with various active G2/M-phase anticancer drugs in human tumour-derived cell lines. *Inv New Drugs* **18:** 139-147.

Tew KD (1994) Glutathione-associated enzymes in anticancer drug resistance. *Cancer Res* **54:** 4313-4320.

Tewey KM, Rowe TC, Yang L, Halligan BD, Liu LF (1984) Adriamycin-induced DNA damage mediated by mammalian DNA topoisomerase II. *Science* **226:** 466-468.

Tobey RA, Chrissman HA, Oka MS (1976) Arrested and cycling CHO cells as a kinetic model: studies with adriamycin. *Cancer Treat Rep* **60:** 1829-1837.

Tsao YP, D'Arpa P, Lui LF (1992) The involvement of active DNA-synthesis in campothecin-induced G_2 arrest: altered regulation of p34cdc2/cyclin B. *Cancer Res* **52:** 1823-1829.

Twentyman PR, Luscombe M (1987) A study of some variables in a tetrazolium dye (MTT) based assay for cell growth and chemosensitivity. *Br J Cancer* **56:** 279-285.

Tyson JJ, Chen K, Novak B (2001) Network dynamics and cell physiology. *Nat Rev Mol Cell Biol* **2:** 908-916.

Ubezio P (1985) Microcomputer experience in analysis of flow cytometric DNA distributions. *Comput Programs Biomed* **19:** 159-166.

Ubezio P, Filippeschi S, Spinelli L (1991) Method for kinetic analysis of drug-induced cell cycle perturbations. *Cytometry* **12:** 119-126.

Unsal-Kacmaz K, Makhov AM, Griffith JD, Sancar A (2002) Preferential binding of ATR protein to UV-damaged DNA. *Proc Natl Acad Sci USA* **99:** 6673-6678.

Urbani L, Sherwood SW, Schimke RT (1995) Dissociation of nuclear and cytoplasmic cell cycle progression by drugs employed in cell synchronization. *Exp Cell Res* **219:** 159-168.

Vahrmeijer AL, van Dierendonck JH, Schutrups J, van de Velde CJH, Mulder GJ (1999) Effect of glutathione depletion on inhibition of cell cycle progression and induction of apoptosis by melphalan (L-phenylalanine mustard) in human colorectal cancer cells. *Biochem Pharmacol* **58:** 655-664.

Valeriote F, van Putten L (1975) Proliferation-dependent cytotoxicity of anticancer agents: a review. *Cancer Res* **35:** 2619-2630.

Vermeulen K, Van Bockstaele DR, Berneman ZN (2003) The cell cycle: a review of regulation, deregulation and therapeutic targets in cancer. *Cell Prolif* **30:** 131-149.

Vermorken JB, Kobierska A, van der Burg ME, Chevallier B, Zanaboni F, ten Bokkel Huinink WW, Forni M, Pawinski A, van der Putten E, Bolis G (1995) High-dose epirubicin in platinum-pretreated patients with ovarian carcinoma: the EORTC-GCCG experience. *Eur J Gynaecol Oncol* **16:** 433-438.

Vikhanskaya F, Colella G, Valenti M, Parodi S, D'Incalci M, Broggini M (1999) Cooperation between p53 and hMLH1 in a human coloncarcinoma cell line in response to DNA damage. *Clin Cancer Res* **5:** 937-941.

Villunger A, Michalak EM, Coultas L, Mullauer F, Bock G, Ausserlechner MJ, Adams JM, Strasser A (2003) p53- and drug-induced apoptotic responses mediated by BH3-only proteins puma and noxa. *Science* **302:** 1036-1038.

Vistica DT, Toal JN, Rabinovitz M (1978) Amino acid-conferred protection against melphalan: characterization of melphalan transport and correlation uptake with cytotoxicity in cultured L1210 murine leukemia cells. *Biochem Pharmacol* **27:** 2865-2870.

Vogelstein B, Lane D, Levine AJ (2000) Surfing the p53 network. *Nature* **408:** 307-310.

von Horsten S, Helfritz A, Kuhlmann S, Nave H, Tschernig T, Pabst R, Ben-Eliyahu S, Meyer D, Schmidt RE, Schmitz C (2000) Stereological quantification of carboxyfluorescein-labeled rat lung metastasis: a new method for the assessment of natural killer cell activity and tumor adhesion in vivo and in situ. *J Immunol Methods* **239:** 25-34.

Vousden KH, Lu X (2002) Live or let die: the cell's response to p53. *Nat Rev Cancer* **2:** 594-604.

Wadler S, Yeap B, Vogl S, Carbone P (1996) Randomized trial of initial therapy with melphalan versus cisplatin-based combination chemotherapy in patients with advanced ovarian carcinoma: initial and long term results – Eastern Cooperative Oncology Group Study E2878. *Cancer* **77:** 733-742.

Waga S, Li R, Stillman B (1997) p53-induced p21 controls DNA replication. *Leukemia* **3:** 321-323.

Waldman T, Kinzler KW, Vogelstein B (1995) p21 is necessary for the p53-mediated G_1 arrest in human cancer cells. *Cancer Res* **55:** 5187-5190.

Waldman T, Zhang Y, Dillehay L, Yu J, Kinzler K, Vogelstein B, Williams J (1997) Cell-cycle arrest versus cell death in cancer therapy. *Nat Med* **3:** 1034-1036.

Wall JG, Burris HA, Von Hoff DD, Rodriguez G, Kneuper-Hall R, Shaffer D, O'Rourke T, Brown T, Weiss G, Clark G (1992) A phase I clinical and pharmacokinetic study of the topoisomerase I inhibitor topotecan (SK&F 104864) given as an intravenous bolus every 21 days. *Anticancer Drugs* **3:** 337-345.

Wall ME (1993) Chronicles of Drug Discovery, Ed. Lednicer D. American Chemical Society, Washington DC, 3: 327.

Wall ME, Wani MC, Cook CE, Palmer KH (1966) Plant antitumor agents: the isolation and structure of camptothecin, a novel alkaloidal leukemia and tumor inhibitor from *Camptotheca acuminata*. *J Am Chem Soc* **88:** 3888-3890.

Walton MI, Whysong D, O'Connor PM, Hockenbery D, Korsmeyer SJ, Kohn KW (1993) Constitutive expression of human Bcl-2 modulates nitrogen mustard and camptothecin induced apoptosis. *Cancer Res* **53:** 1853-1861.

Wang JJ, Chervinsky DS and Rosen JM (1972) Comparative biochemical studies of adriamycin and daunomycin in leukemic cells. *Cancer Res* **32:** 511-515.

Wani MA, Zhu QZ, El-Mahdy M, Wani AA. (1999) Influence of p53 tumor suppressor protein on bias of DNA repair and apoptotic response in human cells. *Carcinogenesis* **20:** 765-772.

Warren HS (1999) Using carboxyfluorescein diacetate succinimidyl ester to monitor human NK cell division: analysis of the effect of activating and inhibitory class I MHC receptors. *Immunol Cell Biol* **77:** 544-551.

Webb CD, Latham MD, Lock RB, Sullivan DM (1991) Attenuated topoisomerase II content directly correlates with a low level of drug resistance in a Chinese hamster ovary cell line. *Cancer Res* **51:** 6543-6549.

Weston SA, Parish CR (1990) New fluorescent dyes for lymphocyte migration studies. Analysis by flow cytometry and fluorescence microscopy. *J Immunol Methods* **133:** 87-97.

Wolfel T, Hauer M, Schneider J, Serrano M, Wolfel C, Klehmann-Hieb E, De Plaen E, Hankeln T, Meyer zum Buschenfelde KH, Beach D (1995) A p16INK4a-insensitive CDK4 mutant targeted by cytolytic T lymphocytes in a human melanoma. *Science* **269:** 1281-1284.

Wu J, Liu LF (1997) Processing of topoisomerase I cleavable complex into DNA damage by transcription. *Nucleic Acid Res* **25:** 4181-4186.

Wu J, Yin MB, Hapke G, Toth K, Rustum YM (2002) Induction of biphasic DNA double strand breaks and activation of multiple repair protein complexes by DNA topoisomerase I drug 7-ethyl-10-hydroxy-camptothecin. *Mol Pharmacol* **61:** 742-748.

Yamaguchi T, Matsuda K, Sagiya Y, Iwadate M, Fujino MA, Nakamura Y, Arakawa H (2001) p53R2-dependent pathway for DNA synthesis in a p53-regulated cell cycle checkpoint. *Cancer Res* **61:** 8256-8262.

Yao S, Murali D, Seetharamulu P, Haridas K, Petluru PNV, Reddy DG, Hausheer FH (1998) Topotecan lactone selectively binds to double- and single-stranded DNA in the absence of topoisomerase I. *Cancer Res* **58:** 3782-3786.

Yu Q, Geng Y, Sicinski P (2001) Specific protection against breast cancers by cyclin D1 ablation. *Nature* **411:** 1017-1021.

Zamble DB, Jacks T, Lippard SJ (1998) p53-Dependent and -independent responses to cisplatin in mouse testicular teratocarcinoma cells. *Proc Natl Acad Sci USA* **95:** 6163-6168.

Zhang H, D'Arpa P, Liu LF (1990) A model tumor cell killing by topoisomerase poisons. *Cancer Cells* **2:** 23-27.

Zhou BB, Elledge SJ (2000) The DNA damage response: putting checkpoints in perspective. *Nature* **408:** 433-439.

Zhou BB, Bartek J (2004) Targeting the checkpoint kinases: chemosensitization versus chemoprotection. *Nature Rev Cancer* **4:** 1-10.

Zuco V, Supino R, De Cesare M, Carenini N, Perego P, Gatti L, Pratesi G, Bucci F, Zanier R, Carminati P, Zunino F (2003) Cellular bases of the antitumor activity of a 7-substituted camptothecin in hormone-refractory human prostate carcinoma models. *Biochem Pharm* **65:** 1281-1294.

LIST OF ABBREVIATIONS

ALL	Acute lymphoblastic leukaemia
Ara-C	Cytosine arabinoside
ATM	Ataxia telangiectasia mutated
ATR	ATM-related
BER	Base-excision repair
BrdUrd	5-bromo-2'-deoxyuridine
CDK	Cyclin-dependent kinases
CFDASE	5-(and-6)-Carboxyfluorescein diacetate succinimidyl ester
CFSE	Carboxyfluorescein
Chk1 and Chk2	Checkpoint kinase 1 and checkpoint kinase 2
CKI	CDK inhibitors
CML	Chronic myeloid leukaemia
CPT	Camptothecin
CV	Coefficient of variation
DSB	Double-strand break
DDP	Cisplatin
DMSO	Dimethylsulfoxide
DXR	Doxorubicin
EDTA	Ethylenediaminetetraacetic acid
EGFR	Epidermal growth factor receptor
FITC	Fluorescein isothiocyanate
FSC	Froward scatter
GSH	Glutathione
GST	Glutathione S-transferases

IMDM	Iscove's Modified Dulbecco's Medium
L-PAM	L-phenylalanine mustard - melphalan
LU	Labelled undivided (cells)
MDR	Multidrug resistance
MMR	Mismatch repair
MRP	MDR-associated protein
MTT	3-[4,5-dimethyl(thiazol-2-yl)-3,5-diphenyl] tetrazolium bromide
NER	Nucleotide-excision repair
NGS	Normal goat serum
PBS	Phosphate buffer solution
PCNA	Proliferating cell nuclear antigen
PE	Phycoerythrin
P-gp	P-glycoprotein
PI	Propidium iodide
PMT	Photomultiplier tube
Rb	Retinoblastoma
SCLC	Small cell lung cancer
SRB	Sulphorhodamine blue
SSC	Side scatter
TdT	Terminal deoxynucleotidyl transferase
TPT	Topotecan
TUNEL	TdT-mediated dUTP nick end labelling technique

LIST OF PUBLICATIONS

Publications of the candidate not strictly related to the work presented here

Babetto E, Mangolini A, Rizzardini M, Lupi M, Conforti L, Rusmini P, Poletti A, Cantoni L (2005) Tetracycline-regulated gene expression in the NSC-34-tTA cell line for investigation of motor neuron disease. *Brain Res Mol Brain Res* **140:** 63-72.

Rizzardini M, Mangolini A, Lupi M, Ubezio P, Bendotti C, Cantoni L (2005) Low levels of ALS-linked Cu/Zn superoxide dismutase increase the production of reactive oxygen species and cause mitochondrial damage and death in motor neuron-like cells. *J Neurol Sci* **232:** 95-103.

Tomasoni D, Lupi M, Brikci FB, Ubezio P (2003) Timing the changes of cyclin E cell content in G1 in exponentially growing cells. *Exp Cell Res* **288:** 158-167.

Rizzardini M, Lupi M, Bernasconi S, Mangolini A, Cantoni L (2003) Mitochondrial dysfunction and death in motor neurons exposed to the glutathione-depleting agent ethacrynic acid. J Neurol Sci 207: 51-58.

Chiorino G, Lupi M (2002) Variability in the timing of G(1)/S transition. *Math Biosci* **177-178:** 85-101.

Bettega D, Calzolari P, Belloni F, Di Lena F, Genchi S, Lupi M, Massariello P, Orsini S, Tallone L, Tomasoni D, Ubezio P, Redpath JL (2001) Solar UV radiation: differential effectiveness of UVB subcomponents in causing cell death,

micronucleus induction and delayed expression of heritable damage in human hybrid cells. *Int J Radiat Biol* **77:** 963-970.

Cappella P, Tomasoni D, Faretta M, Lupi M, Montalenti F, Viale F, Banzato F, D'Incalci M, Ubezio P (2001) Cell cycle effects of gemcitabine. *Int J Cancer* **93:** 401-408.

Publications of the candidate arisen from the work reported here

Lupi M, Cappella P, Matera G, Natoli C, Ubezio P (2005) Interpreting cell cycle effects of drugs: the case of melphalan. *Cancer Chemother Pharmacol* [Epub ahead of print].

Matera G, Lupi M, Ubezio P (2004) Heterogeneous cell response to topotecan in a CFSE-based proliferation test. *Cytometry A* **62:** 118-128.

Lupi M, Matera G, Branduardi D, D'Incalci M, Ubezio P (2004) Cytostatic and cytotoxic effects of topotecan decoded by a novel mathematical simulation approach. *Cancer Res* **64:** 2825-2832.